Université de Montréal

Role of Nuclear Angiotensin-II Receptor Mediated Signalling in Cardiovascular Remodelling

par
Artavazd Tadevosyan

Département de Sciences Biomédicales
Faculté de Médecine

Thèse présentée à la Faculté des études supérieures et postdoctorales
en vue de l'obtention du grade de Doctorat
en Sciences Biomédicales

Février, 2015

Université de Montréal
Faculté des études supérieures et postdoctorales

Cette thèse intitulée:
Role of Nuclear Angiotensin-II Receptor Mediated Signalling in Cardiovascular Remodelling

présentée par:
Artavazd Tadevosyan

a été évaluée par un jury composé des personnes suivantes :

Dr Martin G Sirois	Président-rapporteur
Dr Stanley Nattel	Directeur de recherche
Dr Bruce G Allen	Co-Directeur de recherche
Dr Nicolas Bousette	Membre du jury
Dr Timothy O'Connell	Examinateur externe
Dr Denis deBlois	Représentant du doyen de FESP

Résumé

Le remodelage cardiaque est le processus par lequel la structure ou la fonction cardiaque change en réponse à un déséquilibre pathophysiologique tel qu'une maladie cardiaque, un contexte d'arythmie prolongée ou une modification de l'équilibre hormonal. Le système rénine-angiotensine (SRA) est un système hormonal largement étudié et il est impliqué dans de nombreuses activités associées au remodelage cardiovasculaire. L'existence d'un système circulatoire couplé à un système de tissus locaux est une représentation classique, cependant de nouvelles données suggèrent un SRA indépendant et fonctionnellement actif à l'échelle cellulaire. La compréhension de l'activité intracellulaire du SRA pourrait mener à de nouvelles pistes thérapeutiques qui pourraient prévenir un remodelage cardiovasculaire défavorable. L'objectif de cette thèse était d'élucider le rôle du SRA intracellulaire dans les cellules cardiaques.

Récemment, les récepteurs couplés aux protéines G (RCPG), les protéines G et leurs effecteurs ont été détectés sur des membranes intracellulaires, y compris sur la membrane nucléaire, et les concepts de RCPG intracellulaires fonctionnels sont en voie d'être acceptés comme une réalité. Nous avons dès lors fait l'hypothèse que la signalisation du SRA délimitant le noyau était impliquée dans le contrôle de l'expression des gènes cardiaques. Nous avons démontré la présence de récepteurs d'angiotensine de type-1 (AT1R) et de type-2 (AT2R) nucléaires dans les cardiomyocytes ventriculaires adultes et dans une fraction nucléaire purifiée de tissu cardiaque. Des quantités d'Ang II ont été détectées dans du lysat de cardiomyocytes

et des microinjections d'Ang-II-FITC ont donné lieu à des liaisons préférentielles aux sites nucléaires. L'analyse transcriptionnelle prouve que la synthèse d'ARN de novo dans des noyaux isolés stimulés à l'Ang-II, et l'expression des ARNm de NF-κB étaient beaucoup plus importants lorsque les noyaux étaient exposés à de l'Ang II par rapport aux cardiomyocytes intacts. La stimulation des AT1R nucléaires a engendré une mobilisation de Ca^{2+} via les récepteurs de l'inositol trisphosphate (IP3R), et le blocage des IP3R a diminué la réponse transcriptionnelle.

Les méthodes disponibles actuellement pour l'étude de la signalisation intracrine sont limitées aux méthodes indirectes. L'un des objectifs de cette thèse était de synthétiser et caractériser des analogues d'Ang-II cellule-perméants afin d'étudier spécifiquement dans les cellules intactes l'activité intracellulaire du SRA. Nous avons synthétisé et caractérisé pharmacologiquement des analogues photosensibles Ang-II encapsulée en incorporant un groupement 4,5-diméthoxy-2-nitrobenzyl (DMNB) photoclivable sur les sites actifs identifiés du peptide. Chacun des trois analogues d'Ang II encapsulée synthétisés et purifiés: [Tyr(DMNB)^4]Ang-II, Ang-II-ODMNB et [Tyr(DMNB)^4]Ang-II-ODMNB a montré une réduction par un facteur deux ou trois de l'affinité de liaison envers AT1R et AT2R dans les dosages par liaison compétitive et une activité réduite dans la contraction de l'aorte thoracique. La photostimulation de [Tyr(DMNB)^4]Ang-II dans des cellules HEK a augmenté la phosphorylation d'ERK1/2 (via AT1R) et la production de cGMP (via AT2R) alors que dans les cardiomyocytes isolés elle générait une augmentation de Ca^{2+} nucléoplasmique et initiait la synthèse d'ARNr 18S et d'ARNm du NF-κB.

Les fibroblastes sont les principaux générateurs de remodelage cardiaque structurel, et les fibroblastes auriculaires sont plus réactifs aux stimuli profibrotiques que les fibroblastes ventriculaires. Nous avons émis l'hypothèse que l'Ang-II intracellulaire et l'activation des AT1R et AT2R nucléaires associés contrôlaient les profils d'expression des gènes des fibroblastes via des systèmes de signalisation distincts et de ce fait jouaient un rôle majeur dans le développement de la fibrose cardiaque. Nous avons remarqué que les fibroblastes auriculaires expriment l'AT1R et l'AT2R nucléaire et l'Ang-II au niveau intracellulaire. L'expression d'AT1R nucléaire a été régulés positivement dans les cas d'insuffisance cardiaque (IC), tandis que l'AT2R nucléaire a été glycosylé post-traductionnellement. La machinerie protéique des protéines G, y compris Gαq/11, Gαi/3, et Gβ, a été observée dans des noyaux isolés de fibroblastes. AT1R et AT2R régulent l'initiation de la transcription du fibroblaste via les voies de transduction de signal d'IP3R et du NO. La photostimulation de [Tyr(DMNB)^{4}]Ang-II dans une culture de fibroblastes auriculaire déclenche la libération de Ca^{2+} nucléoplasmique, la prolifération, et la synthèse et sécrétion de collagène qui ne sont pas inhibées par les bloqueurs d'AT1R et/ou AT2R extracellulaires.

***Mots-clés**:* Système rénine-angiotensine (SRA), récepteurs intracellulaires, signalisation, remodelage cardiovasculaire

Abstract

Cardiac remodelling is the process by which cardiac structure and/or function change in response to pathophysiological imbalances such as hypertension, cardiac disease, prolonged arrhythmia or altered hormonal balance. The renin-angiotensin system (RAS) is an extensively studied hormonal system involved in numerous processes associated with cardiovascular remodelling. Classically viewed as a circulating and a local tissue system, emerging evidence suggests an independent and functionally active RAS within individual cells. Understanding intracellular RAS actions might lead to new therapeutic avenues that could prevent adverse cardiac remodelling. The purpose of this thesis was to elucidate the role of intracellular RAS in cardiac cells.

Recently, G protein-coupled receptors (GPCRs), G proteins, and their downstream effectors have been detected on intracellular membranes, including the nuclear membrane, and the concept of functional intracellular GPCRs is slowly being accepted as a reality. We therefore hypothesized that nuclear-delimited angiotensin II (Ang-II) signalling is involved in controlling cardiac gene expression. We demonstrated the presence of nuclear angiotensin-type 1 (AT1R) and angiotensin-type 2 (AT2R) receptors in adult ventricular cardiomyocytes and in a purified nuclear preparation from cardiac tissue. Ang-II was detected in cardiomyocyte lysate and microinjected Ang-II-FITC preferentially bound to nuclear sites. Transcriptional analysis demonstrated that Ang-II enhanced de novo RNA synthesis in isolated nuclei and NF-κB mRNA expression was much greater when nuclei were exposed to Ang-II. Nuclear AT1R-stimulation produced Ca^{2+} mobilization via nuclear inositol

1,4,5-trisphosphate receptor (IP3R) Ca^{2+}-channels, and IP3R-blockade attenuated the AT1R-mediated transcriptional responses in isolated nuclei.

Current methods available to study intracrine RAS signalling are limited to indirect methodologies because of a lack of selective intracellularly-acting probes. An aim of this thesis was to synthesize and characterize cell-permeant Ang-II analogues to probe intracellular RAS action with spatial and temporal precision. Using solid-phase peptide technology we synthesized and pharmacologically characterized light-sensitive caged Ang-II analogues. This was achieved by incorporating a photocleavable 4,5-dimethoxy-2-nitrobenzyl (DMNB) moiety on sites of Ang-II responsible for receptor recognition and activation. All of the three synthesized and purified caged-Ang-II analogues: [Tyr(DMNB)^4]Ang-II, Ang-II-ODMNB and [Tyr(DMNB)^4]Ang-II-ODMNB, showed two-to-three orders of magnitude reduced binding affinity towards the AT1R and AT2R in competition binding assays and reduced potency in contraction assays using thoracic aorta. Photolysis of [Tyr(DMNB)^4]Ang-II in HEK cells increased ERK1/2 phosphorylation (via AT1R) and cGMP production (via AT2R) whereas in isolated cardiomyocytes it induced an increase in nucleoplasmic Ca^{2+} and increased the abundance of 18S rRNA and NF-κB mRNA.

Fibroblasts are the main drivers of cardiac structural remodelling. Atrial fibroblasts are more responsive to pro-fibrotic stimuli than ventricular fibroblasts. We hypothesized that intracellular Ang-II and associated nuclear AT1R and AT2R activation control fibroblast gene-expression patterns via discrete signalling systems and thereby play a key role in cardiac fibrosis. Atrial fibroblasts were found to express

Ang-II, and nuclear AT1R and AT2R. The nuclear localisation of AT1R was increased in fibroblasts isolated from failing hearts whereas nuclear AT2R showed alterations in glycosylation. Heterotrimeric G protein subunits including Gαq/11, Gαi/3, and Gβ were observed in isolated fibroblast nuclei. AT1R and AT2R increased fibroblast transcription initiation via IP3R and NO signal transduction pathways, respectively. Photolysis of [Tyr(DMNB)^4]Ang-II in cultured atrial fibroblasts induced an increase in nucleoplasmic Ca^{2+}, proliferation, collagen synthesis and secretion that was not prevented by extracellular AT1R and/or AT2R blockers.

***Keywords**:* Renin-angiotensin system (RAS), intracellular receptors, signalling, cardiovascular remodelling

Table of Contents

Résumé i

Table of Contents vii

Liste of Figures and Tables xi

List of Abbreviations xv

Acknowledgements xxi

CHAPTER 1 – Introduction 1

1.1 Overview 2

1.2 Cardiovascular System 2

1.2.1 The Cardiac Muscle 3

1.2.2 The Cardiac Arteries 4

1.2.3 The Cardiac Valves 5

1.2.4 The Cardiac Electrical System 6

1.2.5 The Pericardium 10

1.3 Cardiac Remodelling 10

1.4 Concepts of Cardiac Remodelling 13

1.5 Components of Cardiac Remodelling 15

1.5.1 The Role of Cardiac Myocyte Growth 15

1.5.2 The Role of Cardiomyocyte Apoptosis, Necrosis, and Autophagy 16

1.5.3 The Role of Fibroblast Proliferation 17

1.6 Influences on Cardiac Remodelling 18

1.6.1 Mechanical Signals 19

1.6.2 Neurohormonal Signals 22

1.7 Renin-Angiotensin System 22

1.7.1 Angiotensin Type 1 Receptor Signalling 25

1.7.2 Angiotensin Type 2 Receptor Signalling 28

1.7.3 RAS Inhibition to Prevent Cardiac Remodelling....31
1.7.3.1 ACE Inhibitors....31
1.7.3.2 AT1R blockers....31
1.7.3.3 Renin inhibitors....32
1.8 Heart diseases in which the RAS is implicated in adverse cardiac remodelling....32
1.8.1 Cardiac Hypertrophy....32
1.8.2 Atrial Fibrillation....35
1.8.3 Heart Failure....37
1.9 Mediators of RAS Communication in Fibrogenic and Hypertrophic Responses....38
1.9.1 Transforming growth factor-β....38
1.9.2 Connective tissue growth factor....41
1.9.3 Platelet-derived growth factors....43
1.9.4 Fibroblast growth factors....44
1.10 Intracellular RAS: Implications in Cardiovascular Remodelling....46
1.11 Thesis Rationale....48
CHAPTER 2 – Subcellular distribution of Ang-II receptors in ventricular cardiomyocytes and their role in mediating transcriptional responses.....49
Linking Statement and Author Contribution....50
Abstract....52
Introduction....54
Materials and Methods....56
Results....66
Discussion....75
Conclusions....81
References....82
Figure Legends....87
Supplemental Materials....101

CHAPTER 3 – Synthesis and characterisation of novel photoreleasable angiotensin II analogs to probe intracellular actions with spatial and temporal precision 120
Linking Statement and Author Contribution 121
Abstract 123
Introduction 125
Materials and Methods 128
Results 138
Discussion 147
References 153
Figure Legends 160
CHAPTER 4 – Nuclear Compartmentalization of Angiotensin-II Receptor Signaling in Cardiac Fibroblasts Governs de Novo RNA Expression, Proliferation and Collagen Synthesis. 175
Linking Statement and Author Contribution 176
Abstract 178
Introduction 180
Materials and Methods 181
Results 189
Discussion 196
Conclusions 200
References 201
Legends 206
CHAPTER 5 –General Discussion 219
5.1 Summary and Novel Contributions 220
5.2 Current Insights and Directions for Future Research 223

5.2.1 Concepts of Intracellular RAS 223
5.2.2 Significance of the Cardiac Intracellular RAS 225
5.2.2.1 Intracellular ANG II Receptors and Actions 227
5.2.2.2 Novel Routes for Intracellular Ang-II Biosynthesis 229
5.2.2.3 Significance of Parallel Mechanisms 230
5.3 Conclusions 232
References 233

Liste of Figures and Tables

Chapter 1

Figure 1. Anatomy Of The Heart, Structural Constituents Of Cardiac Muscle Fiber And Traces Of Cardiac Conduction System's Electrical Events. 7

Figure 2. Structural Constituents Of Cardiac Muscle Fiber And Traces Of Cardiac Conduction System's Electrical Events. 9

Figure 3. Diagram Representing The Pathophysiological Mechanisms Of The Early And Late Remodelling 14

Figure 4. The Progression Of Myocardial Remodelling 21

Figure 5. Renin-Angiotensin System 23

Figure 6. Signal Transduction Pathways Activated By AT1R / AT2R 26

Figure 7. AT1R Mediated Desensitization, Internalisation, Recycling And Degradation.....30

Figure 8. Schematic Illustrating The Networking Between Ang-II And TGF-β In Cardiac Remodelling 40

Table 1. Differences Between HFpEF and HFrEF at the Cardomyocyte, Intracellular and Interstitial Level.....12

Chapter 2

Figure 1. Immunoreactivity of angiotensin II receptor subtypes 1 and 2 in purified cardiomyocyte nuclei.....92

Figure 2. Subcellular distribution of AT1 and AT2 receptors in adult rat ventricular cardiomyocytes 93

Figure 3. Endocytosis and intracellular trafficking of Ang-II 94

Figure 4. Subcellular localization of intracellularly applied FITC-Ang-II 95

Figure 5. AT1R and AT2R in nuclear membranes regulate cardiomyocyte transcription initiation.....96

Figure 6. Regulation of cardiomyocyte nuclear NF-κB mRNA expression by nuclear ATRs 97

Figure 7. Coupling of ATRs to Ca^{2+} entry in cardiomyocyte nuclear enriched preparations 98

Figure 8. IP3-dependent Ca^{2+} signals from isolated cardiomyocyte nuclei.....99

Figure 9. Role of IP3R-signalling for AT1R-mediated transcription initiation 100

On-line Figures and Tables

On-line Table I. Primary Antibody Information.....103

On-line Table II. Primers Information.....104

Figure 1. Assessment of cardiomyocyte preparation and expression of renin-angiotensin components in cardiomyocytes 110

Figure 2. Immunoreactivity of angiotensin II receptor subtypes 1 and 2 in purified cardiac nuclei 111

Figure 3. Endocytosis and intracellular trafficking of Ang-II 113

Figure 4. AT1R and AT2R in nuclear membranes regulate transcription initiation .114

Figure 5. Regulation of nuclear NFκB mRNA expression by nuclear ATRs.....115

Figure 6. Vehicle control for calcium transients 116

Figure 7. Coupling of ATRs to Ca^{2+} entry in nuclear enriched preparations 117

Figure 8. IP3-dependent Ca^{2+} signals from isolated nuclei.....118

Figure 9. Role of IP3R-signalling for AT1R-mediated transcription initiation 119

Chapter 3

Table 1. Physicochemical and binding properties of Ang-II.....165

Figure 1. Structures of the caged Ang-II analogues and competitive displacement of [^{125}I]Ang-II by caged Ang-II analogues 166

Figure 2. Concentration-dependent responses of rat thoracic aortic rings to various analogues without uncaging 167

Figure 3. Photolysis kinetics of various analogues 168

Figure 4. Contractile responses of rat thoracic aortic rings following photolysis of various analogues 169

Figure 5. AT1R-dependent ERK-phosphorylation following photolysis of [Tyr(DMNB)^4]Ang-II 170

Figure 6. AT2R-dependent cGMP production following photolysis of [Tyr(DMNB)^4]Ang-II 171

Figure 7. Cellular uptake of fluorescein-[Ahx^0,Tyr(DMNB)^4]Ang-II.....172

Figure 8. Response of nucleoplasmic and cytosolic [Ca^{2+}] to photolysis of intracellular [Tyr(DMNB)^4]Ang-II 173

Figure 9. Photolysis of intracellular [Tyr(DMNB)^4]Ang-II regulates gene-transcription 174

Chapter 4

Figure 1. Endogenous AT1R and AT2R localize to the nucleus in canine atrial fibroblasts 211

Figure 2. AT1R and AT2R colocalize with TOPRO-3 nucleic acid stain in canine atrial fibroblasts 212

Figure 3. Ventricular tachypacing increases nuclear AT1R immunoreactivity and alters AT2R glycosylation in fibroblasts 213

Figure 4. Presence of G protein subunits in fibroblast nuclei. 214

Figure 5. Nuclear AT1R and AT2R regulate gene expression. 215

Figure 6. Photolysis of Intracellular cAng-II increases $[Ca^{2+}]_n$ 216

Figure 7. Intracellular Ang-II regulates fibroblast proliferation.....217

Figure 8. Intracellular Ang-II regulates collagen synthesis and secretion 218

List of Abbreviations

αSMA	α-Smooth muscle actin
AAV	Adeno-associated virus
AC	Adenylyl cyclase
ACE	Angiotensin converting enzyme
ACE-2	Angiotensin converting enzyme-2
ACEI	ACE inhibitor
AF	Atrial fibrillation
ANF	Atrial natriuretic factor
Ang-II	Angiotensin II
ARB	AT1R inhibitor
AT1R	Ang-II type 1 receptor
AT2R	Ang-II type 2 receptor
AV	Atrioventricular
β-MyHC	Beta-myosin heavy chain
bFGF	Basic fibroblast growth factor
BNP	Brain natriuretic peptide
Bpm	Beats per minute
Ca^{2+}	Calcium
Cav	Caveolins
cGMP	Cyclic guanosine 3’,5’-monophosphate
CRP	C-reactive protein
CT	Carboxyl-terminal

CTGF	Connective tissue growth factor
CVD	Cardiovascular disease
Cx	Connexins
DAG	1,2-diacylglycerol
DOCA	Desoxycorticosterone
ECG	Electrocardiogram
ECM	Extracellular matrix
ERK	Extracellular signal-regulated kinase
ET-1	Endothelin-1
FAK	Focal adhesion kinase
FGF	Fibroblast growth factor
FGFR-1	FGF receptor-1
GDP	Guanosine 5′-diphosphate
GEF	Guanine nucleotide exchange factors
GPCR	G protein-coupled receptor
G proteins	GTP-binding protein
Grb2	Growth factor receptor-bound protein 2
GRK	G protein-coupled receptor kinase
GTP	Guanosine-5'-triphosphate
H_2O_2	Hydrogen peroxide
HF	Heart failure
HFpEF	Heart failure with a preserved ejection fraction
HFrEF	Heart failure with a reduced ejection fraction

iAng-II	Intracellular Ang-II
ICa	Inward calcium current
IGF	Insulin-like growth factor
IL	Interleukin
IP3	1,4,5-inositol trisphosphate
iRAS	Intracellular RAS
JAK/STAT	Janus tyrosine kinase/signal transducers and activators of transcription
JNK	C-Jun N-terminal kinase
KLF5	Kruppel-like zinc-finger transcription factor
LTBP	Latent TGF-β binding protein
LVH	Left ventricular hypertrophy
MAPK	Mitogen-activated protein kinase
MI	Myocardial infarction
MKP-1	Mitogen-activated protein kinase phosphatase-1
MMP	Matrix metalloproteinase
MPTP	Mitochondrial permeability transition pore
MRI	Magnetic resonance imaging
mTOR	Mammalian target of rapamycin
NADPH	Nicotinamide adenine dinucleotide phosphate-oxidase
NCX	Na+/Ca^{2+} exchanger
NF-κB	Nuclear factor κB
NFAT	Nuclear factor of activated T cells
NO	Nitric oxide

NOS	Nitric oxides synthase
NRK	Normal rat kidney
NRVM	Neonatal rat ventricular myocytes
O_2^-	Superoxide anion
PVP	Prolylcarboxypeptidase
PDGF	Platelet-derived growth factor
PEP	Prolylendopeptidase
PI3K	Phosphatidylinositol 3-kinase
PKB	Protein kinase B
PKC	Protein kinase C
PLC	Phospholipase C
PP2A	Protein phosphatase 2A
PPARγ	Peroxisome proliferator-activated receptor-gamma
PTPase	Protein tyrosine phosphatases
RAS	Renin-angiotensin systems
ROCK	Rho/Rho-kinase
ROS	Reactive oxygen species
SA	Sinoatrial
SERCA	Sarco/endoplasmic reticulum calcium ATPase
Shc	Src homology 2 domain containing
SHP-1	Src homology region 2 domain-containing phosphatase-1
SKA	Skeletal alpha actin
SMAD	Small mothers against decapentaplegic

SNS	Sympathetic nervous system
SOS	Son of sevenless
TGF-β	Transforming growth factor beta
TGF-βR1	TGF-β type I receptor
TGF-βR2	TGF-β type II receptor
TIMP	Tissue inhibitors of metalloproteinase
TNFα	Tumor necrosis factor alpha
TPA	Tissue plasminogen activator
TSP-1	Thrombospondin type 1
T-tubule	Transverse tubule
VSMC	Vascular smooth muscle cell
VWC	Von Willebrand factor type C

“The important thing is to never stop questioning” – Albert Einstein

Acknowledgements

First and foremost, I offer my deepest gratitude to two exceptional academics at the Montreal Heart Institute: Dr. Stanley Nattel and Dr. Bruce G Allen, for their supervision, guidance, inspirational and timely advice, constant encouragement and enthusiasm from the very early stages of this research, as well as for giving me extraordinary experiences throughout my training. I have learned a great deal from their unique perspectives on research, their sharp insight on almost any issue, and their personal integrity and expectations of excellence.

I would like to thank several knowledgeable and friendly people who invested immeasurable personal and professional resources into my training. From Allen lab: Dr. George Vaniotis, Dr. Clémence Merlen and Dr. Dharmendra Dingar. From Nattel lab: Dr. Mona Aflaky, Dr. Ling Xiao, Dr. Kristin Dawson, Dr. Xiaoyan Qi, Dr. Sirirat Surinkaew, Dr. Begona Benito, Yolanda Chen, Eric Duong, Dr. Martin Aguilar, Dr. Brett Burstein, Dr. Reza Wakili, Dr. Balazs Ordog, Dr. Attila Farkas, Dr. Xiaobin Luo, Dr. Masahide Harada, Dr. Yuki Iwasaki, Dr. Chia-Tung Wu, Dr. Hai Huang, Dr. Marc Lemoine, Dr. Sebastian Clauss, Dr. Samy Makary, Dr. Takashi Kato, Dr. Kunihiro Nishida, Dr. Feng Xiong, Dr. Ali Kazemi, Dr. Eduard Guasch, Dr. Ange Maguy, Dr. Patrice Naud, Dr. Claire Louault, Patrick Vigneault and Yiguo Sun.

I would like also to acknowledge my collaborators. From McGill University: Dr. Terence E. Hébert and Dr. Danny Del Duca, for their help, support and for many productive scientific discussions. From INRS-IAF: Dr. Alain Fournier, Dr. David Chatenet and Myriam Létourneau for helping me to synthesize and characterise

photo-releasable angiotensin-II analogs. I also appreciated the amazing and unrestricted assistance I received from: Nathalie l'Heureux, Chantal St-Cyr, Louis Villeneuve, Aida Mamarbachi, Jennifer Bacchi, France Thériault and France Fauteux.

Special thanks to Dr. Martin G. Sirois, Dr. Nicolas Bousette, Dr. Timothey O'Connell and Dr. Denis deBlois for accepting to evaluate my thesis.

I would like also to acknowledge funding agencies that provided financial support throughout my training: Canadian Institutes of Health Research (CIHR), Le Fonds de recherche du Québec - Santé (FRQS), Heart and Stroke Foundation Canada (HSFC), Réseau en santé cardiovasculaire (RSCV), Fondation de l'Institut de Cardiologie de Montréal and Université de Montréal.

Last but not least, I would like to thank my parents, Samuel and Suzanna, for their unflagging love and unconditional support throughout my life and my studies. Special thanks to my sister, Nara, for all her advice and absolute confidence in me, she has been my best friend all my life and I love her dearly. I also want to extend my sincerer gratitude to my brother in law, Daniel, for all the entertaining discussions and encouragements, and to my nephews, Edward and Alexander, who have bought great joy to my life and their presence have been a continuous source of motivation and inspiration throughout the writing of my thesis.

CHAPTER 1 – Introduction

1.1 Overview

Cardiovascular diseases (CVDs) remain the major cause of morbidity and mortality in the industrialized world. Epidemiologists predict that by 2030 - in a mere fifteen years - CVDs will be responsible for 30% of all deaths and will remain the single leading cause of mortality [1]. G-protein coupled receptors (GPCRs) are a conserved family of heptahelical receptors and are one of the largest and most diverse classes of receptors in the human genome to be targeted by therapeutics in clinical use [2]. Among 200 GPCRs expressed in various cardiac cell types, pharmacological drugs targeting only adrenergic and angiotensin GPCR signaling mechanisms account for the majority of clinical prescriptions in regulation of the cardiovascular system [3]. However, heart failure progression with high morbidity and mortality rates continues. Studies of the newly recognized GPCRs, in particular intracellular GPCRs and investigations that define their molecular signaling mechanisms, expression patterns, cross-talk with other sub-systems, and regulation in cardiac diseases may provide a mechanistic basis and new attractive targets for improving heart failure treatment.

1.2 Cardiovascular System

The cardiovascular system is powered by the body's hardest working vital organ for sustaining life – the heart. The heart is a muscular pump and is divided into four pumping chambers: the right and left atria and the right and left ventricles (Figure 1). The right side of the heart is where the deoxygenated or ‘‘bad’’ blood enters from

our body. The left side of the heart sends the oxygenated ‘‘good’’ blood to the rest of our body through the aortic valve to serve physiological needs. At rest, the average human heart efficiently pumps approximately 5 liters of blood throughout the body every minute and helps to deliver oxygen to cells and maintain homeostasis of nutrients, metabolic wastes and gases [4]. Angiotensin II (Ang-II) via Ang-II type 1 (AT1R) and Ang-II type 2 (AT2R) receptors, endothelin-1 via ETA and ETB receptors, acetylcholine via muscarinic receptors, adenosine via A1 and A2 receptors and catecholamines via α-/β-adrenergic receptors are among the most widely studied extracellular ligands that control cardiac pump performance by recognizing and binding to specific GPCRs. These signals can regulate heart rate and contractile strength to preserve continuous perfusion of all vascular system with oxygenated and nutrient-rich blood. Whereas acute activation of GPCR signaling system is beneficial, prolonged activation can also promote remodeling of the heart by increasing cardiac cell dimensions, tissue fibrous composition, chamber size, heart size and altered expression of proteins that control cardiac excitability and contractility [5]. The main cellular constituents of the heart are cardiac myocytes, cardiac fibroblasts, vascular smooth muscle cells and endothelial cells. The heart’s five central components are: the muscle, the arteries, the valves, the electrical system and the pericardium.

1.2.1 The Cardiac Muscle

The main pumping part of the heart responsible for contraction of cardiac tissue and distribution of blood is the cardiac muscle, or the myocardium. The heart muscle contains cardiac contractile cells and sarcomeres, highly resistant to fatigue,

which allows the heart to beat our entire lifetime. The cardiac contractile cells, or cardiomyocytes, are surrounded by a sarcolemma, which invaginates, perpendicular to the length of the cell to form transverse tubules (T-tubule) (Figure 2A). T-tubules are rich in calcium (Ca^{2+}) channels, carriers, pumps and control the contraction of the muscle [6]. Ca^{2+} signals in cardiomyocytes are modulated by the actions of Ang-II and overexpression of AT1R alters excitation-contraction coupling [7]. Cardiomyocyte contraction is initiated by a transient increase in intracellular Ca^{2+} as the action potential from the sinoatrial node sweeps over the heart. The cellular depolarization subsequently activates voltage-operated Ca^{2+} channels, which triggers the release of Ca^{2+} fom the sarcoplasmic reticulum into the cytoplasm. Ryanodine-sensitive Ca^{2+} release channels activated by the voltage-dependant Ca^{2+} influx, a process termed as Ca^{2+}-induced Ca^{2+}-release. Relaxation occurs as Ca^{2+} returns back to resting levels through the actions of both sarcoendoplasmic reticulum Ca^{2+} ATPase (SERCA) and sarcolemma Na+/Ca^{2+} exchanger (NCX) [8]. The sarcomeres are composed of fibrous protein filaments, myosin and actin, and originate muscle contraction after sliding [9]. The heart's contraction efficacy, clinically termed as the ejection fraction, is a measurement of the percentage of blood pumped out of a filled ventricle with every heartbeat. A healthy human heart's ejection fraction is in the range of 55% to 70% and may decrease by thickening, stiffening or weakening of the heart muscle [10].

1.2.2 The Cardiac Arteries

Coronary arteries are the blood vessels that encircle the heart like a crown and are vital to heart function as they carry virtually all of the blood that supplies the heart.

The major coronary arteries are the right coronary artery, the left coronary artery, the circumflex coronary artery and the left anterior descending artery. The endothelium, skin-like tissue that lines the aforementioned arteries, maintains vascular tone through the release of nitric oxide (NO), prostacyclin, bradykinin, endothelium-derived hyperpolarizing factor, endothelin and Ang-II. Ang-II activates endothelial nicotinamide adenine dinucleotide phosphate (NADPH) oxidase and upregulates nuclear factor κB (NF-κB) [11]. In arteries, NF-κB promotes CVD through the activation of genes involved in inflammation, oxidation and adhesion. NADPH oxidase plays a fundamental role in the generation of reactive oxygen species (ROS) and catalyzes the production of superoxide anion (O_2^-) which in turn is broken down to hydrogen peroxide (H_2O_2) by superoxide dismutases [12]. The balance between ROS and NO governs the state of health of the endothelium. The endothelium also regulates vascular smooth muscle cell (VSMC) proliferation, thrombogenesis and fibrinolysis [13-15].

1.2.3 The Cardiac Valves

The cardiac valves, composed of papillary muscle, chordae tendineae and mitral valve annulus, regulate the blood flow through the four pumping chambers. The four heart valves include: right atrioventricular (triscupid) valve, left atrioventricular (mitral) valve, pulmonary valve and aortic valve. An abnormal valve opening when the valve should remain closed, medically termed regurgitation, permits blood to leak abnormally (e.g. the left atrium for mitral regurgitation) and causes a heart murmur. Rupture of a papillary muscle, which sometimes occurs after myocardial infarction

(MI), causes severe mitral regurgitation and is often a surgical emergency that requires rapid intervention for optimal outcomes [16]. Narrowing of a valve orifice, known as stenosis, inhibits the ability of the heart to pump efficiently. Ang-II contributes to the pathogenesis of aortic valve disease by inducing monocyte chemoattractant protein-1 gene expression as well as collagen synthesis through the activation of transforming growth factor-beta (TGF-β) [17]. Aortic stenosis is typically triggered by rheumatic heart fever or aging-related calcification and affects up to 5% of the elderly population [18,19].

1.2.4 The Cardiac Electrical System

The electrical impulses generated and conducted through specialized myocardial cells initiate and control the heartbeat in a coordinated fashion. Resting average normal heart rate is in the range of 100 to 160 beats per minute (bpm) for an infant and 60 to 100 bpm for adults [20,21]. A fast sustained adult heart rate (>100 bpm) is referred to as tachycardia and a slow adult heart rate (<60 bpm) is termed bradycardia. The electrical signals that set the contractions in motion begin in the sinoatrial (SA) node. The impulse rapidly propagates through the atrium to the atrioventricular (AV) node and after encountering a delay in the AV node, the impulse rapidly spreads through the bundle of His, then the bundle branches, the Purkinje

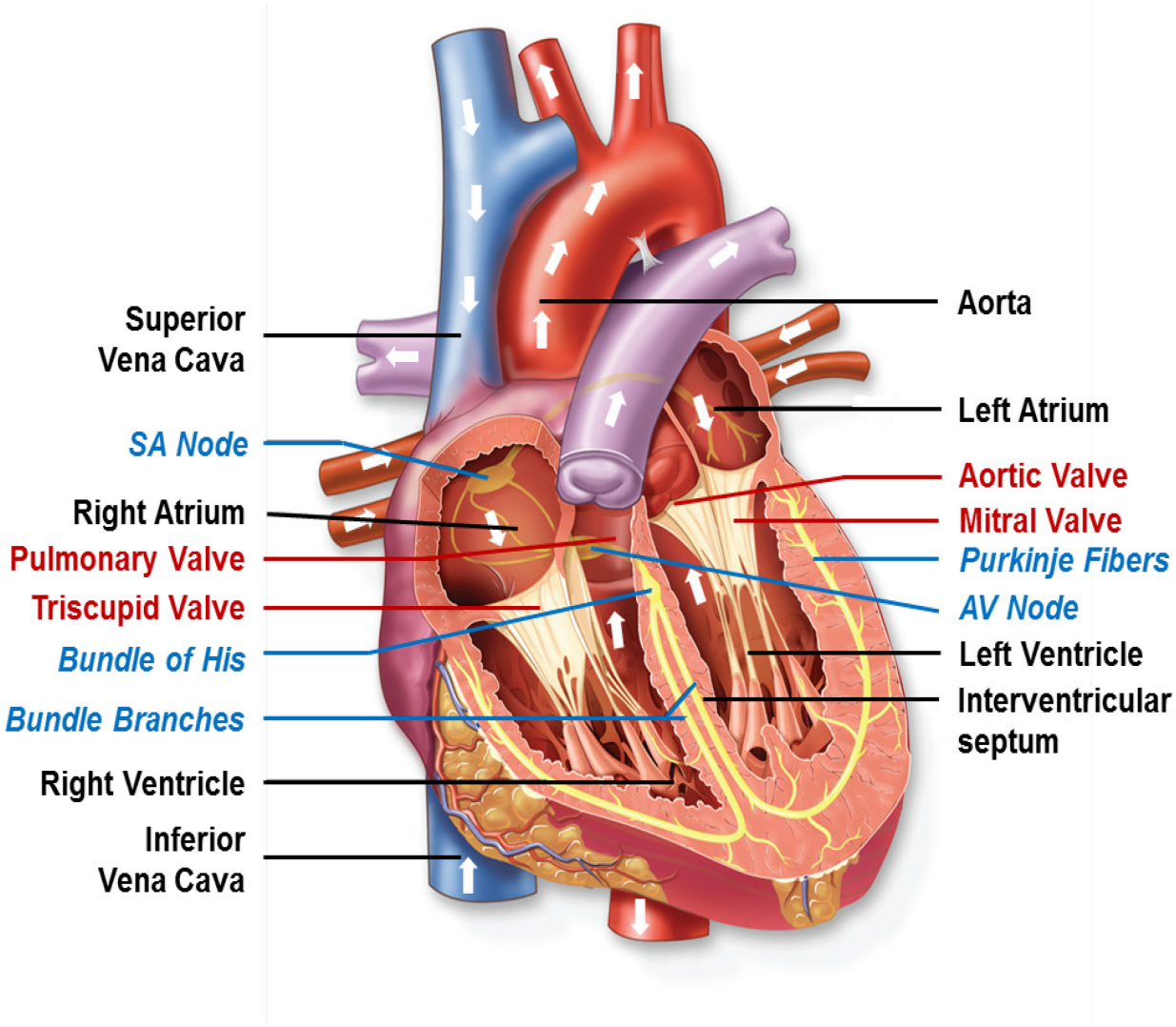

FIGURE 1. ANATOMY OF THE HEART, STRUCTURAL CONSTITUENTS OF CARDIAC MUSCLE FIBER AND TRACES OF CARDIAC CONDUCTION SYSTEM'S ELECTRICAL EVENTS.

Schematic of the heart. The heart is composed of four chambers: right and left atria and right and left ventricles. Blood passes through valves before leaving each cardiac chamber. The four heart valves (red lines) include: aortic, mitral, pulmonary and tricuspid. The rhythmic heart beat is maintained by the cardiac conducting system which fires sequentially from atria to ventricle (blue lines) composed of SA node, AV node, bundle of His, bundle branches, and Purkinje network. The blood flow in the heart is represented by white arrows.

network, and finally the ventricular myocardium. The electrocardiogram (ECG), used to diagnose heart conditions, records cardiac electrical activity (Figure 2B). In an ECG a P wave is caused by atrial depolarization (atrial contraction), QRS wave complex is generated by ventricular depolarization (ventricular contraction) and the T wave is generated by ventricular repolarization (ventricular relaxation). Abnormalities in the cardiac electrical system are called arrhythmias (e.g. atrial fibrillation, ventricular fibrillation) and their occurrence and underlying electrophysiological properties, among other factors, are influenced by gender-related dynamics [22-24]. Cardiac electrical activity is associated with the generation of action potentials in single cardiac cells and reflects the coordinated activation and inactivation of ion channels that regulate depolarization (inward Na^+, Ca^{2+}) and repolarization (outward K^+) membrane currents [25]. Ang-II modulates the electrical properties of the myocardium by downregulating L-type Ca^{2+} current and transient outward current (Ito) and by regulating the membrane expression of the pore-forming α-subunit underlying Ito, Kv 4.3 [26]. Ang-II also induces arrhythmic events by modulating gap junctions formed by connexins, key channels for impulse propagation between neighboring cardiomyocytes [27]. Furthermore, Ang-II initiate delayed after-depolarization in pulmonary vein cardiomyocytes [28].

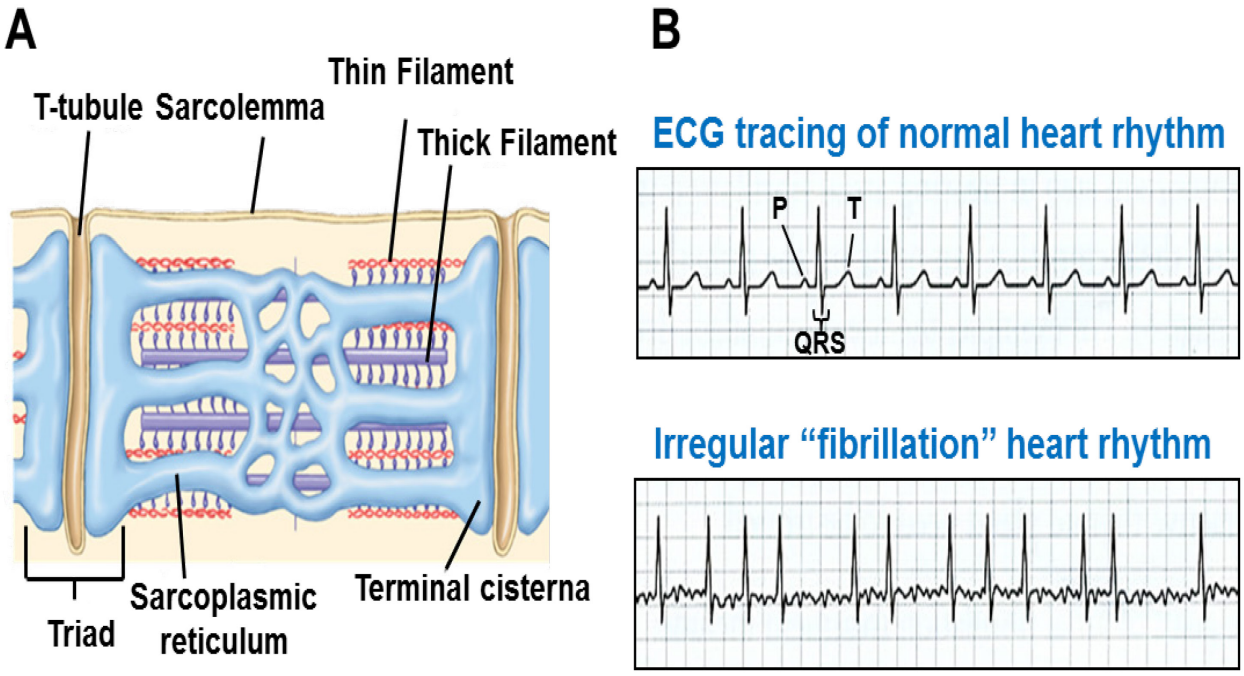

FIGURE 2. STRUCTURAL CONSTITUENTS OF CARDIAC MUSCLE FIBER AND TRACES OF CARDIAC CONDUCTION SYSTEM'S ELECTRICAL EVENTS.

A- Characteristics of cardiac muscle fiber. The sarcolemma is the membrane bilayer that surrounds each muscle cell/fiber. T-tubules, perpendicular to the length of the cell, are invaginations of the sarcolemma and are rich in ion channels and proteins critical for synchronous activation of the cardiac muscle. T-tubules are surrounded with two terminal cisternae (triads in skeletal muscle, dyads in cardiac muscle) that serve as Ca^{2+} stores. The sarcoplasmic reticulum contains high levels of the ATP-dependent Ca^{2+} pump (SERCA) and controls cardiac muscle contractility. The contractile units (sarcomeres) of the cardiac cell are composed of thin and thick filaments.

B- Upper panel: ECG recordings of normal heart rhythm. P wave (atrial depolarization) precedes each QRS complex (ventricular depolarization) and follows T wave (ventricular repolarization). The P-waves are much smaller in size and shape compared to the QRS complex. Lower panel: ECG recordings from irregular "fibrillating" heart rhythm. The baseline appears noisy, no distinct P waves are seen and the QRS complexes appear at erratically irregular intervals.

1.2.5 The Pericardium

The fibroelastic sac that encloses the heart, also known as the pericardium, consists of mesothelial cells and a dense fibrous layer primarily composed of collagen with interspersed elastic fibrils. The pericardium separates the heart from the rest of the thoracic cavity, preventing the heart from overfilling with blood, and protects it from nearby infection. Pericardial inflammation, manifested by elevated erythrocyte sedimentation rate, leukocytosis and abnormal C-reactive protein (CRP) levels, produces severe retrosternal chest pain and triggers vagally-mediated reflexes [29,30]. The pericardium secrets prostaglandins, in the pericardial fluid, hence the pericardium modulates cardiac electrophysiological properties and coronary tone [31].

1.3 Cardiac Remodelling

Heart failure is the common end product of CVD and the leading cause of mortality worldwide, despite recent progresses in treatment [32]. The fundamental pathophysiological process leading to heart failure is cardiac remodelling. Adverse cardiac remodelling is strongly associated with increases in cardiovascular morbidity and mortality [33]. Cardiac functional and structural changes, including ventricular enlargement and/or progressive ventricular dilatation are manifestations of the clinical progression of heart failure and cardiac dysfunction [34]. There is great interest in understanding the basic mechanisms of cardiac remodelling, to allow better understanding of the pathophysiological progression, which may generate novel clinical therapies to attenuate and/or reverse the remodelling.

Heart failure (HF) patients can now be classified into subcategories according to their ejection fraction: heart failure associated with reduced ejection fraction (HFrEF) and heart failure with a preserved ejection fraction (HFpEF). The occurrence of these subcategories varies with age, HFrEF being more common in younger patients and more repetitively connected with a history of myocardial infarction, whereas patients hospitalized with HFpEF tend to be much older than those with HFrEF and are more frequently female [35]. HFrEF is more regularly associated with the result of loss of myocardial tissue due to a myocardial damage and therefore results into weakening of the pumping ability of the heart. Excessive neurohumoral activation, mitral valve insufficiency, ventricular remodelling, and comorbidities contribute to the severity of HFrEF. In contrast, HFpEF is an important heart failure syndrome with classical haemodynamic and neurohumoral changes of heart failure. Because of the important comorbidities (e.g. hypertension, diabetes, atrial fibrillation, aging) associated with HFpEF, advances in pharmacologic therapy had little positive effect in patients with HFpEF [36]. There are fundamental structural differences between HFrEF and HFpEF. Left ventricular dilation is a key characteristic of HFrEF while wall thickness relative to chamber dimension is increased in HFpEF, with normal ventricular chamber size [37,38]. There are also important differences at the cardiomyocyte, intracellular and interstitial level (Table 1) [37,39-41].

Table 1. Differences between HFpEF and HFrEF at the Cardomyocyte, Intracellular and Interstitial Level

	HFpEF	HFrEF
Cardiomyocyte diameter	↑	↓
Myofibrillar density	↑	↓
Cardiomyocyte resting tension	↑↑	↑
Cardiomyocyte calcium sensitivity	↑↑	↑
Abnormal phosphorylation of sarcomeric proteins	↑↑	↑
Myocardial protein kinase G activity	↓	↑
Myocardial oxidative stress	↑	↔
Myocardial cyclic guanosine monophosphate concentration	↓	↑
Myocardial pro-B-type natriuretic peptide-108 expression	↔/↑	↑↑
Mysial collagen volume fraction	↑	↓
Perivascular collagen volume fraction	↑	↑↑
Scar-related collagen volume fraction	↑	↑↑
Myocardial advanced glycation end products in diabetic HF	↑	↑↑

↑, increased; ↑↑, highly increased ↓, decreased; ↔, no change

1.4 Concepts of Cardiac Remodelling

Cardiac remodelling is a maladaptive process by which the function, shape, and size of the heart are influenced by genetic factors, haemodynamic load, neurohormonal activation, inflammation, apoptosis, necrosis and fibrosis [42]. The cardiac structural and functional equilibrium can be challenged by internal and external factors causing altered transcriptional (RNA), posttranscriptional (microRNA), translational (protein), cellular, electrophysiological and interstitial changes of the heart. Compensatory mechanisms are triggered to reduce the adverse effects of remodelling and if possible, restore the equilibrium. Cardiac remodelling may be "physiological" and adaptive during normal growth, in healthy individuals after endurance training, and throughout pregnancy or may be "pathological" due to MI, pressure overload (aortic valve stenosis, long-standing hypertension), volume overload (valvular regurgitation), myocarditis, and/or cardiomyopathy [33]. Although the origins of remodelling are varied, they share similar molecular, biochemical and cellular behaviours that jointly change the structure and function of the myocardium.

Cardiac remodelling following an acute MI results from myocyte necrosis and a rapid increase in loading conditions. In MI, neutrophils, monocytes and macrophages migrate to the infarct zone to initiate the reparation of the necrotic area [43]. The healing of necrotic tissue after MI triggers a cascade of cellular events that initiates reparative structural alterations, including dilatation, hypertrophy, and the formation of a collagen scar (Figure 3). The degree of cardiomyocyte loss, stimulation of the sympathetic nervous system, activation of the neurohormonal systems and release of natriuretic peptides govern the degree of remodelling. Postinfarction remodelling has

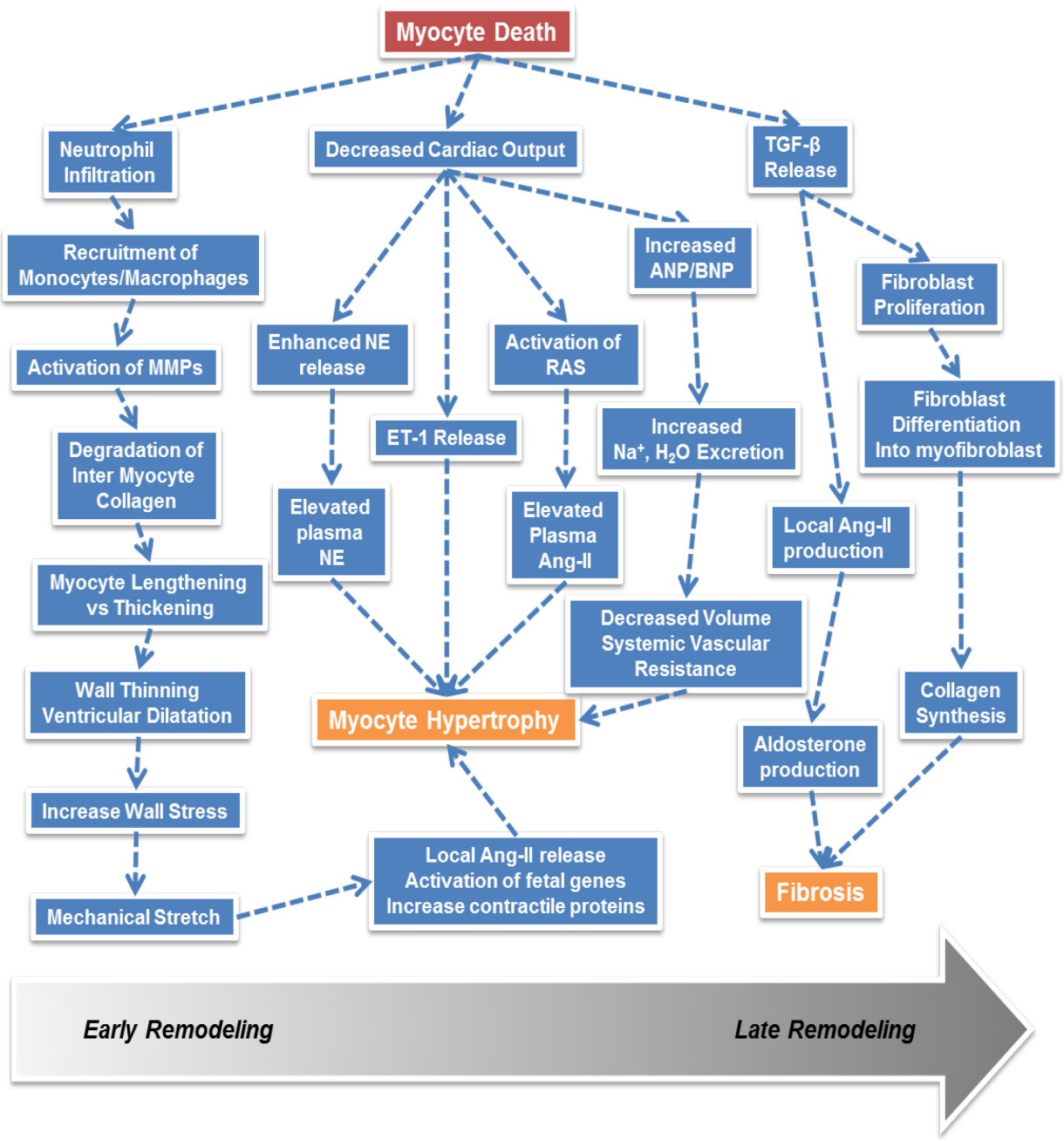

FIGURE 3. DIAGRAM REPRESENTING THE PATHOPHYSIOLOGICAL MECHANISMS OF THE EARLY AND LATE REMODELLING

The early phase of postinfarction remodelling result in expansion of the infarct zone, whereas late remodelling is associated with time dependent dilatation, hypertrophy and fibrosis.

been divided into the early phase (<72 hours after coronary occlusion) which involves expansion and stretching of the infarct zone and late phases (>72 hours) which involves stretching of the left ventricle globally, dilatation with subsequent distortion of ventricular shape, hypertrophy and deterioration of systolic function [44-46]. Most of above-mentioned cardiac remodelling stimuli initially lead to compensatory cardiac hypertrophy in order to maintain cardiac pump function and reduce ventricular wall tension, but in the long run, cardiac hypertrophy itself predisposes patients to progressive heart failure, life-threatening arrhythmia and sudden cardiac death. The cardiac myocytes and cardiac fibroblasts, vital cells for the maintenance of electrical, biochemical, and biomechanical responsive nature of the heart, are strongly involved in the remodelling process (Figure 4).

1.5 Components of Cardiac Remodelling

1.5.1 The Role of Cardiac Myocyte Growth

Cardiomyocytes are profoundly involved in cardiac remodelling processes. In contrast to other cell types in the heart, cardiomyocytes lose the ability to differentiate soon after birth [47]. Therefore, in response to an increase in biomechanical stress or to high levels of neurohormonal stimulation, cardiomyocytes become elongated or hypertrophied as part of a primary compensatory process to preserve stroke volume. Stretching of cardiomyocytes by pressure and/or volume overloading ultimately leads to the increased synthesis of the products of early-response genes: c-myc, c-fos, c-jun and the fetal genes: beta-myosin heavy chain (β-MyHC), atrial natriuretic factor

(ANF) and skeletal alpha-actin (SKA), which are employed as biomarkers of cardiac hypertrophy [48,49]. These changes in gene expression result in the assembly of additional sarcomeres. The arrangements in which these sarcomeres are laid down (parallel vs. longitudinal) define whether cardiomyocytes elongate or increase in thickness.

1.5.2 The Role of Cardiomyocyte Apoptosis, Necrosis, and Autophagy

Programmed cellular death or apoptosis, of cardiomyocytes in the adult mammalian heart is activated by cardiac injury (MI, ischemia, reperfusion) and contributes to adverse cardiac remodelling. At the cellular level, apoptosis can be induced by biomechanical stretch, ROS, insufficiencies of nutrients/oxygen/survival factors, cell cycle perturbations and deoxyribonucleic acid (DNA) damage [50]. Intracellular cysteine-aspartic proteases or caspases that trigger the apoptotic response can also be activated by cell death receptor ligands such as tumor necrosis factor alpha (TNFα). The apoptotic rate in the myocardium is correlated with ventricular dilation, wall thinning and symptomatic evidence of heart failure [51,52].

Necrotic cardiomyocyte death plays a critical role in myocardial infarction and heart failure. In contrast to apoptotic cell death, necrosis is characterized by cardiomyocyte and organelle swelling, cell membrane rupture and loss of ATP. Necrotic cell death originates at the level of the mitochondria following sustained Ca^{2+} stress, oxidative damage, hypoxia and mitochondrial permeability transition pore (MPTP) opening [52,53]. Activation of TNFα represents alternative necrosis pathway

in cardiomyocytes under heart failure and activation of neurohumoral factors such as norepinephrine and Ang-II induces TNFα biosynthesis through PKC-dependent pathway [54,55]

One of the crucial cellular mechanisms that mediate ischemia-induced adaptation and damage control is authophagy. In cardiomyocytes autophagy occurs via the mammalian target of rapamycin (mTOR)-dependent process in response to ROS, hypoxia, nutrient deprivation, injured organelles to maintain intracellular homeostasis and cell integrity [56]. Recent evidence suggests that autophagosome processing is impaired in response to prolonged cardiac stress and promote cardiomyocyte death, contractile dysfunction and heart failure through excessive digestion of vital organelles and proteins [57,58].

1.5.3 The Role of Fibroblast Proliferation

Fibroblasts make up the largest nonexcitable cellular populations of the heart. The role of cardiac fibroblasts in the pathogenesis of cardiac remodelling is well established. In response to various biological stressors, fibroblasts can migrate, proliferate and differentiate into myofibroblasts [59,60]. Myofibroblasts, which express several smooth muscle proteins, are the main sources of production of cytokines, growth factors (TNFα, TGF-β, platelet-derived growth factor (PDGF), interleukin (IL)-1β, IL-6) and extracellular matrix (ECM) proteins (collagens, glycoproteins, proteoglycans, proteases). Disturbances of the balance between collagen synthesis and the activity of enzymes that degrade collagen molecules (matrix

metalloproteinases (MMPs), and tissue inhibitors of metalloproteinases (TIMPs)) can induce fibrotic changes that contribute significantly to cardiac remodelling [61]. Furthermore, mechanical stress can elicit differentiation of fibroblasts into myofibroblasts both in vitro as seen in response to cyclic stretching or extended culture conditions and in vivo in pressure overload heart failure models [62]. The differentiation of fibroblast into myofibroblast is marked by increased α-smooth muscle actin (αSMA). The myofibroblasts contain a widespread rough endoplasmic reticulum and are remarkably different in terms of gene expression and phenotype [63]. There is growing evidence that Ang-II by inducing TGF-β secretion and PKC-NADPH oxidase-ROS pathway induces fibroblasts to differentiate into myofibroblasts and plays a critical role in the progression of pathological cardiac remodeling [64,65].

In addition, fibroblasts may be connected to cardiomyocytes through gap junctional channels, composed mainly of connexins (Cx40, Cx43, and Cx45), that are critical for maintaining cardiac intercellular electrical and metabolic communications [66]. Fibrosis can form a barrier between cardiomyocytes and/or fibroblasts (generating abnormal cardiac electrical activity) and produce changes in cardiac mechanical properties that in the long run can lead to profound cardiac dysfunction [67].

1.6 Influences on Cardiac Remodelling

Cardiovascular remodelling can be initiated in the myocardium by means of two functionally disparate triggers: mechanical and neurohormonal.

1.6.1 Mechanical Signals

The biomechanical stress generated by the physical stretching of adult cardiomyocytes is sufficient to trigger a phenotypic hypertrophic response (heart geometry changes from elliptical to spherical), even in the absence of neurohumoral signalling.

When the heart faces increased hemodynamic/pressure load in conditions such as hypertension or aortic stenosis, initial changes in the ventricular morphology, including increased mural thickness and ventricular mass due to the enlargement of cardiomyocytes, assumes a crucial role in the compensation for overload and maintains cardiac output. This early remodelling leads to concentric hypertrophy, in which the ratio of wall thickness/chamber dimension increases. On the other hand, when the heart faces increased hemodynamic/volume load in conditions such as aortic regurgitation or mitral regurgitation, salt and water retention increases ventricular volume. Volume overload leads to compensatory eccentric hypertrophy with cavity dilation and decrease in the ratio of wall thickness/chamber dimension [68].

According to LaPlace's law, cardiac wall stress can be altered by changes in the pressure, radius or thickness of the ventricle: (pressure × radius) / (2 × wall thickness). However, myocardial wall tension and stress increase as a result of progressive ventricular dilation and insufficient development of compensatory ventricular hypertrophy deviating clearly from LaPlace's feedback loop [69]. The mechanisms of stress-induced remodelling are not fully elucidated to date, even though there seems to be some overlap in the origin between mechanical and

neurohormonal remodelling. Nevertheless, mechanical stretch is sufficient to upregulate the expression of AT1R mRNA in cardiomyocytes and cause a rapid secretion of vasoactive Ang II [70]. Clarifying the underlying molecular mechanisms of mechanical stress induced remodelling may be a major factor in the early prognosis of heart failure.

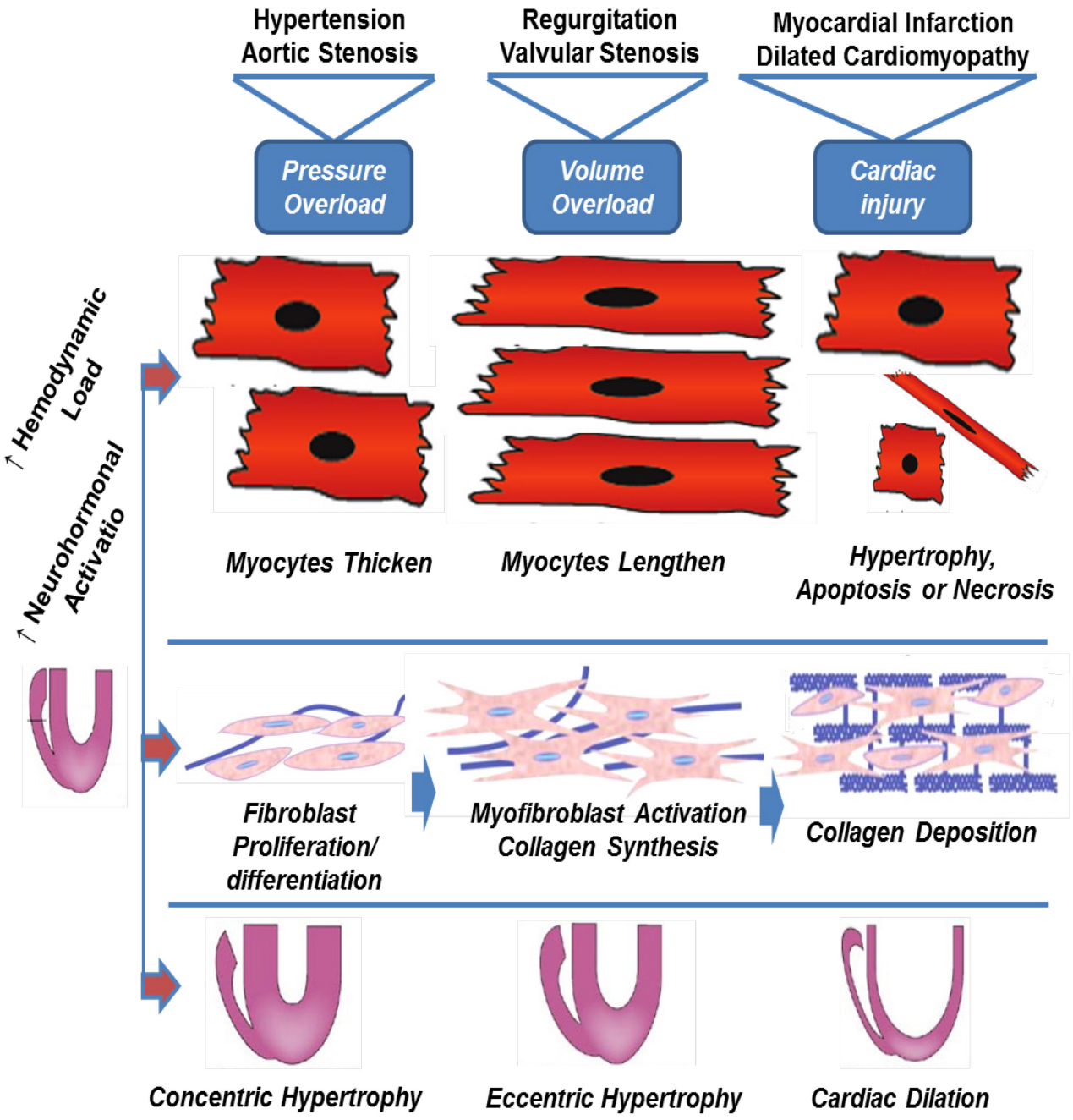

FIGURE 4. THE PROGRESSION OF MYOCARDIAL REMODELLING

Myocardial stress including a rise in hemodynamic load, neurohormonal activation and cardiac injury may induce a remodelling process, both at the cardiomyocyte and fibroblast level that over time may cause functional and structural deterioration of the heart leading to cardiac dysfunction and failure.

1.6.2 Neurohormonal Signals

Initially, hormonal signals intervene and mediate compensatory changes in response to abnormal cardiac output; however, similar to mechanical signals, they are deeply involved in disease continuum and in the remodelling process [71]. Ang-II is one of the most important hormonal stimuli that is related to pathological cardiac remodelling and progression of heart failure. Mediators of Ang-II signaling in fibrogenic and hypertrophic responses consist of growth factors including: TGF-β, fibroblast growth factor (FGF), insulin-like growth factor (IGF), PDGF and connective tissue growth factor (CTGF). This will be expanded upon in succeeding sections.

1.7 Renin-Angiotensin System

Circulatory and tissue renin-angiotensin systems (RAS) remain one of the most important cardiovascular pathophysiological regulatory systems. In the human body, RAS play a crucial role in conserving haemodynamic stability, electrolyte and water homeostasis. Overstimulation of RAS is an important contributor to the pathophysiology of cardiac hypertrophy, failure, and arrhythmias.

RAS activation starts when angiotensinogen, a serum α2-globulin produced in the liver, is excreted and converted into a decapeptide, angiotensin I, through hydrolysis by renin. Renin is a glycoproteolytic enzyme produced by the juxtaglomerular cells of the afferent arterioles of the kidney. The biologically inactive angiotensin I is cleaved by a dipeptidyl carboxypeptidase, angiotensin converting enzyme (ACE), to form the major bioactive product of the system, Ang-II [72]. ACE,

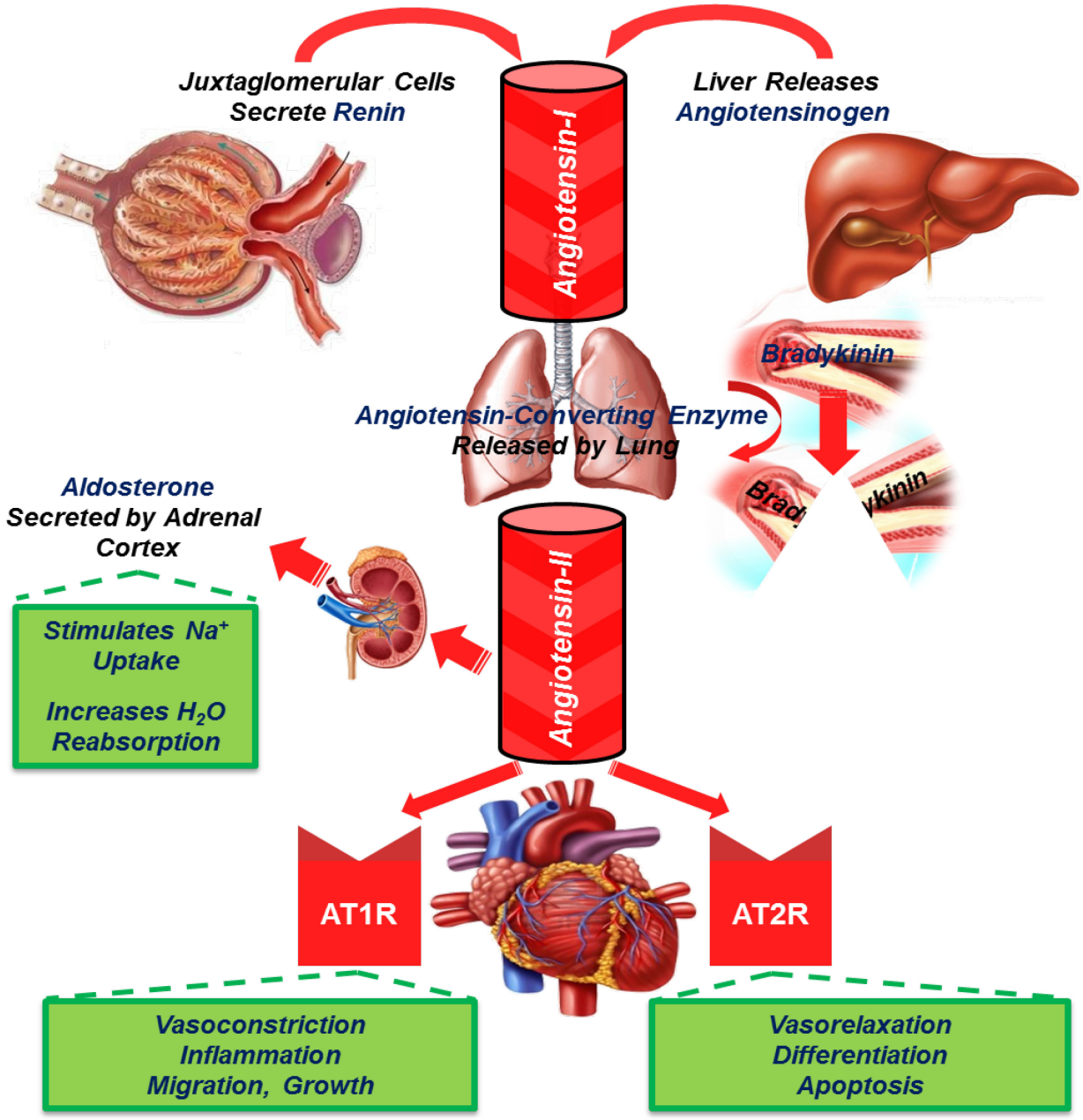

FIGURE 5. RENIN-ANGIOTENSIN SYSTEM

In the classical renin-angiotensin system, angiotensinogen released from the liver is cleaved by renin, secreted from the kidney, to form the inactive decapeptide angiotensin-I. Angiotensin-converting enzyme cleaves bradykinin into inactive fragments and also the two amino acids from angiotensin-I to produce the active hormone of the system, Ang-II. The effects of Ang-II on the cardiovascular system are principally mediated by receptors (AT1R, AT2R) or via the release of aldosterone.

apart from playing a fundamental role in the production of vasoactive octapeptide Ang-II, it degrades bradykinin, a potent endothelium-dependent vasodilator (Figure 5) [73]. Ang-II, the key effector of the RAS with a variety of cardiac physiological and pathophysiological actions, can also be produced directly from angiotensinogen via ACE-independent pathways, including ACE-2-dependent pathways, tonin, tissue plasminogen activator (tPA), kallikrein, cathepsin G and chymase [74-77].

A large body of evidence now indicates that the heptapeptide Ang-(1-7) plays an important biological role in the cardiac RAS. Ang-(1-7) is formed directly from Ang-II through hydrolysis by angiotensin-converting enzyme (ACE-2), as well as prolylcarboxypeptidase (PCP) and prolylendopeptidase (PEP). [78,79] In cardiomyocytes, Ang-(1-7) binds to the Mas receptor and activates the phosphatidylinositol 3-kinase (PI3-K)-protein kinase B (Akt)-signaling cascade, causing nitric oxide synthase (NOS) 3 activation and NO/cGMP generation [80]. Furthermore, Ang-(1-7) prevents Ang-II-induced pathological remodeling by preventing nuclear factor of activated T cells (NFAT) translocation to the nucleus and activation of hypertrophic genes [81]. Cardiomyocyte specific genetic ablation of the Mas receptor leads to reduced SERCA2 expression, Ca^{2+} transients and slower Ca^{2+} uptake [80].

Ang-II mediates its physiological effects by stimulating two distinct biological receptors, AT1R and AT2R and by inducing secretion of aldosterone from the adrenal gland. Both Ang-II receptors are formed by seven transmembrane-spanning α-helices and are members of the GPCR superfamily commonly recognized as integral plasma membrane proteins. In the human myocardium, both AT1R and AT2R are expressed

at the mRNA and protein levels and have similar affinities for Ang-II [82]. Radioligand binding studies on rat cardiomyocyte membrane-enriched preparations revealed that cardiomyocytes possess similar levels of AT1R and AT2R and that their expression is upregulated during the neonatal period and after myocardial infarction[83]. Similarly, RT-PCR experiments confirmed that both AT1R and AT2R are expressed in human cardiac fibroblasts with AT1R being the predominant isoform [84].

1.7.1 Angiotensin Type 1 Receptor Signalling

The AT1R mediates most of the known physiological actions of Ang-II in cardiovascular, neuronal, renal, endocrine, hepatic and other target cells. The physiological effects are initiated when the ligand binds to the extracellular side of the receptor, causing a change in receptor conformation. This leads to an interaction between the receptor and a heterotrimeric GTP-binding protein (G protein) consisting of alpha (α), beta (β) and gamma (γ) subunits. Agonist binding promotes the receptor to adopt an active conformational status that accelerates the hydrolysis of guanosine 5′-triphosphate (GTP) to guanosine 5'-diphosphate (GDP) by the Gα subunit and causes dissociation of the Gα from the Gβγ complex. Both Gα and Gβγ may interact with effectors or ion channels and regulate their activity.

AT1R signalling involves the activation of multiple Gα subunits including $G_{q/11}$, G_i, $G_{o,}$ G_{12}, G_{13} in various cellular contexts, followed by activation of effectors such as phospholipase C (PLC) and adenylyl cyclase (AC) (Figure 6) [85]. Once activated, PLC hydrolyses PIP2 to generate IP_3 plus 1,2-diacylglycerol. IP3, in turn, binds to IP_3 receptors, releasing calcium ions (Ca^{2+}) from intracellular stores. The resulting rise in

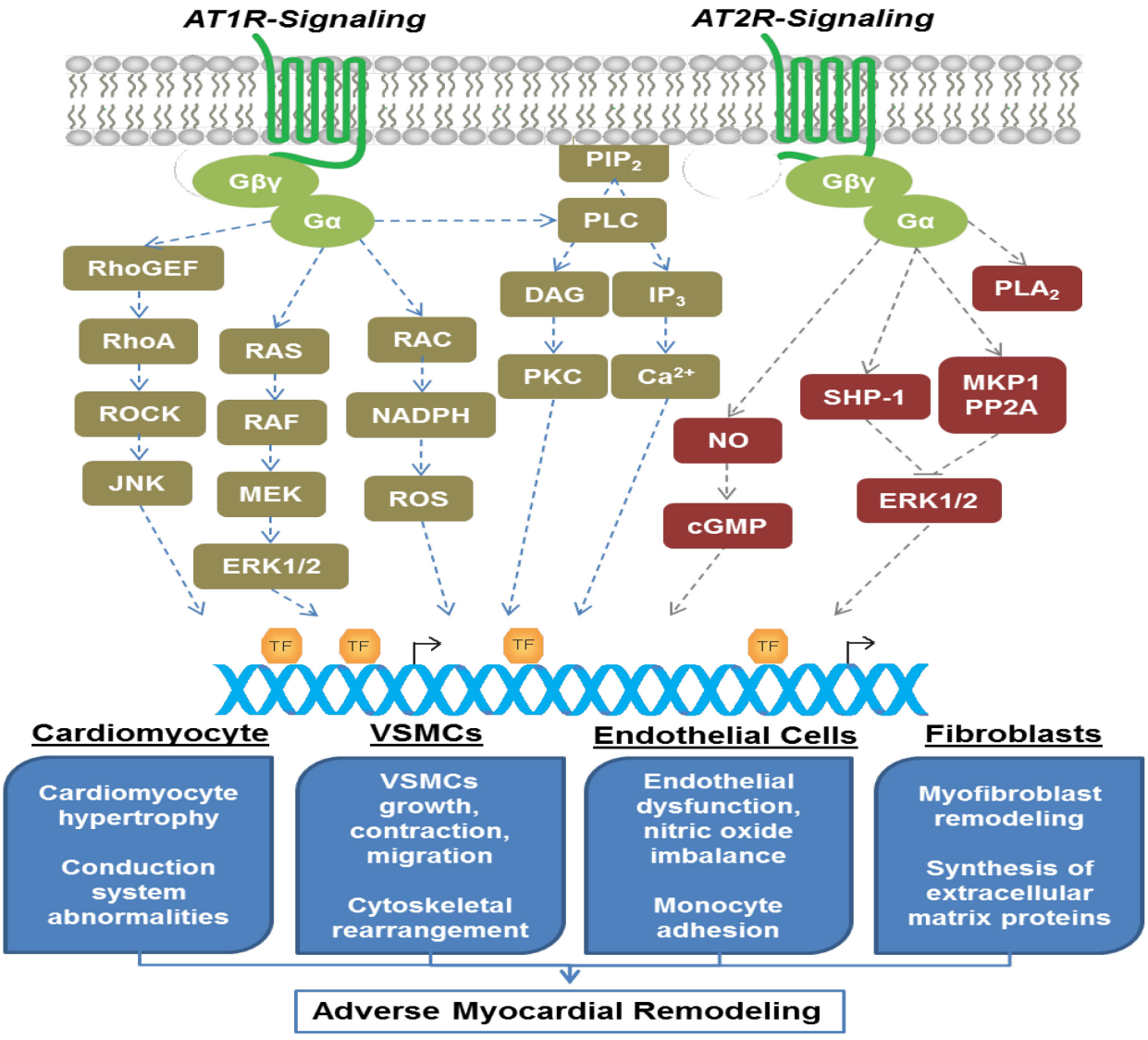

FIGURE 6. SIGNAL TRANSDUCTION PATHWAYS ACTIVATED BY AT1R / AT2R

AT1R signalling involves the hydrolysis of PIP2 by PLC to produce DAG and IP3. IP3 stimulates the release of calcium, whereas DAG activates PKC. AT1R leads to the activation of Rac-NADPH oxidase, a major source of cellular ROS. Activated AT1R can also transactivate RAS-RAF-MEK-ERK1/2 and RhoGEF-RhoA-ROCK-JNK signalling cascades. AT2R signalling is coupled to protein phosphatases (SHP-1, MKP-1, PP2A) that leads to inhibition of ERK1/2 pathway. AT2R also regulates the NO-cGMP system and stimulates PLA2. Signalling pathways activated by Ang-II have been correlated to specific negative responses in cardiomyocytes, VSMCs, endothelial cells and fibroblasts.

Ca^{2+} concentration can activate downstream Ca^{2+}-dependent enzymes and induce cell growth responses in cardiac myocytes, cardiac fibroblasts and VSMCs [86-88]. AT1R also activates receptor and non-receptor tyrosine and serine/threonine kinases such as extracellular-signal-regulated kinase (ERK1/2), c-Jun N-terminal kinase (JNK), protein kinase B (Akt/PKB), PI3K and protein kinase C (PKC) [89]. Ang-II can also activate small GTP-binding proteins including Ras, Rac, Rho, and Arf through AT1R in cardiomyocytes. Ang-II activates Ras by recruitment of guanine nucleotide exchange factors (GEFs) such as SOS (son of sevenless) through adaptor proteins Shc (Src homology 2 domain containing) and Grb2 (growth factor receptor-bound protein 2) and consequently activates ERK1/2-dependent pathways [90]. In cardiac cells, Rac mediates Ang-II stimulation of ROS production through NADPH-oxidase activation [91,92]. Rho plays an essential role in actin cytoskeleton remodelling and in the Ca^{2+} sensitization of VSMC contraction: Rho/Rho-kinase (ROCK) signalling is critical for vascular remodelling induced by Ang-II [90]. In cardiomyocyte AT1R activation via $G_{12/13}$ Rho/ROCK through RhoGEF mediate JNK and p38 MAPK activation and leads to increased cell contraction and hypertrophy [93].

β-arrestin and the GTPase activity of dynamin-dependent process play a central role in regulating AT1R desensitization (uncoupling of AT1R from G-protein signalling) through G protein-receptor kinase (GRK)-mediated phosphorylation at physiological Ang-II concentrations [94]. Moreover, increasing experimental evidence suggests that selective activation of AT1R signaling through β-arrestin, referred to as biased signaling, promotes cardioprotective biochemical signaling in cardiac cells [95]. Selective activation of AT1R by β-arrestin-biased AT1R ligand, TRV027,

increases cardiac contractility, promotes cardiac unloading, promotes cardiomyocyte survival, and blocks cardiac hypertrophy [96,97]. AT1R endocytosis (ligand bound cell surface AT1R internalization) in rat aortic smooth muscle and adrenal glomerulosa cells occurs via clathrin-coated vesicles [98,99]. Internalized receptors are either degraded in lysosomes or dephosphorylated and recycled (Figure 7). In cardiac muscle cells, lipid raft-associated caveolins (Cav1, 2, and 3) have been identified as trafficking chaperones and serve a central role in AT1R maturation and transport to the cell surface [100].

1.7.2 Angiotensin Type 2 Receptor Signalling

The AT2R shares almost 35% sequence homology with the AT1R and contains in its extracellular N-terminus five glycosylation sites [101]. AT2R is distinct from AT1R in tissue specific expression, intracellular signal transduction mechanisms and physiological actions. AT2R is the predominant subtype during fetal development, is particularly expressed in the heart, adrenals, and uterus and is upregulated in pathological conditions associated with tissue remodelling or inflammation. The expression of AT2R is modulated by IGF, TGF-β and basic fibroblast growth factor (bFGF) [101]. In contrast to AT1R, AT2R exerts anti-growth, anti-hypertrophic and pro-apoptotic effects. The growth-inhibitory actions of AT2R are mediated by the activation of a series of cytosolic protein serine-threonine and tyrosine phosphatases (PTPases) including Src homology region 2 domain-containing phosphatase-1 (SHP-1), the serine/threonine protein phosphatase 2A (PP2A) and the mitogen-activated protein kinase phosphatase-1 (MKP-1), resulting in inactivation of

ERK 1/2 [102,103]. In neonatal cardiac myocytes and fibroblasts, AT2R activation negatively regulates AT1R-dependent growth, suggesting that Ang-II simultaneously exerts divergent actions on myocardial biology [83,104]. Proapoptotic effects of AT2R have been observed in adult rat VSMCs, R3T3 mouse fibroblasts, human umbilical venous endothelial cells, PC12W cells and R3T3 mouse fibroblasts [105-108]. In vascular endothelial cells, AT2R-G_i activation triggers the production of cyclic guanosine 3',5'-monophosphate (cGMP) through a mechanism involving bradykinin receptors and NO. Unlike AT1R, AT2R does not undergo rapid desensitization and internalization. AT2R is phosphorylated by PKC, but not GRK. Thus AT2R does not interact with β-arrestins, which may explain its lack of agonist-induced internalization [109].

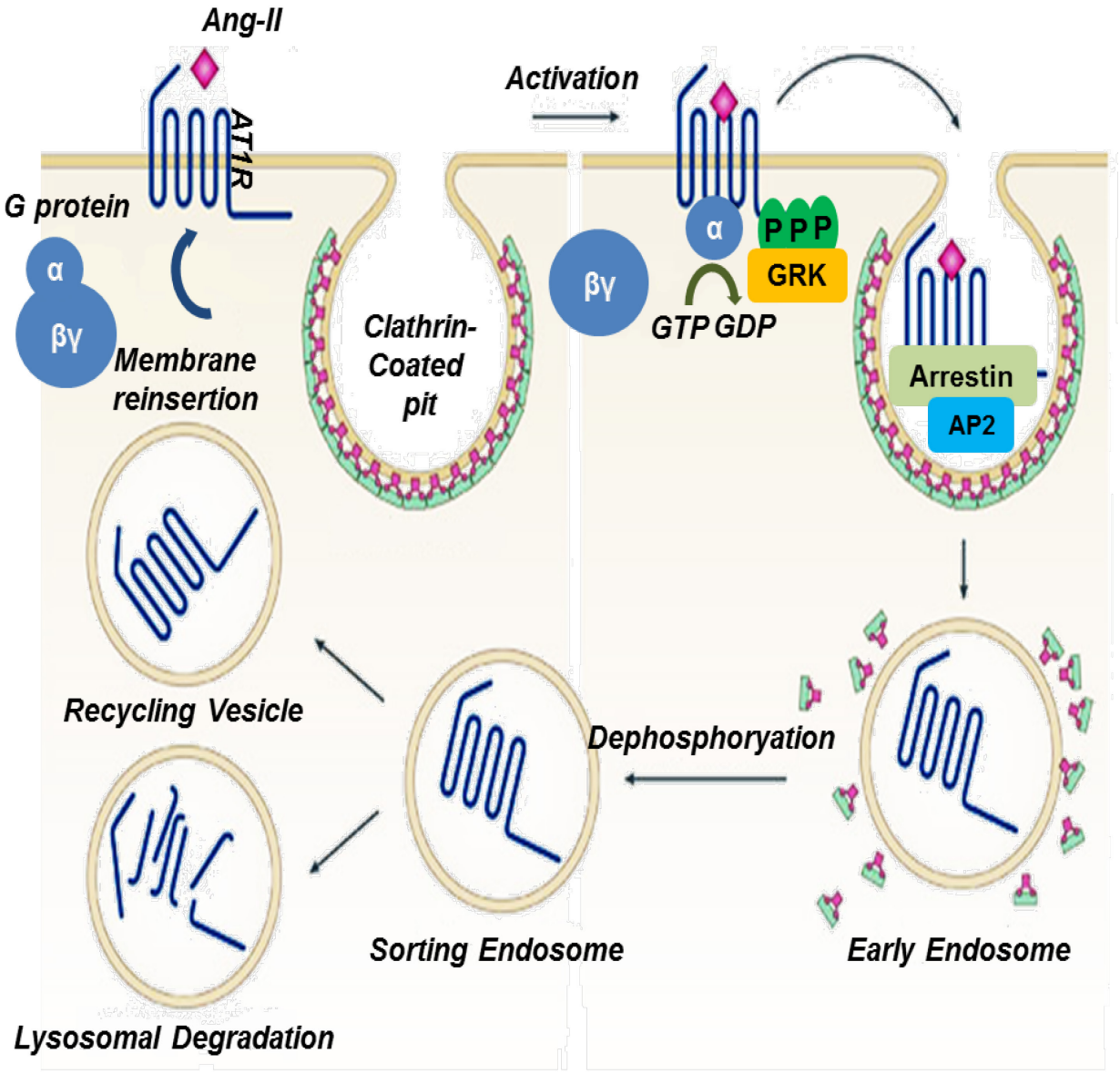

FIGURE 7. AT1R MEDIATED DESENSITIZATION, INTERNALISATION, RECYCLING AND DEGRADATION

Upon Ang-II stimulation, the AT1R is phosphorylated on serine/threonine residues by GRK, which facilitates the translocation and binding of β-arrestins. β-arrestin binding sterically precludes the interaction between the AT1R and heterotrimeric G proteins leading to termination of intracellular signalling. The AT1R/β-arrestin complex then recruits and binds components of the clathrin-mediated endocytic pathway, including clathrin and adaptor protein 2 (AP-2). Following receptor sequestration, the AT1R accumulate in endocytic vesicles and are sorted for either degradation or recycling back to the membrane.

1.7.3 RAS Inhibition to Prevent Cardiac Remodelling

RAS inhibition has become one of the most successful therapeutic approaches in cardiovascular medicine. RAS inhibition has repeatedly been shown in clinical trials to attenuate adverse myocardial remodelling and improve cardiac function in heart failure patients.

1.7.3.1 ACE Inhibitors

ACE inhibitors (ACEI) block the ACE-mediated conversion of angiotensin-I to Ang-II and also antagonize the breakdown of vasoactive bradykinin into inactive fragments. However, because of the existence of several alternative enzymatic pathways, the ability of ACEIs to completely suppress Ang-II production may be limited.

1.7.3.2 AT1R blockers

AT1R blockers (ARBs) prevent the interaction of Ang-II with AT1R receptor and hence inhibit the activation of intracellular cascades leading to adverse changes at the transcriptional level. Because ARBs block the effects of Ang-II from any source (including non-ACE systems) they might be expected to be more effective than ACEI in heart disease. However, clinical trials have not provided convincing evidence for the superiority of ARBs compared to ACEI. ARBs remain an excellent substitute in ACEI-intolerant patients. Despite the attractiveness of the pharmacological rationale, clinical evidence does not support the superiority of dual blockade of RAS with a combination of ARBs and ACEIs.

1.7.3.3 Renin inhibitors

Incomplete inhibition of RAS with ACEIs and ARBs lead to a substantial compensatory increase in the circulating levels of renin. Inhibition of RAS with renin inhibitors was an attractive pharmacological option since it prevents the formation of Ang-II, the activation of AT1R and the alterations in bradykinin metabolism. Clinical trials are currently underway to study this promising means of blocking the RAS.

1.8 Heart diseases in which the RAS is implicated in adverse cardiac remodelling

1.8.1 Cardiac Hypertrophy

Left ventricular hypertrophy (LVH) is a fundamental manifestation of an adaptive response to long-lasting increases in systemic blood pressure directed to counterbalance left ventricular wall stress [110]. The defining features of hypertrophy at the cellular level are an increase in cardiomyocyte size, enhanced protein synthesis, and a higher organisation of the sarcomere. Changes in cardiomyocyte phenotype, both in the case of concentric (muscle fiber thickening) and eccentric hypertrophy (muscle fiber lengthening), are accompanied by a reinduction of the fetal gene program [111]. LVH, clinically detected using electrocardiographic and cardiac magnetic resonance imaging (MRI) techniques, strongly predicts cardiovascular morbidity and mortality events in patients with uncomplicated essential hypertension [112]. Aortic or mitral regurgitation, aortic stenosis, coronary heart disease and dilated

cardiomyopathy contribute to the pathogenesis of LVH. Induction of LVH is multifactorial, sustained by a number of circulating or locally produced growth factors, cytokines, and hormones including aldosterone, Ang-II, and inflammatory mediators [113]. In its early stages, LVH is able to compensate in the face of increased load, but in later stages the diastolic and systolic functions of the left ventricle become impaired, resulting in decompensation leading to heart failure.

The cardiac circulatory and tissue RAS play a key role in the pathophysiology of cardiac hypertrophy. The cardiac RAS is able to regulate Ang-II production levels within the myocardium, independent of systemic Ang-II synthesis. Mechanical stretch, and in vitro model of load-induced cardiac hypertrophy, induces the release of Ang-II from cardiomyocytes, which acts as an initial mediator of stretch-induced hypertrophic remodelling [70]. In neonatal cardiomyocytes, Ang-II induces the expression of immediate-early genes including c-fos, c-jun, jun B, Egr-1, and c-myc (predominantly via AT1R) and fetal genes including SKA and ANF. Furthermore Ang-II augments protein synthesis, enhances TGF-β and PDGF production, and increases cell size [114]. AT1R and AT2R expression, angiotensinogen mRNA, ACE mRNA and activity are all increased in hypertrophy [115,116]. Multiple signal transduction cascades are activated in response to AT1R stimulation to promote molecular and morphological features of the hypertrophic response. Ang-II, acting via AT1R, activates the PLC-PKC-SRE pathway, which induces c-fos gene expression [117]. Ang-II regulates overall protein synthesis, a cardinal feature of hypertrophy, through rapid and sustained activation of 70-kDa S6 kinase ($p70^{S6K}$) [118]. The ERK1/2 pathway

mediates the Ang-II induced increase in ANF expression whereas RhoA mediates the Ang II–induced sarcomeric actin reorganization in cardiac myocytes [119].

In rat models of MI induced by coronary artery ligation, immediate therapy with losartan (ARB) and captopril (ACEI) were equally effective in reducing cardiomyocyte hypertrophy and long-term mortality [120]. In a heart failure model, ACEI and ARBs have a cardioprotective effect manifested by reduction of left ventricular remodelling [121]. In the recent Losartan Intervention For Endpoint reduction in hypertension (LIFE) trial, hypertensive patients with electrocardiographically documented LVH were randomly assigned to receive either losartan or atenolol (β1-adrenergic receptor blocker). Patients taking losartan displayed significantly less hypertrophy; although the blood pressure lowering effects were similar with atenolol, losartan was more effective in preventing cardiovascular morbidity and mortality [122]. Similarly, in the Heart Outcomes Prevention Evaluation (HOPE) study, the ACEI ramipril prevented the development of LVH in hypertensive patients with controlled blood pressure and furthermore was associated with reduced risk of adverse cardiovascular events and improved survival [123]. In patients receiving hemodialysis, ACEI and ARB treatment reduced the incidence of LVH, but the combination of ACEI with ARB did not translate into a prognostic benefit [124]. The Ongoing Telmisartan Alone and in Combination With Ramipril Global End Point Trial (ONTARGET) provided further evidence that the combination of telmisartan (ARB) with Ramipril does not provide any additional benefit in preventing LVH in patients at high risk [125].

1.8.2 Atrial Fibrillation

Atrial fibrillation (AF) is the most frequent disorder of cardiac rhythm encountered in clinical practice. During AF episodes, atrial contractions are irregular and chaotic; the atria fire very rapidly at rates ranging from 300 to 600 bpm; the electrical impulses propagate in a highly irregular manner through the AV node; and the blood flow from the atria to the ventricles is often disturbed [126]. The incidence of AF raises dramatically with advancing age, with an annual incidence of 3.1 cases in man and 1.9 cases in women per 1000 person for those who fall within the age range of 55 to 64, increasing to 38.0 cases in man and 31.4 cases in women per 1000 person for those who fall within the age range of 85 to 94 [127]. The risk of stroke associated with AF also increases with age, from 1.5% for the 50 to 59 age group to 23.5% for the 80 to 89 age group [128]. AF is a progressive cardiac arrhythmia and its likelihood increases with the presence of structural heart disease. Early episodes of erratic electrical signals and rapid heart rate resolve spontaneously within a week (paroxysmal AF) but it can also continue for longer periods (persistent AF). Over time, frequent and longer lasting episodes of paroxysmal and persistent AF can result in permanent AF [129]. The progressive nature of this arrhythmia is consistent with observations that AF causes electrical, contractile and structural remodelling such that AF begets AF [130]. The cornerstones of AF management are rate control and rhythm control, along with anticoagulation therapy.

A hallmark of continuous structural remodelling of the atria associated with AF is atrial dilatation and increased atrial pressure. Atrial dilation cause atrial tissue stretching, modifies effective atrial refractoriness, and triggers activation of hormonal

RAS, which leads to atrial fibrosis [131]. Ang-II production induces atrial dilatation with marked increase in fibrous tissue content, AF and sudden death in a mouse model with 100-fold cardiac ACE overexpression [132]. Ang-II concentrations and ERK1/2 phosphorylation are increased in a canine congestive heart failure model and in patients with atrial fibrosis [133,134]. Ang-II has a direct influence in stimulating atrial fibroblast proliferation and collagen synthesis via the AT1R/MAPK phosphorylation pathway [134]. Levels of ECM-related molecules in the atrium correlate with atrial fibrotic pathophysiology [135,136]. Ang-II interferes with collagen degradation by governing tissue MMP and TIMP expression [137]. Ang-II also upregulates growth factors such as TGF-β, and activates downstream signalling cascades to promote the expression of collagen and enhance atrial fibrosis [138].

Since RAS plays a central role in the development of atrial fibrosis that favours prolonged episodes of AF, inhibitors including ACEIs and ARBs should, in theory, be beneficial in preventing the occurrence and progression of AF. In the recent GISSI-AF trial, valsartan (ARB) didn't reduce the risk of recurrences of AF in patients with a history of AF associated with cardiovascular disease, type 2 diabetes, or left atrial dilatation [139]. In a different clinical trial, irbesartan (an ARB) was not able to reduce cardiovascular events in patients with permanent AF [140]. In ANTIPAF, a prospective multicenter trial, one year olmesartan (ARB) therapy didn't reduce the number of AF episodes in paroxysmal AF patients [141]. The ongoing Canadian Trial on AF (CTAF-2) is presently testing the effect of perindopril (ACEI) on recurrences of AF [142].

1.8.3 Heart Failure

HF is a major clinical and public health problem, associated with substantial mortality, morbidity and healthcare costs, occurring most frequently in the elderly [143]. HF can result from any number of cardiac structural or functional changes and can be subdivided into HFrEF and HFpEF). In HFrEF, cardiac contractility is decreased, whereas in HFpEF there is impaired ventricular relaxation.

Initially, neurohormonal (e.g., SNS, RAS) activation can maintain blood pressure and circulatory homeostasis by increasing cardiac contractility, heart rate and vascular tone in HF. However, in the long run these neurohormones lead to adverse remodelling and result in clinical deterioration of HF and progressive left ventricular dysfunction [144]. In cardiac cells, Ang-II can trigger necrosis, apoptosis and myocardial fibrosis by altering the composition of ECM.

ACE inhibitors are routinely used as first line treatment in all patients with a recent history of MI and reduced ejection fraction to prevent symptomatic HF [145]. The benefits of ACE inhibitors in reducing overall mortality and morbidity have been demonstrated in large, prospective and randomized clinical trials. However, 5% to 20% of patients treated with ACE inhibitors develop renal dysfunction, angioedema, hyperkalemia, and/or cough. ARBs offer an alternative approach to inhibit the RAS for ACE-intolerant patients. In the Candesartan in Heart failure: Assessment of Reduction in Mortality and morbidity (CHARM)-Alternative trial, candesartan was well tolerated and reduced cardiovascular mortality and morbidity in HF patients, however no benefit was seen in patients with HFpEF [146]. In another clinical trial, the

combination of valsartan (ARB) and captopril (ACEI) showed an increase in the rate of adverse events without improving survival versus either agent alone [147].

1.9 Mediators of RAS Communication in Fibrogenic and Hypertrophic Responses

1.9.1 Transforming growth factor-β

TGF-β is a ubiquitously expressed protein that activates the fibrotic response principally through the activation and differentiation of cardiac fibroblasts. TGF-β exists in three isoforms including TGF-β1, TGF-β2 and TGF-β3 and is primarily produced as a complex bound to latent TGF-β binding protein (LTBP) [148]. TGF-β expression can be increased by mechanical stretch, altered pH, high-energy radiation, Ang-II, MMPs, plasmin, or integrins and its synthesis is markedly enhanced in animal models of heart failure [149-151]. Once activated, TGF-β binds directly to the TGF-β type II receptor (TGF-βR2) and subsequently recruits and dimerizes with the TGF-β type I receptor (TGF-βR1) to activate downstream signalling pathways. TGF-β receptors contain a serine/threonine kinase domain that allows TGF-βR2 to phosphorylate TGF-βR1 and then to propagate the signal through the phosphorylation of receptor regulated SMADs (small mothers against decapentaplegic) (rSMADs: SMAD 1,2,3,5, and 8). Phosphorylated rSMADs undergo homotrimerization and associate with a common-mediator SMAD (coSMADs: SMAD 4). The activated SMAD complexes are then translocated into the nuclear

compartment where they bind to transcription promoters/DNA-binding cofactors and regulate the expression of target genes. The inhibitory SMADs (iSMADs: SMAD 6 and 7) compete with rSMADs or coSMADs to negatively regulate TGF-β signalling [152]. Similarly, ubiquitylation of SMADs in the nucleus followed by proteasome-mediated degradation terminates TGF-β signalling [153].

TGF-β critically modifies fibroblast phenotype, promotes myofibroblast differentiation and enhances ECM protein synthesis, particularly of collagen and fibronectin [149]. Responses to Ang-II, which play a fundamental role in producing maladaptive hypertrophy in the failing heart, are mediated in part when Ang-II initiates TGF-β signalling (Figure 8). Serum TGF-β1 levels are correlated with left ventricular mass and diastolic internal dimension in hypertensive patients [154]. Peripheral venous TGF-β1 plasma levels are also increased in aortic stenosis patients and are associated with increased aortic transvalvular gradients and hypertrophy [155]. In addition, atrial myocardial expression of TGF-β1, TGF-βR2 and SMADs (1, 2, 4, 7) are upregulated and lead to structural atrial remodelling/fibrogenesis in patients with AF [156]. Transgenic mice overexpressing TGF-β1 exhibit important myocardial hypertrophy accompanied by increased deposition of ECM constituents [157]. In a rat model of cardiac pressure overload, produced by constricting the suprarenal abdominal aorta, TGF-β expression levels are significantly higher, myocardial fibrosis is progressive and severe diastolic dysfunction develops. In this model, TGF-β blockade reverses pressure overload triggered fibroblast activation, collagen mRNA synthesis, cardiac fibrosis and diastolic dysfunction [158]. Furthermore, in a rat model of chronic NO-synthase inhibition, neutralizing monoclonal antibodies raised against

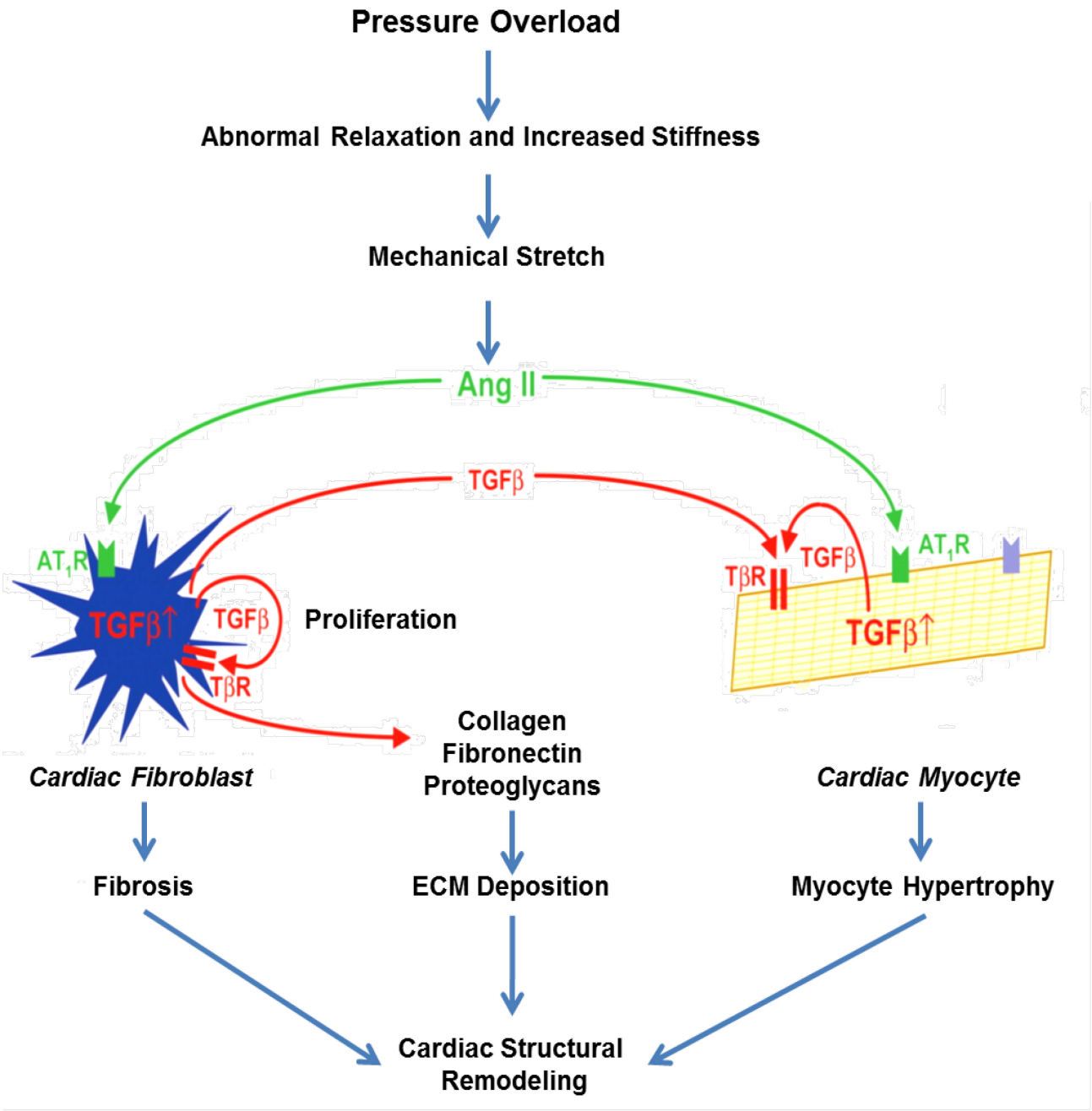

FIGURE 8. SCHEMATIC ILLUSTRATING THE NETWORKING BETWEEN ANG-II AND TGF-β IN CARDIAC REMODELLING

Ang-II released upon pressure overload upregulates TGF- β mRNA and protein in fibroblasts and cardiomyocytes. TGF-β via paracrine and autocrine cellular responses can induce fibrotic and hypertrophic changes leading to cardiac structural remodeling.

TGF-β inhibited fibroblast proliferation and supressed the expression of inflammation-promoting proteins (MCP-1, ICAM-1 and P-selectin) [159].

1.9.2 Connective tissue growth factor

CTGF is a profibrotic actor playing an important role in the pathophysiology of myocardial remodelling. CTGF is a matricellular regulatory protein expressed in cardiomyocytes and fibroblasts, and is involved in intracellular signal transduction pathways leading to hypertrophy, angiogenesis, cellular adhesion and migration, proliferation and myofibroblast differentiation, with subsequent ECM deposition and remodelling ultimately leading to scar formation, tissue remodelling and myocardial fibrosis [160]. CTGF, first extracted from human umbilical vein endothelial cells, is a member of the CCN (Cyr61, Ctgf, Nov) gene family, and contains four conserved structural modular domains composed of insulin-like growth-factor (IGF-1) binding protein domain, von Willebrand factor type C (VWC) repeat domain, thrombospondin type 1 (TSP-1) repeat domain, and a carboxyl-terminal (CT) cysteine-knot domain [161].

In experimental animal models as well as in humans, CTGF mRNA and protein expression are upregulated in heart failure of both ischemic and non-ischemic etiologies and the degree of upregulation is associated with the severity of disease [162,163]. Similarly, in genetically hypertensive rats, cardiac CTGF levels are positively associated with blood pressure [164]. In addition, cardiac CTGF secretion is upregulated by mechanical stretch, static pressure, Ang-II, endothelin-1 (ET-1),

aldosterone, TGF-β and brain natriuretic peptide (BNP) [165,166]. Treatment with the AT1R antagonist losartan prevents the induction of myocardial CTGF mRNA in experimental post-MI rats [167]. Similarly, in adult mouse atrial cells, ETA (BQ123) and ETB (BQ788) inhibitors abolished ET-1 induced CTGF expression and CTGF silencing attenuated ECM accumulation [168]. Cardiovascular remodelling associated with diabetes was reversed in a rat model treated with CTGF inhibitor FG-3019 [169].

CTGF signal transduction triggers changes in cellular responses through interactions with multiple molecules including cytokines and growth factors (IGF-1, BMP, TGF-β, VEGF), matrix proteins (fibronectin, heparin sulfate proteoglycans), integrins and receptors (LRP1, LRP6, TrkA) [169,170]. Luciferase-based gene reporter assays revealed that TGF-β induces CTGF expression by activating its promoter and in cardiac cells CTGF upregulation is correlated with increased production of collagen type I, fibronectin, and plasminogen activator inhibitor-1 [171]. Furthermore, in normal rat kidney (NRK) fibroblasts and human foreskin fibroblast cultures, blockade of CTGF with both specific anti-CTGF antibodies and antisense CTGF gene constructs inhibits TGF-β stimulated collagen synthesis [172]. In cardiac allografts, TGF-β and IL-6 induce CTGF expression and CTGF neutralization improves graft fibrosis and hypertrophy associated with cardiac rejection. SMAD and STAT3 binding response elements were identified in the 5’ region upstream of the CTGF promoter, supporting the role of CTGF as downstream regulator and an interesting target for HF therapy [173].

1.9.3 Platelet-derived growth factors

PDGFs are multifunctional prototypic growth factors with wide-ranging actions, extensively involved in stimulation of cell growth and cell division, and contribute to the maintenance of connective tissue in the adult heart [174]. They are composed of four inactive isoforms (PDGF-A, B, C, D); these form homodimers and/or heterodimers through intermolecular disulfide linkages to become functional after biosynthesis and processing [175]. To exert their biological activities, PDGFs signal through tyrosine kinase α and β PDGF-receptors (PDGFRα, PDGFRβ). PDGF activated cell proliferation is mediated via ligand induced dimerization of PDGFRα and/or PDGFRβ and subsequent phosphorylation resulting in activation of downstream RAS/ERK1/2 signalling pathways [176]. PDGF contributes to Janus tyrosine kinase/signal transducers and activators of transcription (JAK/STAT) pathway activation through ROS production, and plays a key role in cell transformation and inflammatory processes [177]. PDGF also activates cell migration, attachment, proliferation and collagen expression through the focal adhesion kinase (FAK)-phosphatidylinositol 3-kinase (PI3K)-Akt signalling pathway [178,179].

PDGF isoforms and receptors are expressed in cardiomyocytes and fibroblasts and are significantly upregulated in the infarcted myocardium, in cardiac hypertrophy, fibrosis and AF [180-183]. PDGF-C overexpression in a transgenic mouse heart using the α-myosin heavy chain promoter induces progressive fibrosis and hypertrophy leading to dilated cardiomyopathy and HF [184]. Recombinant adeno-associated virus (AAV) PDGF-A, PDGF-B, and PDGF-D gene transfer in mice accelerated cardiac

fibrosis development compared to PDGF-B that displayed minimal fibrotic effect [185]. PDGF-D/PDGFRβ signal transduction promotes fibrogenesis through enhanced synthesis of TGF-β, MMP1, MMP2, MMP9 and TIMP1, TIMP2 in cardiac fibroblasts [186]. In addition, desoxycorticosterone (DOCA) induced salt-sensitive hypertensive rats experience massive collagen deposition through PDGF/PDGFR signalling, and stimulate the growth, differentiation and migration of fibroblasts, resulting in myocardial fibrosis [179]. Similarly, Ang-II upregulates PDGF-A expression through the activation of the Kruppel-like zinc-finger transcription factor (KLF5). KLF5 is a key determinant of cellular response and tissue remodelling. Hearts of KLF5 knockout mice infused continuously for 14 days with Ang-II had comparatively thinner ventricular walls, reduced heart weight to body weight ratio and significantly lower interstitial and perivascular fibrosis compared to wild type Ang-II infused animals [182].

1.9.4 Fibroblast growth factors

FGFs mediate cardiac fibroblast behaviours and restore ECM homeostasis and regulation. They play distinct but overlapping roles in cardiac remodelling. Of the 23 FGF isoforms identified to date, FGF-2 is predominantly expressed in the heart and is the most studied. FGF-2, also recognized as basic FGF (pI>9.0), consists of a low molecular weight (Lo-FGF-2) and a high molecular weight (Hi-FGF-2) isoform produced by alternate initiation of translation from the FGF-2 mRNA, and is highly conserved amongst different species [187]. FGF-2 may be released through

exocytosis by means of Na^+/K^+-ATPase, transient membrane disruptions due to sustained increase in cardiac work, cardiomyocyte contraction and migration of endothelial cells [188-191]. The biological actions of FGF-2 in the heart are mediated by a cell surface tyrosine kinase FGF receptor (FGFR-1). Stimulation of FGFR-1 in cardiac cells results in activation of its downstream target PLC, translocation of PKCε to the plasma membrane and opening of mitochondrial K^+/ATP channels. PKC can also phosphorylate connexin43 leading to decreased cardiomyocyte metabolic coupling [192]. In addition, FGF-2 can also activate ERK1/2, JNK and p38 kinases [193].

Initial studies provided evidence that FGF-2 is a cardioprotective and a physiological survival growth factor acting via autocrine/paracrine actions on cardiac cells. FGF-2 regulates survival of cardiomyocytes early in cardiogenesis and is a key factor in the maintenance of cardiovascular physiology [194]. During ischemia–reperfusion injury, injection of FGF-2 protects against myocardial injury and contractile dysfunction [195]. In vivo, FGF-2 overexpression in transgenic mice increased myocyte viability and reduced infarct size [196].

In contrast to its cardioprotective actions, recent studies have established a role of FGF-2 in the cardiac hypertrophic response. In vitro, FGF-2 increases both fibroblast and myofibroblast proliferation, and is associated with cardiomyocyte growth and reexpression of fetal gene contractile proteins [197]. Mice lacking the FGF-2 gene subjected to aortic coarctation had reduced left ventricular mass, wall thickness and cardiomyocyte cross-sectional area compared to wild-type mice [198]. In neonatal cardiomyocytes, Ang-II binding to AT1R and subsequent activation of

ERK1/2 and p38 MAPKs can increases GATA4 binding activity to the FGF-2 promoter and upregulate the expression of FGF-2 [199]. Ang-II induced hypertensive mice lacking FGF-2 do not develop hypertrophy and MAPK (ERK, p38, JNK) activation appeared to be reduced [200].

1.10 Intracellular RAS: Implications in Cardiovascular Remodelling

Traditionally, the RAS hormonal pathway was viewed as a circulatory and tissue specific system. However, recent studies support the notion of intracellular or intracrine RAS, defined by the presence of complete and functional RAS within a single cell. Internalization of non-glycosylated prorenin, a biosynthetic precursor of renin, in adult cardiomyocytes, results in a significant increase in intracellular Ang-II (iAng-II) levels [201]. iAng-II production in neonatal rat ventricular myocytes (NRVM), using recombinant adenoviral and plasmid expression vectors, induces cytoskeletal reorganization, augments cellular [^{3}H]leucine incorporation, and increases cardiac levels of c-jun, IGF-1 and TGF-β mRNA. Furthermore, injection of adenoviral vectors constructed to express Ang-II intracellularly in adult mouse heart resulted in biventricular cardiac hypertrophy and administration of the AT1R inhibitor, losartan, had no influence on the induction of hypertrophy [202]. In diabetic patients, iAng-II levels are increased in cardiomyocytes by 3.4 fold and in endothelial cells by 3.1 fold compared to non-diabetics. An additional 2-fold increase of iAng-II was observed in diabetic hypertensive patients compared to diabetic non-hypertensive patient group

[203]. When exposed to high glucose, NRVMs synthesize and retain intracellular Ang-II with redistribution of the peptide to the nucleus, via renin and chymase dependant enzyme pathways. Similarly, exposure of neonatal rat ventricular fibroblasts to high glucose-exposure induces the production of iAng-II, which is correlated, with increased levels of collagen-1 and TGF-β [204,205]. Diabetes, triggered in adult rats by streptozotocin, dramatically increases iAng-II concentrations in cardiac cells, leading to increases in oxidative stress, apoptosis and fibrosis [206]. In the latter study the AT1R blocker, candesartan, or the ACE inhibitor, benazepril, didn't provide clear beneficial effects [206]. Intracellular administration of Ang-II by microinjection in isolated cardiomyocytes reduces inward calcium current (I_{Ca}), increases gap junctional resistance and favours the generation of re-entrant arrhythmias [207]. Similarly, injection of Ang-II in cardiomyocytes isolated from cardiomyopathic failing hearts induces an alteration in action potential duration, resting potential and refractoriness [208,209]. Intracellular delivery of Ang-II using a liposomal delivery system in A7r5 vascular smooth muscle cells promotes cell growth and modulates Ca^{2+} homeostasis [210,211]. Many of the observed intracellular Ang-II actions are not inhibited by traditional ARBs, most probably because of their inability of penetrating inside the cell. These observations further support the clinical outcomes that current ARBs and ACEi do not offer anticipated benefits in high-risk cardiovascular conditions [212].

1.11 Thesis Rationale

Despite many new advances in diagnosis, therapy and cardiac assist devices, heart failure remains a leading cause of death worldwide. The progression of heart failure is attributable largely to cardiac remodelling due to maladaptive alterations in cardiomyocyte properties and cardiac architectures. The process of cardiac remodelling is influenced enormously by activation of the phylogenetically ancient renin-angiotensin neurohormonal system. The status of the RAS has evolved into a complex hormonal cardiovascular regulatory system since the original discovery of renin, the rate-limiting enzyme of the RAS, more than a century ago. Since the RAS is involved in many components of the cardiovascular remodelling system, improved targeting of the RAS by more specific inhibition of selected components might help to reduce cardiovascular risk. The intracellular RAS in cardiac myocytes and fibroblasts is poorly understood; a better knowledge of its role may allow for the development of new and hopefully better anti-remodelling strategies. The main objective of this thesis is therefore to elucidate the role of intracellular RAS in cardiac cells, with a view to aiding in the design and synthesis of novel RAS inhibitors to prevent remodelling and improve outcome.

CHAPTER 2 – Subcellular distribution of Ang-II receptors in ventricular cardiomyocytes and their role in mediating transcriptional responses.

Linking Statement and Author Contribution

Several reports provide strong evidence that Ang-II can generate physiologically relevant effects by acting at intracellular sites. Intracellular Ang-II may be generated through internalization from the circulation via clathrin-mediated endocytosis and subsequent release into the cytoplasm from the endosomes, or may be retained intracellularly after biosynthesis. An important issue is the extent to which the intracellular actions of Ang-II are conserved, that is, acting though membrane associated receptors in the intracellular milieu. Since a growing body of experimental data support the notion that GPCRs can activate signalling pathways from nuclear or other endomembranes, we hypothesized that in native ventricular cardiomyocytes intracellular AT1Rs and AT2Rs are activated by Ang-II and control gene-expression via discrete signalling systems.

Tadevosyan A, Maguy A, Villeneuve LR, Babin J, Bonnefoy A, Allen BG, Nattel S. Nuclear-delimited angiotensin receptor-mediated signaling regulates cardiomyocyte gene expression. J Biol Chem. 2010 Jul 16;285(29):22338-49.

A.T., B.G.A. and S.N. participated in conception and experimental design. A.T. carried out all of the cellular fractionations, biochemical/pharmacological assays, de novo RNA transcription experiments, immunohistochemistry, microinjections, calcium recordings, performed statistical analysis and wrote the first draft of the manuscript (Figures 1-9). A.M. provided technical assistance for biochemical assays. L.V. acquired all of the immunocytochemistry images. J.B. and A.B. provided help with the endocytosis experiments. B.G.A and S.N. supervised the project, provided intellectual input and edited the final manuscript.

Nuclear-Delimited Angiotensin Receptor-Mediated Signaling Regulates Cardiomyocyte Gene Expression

Artavazd Tadevosyan[1,3], Ange Maguy[3], Louis R. Villeneuve[3], Judith Babin[1,3], Arnaud Bonnefoy[1,3,4], Bruce G. Allen[1,2,3,5]*, and Stanley Nattel[1,3,5]*

From the Department of Medicine[1], Department of Biochemistry[2], Montreal Heart Institute and Université de Montréal[3]; INSERM U743 Université de Montréal[4]; and Department of Pharmacology and Therapeutics[5], McGill University, Montreal, Quebec, Canada

***Co-senior authors.**

Running head: Nuclear envelope angiotensin receptors

Address correspondence to: Stanley Nattel, 5000 Belanger Street East, Montreal, Quebec, H1T 1C8, Canada. Tel.: 514-376-3330; Fax: 514-376-1355;

Abstract

Angiotensin-II (Ang-II) from extracardiac sources and intracardiac synthesis regulates cardiac homeostasis, with mitogenic and growth-promoting effects largely due to altered gene-expression. Here, we assessed the possibility that angiotensin-1 (AT1R) or angiotensin-2 (AT2R) receptors on the nuclear envelope mediate effects on cardiomyocyte gene-expression. Immunoblots of nucleus-enriched fractions from isolated cardiomyocytes indicated the presence of AT1R and AT2R proteins that copurified with the nuclear-membrane marker nucleoporin-62 and histone-3, but not markers of plasma (calpactin-I), Golgi (GRP-78) or endoplasmic-reticulum (GM130) membranes. Confocal microscopy revealed AT1R and AT2R proteins on nuclear membranes. Microinjected Ang-II preferentially bound to nuclear sites of isolated cardiomyocytes. AT1R- and AT2R-ligands enhanced de novo RNA synthesis in isolated-cardiomyocyte nuclei incubated with [α^{32}P]UTP (e.g. 36.0±6.0 cpm/ng DNA control vs. 246.4±15.4 cpm/ng DNA Ang-II, 390.1±15.5 cpm/ng DNA L-162313 (AT1), 180.9±7.2 cpm/ng DNA CGP42112A (AT2), $P<0.001$). Ang-II application to cardiomyocyte nuclei enhanced NF-κB mRNA-expression, a response that was suppressed by co-administration of valsartan and/or PD123177. Dose-response experiments with Ang-II applied to purified cardiomyocyte nuclei vs. intact cardiomyocytes showed greater increases in NFκB mRNA levels at saturating concentrations with ~2 fold greater affinity upon nuclear application, suggesting preferential nuclear signaling. AT1R- but not AT2R-stimulation induced cardiomyocyte nuclear-preparation [Ca^{2+}]-rises. Inositol-1,4,5-trisphosphate receptor block by 2-aminoethoxydiphenyl-borate prevented AT1R-mediated Ca^{2+}-release and

attenuated AT1R-mediated transcription-initiation responses. We conclude that cardiomyocyte nuclear membranes possess angiotensin-receptors that couple to nuclear signaling-pathways and regulate transcription. Signaling within the nuclear envelope (e.g. from intracellularly synthesized Ang-II) may play a role in Ang-II-mediated changes in cardiac gene-expression, with potentially-important mechanistic and therapeutic implications.

Key Words: angiotensin II, angiotensin receptor subtypes, nuclear envelope, gene regulation, transcription, remodelling

Introduction

Angiotensin-II (Ang-II) is implicated in the regulation of cardiac contractility, cell proliferation and communication through the activation of specific heptahelical membrane-spanning G-protein coupled receptors (GPCRs). Blockers of the renin-angiotensin system (RAS) are widely used in the treatment of hypertension and heart failure (1-3). There is increasing evidence that RAS components can act intracellularly (4-6). Extracellular signaling peptides could operate internally following internalization. Alternatively, intracellular action could occur via production of Ang-II within target cells.

Neonatal cardiomyocyte stimulation by high concentrations of glucose or isoproterenol results in the intracellular synthesis and nuclear trafficking of Ang-II (7). Serum-deprived cardiomyocytes release Ang-II into the culture medium and Ang-II concentrations increase 100-fold upon mechanical stretch (8). Internalization of pro-renin into cardiomyocytes leads to the generation of intracellular Ang-II independently of glycosylation (9). Introduction of Ang-II inside the cell has important effects on transmembrane Ca^{2+}-currents, on cardiomyocyte conductance and potentially on the pathogenesis of cardiac arrhythmias (10). Intracellular Ang-II binding sites have been imaged in renal and hepatocyte nuclei, but whether those receptors represent internalized plasma membrane receptors or a genuine new class of Ang-II receptors (ATRs) remains unclear (11,12). Despite Ang-II's fundamental role in the regulation of heart function and gene expression, direct demonstrations of functional ATRs inside cardiac cells are lacking. Accordingly, the current study investigated the subcellular distribution of type 1 and 2 ATRs (AT1Rs, AT2Rs respectively) in native

ventricular cardiomyocytes, with particular attention to the nuclear envelope, and assessed evidence for coupling of such intracellular receptors to Ang-II-mediated transcriptional responses.

Materials and Methods

Reagents and antibodies

The following antibodies were used for immunoblotting: AT1R, AT2R from Santa Cruz (Santa Cruz, CA) and Alomone Labs (Jerusalem, Israel); calpactin-I, GM130, GRP-78 from BD Biosciences (Franklin Lakes, NJ); histone from Cell Signaling (Danvers, MA) and nucleoporin 62 from ABCAM (Cambridge, MA) (see on line Table I for more details). All the secondary antibodies used for Western and immunostaining were from Jackson ImmunoResearch Laboratories (West Grove, PA). Candesartan was kindly provided by AstraZeneca (Mississauga, Ontario) and valsartan by Novartis (Dorval, Quebec). The primers for quantitative real-time polymerase chain reaction (qPCR) assays were purchased from SuperArray (Frederick, MD)/Invitrogen (Burlington, Ontario). Unless otherwise specified, all reagents were of molecular biology grade and obtained from Fisher (Ottawa, Ontario) or Sigma-Aldrich (Oakville, Ontario).

Isolation of cardiomyocytes

Male Wistar adult rats (200-300 g) were anesthetized with a combination of ketamine/xylazine (10 mg/kg body weight i.p.) and treated with heparin (1.0 U/kg body wt). All animal-handling procedures were approved by the Animal Research Ethics Committee of the Montreal Heart Institute and the procedures complied with guidelines established in the Guide for the Care and Use of Laboratory Animals (NIH Publication 65-23, revised 1996). Hearts were exposed via sternotomy, rapidly excised, and immersed in ice-cold Tyrode solution containing: 140 mM NaCl, 5.5 mM

KCl, 1 mM $MgCl_2$, 0.3 mM KH_2PO_4, 10 mM dextrose, 5 mM HEPES, 2 mM $CaCl_2$, adjusted to pH 7.5 with NaOH. Left-ventricular cardiomyocytes were isolated using a Langendorff-perfusion system. The hearts were cannulated via the ascending aorta and in situ retrograde perfusion of the coronary arteries was started with 200 µM Ca^{2+} in modified Tyrode solution (140 mM NaCl, 5.5 mM KCl, 1 mM $MgCl_2$, 0.3 mM NaH_2PO_4, 5 mM HEPES and 10 mM dextrose adjusted to pH 7.5 with NaOH). After perfusion for 3 min at 6 ml/min, the hearts were perfused with calcium-free Tyrode solution for an additional 5 minutes.. Subsequently, hearts were enzymatically digested by recirculation with Ca^{2+}-free Tyrode solution containing 0.5 mg/ml type II collagenase for approximately 45 min. When the heart softened, the left ventricle was minced into small pieces in Kraftbruhe medium (20 mM KCl, 10 mM KH_2PO_4, 10 mM glucose, 40 mM mannitol, 70 mM L-glutamic acid, 10 mM β-hydroxybutyric acid, 20 mM taurine, 10 mM EGTA and 0.1% albumin; pH 7.5, NaOH). To promote cell dissociation, the solution and tissue fragments were resuspended with a transfer pipette and the suspension was filtered through a 200 µm nylon mesh. Cardiomyocytes were separated from non-cardiomyocyte cells by sedimentation (3x200 g, 3 minutes), the supernatant was discarded or used for fibroblast isolation, and the final cardiomyocyte pellet was resuspended in Joklik's Minimal Essential Medium (25 mM $NaHCO_2$, 1.2 mM $MgSO_4$, 1 mM DL-carnitine, 1 mM $CaCl_2$, adjusted to pH 7.5 with NaOH). All solutions were constantly aerated with 5% CO_2-95% O_2, and solutions and cells were kept at 37°C throughout the isolation process. Ca^{2+}-tolerant, rod-shaped ventricular cardiomyocytes (75 to 90% of all cells) were used on the day of isolation or snap-frozen at -80°C for subsequent biochemical studies.

Nuclei from total cardiac tissue were isolated in a similar general fashion- details are provided in the on-line supplement.

Isolation of cardiomyocyte nuclei

Cardiomyocytes, isolated as described above, were washed 4 times with phosphate buffer before the isolation of myocardial nuclei. Cells were suspended in a hypo-osmotic buffer (10 mM Tris, 1 mM $MgCl_2$, 10 mM NaCl, 5 mM $CaCl_2$; adjusted to pH 7.4 with HCl) for 30 minutes at 4ºC. The cells were sedimented at 1000xg for 10 minutes and then resuspended in 20 ml of hypo-osmotic buffer and sonicated for 90 seconds in a Branson 3200 sonifier. Triton X-100 (TX-100) was added to the sonnicated preparation to a final concentration of 0.1% and then the preparation was centrifuged at 1,000 x g for 10 minutes. The supernatant containing the membrane and cytoplasmic fractions was kept as a control for biochemical analysis. The resulting pellet was resuspended in 15 ml of MC buffer (2.2 M sucrose, 10 mM Tris, 1 mM $MgCl_2$, 0.1 mM PMSF; adjusted to pH 7.4 with HCl). This suspension was transferred to high-resistance centrifugation tubes underlaid with 2.5 ml of MC buffer and centrifuged at 100,000 x g for 60 minutes. The pellet containing the nuclear fraction was resuspended in buffer containing 20 mM Na-HEPES, 25% (volume/volume) glycerol, 0.42 M NaCl, 1.5 mM $MgCl_2$, 0.2 mM EDTA, 0.2 mM EGTA, 0.5 mM PMSF, 0.5 mM DTT, 25 µg/ml leupeptin, 0.2 mM Na_3VO_4, with a final pH of 7.4 (NaOH) or 1x transcription buffer (see below), and either used freshly or aliquoted, snap-frozen with liquid nitrogen, and stored at -80°C. Membrane proteins were separated from cytoplasmic proteins by centrifugation at 100,000 x g (Beckman

TLA 100.3 rotor) for 60 minutes. The membrane-protein containing pellets were re-suspended in extraction buffer containing 25 mM. Tris-HCl (pH 7.4), 5 mM EGTA, 5 mM EDTA, 1 mM Na_3VO_4, 0.5 mM AEBSF, 1 mM iodoacetamide, 1 mM β-2-mercaptoethanol, 10 µg/mL aprotinin, 10 µg/mL leupeptin and 1 µg/mL pepstatin, supplemented with 1% Triton X-100 and stored at -80°C. Protein concentrations were determined by Bradford assay using a NanoDrop ND-1000 Spectrophotometer (Wilmington, DE).

Non-cardiomyocyte cell and tissue extracts used to test selectivity of the cardiomyocyte-isolation procedure. The purity of isolated cardiomyocytes was assessed by Western blot, using protein extracts prepared from cardiomyocytes, fibroblasts, smooth muscle cells, endothelial cells and brain rat homogenates. For the isolation of fibroblasts, the supernatant obtained from the cardiomyocyte isolation was centrifuged at 2,500 × g for 10 minutes. The pellet was resuspended in Dulbecco's minimal essential medium (DMEM) containing 10% fetal calf serum (FCS, Biochrom), 1% penicillin/streptomycin and plated on 58-cm^2 dishes. Four hours later, the media were changed and adherent cells were washed free of debris and non-attached cells. Smooth muscle and endothelial cells were obtained by a previously described method (13). The rat brain homogenate protein fraction was a gift from Dr Ling Xiao.

Immunoblot analysis

Samples were separated by sodium dodecyl sulphate (SDS)-polyacrylamide gel electrophoresis (PAGE) on 8% (w/v) acrylamide running gels with 4% (w/v) acrylamide stacking gels. Proteins were transferred onto PVDF membranes at 300

mA and 4°C for 60 min in a transfer buffer consisting of 25 mM Tris-base, 192 mM glycine and 20% (v/v) ethanol. Membranes were blocked for 120 min with a solution of skimmed milk powder 5% (w/v) and 0.1% (v/v) Tween 20 in PBS at ambient temperature. Following blocking, membranes were incubated with the primary antibody (on-line Table I) overnight at 4°C with continuous mixing. The following day, membranes were washed (4x12 min) with a solution containing 0.5% (w/v) skimmed milk powder and 0.1% (v/v) Tween 20 in PBS, then incubated with the appropriate horseradish peroxidase-conjugated secondary antibody (60 min at room temperature). Membranes were thoroughly washed with PBS-Tween 20 (4x12 min) and immunoreactive bands revealed using Enhanced Chemiluminescence Reagent in conjunction with Bio-Max MR film (PerkinElmer Life Sciences, Waltham, MA). Preliminary experiments were performed to establish exposure times that avoided film saturation and permitted quantification. To ensure equal protein loading, blots were stripped and stained using Ponceau S (0.5% Ponceau S, 1% glacial acetic acid, in deionized water). Immunoblots were scanned (1200 dpi) and band intensities quantified with Quantity One 1D analysis software (Bio-Rad Laboratories, Hercules, CA).

Confocal microscopy and deconvolution

Freshly-isolated cardiomyocytes were plated on 18-mm laminin (10 µg/ml)-coated coverslips for 60 min (37ºC, 95% O_2-5% CO_2), fixed with 2%-paraformaldehyde for 20 min and permeabilized with blocking buffer comprising 2% normal donkey serum (NDS) and 0.2% (v/v) TX-100 in PBS for 60 min. After extensive washing to remove

the excess serum, cells were incubated overnight at 4ºC with the primary antibody diluted in PBS containing 1% NDS and 0.05% TX-100. Coverslips were then rinsed several times with PBS and incubated for 60 min at room temperature with secondary antibody (Alexa 488 conjugated anti-rabbit antibody or Alexa 555-conjugated anti-mouse antibody diluted in 1% NDS and 0.05% TX-100). After a final wash with PBS, coverslips were mounted and fixed on glass slides with drop of a mixture containing 0.1% diazabicyclo(2.2.2)octane (DABCO)/glycerol. Fluorescence images were acquired using a Zeiss LSM 510 confocal fluorescence microscope (Carl Zeiss, Oberkochen, Germany). Composite images were created using Zeiss LSM510 software. For every secondary antibody, control experiments were performed omitting the primary antibody to confirm the specificity of the primary antibody. Nuclei were visualized using Hoechst 33342 or DRAQ5 nucleic acid stain. Image stacks were digitally deconvolved (0.01% threshold, lowest background and real signal/noise values) for 25 iterations to reduce out-of-focus light using the Maximum Likelihood Estimation algorithm and the appropriate experimentally-determined point spread function with Huygens Professional software (version 3.1.0p1, Scientific Volume Imaging, Hilversum, The Netherlands). Files were stored in ICS format and exported to PowerPoint (Microsoft, Redmond, WA).

[α-^{32}P]UTP RNA transcription initiation assay

Transcription initiation assays were performed using freshly isolated cardiomyocyte nuclei as previously described (14). Briefly, a mixture of nuclei (treated with ligand where indicated), 1x transcription buffer (50 mM Tris, 0.15 M KCl, 1 mM $MnCl_2$, 6 mM

$MgCl_2$, 1 mM ATP, 2 mM DTT, 1 U/µl RNAse inhibitor, pH adjusted to 7.4 with NaOH) and [α-^{32}P]UTP were incubated for 30 min at 30ºC. CTP and GTP were omitted to prevent chain elongation. Following treatment with DNase (10 U/µl), nuclei were solubilized (10 mM Tris-HCl, pH 8.0, 10 mM EDTA and 1% SDS), aliquots transferred onto Whatman GF/C glass fibre filters (Sigma-Aldrich, Oakville, Ontario, Canada), washed with 5% trichloroacetic acid (TCA), and air-dried. ^{32}P-incorporation was measured by Cerenkov counting in a β-counter. The DNA concentration was determined spectrophotometrically and ^{32}P-incorporation is expressed as dpm/ng DNA.

RNA extraction, Reverse transcription, and qPCR

Total RNA was extracted from cardiomyocyte nuclei using the TRIzol method (Invitrogen) after homogenization with a motor-driven mixer. The concentration, quality and purity of total RNA were determined using a BioAnalyzer (Genome Innovation Center, Montreal, Quebec). Total RNA was treated with DNase 1 (10 U for 15 min at 37ºC) to remove potential contamination by genomic DNA. cDNA templates for PCR amplification were synthesized from 1 µg of total RNA with a reverse transcriptase kit (SuperArray).

Quantitative PCR (qPCR) was performed using SuperArray SYBR Green PCR kits and a Stratagene MX3000P qPCR system. Quantitative measurements were performed in triplicate and normalized to the average of three housekeeping internal controls (glyceraldehyde-3-phosphate dehydrogenase, β2-macroglobin, and heat shock protein 90-kDa α, class B member 1). All reactions included 2 µl of cDNA and

0.5 μM primers. Standard curves were made from 10-fold serial dilutions of cDNA pools containing high concentrations of the gene of interest. Data was collected and analyzed using MX3000P software. Relative gene expression was calculated using the comparative threshold cycle (Ct) method (15). The sequences of primers used for qPCR are shown in on-line Table II.

Ca^{2+}-imaging

Ca^{2+} concentration ([Ca^{2+}]) was measured in isolated nuclei with the ratiometric calcium indicator Fura-2/AM (Sigma-Aldrich). Fura2/AM was prepared daily as a 5mM stock solution in dimethylsulfoxide (DMSO). Right after the isolation, freshly isolated cardiomyocyte nuclei were resuspended in 0.5 ml of loading buffer containing 25 mM HEPES, 100 mM KCl, 2 mM K_2HPO_4 and 4 mM $MgCl_2$. Fura-2/AM was added to the suspension of isolated nuclei for a final concentration of 7.5 μM and incubated on ice for 45min. After an initial loading period, nuclei were washed of extracellular Fura-2/AM by centrifugation (2700 x g for 5 min, 4 ºC) to remove non-incorporated Fura-2/AM and were then added with 1000 μl of loading buffer containing 800 nM CaCl2 onto fluorodish. Ang-II, the AT1 agonist L162313, the AT2 agonist CGP42112A, IP3 or vehicle (DMSO) were added, directly in the bath, close to a single nuclei, pre-treated or free of selective blockers (candesartan, PD123177 or 2-aminoethoxydiphenyl-borate (2-APB)) to make a final concentration of 10 μM. A microspectrofluorimeter (IonOptix, Milton, MA) was used for fluorescence measurements. Excitation wavelengths were 340 and 380 nm. Fluorescence emission was detected at 509 nm and was expressed as the ratio of the two

excitation wavelengths (F340/F380). The amplitudes of Ca^{2+}-transients were calculated by subtraction of the baseline F340/F380 ratio from peak values. Ca^{2+}-concentrations were determined by calibrating the fluorescent signal by sequential addition of 9 µM ionomycin plus 1 mM $CaCl_2$ to obtain the maximal fluorescence ratio (Rmax) and 4 mM EGTA to obtain the minimum fluorescence ratio (Rmin). Autofluorescence was determined by subtracting fluorescence from non-loaded nuclei and from the fluorescence produced by fura-2-loaded nuclei.

Assessment of intracellular components of angiotensin synthesis system Cardiomyocytes were lysed by sonication in ice-cold 1 M acetic acid containing a protease/inhibitor mixture (Sigma S8820). The lysate was sedimented at 15,000 × g for 15 min, and the supernatant was dried in a vacufuge, followed by reconstitution in 1% acetic acid. The samples were applied to a conditioned DSC-18 column (Supelco), washed, and eluted with methanol. The eluted samples were dried and reconstituted in PBS for enzyme-linked immunosorbent assay (ELISA, Peninsula Labs). Ang-II was measured by quantitative competitive ELISA, using a specific anti-Ang-II antibody (Peninsula Labs), which was previously validated by high-performance liquid chromatography chip/mass spectrometric analysis (7). ELISA was performed on anti-Ang-II antibody-coated 96-well dishes. Competitive binding of synthetic biotinylated Ang-II, in the presence of the extracted peptide, was detected with streptavidin-horseradish peroxidase conjugate. A standard curve, generated from binding of a constant amount of biotinylated Ang-II with increasing concentrations of non-biotinylated synthetic Ang-II, was used to calculate the concentration of the

peptide in the sample. The concentration of Ang-II in the cell lysates is expressed as femtomoles per milligram of protein. Components of the Ang-II biosynthetic pathway (angiotensinogen, renin, angiotensin converting enzyme, and cathepsin) were quantified in cardiomyocyte lysates by qRT-PCR, as described above.

Statistical analysis

Data are expressed as mean ± S.E.M. ANOVA with Tukey's post-hoc test was used for statistical comparison. A P-value <0.05 was considered statistically significant.

Results

Endogenous AT1 and AT2 Receptors Localize to Nuclei Isolated from Cardiomyocytes and Cardiac Tissue

To examine the intracellular localization of AT1 and AT2 receptors, we isolated membrane, cytosolic, and nuclear fractions from isolated cardiac myocytes and from whole adult rat hearts. In initial studies, we characterized nuclear AT1 and AT2 receptors from intact cardiac tissue preparations. However, to be sure that biochemical results applied specifically to cardiomyocytes, we developed a nucleus-enriched preparation from isolated cardiomyocytes. All results shown in this paper were obtained from cardiomyocyte nuclei, whereas the results from cardiac tissue preparations are provided under supplemental data. The specificity of the isolated cardiomyocyte preparation was characterized by immunoblot with antibodies to various tissue-selective protein markers and cell populations (supplemental Fig. S1A). Isolated cardiomyocytes showed strong immunoreactive signals for myosin heavy chains, and no signals for Van Willebrand factor, neuron-specific enolase, discoidin domain receptor 2, or α-smooth muscle actin, which were found in the expected non-cardiomyocyte samples.

Cellular fractionations were validated by Western blots for calpactin-I (cell membrane, 38 kDa), GRP-78 (endoplasmic reticulum, 78 kDa), Nup62 (nuclear pore central plug, 62 kDa), histone-3 (cell nuclei, 17 kDa), and GM130 (Golgi cisternae, 130 kDa), respectively (Fig. 1A and supplemental Fig. 2A). Both AT1R (~43 kDa) and AT2R

(~47 kDa) immunoreactivity was detected in the membrane or crude cell fraction A, as were calpactin I, GRP-78, and GM130. After further purification steps, the final nuclear fraction or fraction D was enriched in nucleoporin 62 (Nup62), histone-3, AT1R, and AT2R immunoreactivity. In contrast, fraction D was significantly depleted of calpactin-I, GRP-78, and GM130 immunoreactivity. Both N (Alomone) and C (Santa Cruz) terminal antibodies recognized AT1R and AT2R in the nuclear fraction (D); results shown are with the Santa Cruz antibody. Fig. 1B shows mean intensities of the various bands in cytosolic (fraction B) and nuclear (fraction D) fractions as a ratio of calpactin-I immunoreactivity in the membrane (fraction A), and demonstrates a substantial reduction in non-nuclear markers (GRP-78 and GM130) and increase in nuclear markers (Nup62 and histone-3), along with AT1R/AT2R, in nuclear-enriched preparations. The morphological properties of rat cardiomyocyte nuclei were analyzed as shown in Fig. 1C, and similar to those of nuclei obtained from cardiac tissue (supplemental Fig. S2C). Phase-contrast microscopic imaging (lower panel) reveals the integrity of the nuclei, with an intact nuclear envelope surrounding each nucleus. The freshly isolated nuclei were stained by DNA interactive agents DRAQ5 (Fig. 1C) or Hoechst 33342 dye (supplemental Fig. S2C). Finally, very high concentrations of DNA were found in the isolated nuclei (e.g. nuclear 909 ± 46 μg/ml, versus cytoplasmic supernatant 114 ± 17 μg/ml, $p < 0.001$, $n = 8$/group; Fig. 1D). The data in Fig. 1 confirm that both AT1R and AT2R are present in cardiomyocyte nuclei.

To further investigate the subcellular localization of ATRs, we used confocal immunofluorescence microscopy with deconvolution to image isolated adult rat

ventricular cardiomyocytes decorated with antibodies against AT1R and AT2R, as illustrated in Fig. 2. AT1R and AT2R antibodies revealed a striated pattern consistent with the presence at the T-tubular network (Fig. 2, Aa and Ba). Immunofluorescence was also observed around the nucleus. Fig. 2, Ab and Bb, show the same cardiomyocytes stained for Nup62. Fig. 2, Ac and Bc, indicate extensive colocalization, more clearly evident in the higher magnification images in the insets. Phase-contrast reference images of the same cells are shown in Fig. 2, Ad and Bd. Similar results to those shown in Fig. 2 were obtained in all 40 cardiac cells from 10 rats examined for AT1R and all 30 cells from 10 rats studied for AT2R. No signal was observed in cells where the primary antibodies were omitted.

Differential Subcellular Trafficking of Ang-II: Extracellular Versus Intracellular Injection

Fig. 3 shows in vitro fluorescence imaging of intracellular Ang-II distribution after extracellular administration of Ang-II labeled with FITC to freshly isolated cardiomyocytes. High resolution images were then acquired by confocal microscopy at 5-min intervals. A 60-min time course confirmed the trafficking of Ang-II inside the cell, without any clear specificity for the nucleus. FITC-labeled Ang-II trafficking was significantly changed by the AT1R antagonist valsartan (10 μM), indicating that binding to cell membrane AT1R receptors is important for Ang-II internalization (Fig. 3B). (For corresponding dark-field images, see supplemental Fig. S3.) The absence of nuclear Ang-II in Fig. 3A argues against endocytosis as the mechanism for ATR

localization and suggest that ATRs in the nuclear membrane are most likely a result of intracellular synthesis and trafficking.

We then microinjected fluorescently labeled Ang-II into the cytoplasm of single cardiomyocytes to analyze the intracellular distribution of Ang-II (Eppendorf Femtojet; 1 nM Ang-II in 50 to 75 fl per cell), as shown in Fig. 4A. Although FITC-Ang-II rapidly diffused throughout the cytoplasm, the fluorescence was enriched or sequestered in the perinuclear region of injected cells 10–20 s after microinjection. The fluorescence decreased rapidly after 20 s but a clear signal at the nucleus (colocalization with 4′,6-diamidino-2-phenylindole) remained at 30 s and disappeared within 30 s thereafter. At no time was fluorescence detected in cells neighboring the microinjected cell, suggesting that the distribution observed in injected cells was due to intracellularly injected FITC-Ang-II and not extracellular diffusion. Similar results were obtained in 10 microinjected cells. Cells that were microinjected with valsartan (100 nM) prior to FITC-Ang-II showed little or no nuclear Ang-II fluorescence (Fig. 4B). The data in Fig. 4 suggest that nuclei have a higher density of Ang-II binding sites than do other subcellular structures.

Nuclear Ang-II Receptors Regulate Transcription Initiation

β-Adrenergic receptors were recently shown to stimulate [^{32}P]UTP incorporation in isolated nuclei (16). To determine whether nuclear ATRs are able to control transcription, freshly isolated cardiomyocyte (Fig. 5) or cardiac tissue (supplemental

Fig. S4) nuclei were incubated with [α-^{32}P]UTP in addition to ATR ligands and antagonists. Ang-II, L162,313 (AT1R-selective agonist), PD123177 (AT2R-selective agonist), candesartan (AT1R-selective antagonist), and PD123177 (AT2R-selective antagonist) were added directly to the incubation medium (Fig. 5A). Both non-selective and subtype-specific agonists increased the synthesis of RNA, although stimulation with an AT1R agonist produced a greater response than with the AT2R agonist (390 ± 16 cpm/ng of DNA versus 181 ± 7 cpm/ng of DNA, n = 4/group, $p < 0.001$). Both AT1R and AT2R antagonists significantly reduced the ability of Ang-II to enhance transcription.

To determine whether the activation of heterotrimeric G proteins are involved in coupling ATRs within the nuclear membrane to transcription, freshly isolated nuclei were pre-treated for 120 min with pertussis toxin. Pretreatment of isolated cardiomyocyte nuclei with pertussis toxin blocked the ability of Ang-II to increase de novo RNA synthesis (Fig. 5B). Thus, G_i is involved in coupling Ang-II receptors to transcription.

Ribosomal RNA (rRNA) constitutes the most abundant form of RNA. To determine whether stimulation of ATRs on nuclear membranes alters the abundance of rRNA following stimulation of isolated nuclear preparations, total RNA was resolved on 2% agarose gels and visualized by staining with ethidium bromide. Ang-II increased rRNA levels (Fig. 5C). Overall, Ang-II increased the signal strength (18 and 28 S) to 2.09 ± 0.08 OD, compared with 1.02 ± 0.02 OD in control (n = 4/group, $p < 0.001$). The Ang-

II effect was attenuated by valsartan and PD123177, which reduced the signal strength to 1.21 ± 0.04 OD and 1.11 ± 0.07 OD (n = 4/group, $p < 0.001$), respectively. Responses in total cardiac nuclear preparations (supplemental Fig. S4) were qualitatively similar to results from isolated cardiomyocyte nuclei (Fig. 5).

Nuclear Ang-II Receptors Regulate NFκB Gene Expression

Studies have shown that Ang-II is implicated in the activation of various nuclear transcription factors, including NFκB, and control of NFκB gene transcription is a potentially important regulatory mechanism (17). To assess the possible role of nuclear ATRs in the control of NFκB transcription, we treated isolated cardiomyocytes and purified nuclei with different concentrations of Ang-II. Following RNA isolation, the expression of NFκB was assessed by qPCR and normalized to the average of three housekeeping genes, β2-microglobulin, glyceraldehyde-3-phosphate dehydrogenase, and heat shock protein 90-kDa α, class B member 1. The primer sequences are provided in supplemental Table S2. Ang-II produced clear concentration-response curves, both when applied to intact cells and to nuclei isolated from cardiac tissues (supplemental Fig. S5A). Fig. 6A shows dose-response results obtained from 120-min applications of Ang-II to isolated intact cardiomyocytes (extracellular) or to nuclear preparations isolated from cardiomyocytes. At higher concentrations, there was a significantly greater increase in NFκB mRNA expression following Ang-II application to cardiomyocyte-nuclear preparations versus extracellular application to isolated cardiomyocytes. Preincubation of nuclei with valsartan (10−6 M) or PD123177 (10−6

M) prior to Ang-II administration reduced the Ang-II-induced increase in NFκB mRNA abundance (49 and 39% inhibition, respectively, versus Ang-II alone; n = 4/group, $p < 0.001$, Fig. 6B), whereas pretreatment with both antagonists abolished the NFκB mRNA expression response to Ang-II (n = 4, p = NS versus control).

Nuclear AT1R Stimulation Induces Nuclear [Ca^{2+}] Responses via IP3R-mediated Mechanisms and Thereby Influences Transcription Initiation

The nuclear envelope serves as a pool for calcium and has been proposed to regulate nuclear Ca^{2+} signals (18). Several mechanisms for generating Ca^{2+}-transients in the nucleus have been identified (19). The effect of ATR agonists on nuclear Ca^{2+} concentration was examined in freshly isolated nuclei using the ratiometric fluorescent Ca^{2+} indicator, Fura-2/AM. Exposure to vehicle alone did not alter nuclear Ca^{2+} signals (supplemental Fig. S6). Exposure of nuclei to Ang-II (10 μM) produced a prompt increase in [Ca^{2+}]. In the example shown in Fig. 7A, [Ca^{2+}] in nuclei isolated from cardiomyocytes rose from a baseline value of 111 to 243 nM, followed by a return to baseline values. The AT1R-selective agonist L162,313 (10 μM) also caused an intranuclear [Ca^{2+}] response (Fig. 7B), and the Ang-II response was prevented by co-administration with the AT1R inhibitor candesartan (10 μM) (Fig. 7C). Unlike AT1R-selective agonists, the AT2R agonist CGP42112A (10 μM) failed to elicit a nuclear [Ca^{2+}] response (Fig. 7D) and the AT2R antagonist PD123177 (10 μM) was unable to prevent an Ang-II-mediated Ca^{2+} rise (Fig. 7E). Overall mean data (n = 4/group) are summarized in Fig. 7F, indicating a significant increase in nuclear [Ca^{2+}]

with AT1R agonists, which is blocked by an AT1R antagonist. AT2R selective agonists produced no significant change in [Ca^{2+}], nor did antagonism of AT2R significantly attenuate the response to Ang-II. Similar results were obtained in nuclei isolated from whole hearts (supplemental Fig. S7).

IP3 is an important mediator of nuclear Ca^{2+} mobilization via nuclear envelope Ca^{2+} stores (20). We therefore tested the hypothesis that Ang-II regulates nuclear [Ca^{2+}] via IP3-dependent Ca^{2+} release. As shown in Fig. 8A, IP3 (10 μM) caused a transient increase of [Ca^{2+}] in nuclei isolated from cardiomyocytes, whereas the application of IP3 after pre-treatment with the IP3R blocker 2-APB (10 μM) failed to increase nuclear [Ca^{2+}] significantly (Fig. 8B). Pretreatment of nuclei with 2-APB suppressed the nuclear [Ca^{2+}] responses induced by Ang-II (Fig. 8C). Overall mean ± S.E. [Ca^{2+}] response amplitudes are summarized in Fig. 8D. Similar results were seen for nuclei isolated from whole hearts (supplemental Fig. S8).

To examine the potential role of the AT1R-mediated nuclear Ca^{2+} rise in the AT1R-induced transcription response, we pretreated cardiomyocyte nuclei with various concentrations of 2-APB prior to stimulation with Ang-II, L-162,313 (AT1R agonist), or CGP42112A (AT2R agonist). At a threshold concentration of 1 μM, 2-APB significantly decreased transcription initiation by Ang-II (Fig. 9A, n = 4/condition, $p < 0.05$) and by the AT1R agonist L-162,313 (Fig. 9B, n = 4/condition, $p < 0.01$). Maximum inhibition with 200 μM APB suppressed but did not eliminate Ang-II and L-162,313 responses, pointing to Ca^{2+}-dependent and Ca^{2+}-independent components.

Consistent with the lack of nuclear [Ca^{2+}] response to AT2R stimulation, 2-APB failed to alter CGP42112A-induced transcription initiation (Fig. 9C, n = 4/condition). Similar results were obtained with nuclei isolated from intact cardiac tissues (supplemental Fig. S9).

Assessment of Intracellular Components of Angiotensin Synthesis System

We found by ELISA that lysates prepared from isolated cardiomyocytes contain Ang-II at concentrations of 32.7 ± 4.1 fmol/mg of protein in the free cytosol. In addition, we found by qPCR that components required to produce Ang-II such as angiotensin converting enzyme, renin, angiotensinogen, and cathepsin are present inside cardiomyocytes (supplemental Fig. 1B).

Discussion

Main Findings

In the present study, we examined the subcellular localization of Ang-II receptors and their functionality in adult rat ventricular cardiomyocytes. Our data indicate that both AT1R and AT2R localize to and signal at the nuclear envelope, and that this localization is not a result of post-endocytotic trafficking. We also found that nuclear AT1Rs and AT2Rs mediate de novo RNA synthesis, affecting the abundance of both rRNA and NFκB mRNA, and that G_i availability is essential for this Ang-II effect. Ang-II signaling via AT1Rs induces [Ca^{2+}] responses in isolated nuclei via IP3R-dependent pathways, which participate in AT1R-induced de novo RNA synthesis.

Relation to Previous Studies of GPCR Nuclear Receptors

Classically, GPCRs, which comprise the largest protein superfamily in the human genome, are thought to induce intracellular effects via downstream signaling pathways from the plasma membrane (21, 22). In recent years, we and others have confirmed that endothelin (15), β- and α-adrenergic (17, 23), prostaglandin E2 (24) receptors, in addition to the signaling molecules associated with many GPCRs, including adenylate cyclase (25), G-protein coupled receptor kinases (GRK) (26, 27), phospholipase proteins (22), Gi, Gs, and Gq, are present on the nuclear/perinuclear membranes in a constitutive manner, independent of agonist stimulation. Determining

the subcellular localization of proteins provides crucial information concerning their function and interaction with other molecules in a specific microenvironment, and thus represents a critical step in genome annotation.

The data in the present paper suggest that Ang-II stimulates cardiomyocyte nuclear receptors to induce transcriptional responses in a Gi-dependent manner, similar to previous observations for cardiac nuclear β-adrenoceptors (17). We found that Ang-II increases $[Ca^{2+}]i$ in nuclear-enriched preparations via AT1Rs. Intracellular Ang-II increases nuclear $[Ca^{2+}]$ in vascular smooth muscle cells, an effect that is blocked by intracellular but not extracellular AT1R blockade (28). Intracellular application of Ang-II increases cell $[Ca^{2+}]i$ in A7r5 vascular smooth muscle cells lacking extracellular ATRs, an effect prevented by AT1R, but not AT2R blockers (29). Nuclear Ca^{2+} signaling appears to be an important regulator of gene transcription, particularly in neurons (30), and IP3 receptors are involved in nuclear Ca^{2+} signaling in a muscle cell line (31). Our observation of nuclear AT1R-selective effects to increase nuclear $[Ca^{2+}]$ suggests a potential role for AT1R-mediated nuclear Ca^{2+} changes in transcriptional responses. The degree of $[^{32}P]$UTP incorporation enhancement was greater with nuclear preparation application of the AT1R agonist L-162,313 than with the AT2R agonist CGP42112A (Fig. 5A), consistent with the notion that AT1R-related Ca^{2+}-dependent nuclear signaling may participate in transcriptional responses. However, clearly the Ang-II-induced transcriptional response does not depend solely on increased nuclear $[Ca^{2+}]$, because Ang-II-induced rRNA (Fig. 5C) and NFκB (Fig. 6B) RNA expression changes were sensitive to both AT1R and AT2R blockade, and selective AT2R stimulation with CGP42112A-induced transcriptional

responses. Further work will be needed to characterize in detail how Ang-II induces nuclear [Ca^{2+}] responses and to define nuclear [Ca^{2+}]-sensitive and -insensitive transcriptional control pathways.

Evidence for a Role of Intracellular Ang-II Signaling

The involvement of an intracellular renin-angiotensin system in biological responses has long been debated. We found significant expression of the components needed to produce Ang-II in cardiomyocyte lysates, and measured cytoplasmic Ang-II concentrations of over 30 fmol/mg of protein, of the same order as reported by Singh et al. (5). Ichihara et al. (32) demonstrated the existence of nonproteolytically activated intracardiac prorenin and elevated tissue Ang-II concentrations in genetically hypertensive rats, which produced end organ damage despite prevention of systemic renin-angiotensin activation. By contrast, the prevention of intracellular prorenin activation fully prevented cardiac fibrosis, despite the maintenance of systemic renin-angiotensin activation and severe hypertension (32). Mice engineered to lack intracardiac angiotensinogen lack cardiac hypertrophy and fibrosis despite hypertension comparable with similarly hypertensive control mice (33). In a rat vascular smooth muscle cell line (A7r5) devoid of plasma membrane ATRs, intracellular (liposome-based) Ang-II delivery enhances cell proliferation, whereas extracellular Ang-II has no effect, with intracellular Ang-II responses suppressed by intracellular application of AT1R or AT2R blockers (29). Independent of systemic hemodynamic effects, local cardiac Ang-II may cause deleterious

myocardial remodeling and functional deterioration post-myocardial infarction (34). In summary, there is evidence for a role of intracellular Ang-II signaling in cardiovascular remodeling. Our data, which indicate that AT1Rs and AT2Rs are present on cardiomyocyte nuclei and that Ang-II induces AT1R- and AT2R-mediated transcriptional responses in purified nuclear preparations, suggest that nuclear ATRs may be important mediators of intracellular Ang-II effects on the heart.

Potential Role of Nuclear AT1 and AT2 Receptors in Cardiac Remodeling

Ang-II is an important signaling molecule for cardiac remodeling, although there remains uncertainty over whether cardiac Ang-II signaling alone is enough to induce remodeling or whether Ang-II actions conspire with stressors (like hypertension and excess hemodynamic load) to induce remodeling (35). Overexpression of AT1Rs is a much more potent stimulus to cardiac remodeling than Ang-II overproduction, suggesting that receptor density may be the limiting factor for Ang-II-related remodeling (35). It has long been known that radiolabeled Ang-II preferentially localizes in the perinuclear regions of cardiomyocytes following intraventricular injection (36). The presence of nuclear Ang-II receptors has been demonstrated in the liver (11, 12) and kidneys (37). Similar to our findings, direct application of Ang-II to isolated renal-cortical cell nuclei enhances in vitro transcription of a variety of genes (37). Ang-II activates several nuclear transcription factors and is implicated in the pathogenesis of vascular damage through NFκB (18). NFκB increases the expression of cytokines, enzymes, and adhesion molecules, as well as

other products involved in inflammation, proliferation, and hypertrophy (38). Our observations raise the interesting possibility that direct nuclear receptor signaling may be an important mediator of the action of Ang-II to promote cardiac remodeling via altered gene transcription.

Novel Elements and Potential Implications

Our work is the first demonstration, to our knowledge, that cardiomyocytes express nuclear envelope Ang-II receptors that can induce changes in cardiac gene transcription, that Ang-II stimulation of nuclear receptors can induce nuclear [Ca^{2+}] responses via IP3-mediated pathways in an AT1R-specific fashion, and that blockade of IP3R-mediated nuclear [Ca^{2+}] changes suppress the AT1R-mediated effect on cardiac gene transcription. To demonstrate the properties of the nuclear angiotensin system in cardiomyocytes, we developed and applied a novel nucleus-enriched preparation from isolated cardiomyocytes, to our knowledge for the first time in the literature. Our findings provide mechanistic insights into observations suggesting that Ang-II acts through intracellular receptors to regulate cardiomyocyte growth and induce cardiac remodeling (39).

There is growing interest in the development of intracrine pharmacology, small molecule compounds designed to modulate intracellular signaling systems mediated by compounds synthesized within the target cell (40). Lipid-soluble renin inhibitors and angiotensin converting enzyme inhibitor prodrugs are particularly effective in inhibiting ATR-related glioblastoma (41) and neuroblastoma (42) cell growth, pointing

to the potential importance of blocking intracellular Ang-II signaling. Further information about the nature, role, and significance of cardiomyocyte nuclear ATRs should contribute to the development of rationally based intracrine pharmacology for cardiac remodeling prevention.

Potential Limitations

Transmembrane receptors can exist in monomeric, homodimeric, or heterodimeric states, and the multimeric state of the receptor may alter its pharmacological properties. AT1 and bradykinin B2 receptors form stable heterodimers, increasing G-protein activation (43). The dimerization status of the nuclear membrane ATRs could have important implications for the intracrine physiology of the renin-angiotensin system, but is beyond the scope of the present study. We have not investigated the specific molecular properties of nuclear ATRs, and it remains to be determined whether they are identical to cell-membrane receptors that are simply targeted to the nucleus, or whether a subset of ATRs with specific molecular compositions are selectively targeted to nuclear membranes.

Angiotensin-receptor blockers are known to suppress angiotensin-related cardiac remodeling. To act via nuclear angiotensin-receptor inhibition they would have to achieve significant intracellular concentrations. The extent to which commercially available agents cross the plasma membranes of heart cells is incompletely known, although telmisartan, a lipid-soluble agent, has been shown to achieve 10-fold concentration in the intracellular compartment versus culture medium (44).

Conclusions

The current study provides novel insights into cardiac intracellular Ang-II signaling by demonstrating the existence of nuclear AT1Rs and AT2Rs that are coupled to RNA transcription and nuclear Ca^{2+} signaling in cardiomyocytes. Ang-II acts via AT1Rs to induce Ca^{2+} mobilization in cardiomyocyte nuclear preparations via IP3 receptor-mediated mechanisms. A better understanding of the nature and role of nuclear Ang-II receptors will help to provide a better appreciation of the molecular basis for cardiac remodeling and hopefully lead to the development of improved pharmacological interventions for cardiac disease prevention and therapy.

Acknowledgments

We thank Annick Fortier for expert statistical analysis; George Vaniotis, Dr. Balazs Ordog, and Chantal St-Cyr for excellent technical assistance and suggestions; Dr. Clémence Merlen, Dr. Eric Thorin, and Dr. Ling Xiao for providing endothelial cells, smooth muscle cells, and brain tissue; and France Thériault for secretarial support.

Sources of funding

Supported by the Canadian Institutes of Health Research (MGP 6957) and the European-North American Atrial Fibrillation Research Alliance (ENAFRA) award from Fondation Leducq.

Disclosures section. None.

References

1. Dahlof, B., Devereux, R.B., Kjeldsen, S.E., Julius, S., Beevers, G., de Faire, U., Fyhrquist, F., Ibsen, H., Kristiansson, K., Lederballe-Pedersen, O., Lindholm, L.H., Nieminen, M.S., Omvik, P., Oparil, S., and Wedel, H. (2002) Lancet 359(9311), 995-1003
2. Wachtell, K., Hornestam, B., Lehto, M., Slotwiner, D.J., Gerdts, E., Olsen, M.H., Aurup, P., Dahlof, B., Ibsen, H., Julius, S., Kjeldsen, S.E., Lindholm, L.H., Nieminen, M.S., Rokkedal, J., and Devereux, R.B. (2005) J Am Coll Cardiol 45(5), 705-711
3. Groth, W., Blume, A., Gohlke, P., Unger, T., and Culman, J. (2003) J Hypertens 21(11), 2175 2182
4. De Mello, W.C. (2006) Regul Pept 133(1-3), 10-12
5. Singh, V.P., Le, B., Khode, R., Baker, K.M., and Kumar, R. (2008) Diabetes 57(12), 3297-3306
6. Re, R.N., and Cook, J.L. (2007) Nat Clin Pract Cardiovasc Med 4(10), 549-557
7. Singh, V.P., Le, B., Bhat, V.B., Baker, K.M., and Kumar, R. (2007) Am J Physiol Heart Circ Physiol 293(2), H939-H948
8. Sadoshima, J., Xu, Y., Slayter, H.S., and Izumo, S. (1993) Cell 75(5), 977-984
9. Peters, J., Farrenkopf, R., Clausmeyer, S., Zimmer, J., Kantachuvesiri, S., Sharp, M.G., and Mullins, J.J. (2002) Circ Res 90(10), 1135-1141

10. De Mello, W.C. (1998) Hypertension 32(6), 976-982

11. Booz, G.W., Conrad, K.M., Hess, A.L., Singer, H.A., and Baker, K.M. (1992) Endocrinology 130(6), 3641-3649

12. Tang, S.S., Rogg, H., Schumacher, R., and Dzau, V.J. (1992) Endocrinology 131(1), 374-380

13. Battle, T., Arnal, J.F., Challah, M., Michel, J.B. (1994) Tissue Cell 26(6), 943–955

14. Boivin, B., Chevalier, D., Villeneuve, L.R., Rousseau, E., and Allen, B.G. (2003) J Biol Chem 278(31), 29153-29163

15. Livak, K.J., and Schmittgen, T.D. (2001) Methods 25(4), 402-408

16. Boivin, B., Lavoie, C., Vaniotis, G., Baragli, A., Villeneuve, L.R., Ethier, N., Trieu, P., Allen, B.G., and Hebert, T.E. (2006) Cardiovasc Res 71(1), 69-78

17. Meberg, P.J., Kinney, W.R., Valcourt, E.G., and Routtenberg, A. (1996) Brain Res Mol Brain Res 38(2), 179-190

18. Malviya, A.N., and Rogue, P.J. (1998) Cell 92(1), 17-23

19. Zima, A.V., Bare, D.J., Mignery, G.A., and Blatter, L.A. (2007) J Physiol 584(Pt 2), 601-611

20. Gerasimenko, O., and Gerasimenko, J. (2004) J Cell Sci 117(Pt 15), 3087-3094

21. Bockaert, J., and Pin, J.P. (1999) EMBO J 18(7), 1723-1729

22. Gether, U. (2000) Endocr Rev 21(1), 90-113

23. Wright, C.D., Chen, Q., Baye, N.L., Huang, Y., Healy, C.L., Kasinathan, S., and O'Connell, T.D. (2008) Circ Res 103(9), 992-1000

24. Bhattacharya, M., Peri, K.G., Almazan, G., Ribeiro-da-Silva, A., Shichi, H., Durocher, Y., Abramovitz, M., Hou, X., Varma, D.R., and Chemtob, S. (1998) Proc Natl Acad Sci U S A 95(26), 15792-15797

25. Willard, F.S., and Crouch, M.F. (2000) Immunol Cell Biol 78(4), 387-394

26. Martini, J.S., Raake, P., Vinge, L.E., DeGeorge, B., Jr., Chuprun, J.K., Harris, D.M., Gao, E., Eckhart, A.D., Pitcher, J.A., and Koch, W.J. (2008) Proc Natl Acad Sci U S A 105(34), 12457-12462

27. Sorriento, D., Ciccarelli, M., Santulli, G., Campanile, A., Altobelli, G.G., Cimini, V., Galasso, G., Astone, D., Piscione, F., Pastore, L., Trimarco, B., and Iaccarino, G. (2008) Proc Natl Acad Sci U S A 105(46), 17818-17823

28. Haller, H., Lindschau, C., Erdmann, B., Quass, P., and Luft, F.C. (1996) Circ Res 79(4), 765-772

29. Filipeanu, C.M., Henning, R.H., de Zeeuw, D., and Nelemans, A. (2001) Br J Pharmacol 132(7), 1590-1596

30. Bezin, S., Charpentier, G., Lee, H.C., Baux, G., Fossier, P., and Cancela, J.M. (2008) J Biol Chem 283(41), 27859-27870

31. Kusnier, C., Cárdenas, C., Hidalgo, J., and Jaimovich, E. (2006) Biol Res 39(3), 541-553

32. Izchihara, A., Kaneshiro, Y., Takemitsu, T., Sakoda, M., Suzuki, F., Nakagawa, T., Nishiyama, A., Inagami, T., and Hayashi, M. (2006) Hypertension 47(5), 894-900

33. Kang, N., Walther, T., Tian, X.L., Bohlender, J., Fukamizu, A., Ganten, D., and Bader, M. (2002) J Mol Med 80(6), 359-366

34. Xu, J., Carretero, O.A., Lin, C.X., Cavasin, M.A., Shesely, E.G., Yang, J.J., Reudelhuber, T.L., and Yang, X.P. (2007) Am J Physiol Heart Circ Physiol 293(3), H1900-H1907

35. Reudelhuber, T.L., Bernstein, K.E., and Delafontaine, P. (2007) Hypertension 49(6), 1196-1201

36. Robertson, A.L., Jr., and Khairallah, P.A. (1971) Science 172(988), 1138-1139

37. Li, X.C., and Zhuo, J.L. (2008) Am J Physiol Cell Physiol 294(4), C1034-C1045

38. Barnes, P.J., and Karin, M. (1997) N Engl J Med 336(15), 1066-1071

39. Baker, K.M., Chernin, M.I., Schreiber, T., Sanghi, S., Haiderzaidi, S., Booz, G.W., Dostal, D.E., and Kumar, R. (2004) Regul Pept 120(1-3), 5-13

40. Re, R.N., and Cook, J.L. (2008) J Clin Pharmacol 48(3), 344-350

41. Juillerat-Jeanneret, L., Celerier, J., Chapuis Bernasconi, C., Nguyen, G., Wostl, W., Maerki, H.P., Janzer, R.C., Corvol, P., and Gasc, J.M. (2004) Br J Cancer 90(5), 1059-1068

42. Chen, L., Re, R.N., Prakash, O., and Mondal, D. (1991) Proc Soc Exp Biol Med 196(3), 280-283

43. AbdAlla, S., Lother, H., and Quitterer, U. (2000) Nature 407(6800), 94-98

44. Shao J., Nangaku M., Inagi R., Kato H., Miyata T., Matsusaka T., Noiri E., Fujita T. (2007) J. Hypertens. 25, 1643–1649

Figure Legends

Figure 1. Immunoreactivity of angiotensin II receptor subtypes 1 and 2 in purified cardiomyocyte nuclei. A, Western blots showing expression of various markers on cardiomyocyte fractions. Isolated cardiomyocytes were fractionated into three fractions: membrane, cytosolic, and nuclear. Aliquots (40 µg) of each fraction were separated by SDS-PAGE and transferred onto PVDF-membranes. After blocking, membranes were incubated with antisera specific for calpactin-I, GRP-78, GM130, histone-3, Nup62, AT1 or AT2. Immunoreactive bands were visualized by ECL. B, Mean±SEM expression levels for GRP-78, GM130, histone-3, Nup62, AT1, AT2 normalized to calpactin-I. (N=6/antibody/fraction) **P<0.01, ***P<0.001 vs. respective cytosolic fraction. C, Representative images of a purified nuclear preparation. Top: DNA-staining with DRAQ 5; Bottom: Corresponding phase-contrast image. D, Mean±SEM DNA content (µg/ml) of cytoplasmic or nuclear fraction (N=8/group). ***P<0.001 vs. cytoplasmic.

Figure 2. Subcellular distribution of AT1 and AT2 receptors in adult rat ventricular cardiomyocytes. A, Panels a-d show representative results from a single cell. Panel a is a confocal image demonstrating the nuclear localisation of AT1R (green), b shows nuclear staining with nucleoporin p62 (red), c is a superimposed confocal image showing the colocalization of AT1R with Nup 62, coincident signals appear in yellow (Merge), d is a phase contrast image of the same cell. Data are representative

of 40 cells from 10 rats. B, Panels a-d show representative results from a single cell. Panel a is a confocal image demonstrating the nuclear localisation of AT2R (green), b shows nuclear staining with nucleoporin p62 (red), c is a superimposed confocal image showing the colocalization of AT2R with Nup 62, coincident signals appear in yellow (Merge), d is a phase contrast image of the same cell. Data are representative of 30 cells from 10 rats.

Figure 3. Endocytosis and intracellular trafficking of Ang-II. A, FITC-Ang-II (1 nM) was applied extracellularly to the bathing medium. Images are shown immediately after Ang-II application (0 min) and then 30 and 60 min later. Merged images are superimposed fluorescent images. B, cells were preincubated with valsartan (10 μM, for 25 min) prior to administration of Ang-II. Hoechst 33342 was used as a nuclear marker. Z-stacks were acquired every 5 min using a Zeiss LSM-510 confocal microscope. (N=6/group)

Figure 4. Subcellular localization of intracellularly applied FITC-Ang-II. A, phase contrast image showing myocyte immediately prior to injection. FITC-Ang-II (1 nM) was microinjected into freshly isolated cardiomyocytes and fluorescence visualized at 10, 20 seconds post-injection. B, Cells were microinjected with valsartan (100 nM) prior to FITC-Ang-II injection. DAPI was used as a nuclear marker. No fluorescence was observed in adjacent cells at any time. (Results similar to those in A and B were obtained for 10 microinjected cells from 10 rats each.)

Figure 5. AT1R and AT2R in nuclear membranes regulate cardiomyocyte transcription initiation. A, De novo RNA synthesis. Isolated cardiomyocyte nuclear preparations were stimulated with Ang-II, L 162,313 (a non-peptide AT1R-selective agonist), CGP 42112A (an AT2R-selective agonist), candesartan plus Ang-II, or PD123177 plus Ang-II (all at 10-μM), as indicated. Following the addition of antagonists candesartan (Cand) and PD123177, nuclei were preincubated for 30 min prior to the addition of Ang-II. ***P<0.001 vs. control; +P<0.05, +++P<0.001 vs. Ang-II. B, Cardiomyocyte nuclei were treated with PTX 5 μg/ml for 2 hours and then stimulated with Ang-II. Data represent mean ± SEM of at least five separate experiments performed in triplicate and normalized to control. ***P<0.001 vs. control; N.S. = non-significant vs. control. C, Representative 2% agarose gel electrophoresis of RNA extracted from purified cardiomyocyte nuclei of 2 separate experiments stained with ethidium bromide (GTP and CTP not omitted) under the following conditions: non-stimulated (lane 1 and 2); stimulated with Ang-II (10 μM, lane 3 and 4); stimulated with Ang-II in the presence of valsartan (10 μM, lane 5 and 6); stimulated with Ang-II in the presence of PD123177 (10 μM, lane 7 and 8). Results in lanes 1, 3, 5, and 7 are from one experiment, lanes 2, 4, 6, and 8 from another. 1 μg of each sample was loaded. Bottom panel shows mean±SEM results as arbitrary optical density (O.D.) units from 4 different experiments/condition. ***P<0.001 vs. control, ++P<0.01 vs. Ang-II.

Figure 6. Regulation of cardiomyocyte nuclear NF-κB mRNA expression by nuclear ATRs. Isolated nuclei were treated for 2 hours with Ang-II at different concentrations.

NF-κB mRNA was quantified by qPCR. A, Data are presented as NF-κB mRNA expression relative to an average of three housekeeping genes (N=6/concentration/group). *P<0.05 **P <0.01, ***P<0.001 vs. intact cells. B, Valsartan (10 μM) or PD123177 (10 μM) significantly reduced the Ang-II (10 μM) induced NF □B activity, antagonists completely abolished the NF-κB gene expression-response. Results are expressed as mean±SEM ***P<0.001 vs. Ang-II.

Figure 7. Coupling of ATRs to Ca^{2+} entry in cardiomyocyte nuclear enriched preparations. FURA-2/AM-loaded freshly isolated cardiomyocyte nuclei were seeded onto glass slides and nuclear Ca^{2+} concentration [Ca^{2+}] was measured with an IonOptix microspectrofluorimeter (λex = 340 and 380 nm; λem = 509 nm). Typical recordings of internal Ca2+ are shown, with recordings from all preparations studied shown in insets, after administration of: A, Ang-II (10 μM); B, L-162,313 (10 μM); C, candesartan (10 μM) plus Ang-II (10 μM); D, CGP 42112A (10 μM); E, PD123177 (10 μM) plus Ang-II (10 μM). F, Summary of mean±SEM [Ca^{2+}] transient amplitudes (N=4/group/condition) ***P<0.001 vs. control, N.S. = non-significant vs. control; arrows in A-E indicate the time of drug application.

Figure 8. IP3-dependent Ca^{2+} signals from isolated cardiomyocyte nuclei. Isolated nuclei were exposed to A, IP3 (10 μM). B, the IP3R blocker 2-APB (10 μM) followed by exposure to IP3. C, the IP3R blocker 2-APB (10 μM) followed by exposure to Ang-

II (10 μM). D, summary of [Ca^{2+}] transient amplitudes, mean±SEM (N=5/group/condition) **P<0.01 ***P<0.001; arrows indicate the time of drug application in A-C.

Figure 9. Role of IP3R-signaling for AT1R-mediated transcription initiation. Isolated nuclei were pre-treated with various concentrations of 2-APB for 30 minutes and incubated with: A, Ang-II B, L-162,313 or C, CGP42112A (all at 10 μM) and de novo RNA synthesis was measured by ^{32}P-UTP incorporation. ***P<0.001, **P<0.01 or *P<0.05 vs. agonist alone (Ang-II or L-162,313); #P<0.05 vs. 2 APB (50 μM), DMSO or H2O alone in A and B; N.S = non-significant from each other.

Figure 1

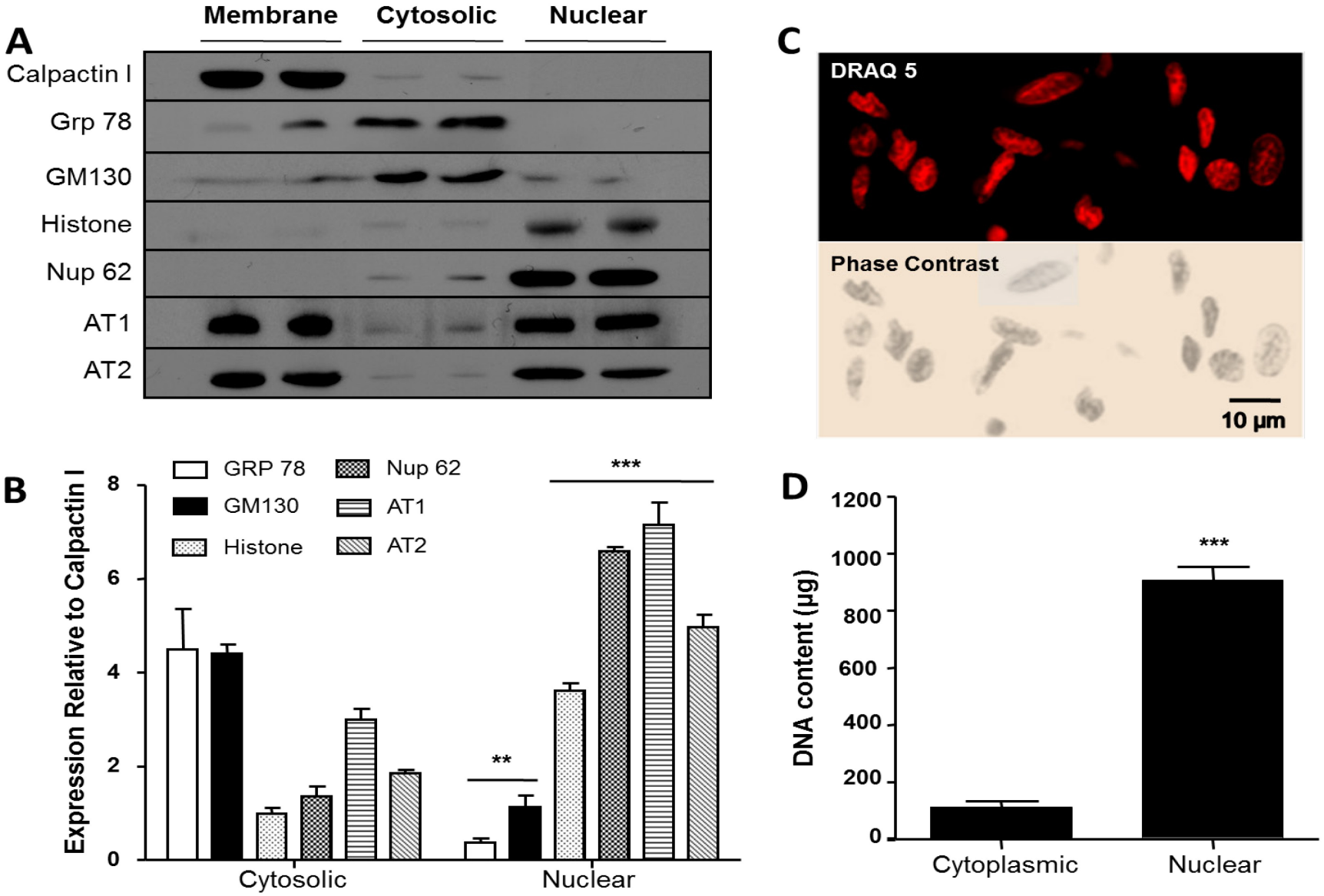
A
Membrane
Cytosolic
Nuclear
Calpactin I
Grp 78
GM130
Histone
Nup 62
AT1
AT2
B
GRP 78
GM130
Histone
Nup 62
AT1
AT2
Expression Relative to Calpactin I
0
2
4
6
8
**
***
Cytosolic
Nuclear
C
DRAQ 5
Phase Contrast
10 µm
D
DNA content (µg)
0
200
400
600
800
1000
1200
***
Cytoplasmic
Nuclear

Figure 2

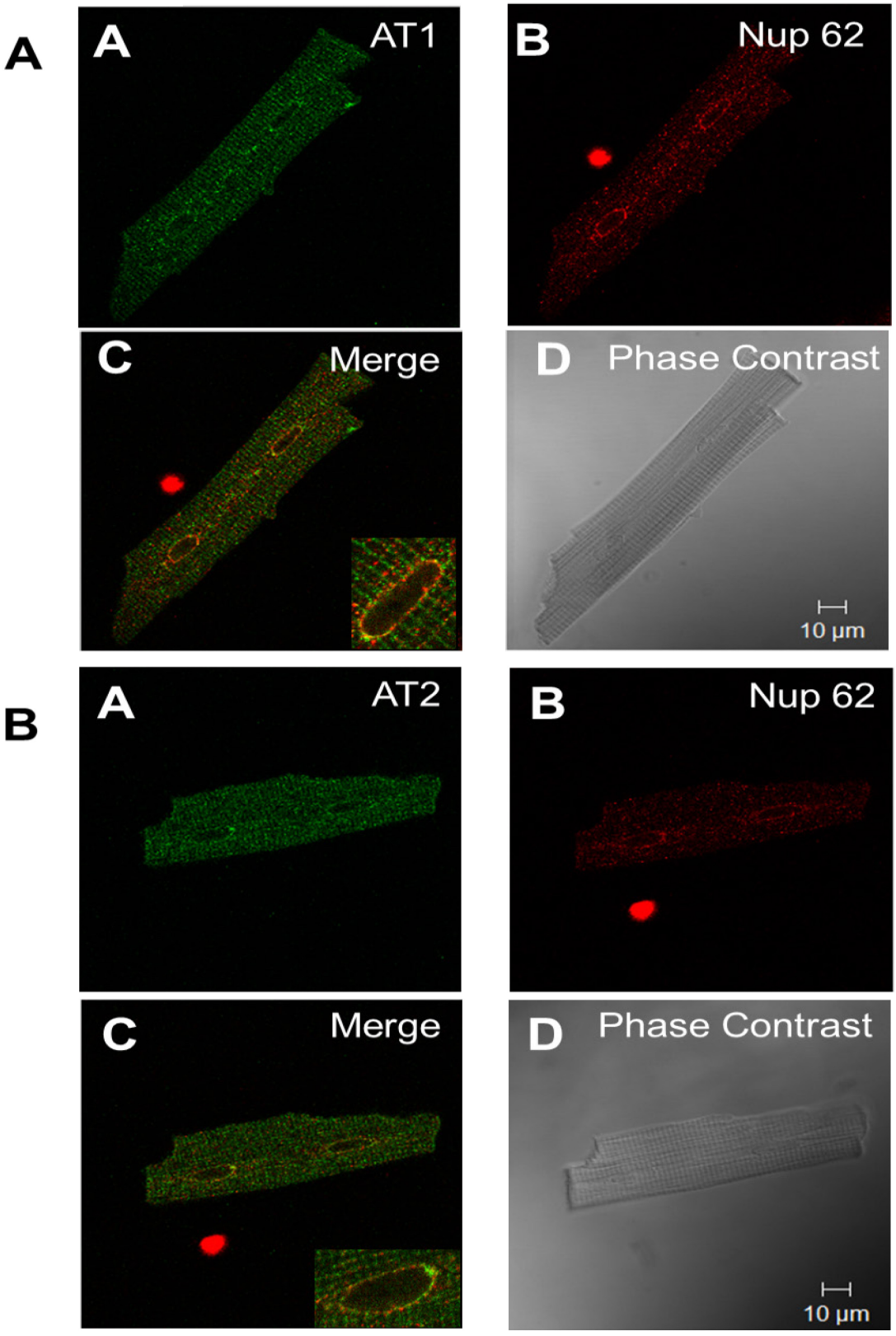
A
A
AT1
B
Nup 62
C
Merge
D
Phase Contrast
10 µm
B
A
AT2
B
Nup 62
C
Merge
D
Phase Contrast
10 µm

Figure 3

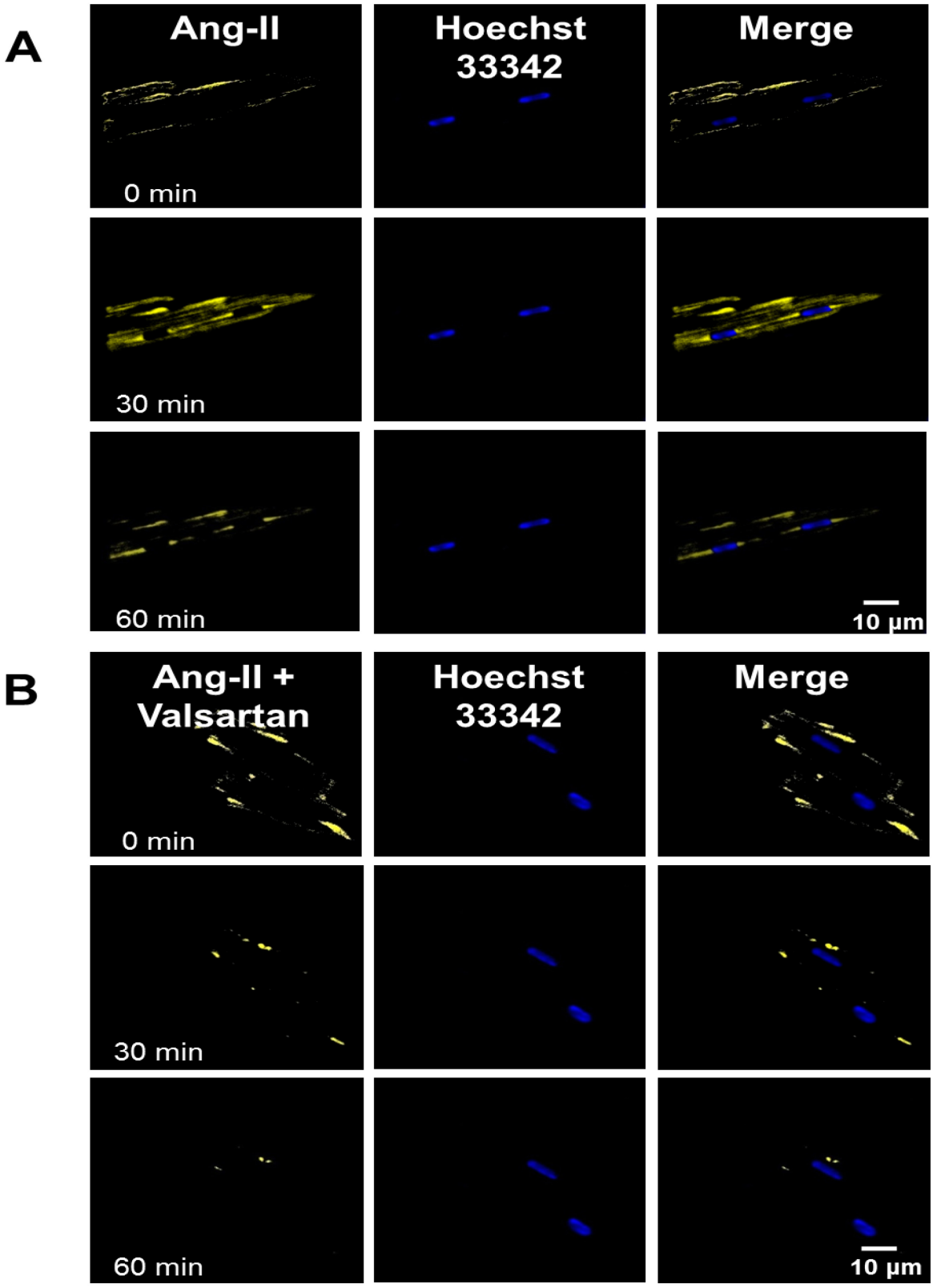
A
Ang-II
Hoechst 33342
Merge
0 min
30 min
60 min
10 µm
B
Ang-II + Valsartan
Hoechst 33342
Merge
0 min
30 min
60 min
10 µm

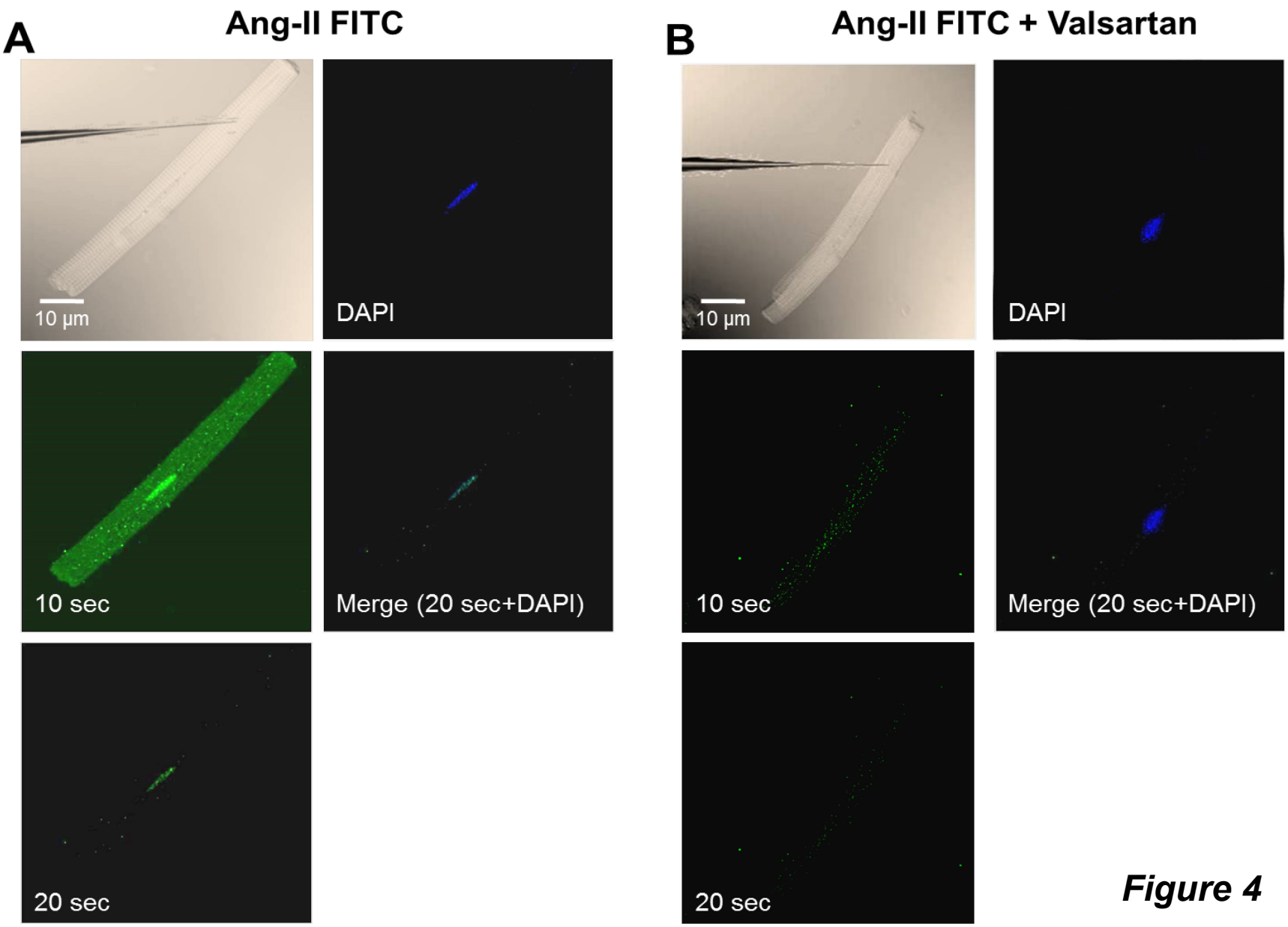
A
Ang-II FITC
10 µm
DAPI
10 sec
Merge (20 sec+DAPI)
20 sec
B
Ang-II FITC + Valsartan
10 µm
DAPI
10 sec
Merge (20 sec+DAPI)
20 sec

Figure 4

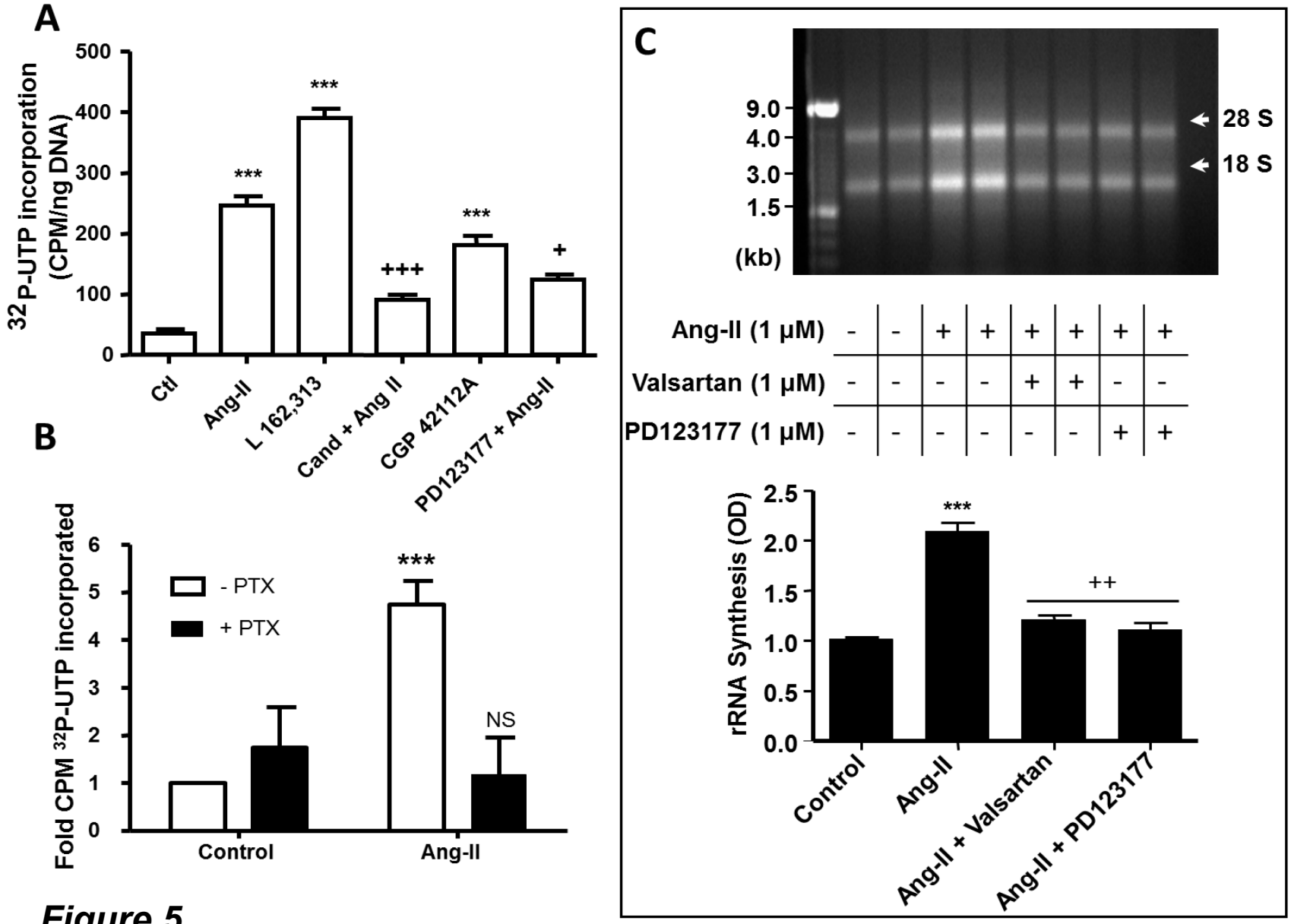
A
32P-UTP incorporation (CPM/ng DNA)
500
400
300
200
100
0
***
***
***
+++
+
Ctl
Ang-II
L 162,313
Cand + Ang II
CGP 42112A
PD123177 + Ang-II
B
Fold CPM 32P-UTP incorporated
6
5
4
3
2
1
0
- PTX
+ PTX
***
NS
Control
Ang-II
C
9.0
4.0
3.0
1.5
(kb)
28 S
18 S
Ang-II (1 μM) - - + + + + + +
Valsartan (1 μM) - - - - + + - -
PD123177 (1 μM) - - - - - - + +
rRNA Synthesis (OD)
2.5
2.0
1.5
1.0
0.5
0.0
***
++
Control
Ang-II
Ang-II + Valsartan
Ang-II + PD123177

Figure 5

Figure 6

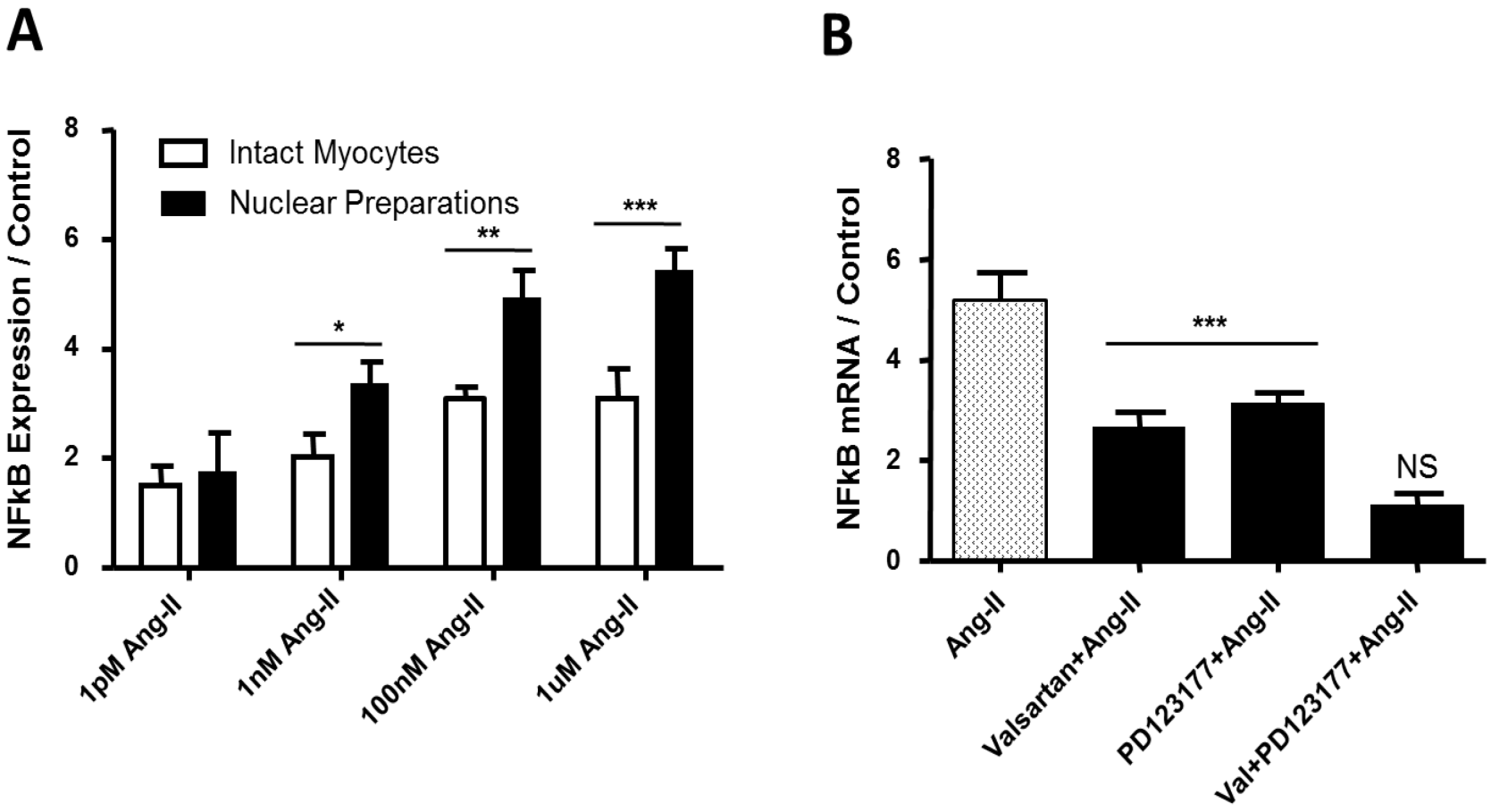
A
NFkB Expression / Control
0
2
4
6
8
Intact Myocytes
Nuclear Preparations
*
**
***
1pM Ang-II
1nM Ang-II
100nM Ang-II
1uM Ang-II
B
NFkB mRNA / Control
0
2
4
6
8
***
NS
Ang-II
Valsartan+Ang-II
PD123177+Ang-II
Val+PD123177+Ang-II

Figure 7

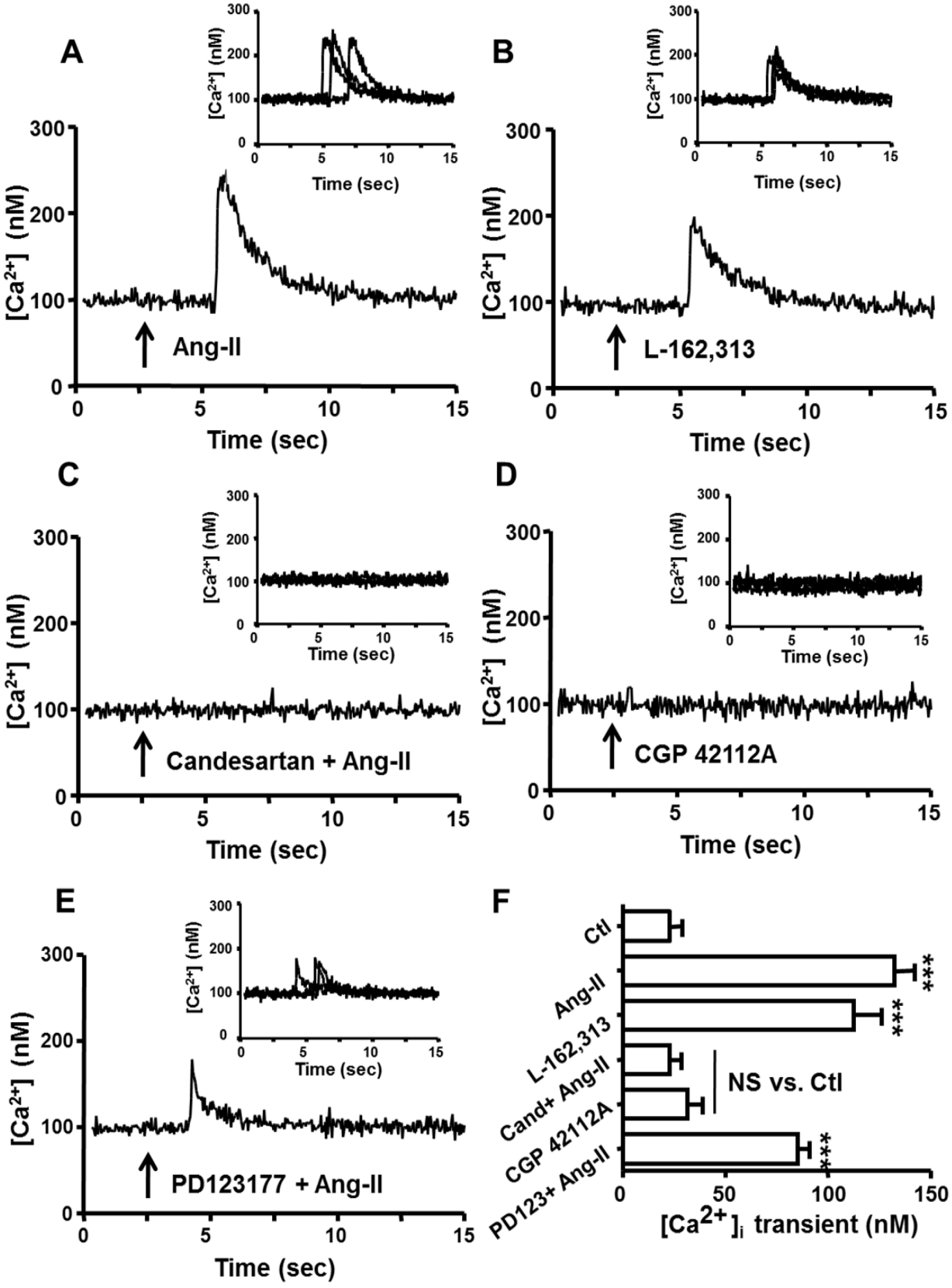
A
B
C
D
E
F
[Ca2+] (nM)
Time (sec)
Ang-II
L-162,313
Candesartan + Ang-II
CGP 42112A
PD123177 + Ang-II
Ctl
Ang-II
L-162,313
Cand+ Ang-II
CGP 42112A
PD123+ Ang-II
NS vs. Ctl
***
[Ca2+]i transient (nM)

Figure 8

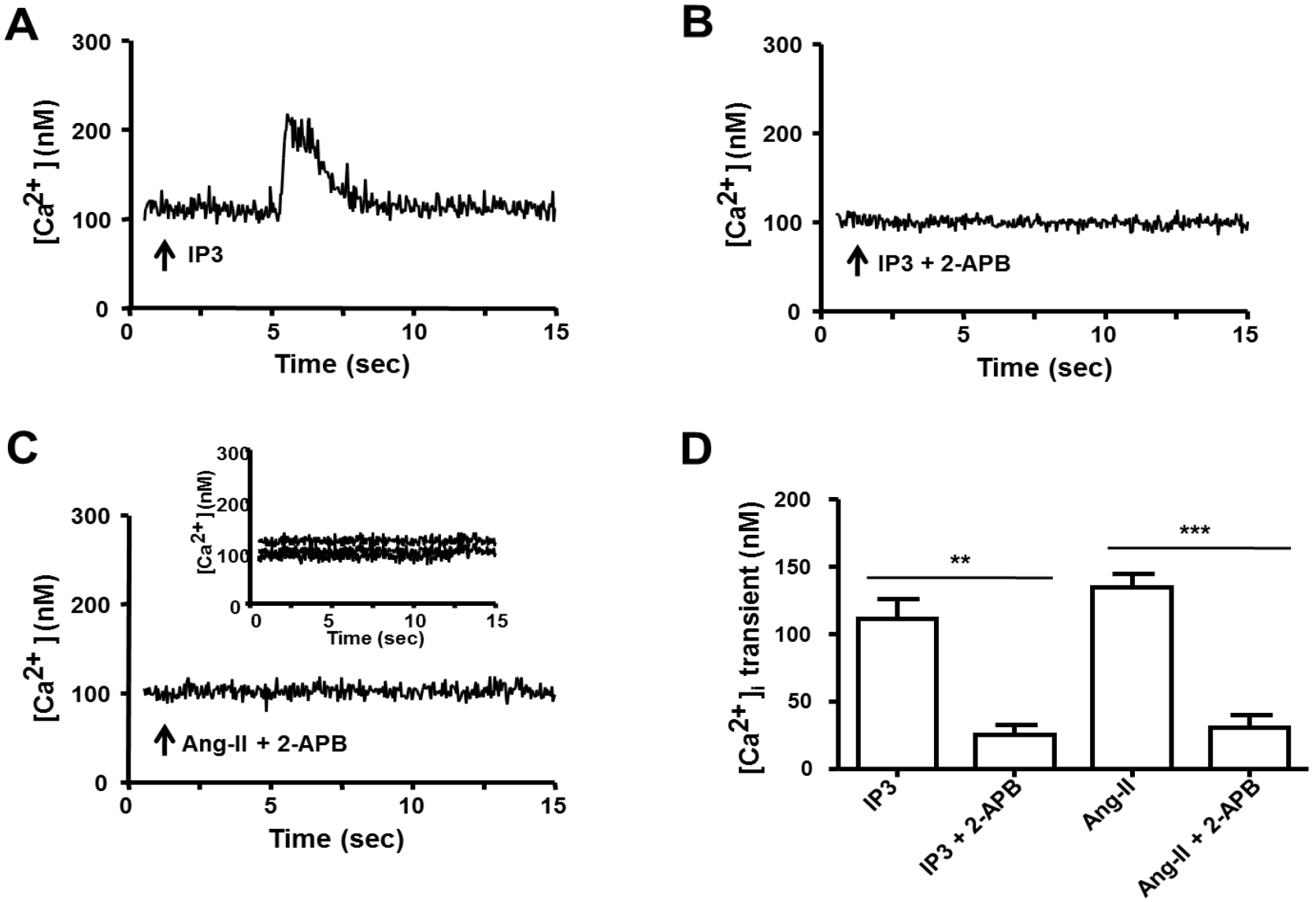
A
300
200
100
0
[Ca2+](nM)
IP3
0
5
10
15
Time (sec)
B
300
200
100
0
[Ca2+](nM)
IP3 + 2-APB
0
5
10
15
Time (sec)
C
300
200
100
0
[Ca2+](nM)
Ang-II + 2-APB
0
5
10
15
Time (sec)
300
200
100
0
[Ca2+](nM)
0
5
10
15
Time (sec)
D
200
150
100
50
0
[Ca2+]i transient (nM)
**
***
IP3
IP3 + 2-APB
Ang-II
Ang-II + 2-APB

Figure 9

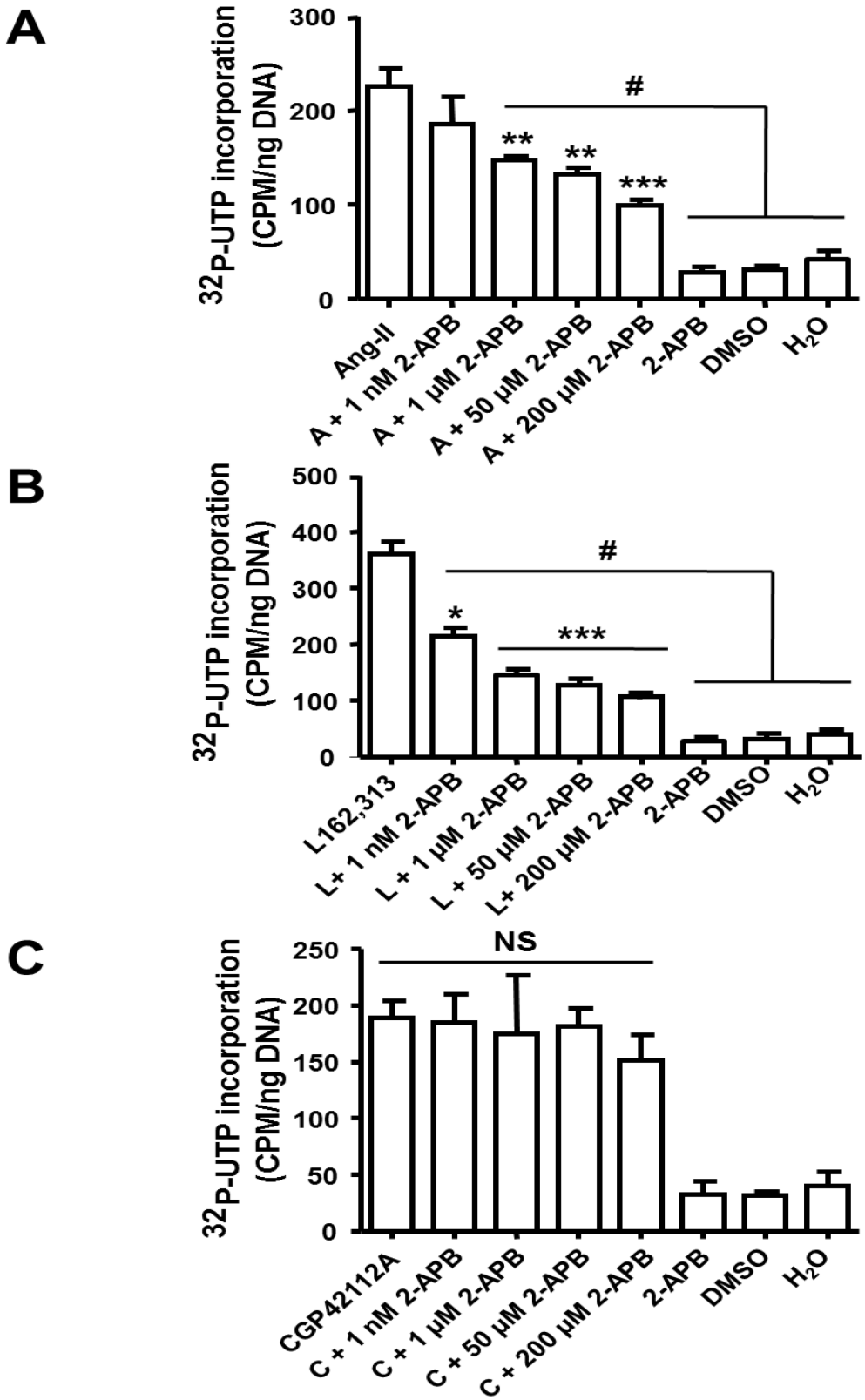
A
^{32}P-UTP incorporation (CPM/ng DNA)
300
200
100
0
#
**
**
***
Ang-II
A + 1 nM 2-APB
A + 1 µM 2-APB
A + 50 µM 2-APB
A + 200 µM 2-APB
2-APB
DMSO
H2O
B
^{32}P-UTP incorporation (CPM/ng DNA)
500
400
300
200
100
0
#
*
***
L162,313
L+ 1 nM 2-APB
L + 1 µM 2-APB
L + 50 µM 2-APB
L+ 200 µM 2-APB
2-APB
DMSO
H2O
C
^{32}P-UTP incorporation (CPM/ng DNA)
250
200
150
100
50
0
NS
CGP42112A
C + 1 nM 2-APB
C + 1 µM 2-APB
C + 50 µM 2-APB
C + 200 µM 2-APB
2-APB
DMSO
H2O

Supplemental Materials

Isolation of heart nuclei.

Nuclear isolation was performed according to a modified version of a previously-described method (13). Briefly, rat hearts were manually ground into a powder under liquid nitrogen, resuspended in cold phosphate-buffered saline (PBS) (137 mM NaCl, 10 mM phosphate, 2.7 mM KCl with a final pH of 7.4, NaOH) and homogenized with a Polytron. The total extract was labelled Fraction A. The subsequent steps were carried out on ice or in a cooling cabinet at 4°C. Homogenates were centrifuged at 1400 × g for 15 min and the supernatant, denoted Fraction B, was diluted 1:1 with buffer A (10 mM K-HEPES, 1.5 mM $MgCl_2$, 10 mM KCl, 1 mM DTT, 25 µg/ml leupeptin, 0.2 mM Na_3VO_4 with a final pH of 7.4, NaOH), incubated for 10 min on ice and re-centrifuged at a higher speed (3500 x g) for 15 min. The resulting supernatant was discarded and the pellet, containing crude nuclei (designated Fraction C) was resuspended in buffer B (0.3 M K-HEPES, 1.5 M KCl, 0.03 M $MgCl_2$, 25 µg/ml leupeptin, 0.2 mM Na_3VO_4 with a final pH of 7.4, NaOH), incubated on ice for 10 min, and centrifuged for 30 min at 5000 × g. The pellet, comprising a nuclear-enriched fraction (designated Fraction D), was resuspended in buffer C (20 mM Na-HEPES, 25% (volume/volume) glycerol, 0.42 M NaCl, 1.5 mM $MgCl_2$, 0.2 mM EDTA, 0.2 mM EGTA, 0.5 mM phenylmethylsulfonyl fluoride, 0.5 mM DTT, 25 µg/ml leupeptin, 0.2 mM Na_3VO_4 with a final pH of 7.4, NaOH) or 1× transcription buffer (see below) and either used freshly or aliquoted, snap-frozen with

liquid nitrogen, and stored at -80°C. Protein concentrations were determined by Bradford assay using a NanoDrop ND-1000 Spectrophotometer (Wilmington, DE).

1. Xiao, L., Coutu, P., Villeneuve, L.R., Tadevosyan, A., Maguy, A., Le Bouter, S., Allen, B.G., and Nattel, S. (2008) Circ Res 103(7), 733-742

On-line Table I

Primary Antibody Information

Protein	*Isotype*	*Company*	*Catalogue Number*	*Dilution*
AT1 (43kDa)	Rabbit-polyclonal	Alomone labs	ZZR-011-AN01	1:400
AT1-c18	Goat-polyclonal	Santa Cruz	Sc-31181	1:500
AT2(47kDa)	Rabbit-polyclonal	Alomone labs	AAR-012-AN01	1:400
AT2-c18	Goat-polyclonal	Santa Cruz	Sc-7420	1:500
Calpactin-I (36kDa)	Mouse-monoclonal	BD Biosciences	610068	1:2000
DDR2 (98kDa)	Rabbit-polyclonal	Abcam	Ab5520	1:200
GM-130 (130kDa)	Mouse-monoclonal	BD Biosciences	610823	1:250
GRP78 (75kDa)	Rabbit-polyclonal	Abcam	Ab21685	1:1000
Histone 3 (17kDa)	Rabbit-polyclonal	Cell Signaling	#9715	1:1000
MyHC (223kDa)	Mouse-monoclonal	Abcam	Ab15	1:1000
NSE (47kDa)	Rabbit-polyclonal	Abcam	Ab16873	1:2000
Nup-62 (62kDa)	Mouse-monoclonal	BD Biosciences	610498	1:1000
VWF (130, 190kDa)	Goat-polyclonal	Santa Cruz	Sc-8068	1:100
αSMA (42kDa)	Mouse-monoclonal	Sigma	A5228	1:2000

Secondary Antibody Information

Antibody Description	*Company*	*Catalogue Number*	*Dilution*
Donkey anti-rabbit IgG	Jackson	711-005-152	1:10000
Donkey anti-mouse IgG	Jackson	711-005-150	1:15000
Donkey anti-goat IgG	Jackson	711-005-003	1:10000

On-line Table II

Primers Information

Primers	***Description***	***Sequences***	***RefSeq mRNA***
Ace	Angiotensin-converting enzyme	F: CCTGATCAACCAGGAGTTTGCAGAG R: GCCAGCCTTCCCAGGCAAACAGCAC	NM_012544.1
Agt	Angiotensinogen	F: GACCGCGTATACATCCACCCCTTTCATCTC R: GTCCACCCAGAACTCATGGAGCCCAGTCAG	NM_134432.2
B2m	Beta-2 microglobulin	F: GAATTCAGTGTGAGCCAGGATG R: CAAGTGTACTCTCGCCATCCAC	NM_012512.1
Cts	Cathepsin	F: GGGGGAAATCTACAAAAATG R: AAAGACTCCTATCTGCCTCACT	NM_022597.2
GAPDH	Glyceraldehyde-3-phosphate dehydrogenase	F: TACATGTTCCAGTATGACTC R: TGTGAGGGAGATGCTCAGTG	NM_017008
Hspcb	Heat shock protein 90kDa alpha, class B member 1	F: TGTTTCTTCACCACCTCCTTGA R: CCTACCTGGTGGCAGAGAAAGT	NM_001004082
NFκB1	Nuclear factor of kappa light polypeptide gene enhancer in B-cells 1	F: CTGCGATACCTTAATGACAGCG R: AATTTGGCTTCCTTTCTTGGCT	XM_342346.3
Ren	Renin	F: CTGGGAGGCAGTGACCCTCAACATTACCAG R: GAGAGCCAGTATGCACAGGTCATCGTI'CCT	NM_012642.4

On-line Figure Legends

Figure 1. Assessment of cardiomyocyte preparation and expression of renin-angiotensin components in cardiomyocytes. A, The purity of isolated cardiomyocytes was assessed by Western blot, with aliquots (40 μg each) of proteins isolated from cardiomyocytes, fibroblasts, smooth muscle cells, endothelial cells and whole-brain. Proteins were separated by SDS-PAGE and transferred onto PVDF. After blocking, membranes were incubated with antisera specific for Van Willebrand's Factor (VWF), neuron-specific enolase (NSE), discoidin domain receptor 2 (DDR2), α-smooth muscle actin (αSMA), myosin heavy chain (MyHC) and GAPDH. Immunoreactive bands were visualized by ECL (examples of Western blots are illustrated, we performed 4 separate experiments/antibody/fraction) B, The expression of renin-angiotensin components were confirmed with RNA isolated from the cytosol of cardiac myocytes, by qRT-PCR with primers for angiotensinogen (AGT), angiotensin converting enzyme (ACE), cathepsin and renin, data are presented as mRNA expression relative to an average of three housekeeping genes (N=8/primer)

Figure 2. Immunoreactivity of angiotensin II receptor subtypes 1 and 2 in purified cardiac nuclei. A, Rat hearts were fractionated into four fractions: total extract (A), supernatant (B), crude nuclear (C) and enriched nuclear (D) fractions. Aliquots (30 μg) of each fraction were separated by SDS-PAGE and transferred onto PVDF. After blocking, membranes were incubated with antisera specific for Calpactin I, GRP78,

Nup62, GM130, AT1 or AT2 (examples of Western blots are illustrated, N=6/antibody/per fraction). Immunoreactive bands were visualized by ECL. B, Mean±SEM expression levels for GRP78, GM130, Nup62, AT1, AT2 normalized to Calpactin I. *P<0.05, **P<0.01 vs. respective fraction in B. C, Representative images of a purified nuclear preparation. Left: DNA-staining with Hoechst 33342; Right: Corresponding phase-contrast image. D, Mean±SEM DNA content (µg/ml) of cytoplasmic or nuclear fractions (N=10/group). ***P<0.001 vs. cytoplasmic.

Figure 3. Endocytosis and intracellular trafficking of Ang-II. A, FITC-Ang-II (1 nM) was applied extracellularly to the bathing medium. Images are shown immediately after Ang-II application (0 min) and then 30 and 60 min later. Merged images are superimposed fluorescent images. B, cells were preincubated with valsartan (10 µM, for 25 min) prior to administration of Ang-II. Hoechst 33342 was used as a nuclear marker. Z-stacks were acquired every 5 min using a Zeiss LSM-510 confocal microscope. (N=6/group)

Figure 4. AT1R and AT2R in nuclear membranes regulate transcription initiation. A, De novo RNA synthesis. Isolated nuclear preparations were stimulated with Ang-II, L 162,313 (a non-peptide AT1R-selective agonist), CGP 42112A (an AT2R-selective agonist), candesartan plus Ang-II, or PD123177 plus Ang-II (all at 10 µM), as indicated. Following the addition of antagonists candesartan (Cand) and PD123177, nuclei were preincubated for 30 min prior to the addition of Ang-II. ***P<0.001 vs.

control; ++P<0.01 vs. Ang-II. B, Nuclei were treated with PTX 5 μg/ml for 2 hours and then stimulated with Ang-II. Data represent mean ± SEM of at least five separate experiments performed in triplicate and normalized to control. ***P<0.001 vs. control; N.S. = non-significant vs. control. C, representative 2% agarose gel electrophoresis of RNA extracted from purified nuclei stained with ethidium bromide (GTP and CTP not omitted) under the following conditions: non-stimulated (lane 1); stimulated with Ang-II (10 μM, lane 2); stimulated with Ang-II in the presence of valsartan (10 μM, lane 3); stimulated with Ang-II in the presence of PD123177 (10 μM, lane 4). 1 μg of each sample was loaded. Bottom panel shows mean±SEM results as arbitrary optical density (O.D.) units from 6 different experiments/condition. **P<0.01 vs. control, ++P<0.01 vs. Ang-II.

Figure 5. Regulation of nuclear NFκB mRNA expression by nuclear ATRs. Isolated nuclei were treated for 2 hours with Ang-II at different concentrations. NFκB mRNA was quantified by qPCR. A, Data are presented as NFκB mRNA expression relative to an average of three housekeeping genes (N=6/concentration/group). ***P<0.001 vs. intact cells, N.S. = non-significant. B, Valsartan (10 μM) or PD123177 (10 μM) significantly reduced the Ang-II (10 μM) induced NFκB activity, while pretreatment of nuclei with both AT1 and AT2 antagonists completely abolished the NFκB gene expression-response. Results are expressed as mean±SEM *P<0.05 vs. control, +P<0.01 vs. Ang-II, #P<0.01 vs. valsartan, N.S: non significant vs. control

Figure 6. Vehicle control for calcium transients. Typical recordings of intracellular Ca^{2+} are shown, with recordings from isolated nuclei preparations shown in insets, after administration of DMSO

Figure 7. Coupling of ATRs to Ca^{2+} entry in nuclear enriched preparations. FURA-2/AM-loaded freshly isolated cardiac nuclei were seeded onto glass slides and nuclear Ca^{2+} concentration [Ca^{2+}] was measured with an IonOptix microspectrofluorimeter (λex = 340 and 380 nm; λem = 509 nm). Typical recordings of intracellular Ca^{2+} are shown, with recordings from each preparation studied shown in insets, after administration of: A, Ang-II (10 μM); B, L-162,313 (10 μM); C, candesartan (10 μM) plus Ang-II (10 μM); D, CGP 42112A (10 μM); E, PD123177 (10 μM) plus Ang-II (10 μM). F, Summary of mean±SEM [Ca^{2+}] transient amplitudes (N=6/group/condition) *P<0.05 vs. control, N.S. = non-significant vs. control; arrows in A-E indicate the time of drug application.

Figure 8. IP3-dependent Ca^{2+} signals from isolated nuclei. Isolated nuclei were exposed to A, IP3 (10 μM). B, the IP3R blocker 2-APB (10 μM) followed by exposure to IP3. C, the IP3R blocker 2-APB (10 μM) followed by exposure to Ang-II (10 μM). D, summary of [Ca^{2+}] transient amplitudes, mean±SEM (N=5/group/condition) ***P<0.001; arrows indicate the time of drug application in A-C.

Figure 9. Role of IP3R-signaling for AT1R-mediated transcription initiation. Isolated nuclei were pre-treated with various concentrations of 2-APB for 30 minutes and incubated with: A, Ang-II B, L-162,313 or C, CGP42112A (all at 10 μM) and de novo RNA synthesis was measured by ^{32}P-UTP incorporation. ***P<0.001 or **P<0.01 vs. agonist alone (Ang-II or L-162,313); ##P<0.01 or #P<0.05 vs. DMSO or 2-APB alone (15 μM); N.S: non-significant.

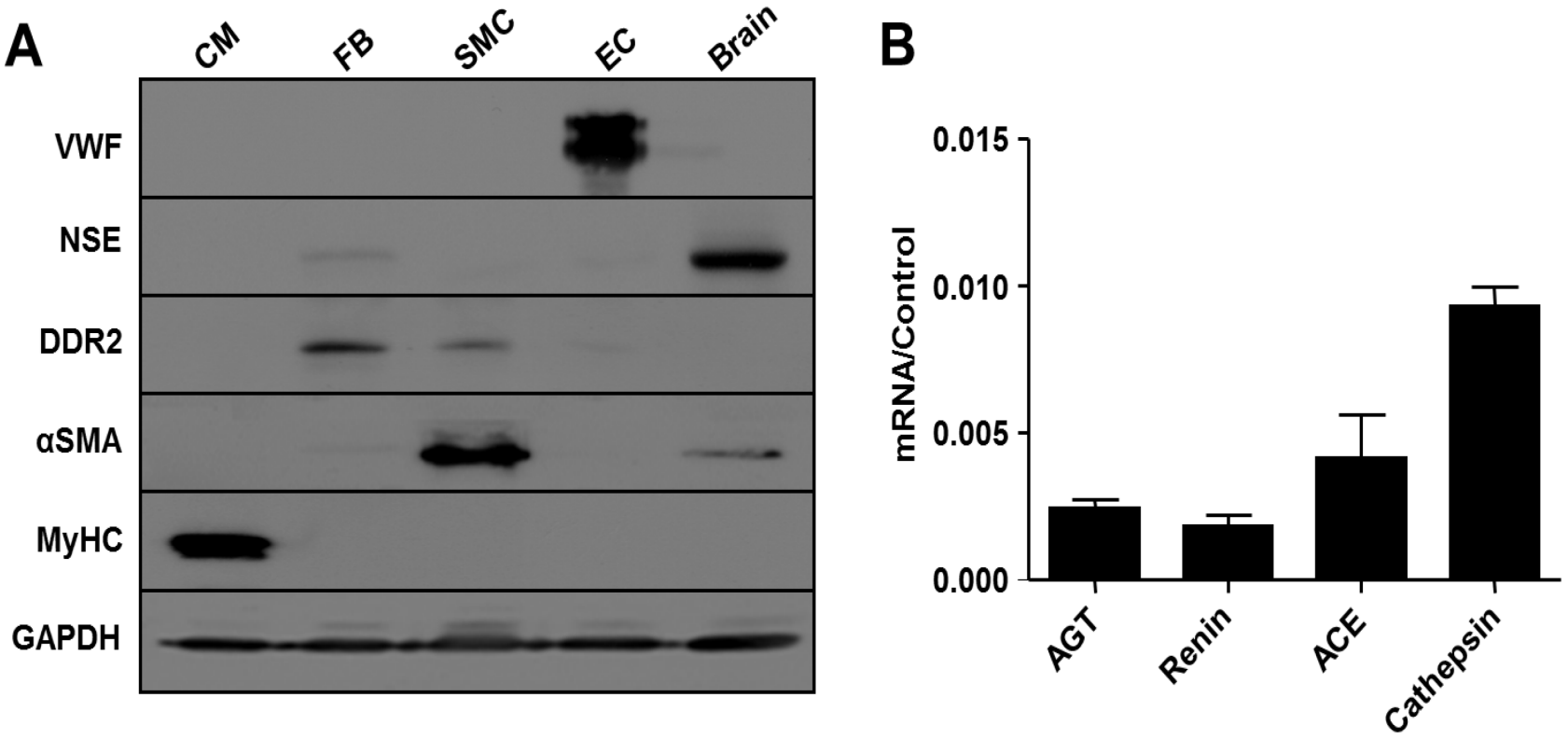

On-line Figure 1

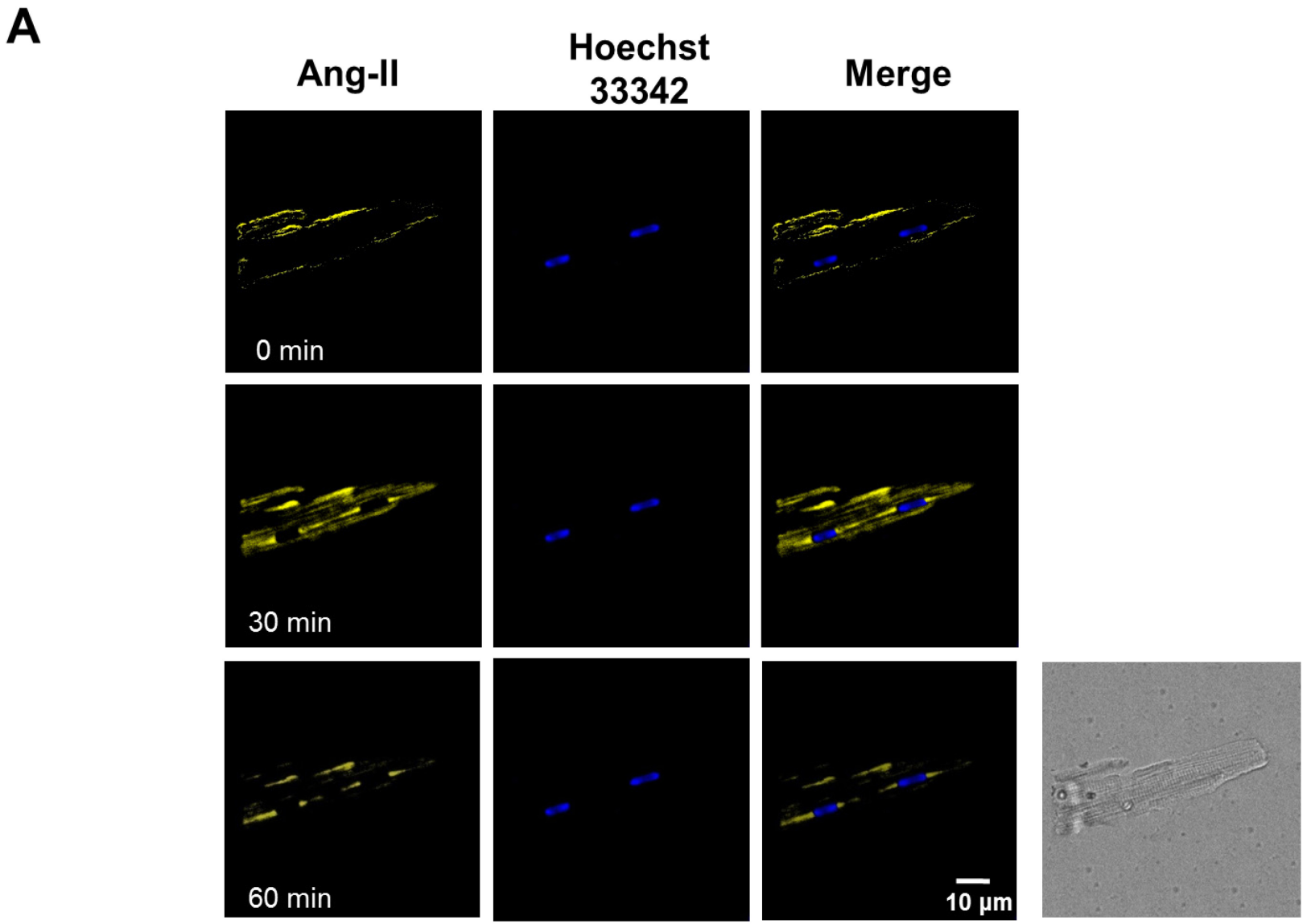

On-line Figure 2A

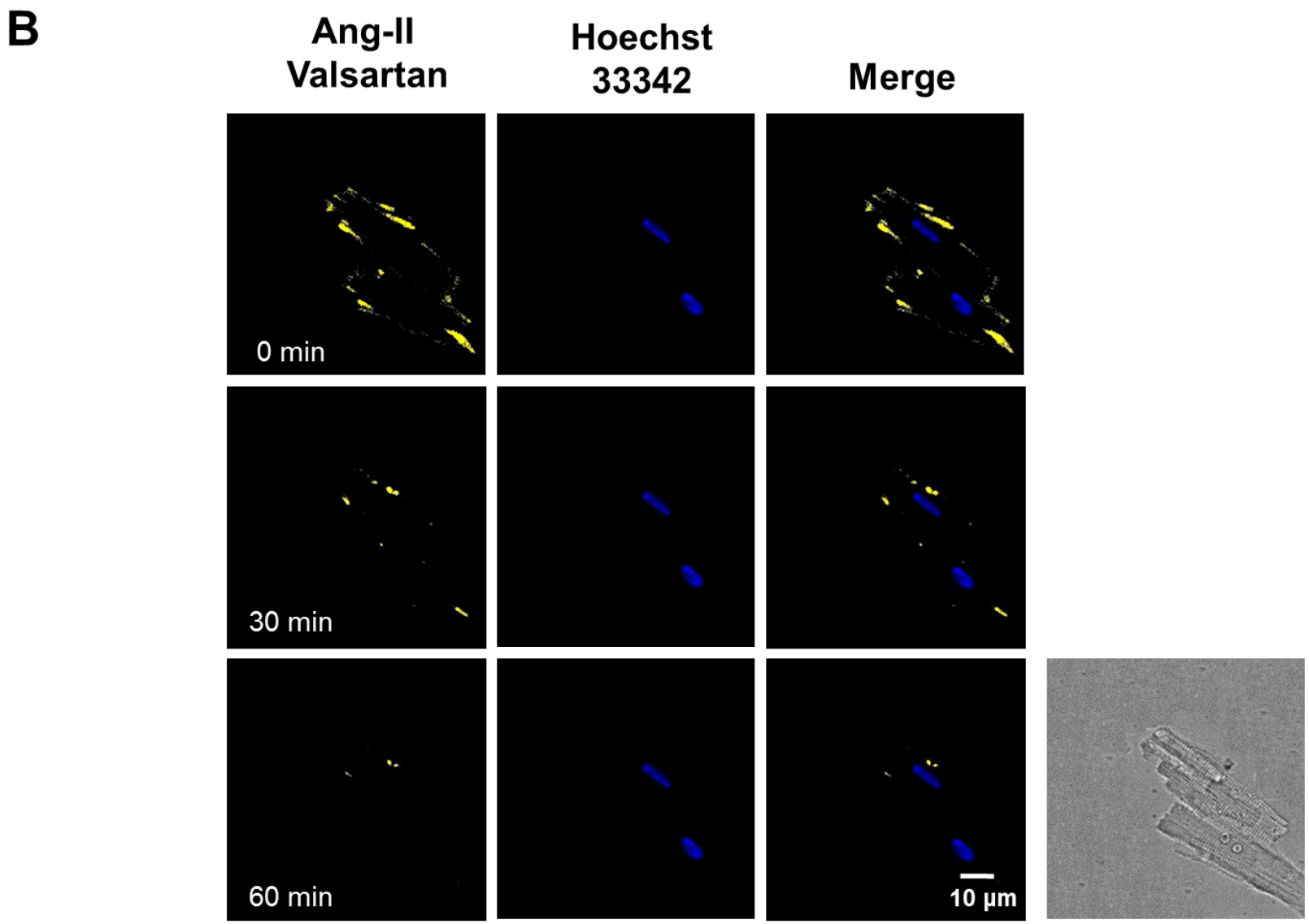

On-line Figure 2B

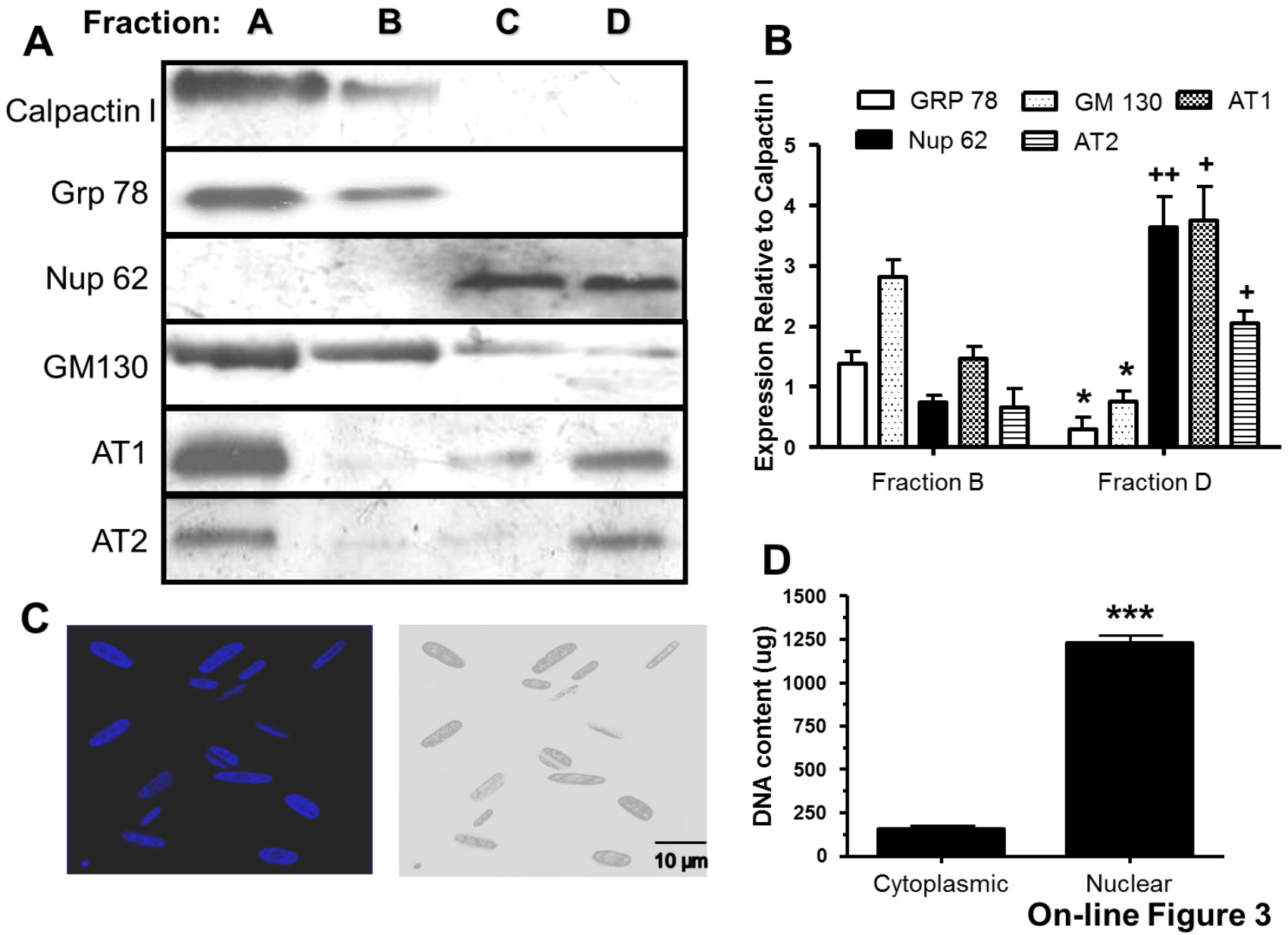

On-line Figure 3

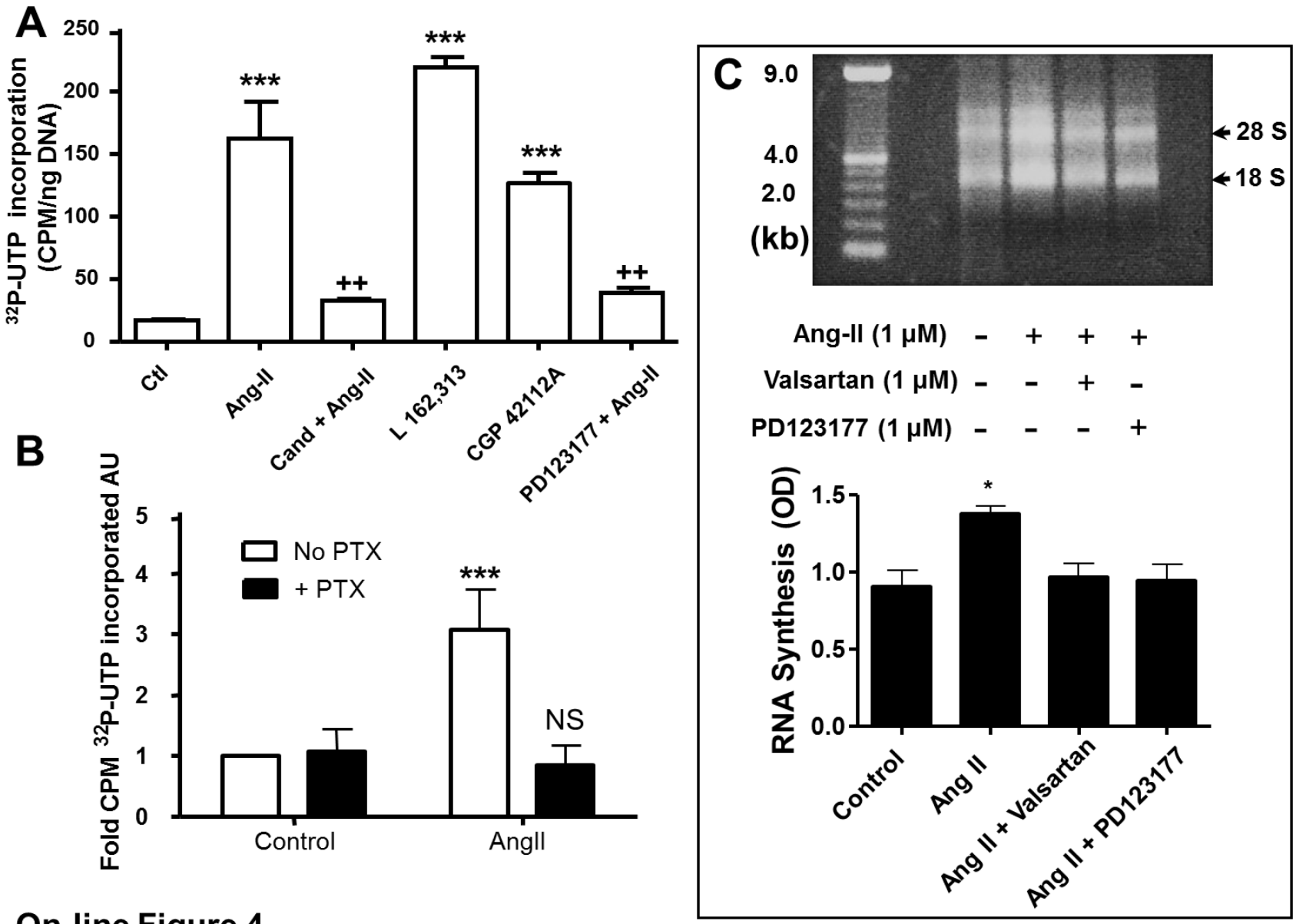

On-line Figure 4

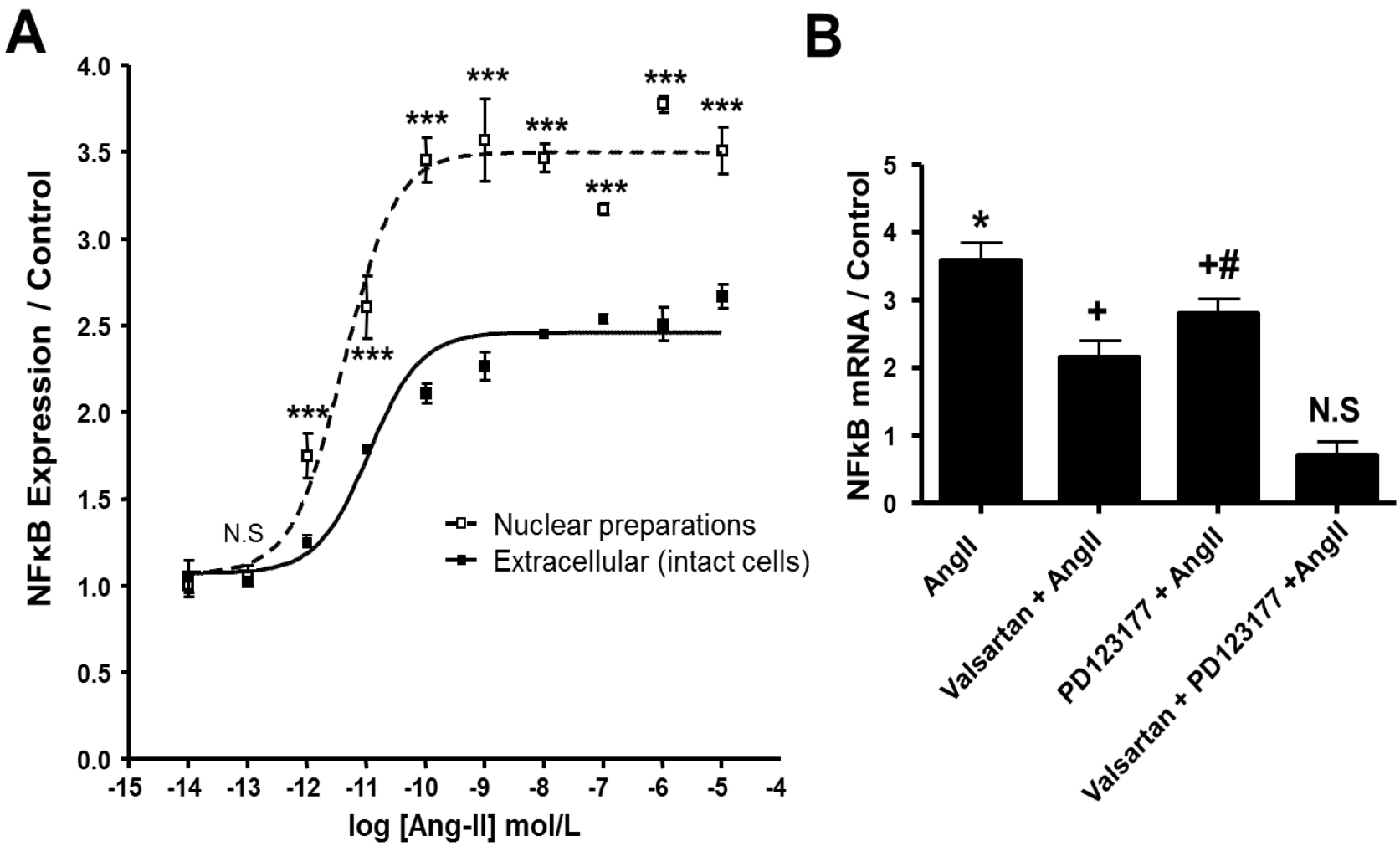

On-line Figure 5

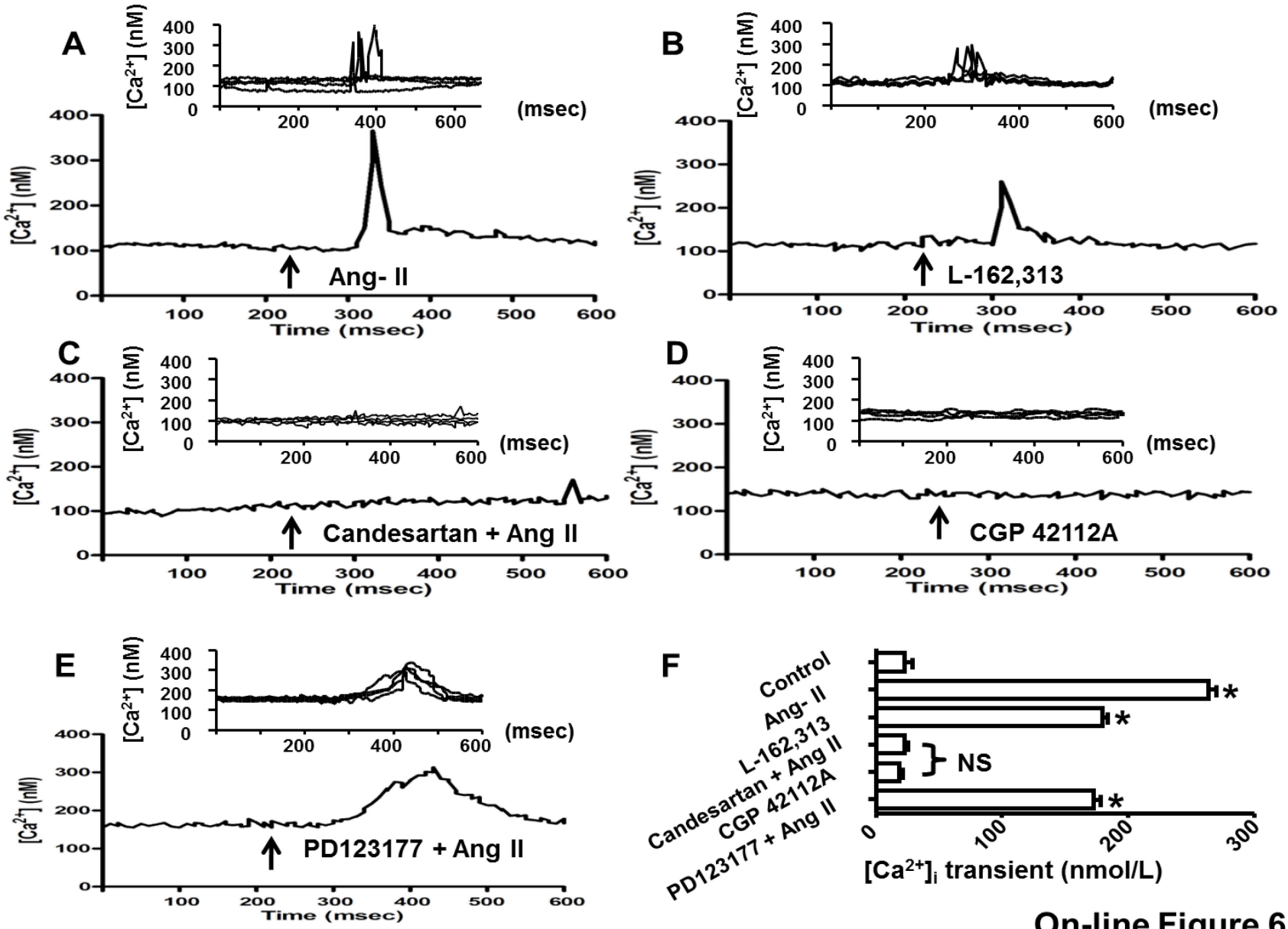

On-line Figure 6

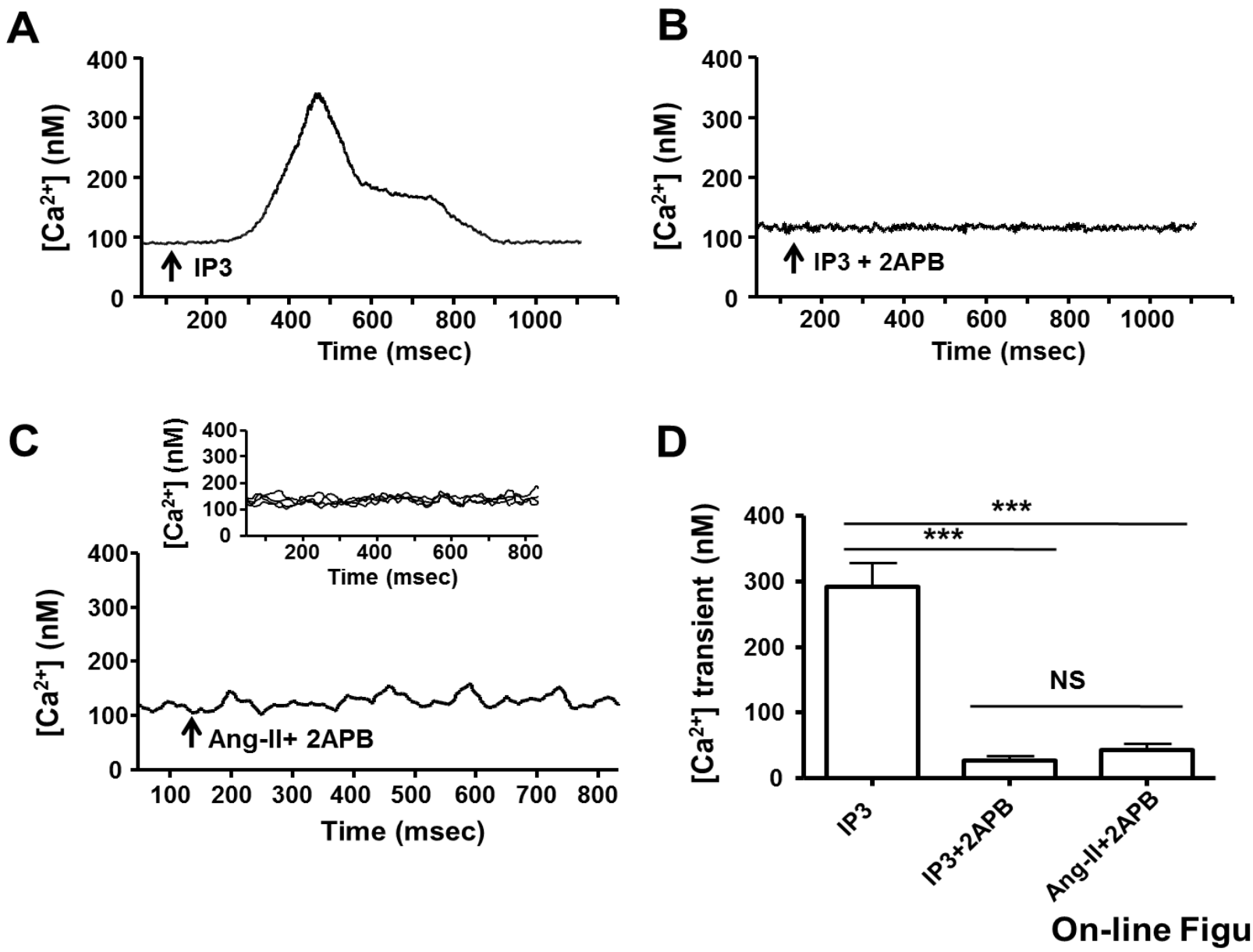

On-line Figure 7

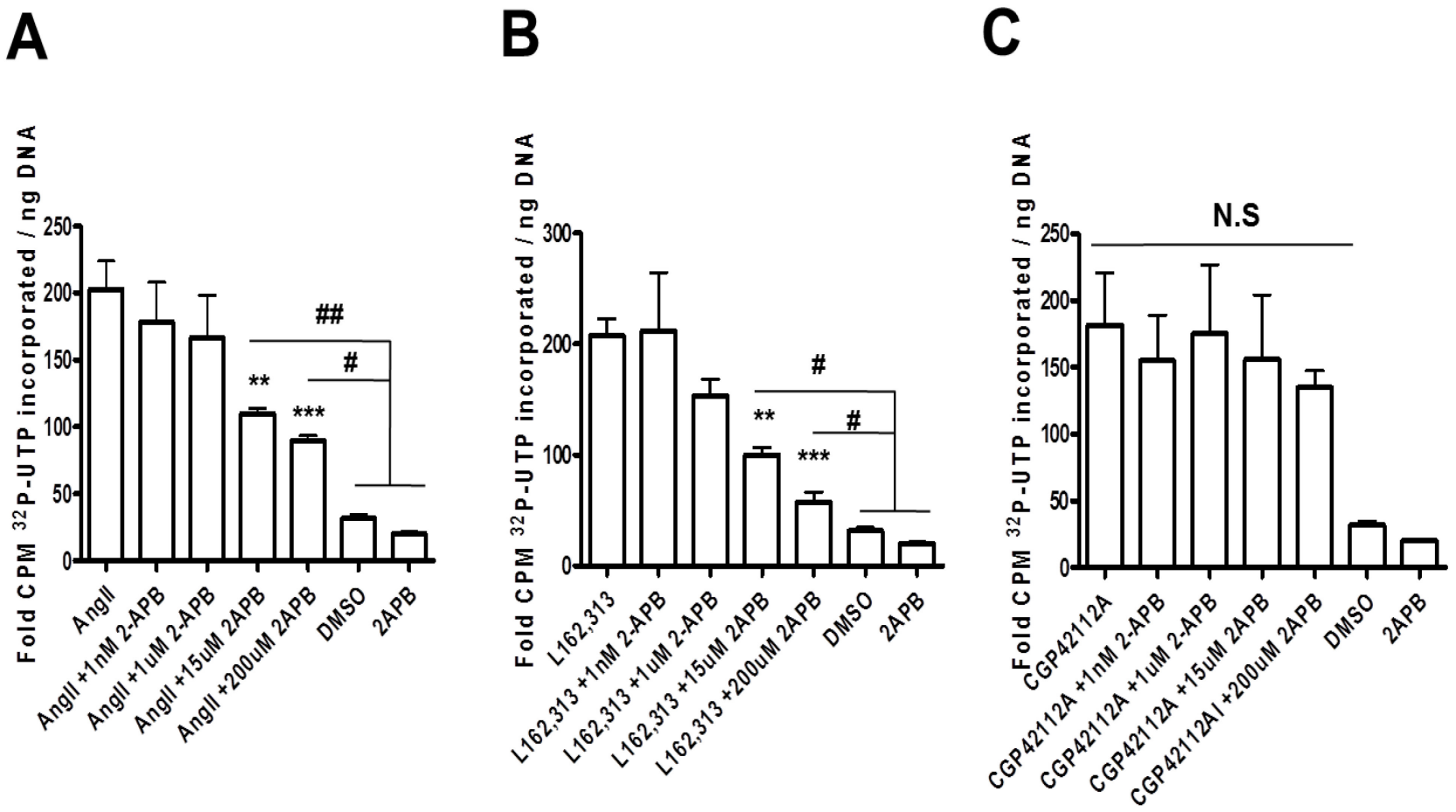

On-line Figure 8

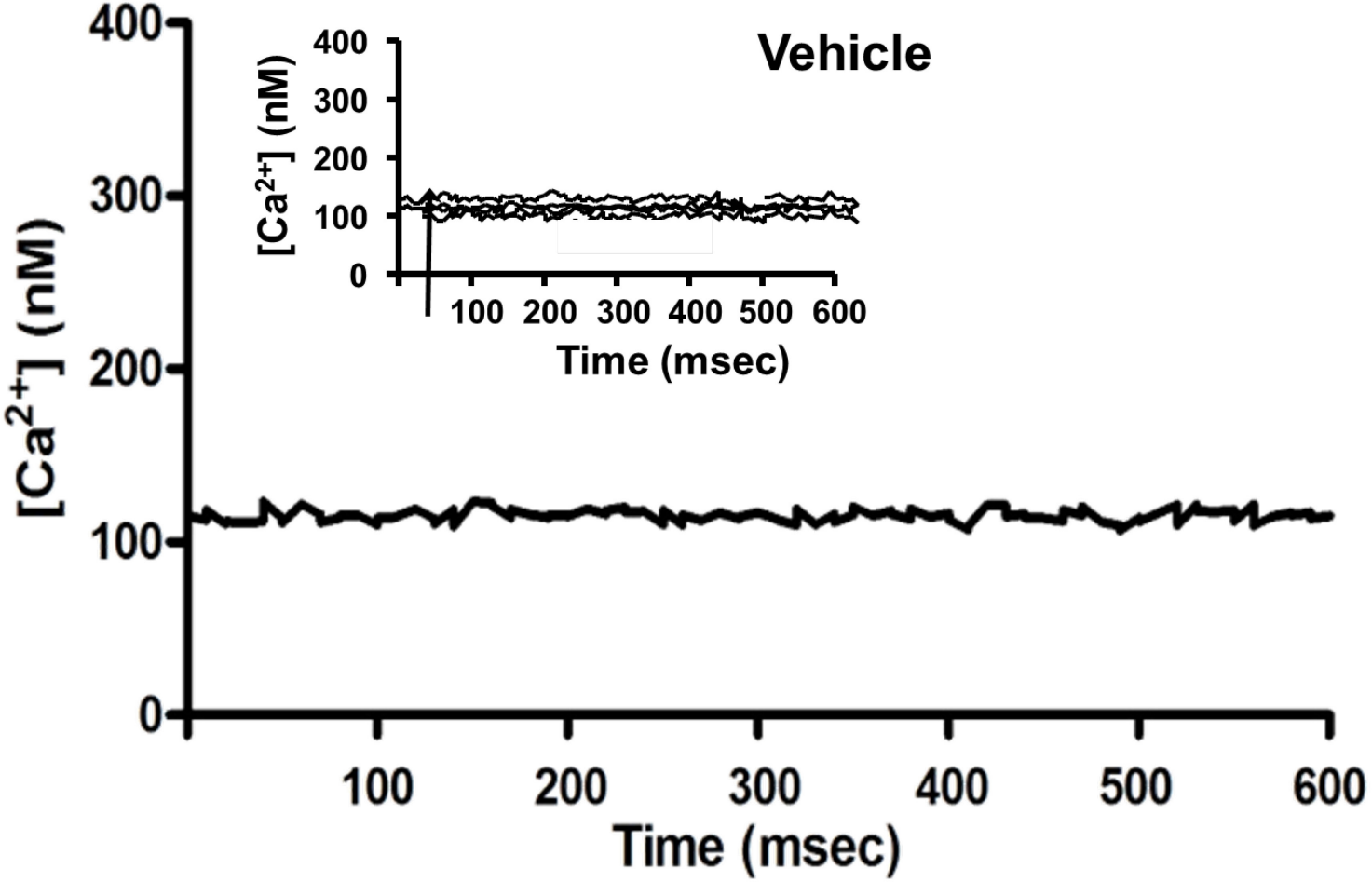

On-line Figure 9

CHAPTER 3 – Synthesis and characterisation of novel photoreleasable angiotensin II analogs to probe intracellular actions with spatial and temporal precision

Linking Statement and Author Contribution

The localisation of functional AT1R and AT2R on nuclei isolated from cardiomyocytes strongly supports the intracellular RAS (iRAS) paradigm. However, novel direct cellular and molecular approaches need to be developed that allow for the direct study of iRAS in whole cell models and the delineation of the roles of iRAS in cardiac physiology and pathophysiology. Here, to further investigate the biological relevance of iAng-II, we synthesized and pharmacologically/physiologically characterized cell-permeable photolabile caged Ang-II analogues. These compounds are biologically inert precursors of Ang-II that release active Ang-II intracellularly when exposed to ultraviolet light.

Tadevosyan A, Letourneau M, Folch B, Doucet N, Villeneuve LR, Mamarbachi AM, Pétrin D, Hébert TE, Fournier A, Chatenet D, Allen BG, Nattel S. Photo-Releasable Ligands to Study Intracrine Angiotensin II Signalling.
J Physiol. 2015 Feb 1;593(3):521-39. Epub Nov 28 2014

A.T., A.F., D.C., B.G.A. and S.N. participated in conception and experimental design. A.T., M.L. and D.C. carried out all of the peptide synthesis, binding assays, biochemical and physiological experiments. B.F. and N.D. performed computer simulation experiments needed to design Ang-II analogues and plan their synthesis. A.M.M., D.P. and T.E.H participated in purification and expression in HEK 293 cells of expression vectors encoding AT1R-Venus and AT2R-Venus. A.T. and L.R.V. performed and analysed immunohistochemical and calcium imaging experiments. A.T., B.G.A. and S.N. participated in analysis and interpretation of data, and drafting and revising the manuscript.

Photo-Releasable Ligands to Study Intracrine Angiotensin II Signalling

Artavazd Tadevosyan, MSc[a,b], Myriam Létourneau, MSc[c,d], Benjamin Folch, PhD[c], Nicolas Doucet, PhD[d,e,f], Louis R Villeneuve, MSc[b], Aida M Mamarbachi, MSc[b], Darlaine Pétrin, MSc[g], Terence E. Hébert, PhD[g], Alain Fournier, PhD[c,d], David Chatenet, PhD[c,d], Bruce G Allen, PhD[a,b,g,h], Stanley Nattel, MD[a,b,g]

[a]Department of Medicine, Université de Montréal, [b]Montreal Heart Institute, [c]INRS–Institut Armand-Frappier, Université du Québec, [d]Laboratoire International Associé Samuel de Champlain, [e]PROTEO, Québec Network for Research on Protein Function, Structure, and Engineering, Université Laval, [f]Groupe de Recherche Axé sur la Structure des Protéines, McGill University, [g]Department of Pharmacology and Therapeutics, McGill University, [h]Department of Biochemistry and Molecular Medicine, Université de Montréal.

Running title: Photoreleasable Ang-II for intracrine physiology

Correspondence to: Stanley Nattel OR Bruce G. Allen, 5000 Bélanger St., Montréal, Québec, H1T 1C8, Canada. Tel.: (514)-376-3330; Fax: (514)-376-1355;

Abstract

Several lines of evidence suggest that intracellular angiotensin II (Ang-II) contributes to the regulation of cardiac contractility, renal salt reabsorption, vascular tone and metabolism; however, work on intracrine Ang-II signalling has been limited to indirect approaches because of a lack of selective intracellularly-acting probes. Here, we aimed to synthesize and characterize cell-permeable Ang-II analogues that are inactive without uncaging, but release active Ang-II upon exposure to a flash of ultraviolet light, as novel tools to study intracrine Ang-II physiology. We prepared three novel caged Ang-II analogues, [Tyr(DMNB)^4]Ang-II, Ang-II-ODMNB and [Tyr(DMNB)^4]Ang-II-ODMNB, based upon the incorporation of the photolabile moiety 4,5-dimethoxy-2-nitrobenzyl (DMNB). Compared to Ang-II, the caged Ang-II analogues showed 2-3 orders of magnitude reduced affinity toward both angiotensin type-1 (AT1R) and type-2 (AT2R) receptors in competition binding assays, and greatly-reduced potency in contraction assays of rat thoracic aorta. Following ultraviolet irradiation, all three caged Ang-II analogues released Ang-II and potently induced contraction of rat thoracic aorta. [Tyr(DMNB)^4]Ang-II showed the most rapid photolysis upon ultraviolet irradiation and was the focus of subsequent characterization. Whereas Ang-II and photolysed [Tyr(DMNB)^4]Ang-II increased ERK1/2 phosphorylation (via AT1R) and cGMP production (AT2R), caged [Tyr(DMNB)^4]Ang-II did not. Cellular uptake of [Tyr(DMNB)^4]Ang-II was 4-fold greater than that of Ang-II and significantly greater than uptake driven by the positive-control HIV TAT(48-60) peptide. Intracellular photolysis of [Tyr(DMNB)^4]Ang-II induced an

increase in nucleoplasmic Ca^{2+} ($[Ca^{2+}]n$), and initiated 18S rRNA and NF-κB mRNA synthesis in adult cardiac cells. We conclude that caged Ang-II analogues represent powerful new tools to selectively study intracrine signalling via Ang-II.

Keywords: Intracrine signalling; Biochemistry and metabolism; Angiotensin converting enzyme; Angiotensin receptors

Abbreviations AT1R, angiotensin II type 1 receptor; AT2R, angiotensin II type 2 receptor; ACE, angiotensin-converting enzyme; DMNB, 4,5-dimethoxy-2-nitrobenzyl group; PACAP(28-38), peptide corresponding to amino acids 28-38 of the pituitary adenylyl cyclase-activating polypeptide; TAT(48-60), peptide corresponding to amino acids 48-60 of the HIV-1 TAT protein; UV, ultraviolet.

Introduction

The renin-angiotensin system (RAS) is critically involved in controlling functions at various levels, from cells to tissues to the entire organism. The physiological actions of RAS and its blockade have been translated into clinical settings, improving both quality and duration of life for patients with hypertension, heart failure, renal insufficiency, myocardial infarction, and stroke (Kobori et al., 2007; Lang & Struthers, 2013). RAS activation is initiated following cleavage of angiotensinogen into angiotensin-I (Ang-I), via renin synthesized in juxtaglomerular cells of renal afferent arterioles. Subsequently, angiotensin-converting enzyme (ACE) hydrolyses the inactive decapeptide Ang-I into the biologically active octapeptide angiotensin-II (Ang-II), which exerts actions via heterotrimeric G protein-coupled type-1 (AT1R) and type-2 (AT2R) receptors.

Although the RAS has been traditionally viewed as an endocrine system, a variety of studies point to intracellular ("intracrine") Ang-II actions. Angiotensin receptors are localized on the nuclear envelope of numerous cell types (Robertson & Khairallah, 1971; Haller et al., 1999; Cook et al., 2006). Exposure of isolated cardiac nuclei to Ang-II causes inositol 1,4,5-trisphosphate (IP3)-dependent Ca^{2+}-release and de novo RNA synthesis (Tadevosyan et al., 2010; Tadevosyan et al., 2012). Hyperglycemia stimulates local Ang-II production in the hearts of diabetic patients and is implicated in increased expression of transforming growth factor-β (TGF-β) and collagen (Frustaci et al., 2000; Singh et al., 2008). The intracrine actions attributed to Ang-II are not prevented by acute extracellular application of angiotensin receptor

blockers or ACE inhibitors (Tadevosyan et al., 2010). As these compounds have a limited capacity to cross the plasma membrane, they are unable to abolish the cytosolic synthesis of Ang-II or its binding to cognate receptors on the nuclear membrane (Schwab et al., 1990; Singh et al., 2007). Direct demonstration of the intracrine effects of Ang-II has been hampered because of difficulty in selectively targeting intracellular Ang-II receptors without activating cell-surface receptors; therefore, the role of intracellular Ang-II signalling in mediating the effects of RAS activation remains poorly understood.

Better spatial and temporal resolution of biologically active molecules can be achieved with the use of “caged compounds”, characterized by the addition of a photo-labile group on a substituent essential for receptor recognition (Yu et al., 2010). This approach has been used to study cellularly localized actions of a range of molecules, including ATP (McCray et al., 1980), GTP (Schlichting et al., 1989), endothelin-1, (Bourgault et al., 2007; Merlen et al., 2013), isoproterenol (Muralidharan & Nerbonne, 1995; Vaniotis et al., 2013), phenylephrine (Muralidharan et al., 1993), γ-aminobutyric acid (Wang & Augustine, 1995), urotensin II (Bourgault et al., 2005), endothelin receptor antagonists (Merlen et al., 2013), IP3 (Li et al., 1998; Tertyshnikova & Fein, 1998), cofilin (Ghosh et al., 2004), DNA (Monroe et al., 1999) and RNA (Chaulk & MacMillan, 1998; Ando et al., 2001). Caged molecules can be introduced non-invasively into the cell in an inert form and then subsequently uncaged with a focused pulse of ultraviolet (UV) light, allowing downstream effects to be monitored without disrupting other aspects of the system (Merlen et al., 2013; Vaniotis et al., 2013), a feature not exhibited by conventional reagents.

Ang-II displays stringent conformational and dynamic requirements for the amino acids at position 4 (tyrosine) and 8 (phenylalanine) for receptor binding (Aumelas et al., 1985; Samanen et al., 1989; Bovy et al., 1990; Noda et al., 1995). Ang-II analogues bearing modifications at positions 4 or 8 differentially activate post-receptor signalling in a biased fashion, thus giving rise to distinct biological outcomes (Zimmerman et al., 2012). To develop a tool with which to study the consequences of selective activation of intracellular Ang-II receptors, we synthesized photo-activatable caged analogues of Ang-II by adding a photo-labile DMNB residue on the phenolic group of tyrosine-4 and/or on the α-COOH of phenylalanine 8, thereby creating three "caged" analogues of Ang-II: [Tyr(DMNB)^4]Ang-II, Ang-II-ODMNB and [Tyr(DMNB)^4]Ang-II-ODMNB. Here, we report for the first time the design, synthesis and characterization of these compounds that can be photo-triggered to release Ang-II. We go on to show that photoactive [Tyr(DMNB)^4]Ang-II demonstrates intracrine regulation of cardiomyocyte nuclear calcium content and gene-expression.

Materials and Methods

Cell Culture and AT1R/AT2R Transfection

Human embryonic kidney 293 (HEK 293) cells were cultured in Dulbecco's modified Eagle's medium (DMEM) supplemented with 10% fetal bovine serum (FBS), 100 µg/mL streptomycin, 100 units/mL penicillin, and 2 mM L-glutamine at 37°C in a humidified 5% CO_2-containing atmosphere. HEK 293 cells were seeded at a density of 4×104 cells per 20 mm well of 24-well plates, 1×105 cells per 35 mm well of 6-well plates, or 106 cells per 100 mm culture dish. For transient expression in HEK 293 cells, expression vectors encoding AT1R-Venus or AT2R-Venus were transfected into cells with polyethylenimine (PEI) at a final concentration of 9 µg/mL (Zhang et al., 2009). Radioligand binding assays, immunoblots, or ELISA experiments were carried out 48 h after transfection.

Synthesis and Purification of Caged Angiotensin-II Analogues

All Ang-II analogues were synthesized manually on a 2-chlorotrityl chloride resin (0.7 mmol/g) using solid-phase peptide synthesis with Fmoc chemistry. Synthesis of Fmoc-Tyr(DMNB)-OH was performed as previously described (Bourgault et al., 2005, 2007). Coupling of protected amino acids, monitored with the qualitative ninhydrin-test, was performed with a 3-equivalent excess of the protected amino acids, based on the original substitution of the resins, benzotriazol-1-yl-oxy-tris(dimethylamino)phosphonium hexafluorophosphate (BOP; 3 equiv) and N,N-diisopropylethylamine (DIPEA; 6 equiv) in N,N-dimethylformamide (DMF) for 45 min.

Fmoc removal was achieved with 20% piperidine in DMF for 20 min. After deprotection, the resin was washed extensively with DMF (1x), methanol (1x), methylene chloride (DCM) (1x) and DMF (2x) before starting another cycle for the introduction of the next amino acid. Cleavage of Ang-II and [Tyr(DMNB)^4]-Ang-II from the resin was performed with a mixture of trifluoroacetic acid (TFA)/triisopropylsilane/phenol/water (92/2.5/3/2.5) for 2 h. Following evaporation of the solvent, the crude peptides were precipitated by addition of cold diethyl ether. The products were isolated, dissolved in water and freeze-dried. For C-terminally modified peptides Ang-II-ODMNB and [Tyr(DMNB)^4]-Ang-II-ODMNB, cleavage from the solid support was carried out with AcOH/trifluoroethanol/DCM (1:1:8; v/v/v) to produce fully protected peptides with a free carboxy-terminal function. The C-terminal carboxylic acid was reacted with 4,5-dimethoxy-2-nitrobenzyl alcohol (DMNBA), as described by Bourgault et al. (Bourgault et al., 2007) C-terminally caged Ang-II analogues were obtained by stirring the protected peptides bearing a C-terminal DMNB ester group with TFA/triisopropylsilane/phenol/water (92/2.5/3/2.5). Similarly, to obtain fluorescein-conjugated peptides, a N-protected ε-amino acid spacer (Fmoc-aminohexanoic acid-OH; Fmoc-Ahx-OH) was coupled to peptidyl-resins using the BOP reagent condensation methodology (see above). After Fmoc removal, the free amino group was allowed to react overnight with fluorescein isothiocyanate (FITC; 1.2 equiv) in a DMF/DCM mixture (1:1), in presence of triethylamine (20 equiv) (Jullian et al., 2009). TFA cleavage (TFA/triisopropylsilane/phenol/water; 92/2.5/3/2.5; 2 h) produced the expected fluorescent peptides. Crude peptides were purified by preparative reverse phase high performance liquid chromatography (RP-HPLC) using

a Phenomenex C18 column (300 Å pore size, 15 µm bead diameter, 250 mm x 21.2 mm) at a flow rate of 20 mL/min. Peptides were eluted with a linear gradient of 0-100% solution B over 2 h (solution A: 0.06% TFA/H_2O, solution B: 40% CH_3CN in 0.06% TFA/H_2O). The absorbance was monitored at 229 nm (A229). To confirm the purity and mass of the purified products, aliquots of the collected fractions were (1) resolved by analytical RP-HPLC using a CSC-Kromasil C18 column (100 Å pore size, 5 µm bead diameter, 250 mm x 4.6 mm) connected to a Beckman 128 pump and Beckman 168 PDA detector, at a flow rate of 1 mL/min, and (2) assessed by matrix-assisted laser desorption ionization-time of flight (MALDI-TOF) mass spectrometry (Voyager DE system). Fractions from preparative HPLC found to have the expected m/z value and be >95% pure were pooled, lyophilized and stored at -20°C.

Competition Binding Assays

Purified Ang-II (10 µg) was radiolabeled with $Na^{125}I$ (0.3 mCi) using chloramine-T (5 µg) in 0.05 M phosphate buffer (pH 7.4) at room temperature for 60 s. The reaction was stopped by addition of 10 mM sodium metabisulfite and then applied to a Sep-Pak C18 cartridge (Waters Corp, Milford, MA, USA). [^{125}I]Ang-II was eluted with a 60% CH3CN/H20 0.1% TFA solution and stored at -20°C until use. Competition binding assays employed concentrations of unlabelled ligands (Ang-II, [Tyr(DMNB)^4]Ang-II, Ang-II-ODMNB, [Tyr(DMNB)^4]Ang-II-ODMNB) ranging from 10-10 M to 10-5 M. HEK 293 cells transfected transiently with AT1R-Venus or AT2R-Venus were plated in 24-well plates, gently washed twice with phosphate-buffered saline (PBS), and incubated for 45 min at 37°C in binding buffer (DMEM, 0.1% BSA)

containing [^{125}I]Ang-II (50,000 cpm/well) plus the indicated concentrations of unlabelled ligand. At the end of the incubation period, buffer was removed by suction and cells were washed twice with ice-cold PBS, before being treated with 0.5 M NaOH for 10 min at room temperature (Bosnyak et al., 2011). The material in each well, corresponding to bound radioligand, was quantified using a Wallac WizardTM 1470 γ-counter. Non-specific binding was measured in the presence of 1 μM unlabelled Ang-II. The statistical fit of the data with one- or two-site models was initially evaluated with Akaike's information criteria and extra sum-of-squares F test comparisons of model fits, and both AT1 and AT2 data were best fitted by a single-site binding model. To determine the pIC50 values for each Ang-II analogue, data were fit by one-site non-linear regression model using Graphpad Prism 6.0c for Mac OS X (GraphPad Software, La Jolla California USA).

Preparation of Rat Thoracic Aortic Rings and Measurement of Contraction Strength

Aortic rings were prepared from male Sprague Dawley rats (250-300 g) euthanized with CO2 asphyxiation. All animal care and handling procedures were performed in accordance with the Canadian Council for the Care of Laboratory Animals and were approved by the Institutional Animal Research Ethics Committee, Institut National de la Recherche Scientifique - Institut Armand-Frappier and by the Montreal Heart Institute. The descending thoracic aorta was excised, transferred to a Petri dish containing Krebs bicarbonate buffer (118.4 mM NaCl, 4.7 mM KCl, 2.5 mM $CaCl_2$, 1.2 mM KH_2PO_4, 1.2 mM $MgSO_4$, 25 mM $NaHCO_3$, 11 mM glucose, pH 7.4), and cleaned

of connective tissue. The endothelium was removed from aortic rings by gently rubbing the luminal surface and the vessel was cut into 4 mm rings. Single aortic rings were mounted in 5 mL organ baths (37°C) filled with Krebs solution aerated with carbogen gas (95% O_2, 5% CO_2). Isometric force-displacement transducers connected to a Grass 7E polygraph were used to measure changes in contraction. Aortic rings were allowed to equilibrate for 1 h under a resting tension of 1 g with buffer changes every 15 min. Once the tension was stable, a reference contractile response was obtained by stimulating with 40 mM KCl. Aortic rings were then washed multiple times, and the contractile response to Ang-II or the caged Ang-II analogues was determined as cumulative concentration-response curves. For each ring preparation, the contractile response was expressed as a percentage of the change in tension induced by 40 mM KCl.

ERK 1/2 Phosphorylation

HEK 293 cells seeded in uncoated 6-well plates were transfected with either AT1R-Venus or AT2R-Venus as described above. Cells were serum-starved for 24 h prior to stimulation. On the day of the experiment, cells were washed twice with serum-free DMEM and the assay was initiated by adding the indicated ligands and incubated at 37°C. To terminate the incubation, cells were placed on ice, the medium was removed, and then cells were washed twice with ice-cold PBS. They were then scraped into ice-cold lysis buffer (25 mM Na HEPES (pH 7.4), 150 mM NaCl, 25 mM NaF, 10 mM $MgCl_2$, 1 mM EGTA, 1 mM Na_3VO_4, 0.025% sodium deoxycholate, 10%

glycerol (v/v), 10 µg/mL leupeptin, 10 µM benzamidine, 0.5 µM microcystin, 1% Triton X-100 (v/v), 0.1 mM phenylmethylsulfonyl fluoride and 5 mM dithiothreitol). After a 30 min incubation on ice, lysates were cleared by centrifugation at 10000×g for 10 min, and the supernatants retained. The protein concentration of each lysate was determined, before being denatured using Laemmli sample buffer, and resolved by SDS-polyacrylamide gel electrophoresis (SDS-PAGE, precast 10% acrylamide gels, Bio-Rad Laboratories). Proteins were transferred onto polyvinylidene difluoride membranes, probed with a phospho-ERK1/2-specific antibody (Cell Signalling Technology) and then, after stripping the membranes with Re-blot Plus mild antibody stripping solution (Millipore), re-probed using an ERK1/2-specific antibody (Abcam) to assess the total ERK immunoreactivity. Horseradish peroxidase-conjugated secondary antibodies (Jackson ImmunoResearch Inc.) were used and immunoreactive bands were revealed by chemiluminescence and quantified using the Quantity One 1-D analysis software (Bio-Rad Laboratories).

Assessment of Angiotensin Receptor Expression in Thoracic Aorta

HEK 293 cells, HEK 293-AT1R, HEK 293-AT2R or an isolated thoracic aorta were lysed by homogenizing samples in cold 300 mM Sucrose, 60 mM KCl, 0.5 mM EGTA, 2 mM EDTA, 1 mM dithiothreitol (DTT), 1 mM $MgCl_2 \bullet 6H_2O$, 50 mM HEPES, 20 mM NaF, 0.2 mM Na_3VO_4, 20 mM β-glycerophosphate, 0.5 mM AEBSF, 25 µg/ml leupeptin, 10 µg/ml aprotinin, 1 µg/ml pepstatin, 1 µM microcystin, 0.1% NP40, pH 7.4. Samples were then sonicated with two 10-s pulses, and intact cells, nuclei and cell debris were removed by centrifugation (500×g for 10 min). The supernatant was

centrifuged (80,000×g for 60 min) to pellet the membrane fraction, the supernatants discarded and 50 µg of each membrane fraction was resolved on SDS-PAGE. Following transfer, membranes were probed with AT1R (Alomone Labs), AT2R (Alomone Labs) or N-cadherin (BD Bioscience) specific antibodies.

Live-Cell Fluorescence Imaging

To assess the cell permeability of [Tyr(DMNB)^4]Ang-II, fluorescein-conjugated derivatives of Ang-II, [Tyr(DMNB)^4]Ang-II, TAT(48-60), and PACAP(28-38) were synthesized and accumulation of fluorescein-conjugated peptides in HEK 293 cells examined. HEK 293 cells (non-transfected) were grown on glass coverslips, incubated for 60 min at 37°C with the fluorescent peptide in HEPES-Krebs-Ringer (HKR) buffer (5 mM HEPES, 2.68 mM KCl, 137 mM NaCl, 2.05 mM $MgCl_2$, 1.8 mM $CaCl_2$ and 1 g/L glucose, pH 7.4), washed extensively, and then incubated for 5 min with Cell Mask (1:1000; Invitrogen) and DRAQ5 (1:1000; BioStatus) to label the plasma membrane and nucleus, respectively. Fluorescence was then visualized with an Olympus FluoView FV1000 inverted confocal microscope. Separate channels were employed for each fluorophore (i.e. FITC, Cell Mask, DRAQ5) and the emission channels scanned sequentially to minimize crosstalk between overlapping emission spectra. Cells were imaged by serial z-stack progressive scans, background fluorescence subtracted, and fluorescence values quantified using FluoView Software (FV10-ASW).

To visualize changes in nucleoplasmic Ca^{2+} concentration ($[Ca^{2+}]n$), freshly isolated canine ventricular cardiomyocytes were plated at 37°C for 60 min on laminin-coated

35 mm glass bottom culture dishes in Tyrode's physiological buffer. Cells were loaded with 5 μM Fluo-4AM (Invitrogen; from a 2.5 mM Fluo-4AM/10% Pluronic F125/DMSO stock) for 30 min in 10 mM HEPES (pH 7.4), 134 mM NaCl, 6 mM KCl, 10 mM glucose, 2 mM $CaCl_2$, 1 mM $MgCl_2$, and in the absence or presence of [Tyr(DMNB)^4]Ang-II, as described previously (Merlen et al., 2013). Cardiomyocytes were washed three times, stained with a live-cell-permeant DNA dye (DRAQ5; 1 μM) and used for Ca^{2+} imaging within 1 h. Images were obtained using a Zeiss LSM 7 Duo microscope (combined LSM710 and Zeiss Live systems) with a 63x/1.4 oil Plan-Apochromat objective. Fluo-4AM was excited using a 488 nm/100 mW diode (1-5% laser intensity) and fluorescence emitted between 495 nm and 550 nm was collected. Cells were scanned at 30 fps in bi-directional mode. The pixel size was set at 0.2 μm and the pinhole at 1.5 Airy units. After establishing a baseline, [Tyr(DMNB)^4]Ang-II was photolysed by a 70 μW pulse of UV-light using a 405-nm/30 mW diode. The power output from the 405-nm diode was measured at the level of the stage using an EC Plan-Neofluar 10x/0.3 objective lens using an X-Cite XR2100 optical power measurement system (Lumen Dynamics Group Inc). DRAQ5 emissions were used to focus the UV-laser into a 60-μm^2 rectangular region overlapping the nucleus. The microscope stage (Zeiss Observer Z1) was equipped with a BC 405/561 dichroic mirror that permitted simultaneous photolysis of [Tyr(DMNB)^4]Ang-II (LSM 710 405 nm laser) and image acquisition (Zeiss Live). Intranuclear Ca^{2+} levels were expressed as a percentage of fluorescence intensity relative to basal fluorescence (Δ[Ca^{2+}]Nuc(F/F0;%)); basal fluorescence is the fluorescence intensity acquired 1 s prior to uncaging the [Tyr(DMNB)^4]Ang-II.

Flow Cytometry

Uptake of peptides into HEK 293 cells was quantified by flow cytometry. HEK 293 cells were incubated for 60 min at 37°C in the presence of the fluorescein-conjugated derivatives of Ang-II, [Tyr(DMNB)^4]Ang-II, TAT(48-60), or PACAP(28-38) in HKR buffer. Following multiple washes with an isotonic acidic aqueous solution (200 mM glycine, 100 mM NaCl, pH 4.0) and PBS to remove extracellular fluorescein-peptides, cells were detached by trypsinization, centrifuged at 1000×g for 5 min, and resuspended in PBS. To identify non-viable cells, propidium iodide (PI; 0.5 µg/mL) was added prior to analysis. A minimum of 10,000 viable cells per sample were analyzed using a Becton Dickinson FACScan system. The mean fluorescence intensity of the live cell population was used for further analysis using the FlowJo software.

Canine Cardiomyocyte Isolation

Cardiac cell isolation was performed by perfusion with Tyrode's solution containing collagenase (100 U/mL, Worthington, type II) as previously described (Tadevosyan et al., 2015).

Quantitative PCR

RNA from cardiac cells was extracted with Trizol (Life Technologies) following the manufacturer's protocol. cDNA was synthesized from 1 µg RNA with the use of a High Capacity cDNA Reverse Transcription Kit (Applied Biosystems). qPCR assays were performed as described previously (Dawson et al., 2012) using the following

TaqMan probes and primers (Applied Biosystems): eukaryotic 18S rRNA (Assay ID: Hs03003631_g1), NFkB (Assay ID: Cf02622547_m1), HPRT1 (Assay ID: Cf02626255_g1). HPRT1 was used as an internal standard. Each RNA was assessed in duplicate and analyzed with the delta-CT method.

Statistical Analysis

Data from radioligand binding and functional assays were from a minimum of 3 independent experiments and are presented as mean ± SEM. EC50, pEC50, IC50 and pIC50 values were determined by fitting experimental data by non-linear regression with GraphPad Prism version 6.0c for Mac OS X (GraphPad Software, La Jolla California USA). Student's t-tests (for single 2-group comparisons) , 1-way or 2-way ANOVA with Bonferroni post hoc test (multiple groups with a common control) were used for statistical comparisons and $P<0.05$ or less was considered to be statistically significant.

Results

Design and Synthesis of Photoactivable Caged Ang-II Analogues

Previous structure-function studies have shown that Ang-II activates AT1 and AT2 receptors through an induced-fit mechanism; for which the aromatic Tyr4 moiety and the α-COOH group of Phe8 are crucial for biological activity (Aumelas et al., 1985; Bovy et al., 1990; Noda et al., 1995; Samanen et al., 1989) Accordingly, we designed and synthesized three Ang-II analogues incorporating the photo-labile nitrobenzyl substituent (4,5-dimethoxy-2-nitrobenzyl; DMNB) on either the phenolic function of Tyr4, the terminal α-COOH group, or both (Fig. 1A-D). The caging substituent was stable when exposed to 1) 20% piperidine in DMF during removal of the Fmoc N-protecting group and 2) 100% trifluoroacetic acid (TFA) during peptide cleavage from the resin used in solid phase synthesis. Each Ang-II analogue eluted from RP-HPLC as a single major product. The purity of each fraction was assessed and confirmed by analytical HPLC. Analysis of Ang II, [Tyr(DMNB)^4]Ang-II, Ang-II-ODMNB and [Tyr(DMNB)^4]Ang-II-ODMNB by mass spectrometry revealed a major peak corresponding to the calculated molecular mass (Table I). Computational structural analysis using PyMol molecular visualization software predicted that the addition of the DMNB group induces conformational changes, including alterations in both main chain torsion angles and side chain orientation (Fig. 1A-D).

In order to be used in studying intracrine Ang-II signalling in intact cells, a caged Ang-II analogue must possess the following characteristics (relative to unmodified Ang-II): 1) reduced affinity for ATR1 and ATR2 binding, 2) reduced affinity and efficacy for

ATR1 and ATR2 activation, 3) rapid uncaging without inducing cell damage and release of the original unmodified form of the ligand upon uncaging, 4) increased cell permeability, 5) physiological activity of the intracellular form under conditions in which extracellular activation is excluded. What follows is a characterization of [Tyr(DMNB)^4]Ang-II, Ang-II-ODMNB and [Tyr(DMNB)^4]Ang-II-ODMNB according to these criteria.

Pharmacological Characterization of the Caged Ang-II Analogues

Radioligand binding assays showed a strong rightward shift in the displacement curve for all three analogues compared to Ang-II (Fig. 1E and 1F). The shift indicated between 100- and 1000-fold reduced binding affinity. Unmodified Ang-II displaced [^{125}I]Ang-II binding to AT1R or AT2R with IC50 values of 3.2 nM and 32 nM, respectively. In contrast, the caged analogues displaced [^{125}I]Ang-II with much higher IC50 values, indicating affinity-reductions of 2-3 orders of magnitude: for AT1R and AT2R respectively: [Tyr(DMNB)^4]Ang-II, 1.1 μM and 1.6 μM; Ang-II-ODMNB, 0.91 μM and 0.47 μM; [Tyr(DMNB)^4]Ang-II-ODMNB, 1.1 μM and 1.9 μM (Table I).

The ability of the caged Ang-II analogues (in the absence of uncaging) to activate cell-surface angiotensin receptors was evaluated by concentration-response curve bioassays using rat thoracic aortic ring preparations (Figs. 2A-D), which expresses both AT1R and AT2R (Fig. 2E). Ang-II evoked a concentration-dependent contraction with a pEC50 of 8.10±0.15 and a maximal efficacy (Emax) of 134%±11% (N=7). All caged Ang-II analogues were far less potent than Ang-II (Fig. 2F) and

induced no detectable vasoconstriction at concentrations of the order (10-8 M) used to study intracrine signalling.

Photorelease Kinetics and Action of Caged Ang-II Analogues

Photorelease kinetics of the caged Ang-II analogues (10^{-8} M) upon exposure to UV-light were examined by mass spectroscopy (Figs. 3A-C). UV-irradiation (100 W) caused a time dependent decrease in the abundance of each caged Ang-II analogue (indicating its photolysis), with a concomitant increase in free Ang-II (corresponding to Ang-II release via cleavage of the photolabile group). Mass spectrometry revealed that no significant side reactions releasing products other than Ang-II occurred during photolysis. Of the three caged Ang-II analogues, [Tyr(DMNB)^4]Ang-II showed the fastest rate of release (Fig. 3D). The time-course of changes in concentration of the caged compound ([Tyr(DMNB)^4]Ang-II) and the free Ang-II product of photolysis was independently confirmed with 3 different UV-exposure durations (1 second, 1 minute and 3 minutes) by HPLC (Fig. 3E).

We next sought to verify that photolysis resulted in the release of physiologically functional Ang-II. After assessing their contractile response to 40 mM KCl as a reference, we incubated aortic rings with caged Ang-II analogues at concentrations (10^{-8} M) that were inactive in the absence of photolysis, and then photolysis was induced by UV-irradiation while monitoring tension. UV-irradiation in the absence of caged Ang-II did not increase tension (Fig. 4A). In contrast, in the presence of the caged compounds UV-irradiation induced time-dependent increases in tension of aortic ring preparations, following an initial ~2-3 minute delay. The rate of rise of the

tension varied among the compounds (note differences in time-scales of Fig. 4B-D). Photolysis of [Tyr(DMNB)^4]Ang-II induced the fastest-rising response (Fig. 4B D). Fig. 4E shows a quantification of the response from its onset for each probe, with results expressed as percentage of maximal 40 mM KCl-response (mean±SEM values for all experiments with each agent). The fastest-appearing response was clearly seen with [Tyr(DMNB)^4]Ang-II, consistent with its rapid uncaging rate in Fig. 3D. Thus, the caged Ang II analogues described here show very limited ability to bind to and activate ATRs in the absence of photolysis; upon photolysis, they release pharmacologically active Ang-II. Because [Tyr(DMNB)^4]Ang-II displayed minimal intrinsic activity, rapid photolysis, and clear biological activity following UV-irradiation, we focused on the evaluation of [Tyr(DMNB)^4]Ang-II for further study of intracrine Ang-II signalling in live cells.

Photolysis of [Tyr(DMNB)4]Ang-II activates AT1R-mediated ERK signalling

To further examine the biological activity of Ang-II photoreleased from caged analogues, we examined an AT1R-specific response to extracellular Ang-II. Extracellular signal-regulated kinases (ERKs)-1/2 are activated by mitogenic signals, including AT1R-stimulation. Accordingly, we examined the effects of extracellular [Tyr(DMNB)^4]Ang-II and Ang-II via AT1R activation by assessing ERK1/2 phosphorylation in HEK 293 cells transiently transfected with AT1R. Ang-II (5 min, 37°C) increased ERK phosphorylation in a concentration-dependent manner that was half-maximal at ~10-8 M (Fig. 5A). At a concentration as high as 10-6 M, [Tyr(DMNB)^4]Ang-II did not induce ERK1/2 phosphorylation in the absence of

photolysis (Fig. 5B). In contrast, upon photolysis [Tyr(DMNB)^4]Ang-II induced a concentration-dependent increase in ERK1/2 phosphorylation (Fig. 5C) with a maximum level of ERK1/2 phosphorylation similar to Ang-II (Fig. 5D). Consistent with AT1R-mediated ERK activation in HEK 293 cells, Ang-II-induced ERK phosphorylation was inhibited by AT1R blockade with valsartan (Figs. 5E and 5F). UV-irradiation alone did not increase ERK1/2 phosphorylation. Hence, [Tyr(DMNB)^4]Ang-II is unable to activate AT1R-induced ERK-phosphorylation at concentrations as high as 1 μM, but upon photolysis shows full pharmacological activity.

Photolysis of [Tyr(DMNB)^4]Ang-II activates AT2R-mediated cGMP signalling

We then proceeded to examine the AT2-R mediated biological activity of extracellular Ang-II photoreleased from caged analogues. AT2R-dependent cardiac-vessel vasodilation is mediated by the NO/cGMP pathway (Tsutsumi et al., 1999). Therefore, we examined the effects of extracellular [Tyr(DMNB)^4]Ang-II and Ang-II on AT2R activation by measuring cGMP levels by ELISA (Thermo Scientific) in HEK 293 cells transiently transfected with AT2R. cGMP production in Ang-II-treated cells (10 nM, 45 min) was 2-fold greater than vehicle-treated cells (3.63±0.43 versus 1.80±0.22 pmol/mg protein) (Fig. 6). At the same concentration, [Tyr(DMNB)^4]Ang-II had no effect on the cGMP levels (2.24±0.04 versus 2.17±0.24 pmol/mg protein for cells exposed to UV-light alone). Upon uncaging by UV-irradiation, [Tyr(DMNB)^4]Ang-II (10 nM) increased the cellular cGMP content by 2-fold (4.51±0.33 versus 2.17±0.24 pmol/mg protein for cells exposed to UV-light alone). The effects of both Ang-II and

irradiated [Tyr(DMNB)^4]Ang-II were abolished by preincubation with the AT2R-selective antagonist, PD 123319. Similarly, preincubating HEK 293 cells with the non-selective NO synthase inhibitor L-NAME markedly attenuated the increase in cGMP induced by both Ang-II and irradiated [Tyr(DMNB)^4]Ang-II. Hence, [Tyr(DMNB)^4]Ang-II (10 nM) alone is unable to activate AT2R but upon photolysis, it shows strong AT2R-mediated activity.

Cell Permeability of [Tyr(DMNB)^4]Ang-II

To test the ability of [Tyr(DMNB)^4]Ang-II to cross the plasma membrane, we synthesized fluorescein-labelled derivatives of caged (fluorescein-[Ahx^0,Tyr(DMNB)^4]Ang-II) and uncaged (fluorescein-[Ahx^0]Ang-II) angiotensin-II. The uptake of Ang-II and [Tyr(DMNB)^4]Ang-II was compared to that of fluorescein-[Ahx^0]TAT(48-60), a cell permeable peptide derived from the HIV transactivating regulatory protein TAT, and fluorescein-[Ahx^0]PACAP(28-38), a highly basic segment of pituitary adenylyl cyclase-activating polypeptide previously characterized as having no cell-penetrating properties (Doan et al., 2012). Non-transfected HEK 293 cells were employed to minimize receptor-mediated endocytosis of Ang-II. Cells were treated with either fluorescein-[Ahx^0]Ang-II, fluorescein-[Ahx^0,Tyr(DMNB)^4]Ang-II, fluorescein-[Ahx^0]PACAP(28-38) or fluorescein-[Ahx^0]TAT(48-60) and the cellular uptake of the fluorescent peptides was analyzed by both confocal fluorescence microscopy and flow cytometry (Figs 7A and 7B). CellMask™ orange and DRAQ5 (a DNA-binding dye) were used to delineate the plasma membrane and nucleus, respectively. After acidic washes to remove peptides non-specifically bound to the

extracellular surface, images of cellular fluorescence were acquired with a confocal microscope. Fluorescein-[Ahx^0]TAT(48-60) (2936±410) produced a clear intracellular fluorescence signal, whereas almost no intracellular fluorescence was observed with fluorescein-[Ahx^0]PACAP(28-38) (186±61). Overall, we observed significantly greater intracellular fluorescence intensity with fluorescein-[Ahx^0,Tyr(DMNB)^4]Ang-II (3475±338) than with fluorescein-[Ahx^0]Ang-II (726±74) (Fig. 7C). Further analysis with flow cytometry revealed that cells preincubated with fluorescein-[Ahx0,Tyr(DMNB)^4]Ang-II displayed a much greater mean fluorescence signal (77±2) than with fluorescein-[Ahx^0]Ang-II (24±6) and even greater than the cell-permeable standard fluorescein-[Ahx^0]TAT(48-60) (60±3) (Fig. 7D). Thus, Tyr(DMNB)^4]Ang-II is a potent cell-penetrating peptide that permits both 1) delivery of a caged Ang-II analogue into intact live cells and 2) spatial and temporal control of ligand release.

Photolysis of [Tyr(DMNB)^4]Ang-II Inside Cardiac Cells Increases Nuclear Calcium, 18S rRNA and NF κB mRNA levels

Nuclear Ca^{2+} regulates essential cellular processes, including transcription, growth and apoptosis. Ang-II is a potent promoter of Ca^{2+} release but, so far, tools have been lacking to discriminate the contribution from organelle-localized versus cell-surface ATRs. Both AT1R and AT2R are expressed on nuclei of numerous cell types, including cardiomyocytes (Tadevosyan et al., 2012). Here, using live-cell confocal fluorescence microscopy, we examined the effect of intracellular [Tyr(DMNB)^4]Ang-II photolysis on nucleoplasmic Ca^{2+} ([Ca^{2+}]n) and cytoplasmic Ca^{2+} ([Ca^{2+}]c) indices in adult canine cardiomyocytes (Figs 8 A-C). Changes in [Ca^{2+}]n and

$[Ca^{2+}]c$ were visualized using the cell-permeable Ca^{2+} dye Fluo-4 AM. Following exposure to 20 nM [Tyr(DMNB)^4]Ang-II, cells were thrice-washed to ensure removal of the extracellular moiety.

Photolysis of [Tyr(DMNB)^4]Ang-II caused a significant increase in $[Ca^{2+}]n$ whereas non-photolyzed [Tyr(DMNB)^4]Ang-II did not (Figs. 8A and B). To ensure that the photoactivated compound does not act via diffusion out of the cell followed by surface-receptor interaction, cells loaded with [Tyr(DMNB)^4]Ang-II were both pre-treated for 20 min with, and photolyzed in the presence of, 1 μM valsartan. Valsartan did not reduce the magnitude of the increase in $[Ca^{2+}]n$ at 400 s post-photolysis of [Tyr(DMNB)^4]Ang-II, but the increase in $[Ca^{2+}]n$ was more rapid in the presence of valsartan. Hence, following photolysis, Ang-II does not increase $[Ca^{2+}]n$ by leaving the cell and acting on cell-surface receptors; however, there may be cross-talk between cell surface and nuclear ATRs. Cells exposed to 100 μM 2-APB to block inositol trisphosphate (IP3) receptors (the principal angiotensin-dependent nuclear Ca^{2+}-entry pathway (Tadevosyan et al., 2010)) displayed a significant decrease in $[Ca^{2+}]n$ accumulation following photolysis. Sham-loaded cardiomyocytes (i.e. without [Tyr(DMNB)^4]Ang-II in the loading buffer) displayed no change in $[Ca^{2+}]n$ in response to UV-irradiation (Fig. 8B). Extracellular application of 20 nM Ang-II caused a slow and limited increase in $[Ca^{2+}]n$, relative to that induced by intracellular photolysis of [Tyr(DMNB)^4]Ang-II, and this effect was abolished when cells were pretreated with 1 μM valsartan. The changes in $[Ca^{2+}]c$ in response to photolysis of [Tyr(DMNB)^4]Ang-II were generally similar to that of $[Ca^{2+}]n$, but the increases in fluorescence intensity were smaller for $[Ca^{2+}]c$ (Figs 8B and C). To compare directly the $[Ca^{2+}]n$ response

with the $[Ca^{2+}]c$ response, we normalized each to their respective baseline values (Fig 8D). The $[Ca^{2+}]n$ response occurred with or before the $[Ca^{2+}]c$ response, making it very unlikely that the $[Ca^{2+}]n$ increases are secondary to the change in $[Ca^{2+}]c$. Figure 8E indicates the mean response in each group by showing mean baseline (t=10 seconds) versus post-photolysis (t=400 seconds) values.

We have shown previously that Ang-II increases the transcription of ribosomal RNA (rRNA) and NF-κB mRNA in nuclei isolated from rat adult cardiomyocytes (Tadevosyan et al., 2010). Similarly, photolysis of $[Tyr(DMNB)^4]$Ang-II (cAng-II) increased 18S rRNA and NF-κB mRNA, compared to the more slowly photolysed Ang-II-ODMNB, in intact cardiomyocytes (Figs 9A and 9B). Therefore, selective activation of intracellular ATRs in cardiomyocytes increases $[Ca^{2+}]n$ and regulates gene transcription.

Discussion

The intracrine RAS has been suggested to control intracellular Ca^{2+}-fluxes, generation of reactive oxygen species, junctional conductance, cell volume, chromatin solubility, gene transcription and posttranslational histone modifications (Re & Cook, 2011). The presence of functional Ang-II receptors on the nuclear membrane, along with the nuclear localization of carboxy-terminal sequence of the AT1R (Lee et al., 2004), provided additional support for the idea that classical receptor signalling occurs on intracellular membranes (Morinelli et al., 2007). To further examine this concept and develop a tool for exploring it, we synthesized novel caged, cell-permeable Ang-II analogues, [Tyr(DMNB)^4]Ang-II being the most effective, allowing spatio-temporal control of ATR activation within intact cells. Furthermore, we have shown that photolysis of [Tyr(DMNB)^4]Ang-II inside intact cardiomyocytes increases [Ca^{2+}]n, as well as 18S rRNA and NF-κB mRNA levels.

A variety of approaches, each with its own challenges and technical limitations, have been applied in vitro and in vivo to study the role of the intracrine RAS. Redding et al. bred transgenic mice that expressed a construct comprising Ang-II fused in-frame to the cyan fluorescent protein (ECFP), linked by a small spacer arm, under control of the mouse metallothionein promoter (Redding et al., 2010). This construct was developed in a manner that ensures that ECFP-Ang-II is synthesized but retained intracellularly as it was unable to access the secretory pathway. Although this transgene resulted in changed diastolic and systolic blood pressure, as well as thrombotic renal microangiopathy, its expression was ubiquitous rather than

intracellularly targeted. Similarly, Li et al. used the sgtl2 gene promoter to selectively drive expression of ECFP-Ang-II in proximal renal tubules; however, this construct was delivered using an adenovirus and, hence, the effect was transient (Li et al., 2011). Furthermore, in vivo delivery to other organs might have been hampered by host immune responses. There have been several reports in which liposomes were used to deliver hormones intracellularly. Filipeanu et al. demonstrated that liposomal delivery of Ang-II into A7r5 cells induced cell growth through activation of the phosphoinositide 3-kinase and MAPK/ERK pathways (Filipeanu et al., 2001). However, during liposomal delivery only a small fraction (7.2±0.2%) of the administered Ang-II was actually taken up into target cells. Additional disadvantages of the liposomal delivery strategy include inability to target the cargo to a specific cell type, biological instability due to the amphiphilic character of liposomes, interactions with lipoproteins, and interactions with common degradation pathways. De Mello used microinjection to introduce Ang-II into ventricular cardiomyocytes and observed increased inward Ca^{2+} current (ICa) and altered myocardial contractility (De Mello, 1998). Similarly, Haller et al. reported that microinjection of Ang-II into vascular smooth muscle cells (VSMCs) induced a rise in [Ca^{2+}] within the injected cell and also in adjacent cells (Haller et al., 1996). It was concluded that Ang-II stimulated a cluster of VSMCs via release of diffusible intracellular second messengers from the injected cell. Nevertheless, the possibility that observed effects were due to outflow of the peptide that eventually activated neighbouring cell-surface receptors could not be excluded. Moreover, although microinjection provides a way to introduce an agonist (or antagonist) into a cell, it can only be applied realistically to single cell experiments

and, therefore, like liposomal delivery, it is not amenable to biochemical analysis of intracrine effects.

The development of caged, cell-permeable Ang-II analogues will permit the study of the molecular pharmacology and physiological function of endogenous ATRs in a broad range of primary cells and possibly ex vivo tissue preparations. Insights into the structural interactions involving Ang-II and its receptors guided the design of caged peptide analogues to selectively interfere with receptor binding and activation (Chaulk & MacMillan, 1998; Monroe et al., 1999; Ando et al., 2001). The photolabile 4,5-dimethoxy-2-nitrobenzyl group (DMNB) exhibits maximal absorption in the near UV-range (λ=365 nm), excellent solubility in aqueous solution, and is compatible with sensitive biological preparations. In the present study, DMNB was introduced at the phenolic hydroxyl group of Tyr4 and/or at the carboxyl function of Phe8 of Ang-II (Figs. 1A-D). The addition of DMNB enhanced the lipophilicity of Ang-II, allowing [Tyr(DMNB)^4]AngII to cross plasma membranes efficiently, while remaining water soluble. Cell permeability was so effective that the intracellular accumulation of [Tyr(DMNB)^4]AngII was greater than that of a potent cell-penetrating peptide derived from the HIV-1 trans-activating protein, TAT (Fig. 7A-D). All three synthetic caged analogues i.e. [Tyr(DMNB)^4]Ang-II, Ang-II-ODMNB and [Tyr(DMNB)^4]Ang-II-ODMNB) showed greatly decreased ability to bind and activate ATRs in the absence of photolysis. [Tyr(DMNB)^4]Ang-II was the best suited for live-cell studies because of its rapid photolysis kinetics. This characteristic allows the study of events occurring on a rapid time scale and minimizes exposure of target-cells to UV-irradiation. Rapid

photolysis also permits evaluation of the effects of acute ligand application in either single cells or a cell population, an experimental condition that cannot be achieved with liposomes or microinjection. The temporal and spatial control of Ang-II release upon UV-irradiation provides a versatile tool for studying the functional and molecular pharmacology of intracrine Ang-II signalling. We examined the effects of [Tyr(DMNB)^4]Ang-II in isolated tissue preparations, cultured HEK 293 cells, and isolated adult cardiomyocytes. Studies in these systems confirmed the reduction in intrinsic affinity and activity of [Tyr(DMNB)^4]Ang-II, in comparison with Ang-II, and its capacity to demonstrate substantial pharmacological potency and efficacy upon photolysis.

Although we previously demonstrated the mobilization of nuclear Ca^{2+} (which could be blocked by 2-APB) and de novo mRNA synthesis upon exposure to Ang-II in isolated nuclei (Tadevosyan et al, 2010), the physiological significance remained unclear in the absence of convincing evidence in an intact cell system. Here, we used photorelease of Ang-II from a caged analogue to show intracellular Ang-II dependent mobilization of nuclear Ca^{2+}, along with de novo RNA synthesis, in intact cardiomyocytes. This effect was suppressed by 2-APB, potentially implicating IP3 receptors, whereas extracellular valsartan did not alter the response. Thus, the caged compound allowed us for the first time to show convincingly that intracellular Ang-II increases nucleoplasmic and cytosolic [Ca^{2+}] in intact cardiomyocytes, with pharmacological evidence suggesting that this action is independent of extracellular receptors and that IP3 receptors might play an important role. Further work is needed

to clarify the precise mechanisms underlying [Ca^{2+}] changes in various subcellular compartments produced by intracellular Ang-II. In principle the probes developed here could be used to study the role of intracellular Ang-II not only in cardiomyocytes, but in any cell-type.

In summary, we have revealed the effectiveness of incorporating a photosensitive 4,5 dimethoxy-2-nitrobenzyl (DMNB) blocking group on the tyrosine-4 side chain of Ang II in creating a cell-permeable, photoactivable Ang-II analogue. The corresponding caged Ang-II analogue, [Tyr(DMNB)^4]Ang-II, was stable, pharmacologically inactive within the required concentration range, rapidly released upon exposure to UV-light, and rapidly releases active Ang-II upon photolysis. Furthermore, when loaded into live cells, uncaging [Tyr(DMNB)^4]Ang-II with a localized pulse from a UV-laser produces spatial and temporal release of Ang-II that, unlike other means of delivery, allows both pharmacological and functional studies of the intracrine Ang-II system in both primary and cultured cells.

Acknowledgments

The authors thank Nathalie L'Heureux and Chantal St-Cyr for technical assistance, Dr Feng Xiong for statistical analyses and France Thériault for secretarial help with the manuscript.

Funding

Supported by grants from the Canadian Institutes for Health Research (CIHR, 6957 and 68929), the Quebec Heart and Stroke Foundation, and the Fondation Leducq (ENAFRA Network, 07/CVD/03). AT was supported by an FRQS-RSCV/HSFQ doctoral scholarship. BF was supported by a postdoctoral fellowship from the "Fondation universitaire Armand-Frappier de l'INRS" and a Banting Research Foundation grant.

References

Ando H, Furuta T, Tsien RY & Okamoto H. (2001). Photo-mediated gene activation using caged RNA/DNA in zebrafish embryos. Nat Genet 28, 317-325.

Aumelas A, Sakarellos C, Lintner K, Fermandjian S, Khosla MC, Smeby RR & Bumpus FM. (1985). Studies on angiotensin II and analogs: impact of substitution in position 8 on conformation and activity. Proc Natl Acad Sci U S A 82, 1881-1885.

Bosnyak S, Jones ES, Christopoulos A, Aguilar MI, Thomas WG & Widdop RE. (2011). Relative affinity of angiotensin peptides and novel ligands at AT1 and AT2 receptors. Clin Sci (Lond) 121, 297-303.

Bourgault S, Letourneau M & Fournier A. (2005). Development and pharmacological characterization of "caged" urotensin II analogs. Peptides 26, 1475-1480.

Bourgault S, Letourneau M & Fournier A. (2007). Development of photolabile caged analogs of endothelin-1. Peptides 28, 1074-1082.

Bovy PR, O'Neal JM, Olins GM, Patton DR, McMahon EG, Palomo M, Koepke JP, Salles KS, Trapani AJ, Smits GJ, McGraw DE & Hutton WC. (1990). Structure-activity relationships for the carboxy-terminus truncated analogues of angiotension II, a new class of angiotensin II antagonists. J Med Chem 33, 1477-1482.

Chaulk SG & MacMillan AM. (1998). Caged RNA: photo-control of a ribozyme reaction. Nucleic Acids Res 26, 3173-3178.

Cook JL, Mills SJ, Naquin R, Alam J & Re RN. (2006). Nuclear accumulation of the AT1 receptor in a rat vascular smooth muscle cell line: effects upon signal transduction and cellular proliferation. J Mol Cell Cardiol 40, 696-707.

Dawson K, Wu CT, Qi XY & Nattel S. (2012). Congestive heart failure effects on atrial fibroblast phenotype: differences between freshly-isolated and cultured cells. PLoS One 7, e52032.

De Mello WC. (1998). Intracellular angiotensin II regulates the inward calcium current in cardiac myocytes. Hypertension 32, 976-982.

Doan ND, Letourneau M, Vaudry D, Doucet N, Folch B, Vaudry H, Fournier A & Chatenet D. (2012). Design and characterization of novel cell-penetrating peptides from pituitary adenylate cyclase-activating polypeptide. J Control Release 163, 256-265.

Filipeanu CM, Henning RH, de Zeeuw D & Nelemans A. (2001). Intracellular Angiotensin II and cell growth of vascular smooth muscle cells. Br J Pharmacol 132, 1590-1596.

Frustaci A, Kajstura J, Chimenti C, Jakoniuk I, Leri A, Maseri A, Nadal-Ginard B & Anversa P. (2000). Myocardial cell death in human diabetes. Circ Res 87, 1123-1132.

Ghosh M, Song X, Mouneimne G, Sidani M, Lawrence DS & Condeelis JS. (2004). Cofilin promotes actin polymerization and defines the direction of cell motility. Science 304, 743-746.

Haller H, Lindschau C, Erdmann B, Quass P & Luft FC. (1996). Effects of intracellular angiotensin II in vascular smooth muscle cells. Circ Res 79, 765-772.

Haller H, Lindschau C, Quass P & Luft FC. (1999). Intracellular actions of angiotensin II in vascular smooth muscle cells. J Am Soc Nephrol 10 Suppl 11, S75-83.

Jullian M, Hernandez A, Maurras A, Puget K, Amblard M, Martinez J & Subra G. (2009). N-terminus FITC labeling of peptides on solid support: the truth behind the spacer Tetrahedron Lett 50, 260-263.

Kobori H, Nangaku M, Navar LG & Nishiyama A. (2007). The intrarenal renin-angiotensin system: from physiology to the pathobiology of hypertension and kidney disease. Pharmacol Rev 59, 251-287.

Lang CC & Struthers AD. (2013). Targeting the renin-angiotensin-aldosterone system in heart failure. Nat Rev Cardiol 10, 125-134.

Lee DK, Lanca AJ, Cheng R, Nguyen T, Ji XD, Gobeil F, Jr., Chemtob S, George SR & O'Dowd BF. (2004). Agonist-independent nuclear localization of the Apelin, angiotensin AT1, and bradykinin B2 receptors. J Biol Chem 279, 7901-7908.

Li W, Llopis J, Whitney M, Zlokarnik G & Tsien RY. (1998). Cell-permeant caged InsP3 ester shows that Ca2+ spike frequency can optimize gene expression. Nature 392, 936-941.

Li XC, Cook JL, Rubera I, Tauc M, Zhang F & Zhuo JL. (2011). Intrarenal transfer of an intracellular fluorescent fusion of angiotensin II selectively in proximal

tubules increases blood pressure in rats and mice. Am J Physiol Renal Physiol 300, F1076-1088.

McCray JA, Herbette L, Kihara T & Trentham DR. (1980). A new approach to time-resolved studies of ATP-requiring biological systems; laser flash photolysis of caged ATP. Proc Natl Acad Sci U S A 77, 7237-7241.

Merlen C, Farhat N, Luo X, Chatenet D, Tadevosyan A, Villeneuve LR, Gillis MA, Nattel S, Thorin E, Fournier A & Allen BG. (2013). Intracrine endothelin signaling evokes IP3-dependent increases in nucleoplasmic Ca in adult cardiac myocytes. J Mol Cell Cardiol 62, 189-202.

Monroe WT, McQuain MM, Chang MS, Alexander JS & Haselton FR. (1999). Targeting expression with light using caged DNA. J Biol Chem 274, 20895-20900.

Morinelli TA, Raymond JR, Baldys A, Yang Q, Lee MH, Luttrell L & Ullian ME. (2007). Identification of a putative nuclear localization sequence within ANG II AT1A receptor associated with nuclear activation. Am J Physiol Cell Physiol 292, C1398-1408.

Muralidharan S, Maher GM, Boyle WA & Nerbonne JM. (1993). "Caged" phenylephrine: development and application to probe the mechanism of alpha-receptor-mediated vasoconstriction. Proc Natl Acad Sci U S A 90, 5199-5203.

Muralidharan S & Nerbonne JM. (1995). Photolabile "caged" adrenergic receptor agonists and related model compounds. J Photochem Photobiol B 27, 123-137.

Noda K, Saad Y & Karnik SS. (1995). Interaction of Phe8 of angiotensin II with Lys199 and His256 of AT1 receptor in agonist activation. J Biol Chem 270, 28511-28514.

Re RN & Cook JL. (2011). Noncanonical intracrine action. J Am Soc Hypertens 5, 435-448.

Redding KM, Chen BL, Singh A, Re RN, Navar LG, Seth DM, Sigmund CD, Tang WW & Cook JL. (2010). Transgenic mice expressing an intracellular fluorescent fusion of angiotensin II demonstrate renal thrombotic microangiopathy and elevated blood pressure. Am J Physiol Heart Circ Physiol 298, H1807-1818.

Robertson AL, Jr. & Khairallah PA. (1971). Angiotensin II: rapid localization in nuclei of smooth and cardiac muscle. Science 172, 1138-1139.

Samanen J, Cash T, Narindray D, Brandeis E, Yellin T & Regoli D. (1989). The role of position 4 in angiotensin II antagonism: a structure-activity study. J Med Chem 32, 1366-1370.

Schlichting I, Rapp G, John J, Wittinghofer A, Pai EF & Goody RS. (1989). Biochemical and crystallographic characterization of a complex of c-Ha-ras p21 and caged GTP with flash photolysis. Proc Natl Acad Sci U S A 86, 7687-7690.

Schwab AJ, Barker F, 3rd, Goresky CA & Pang KS. (1990). Transfer of enalaprilat across rat liver cell membranes is barrier limited. Am J Physiol 258, G461-475.

Singh VP, Le B, Bhat VB, Baker KM & Kumar R. (2007). High-glucose-induced regulation of intracellular ANG II synthesis and nuclear redistribution in cardiac myocytes. Am J Physiol Heart Circ Physiol 293, H939-948.

Singh VP, Le B, Khode R, Baker KM & Kumar R. (2008). Intracellular angiotensin II production in diabetic rats is correlated with cardiomyocyte apoptosis, oxidative stress, and cardiac fibrosis. Diabetes 57, 3297-3306.

Tadevosyan A, Allen BG & Nattel S. (2015). Isolation and study of cardiac nuclei from canine myocardium and adult ventricular myocytes. MethodsMol Biol 1234, 69-80.

Tadevosyan A, Maguy A, Villeneuve LR, Babin J, Bonnefoy A, Allen BG & Nattel S. (2010). Nuclear-delimited angiotensin receptor-mediated signaling regulates cardiomyocyte gene expression. J Biol Chem 285, 22338-22349.

Tadevosyan A, Vaniotis G, Allen BG, Hebert TE & Nattel S. (2012). G protein-coupled receptor signalling in the cardiac nuclear membrane: evidence and possible roles in physiological and pathophysiological function. J Physiol 590, 1313-1330.

Tertyshnikova S & Fein A. (1998). Inhibition of inositol 1,4,5-trisphosphate-induced Ca2+ release by cAMP-dependent protein kinase in a living cell. Proc Natl Acad Sci U S A 95, 1613-1617.

Tsutsumi Y, Matsubara H, Masaki H, Kurihara H, Murasawa S, Takai S, Miyazaki M, Nozawa Y, Ozono R, Nakagawa K, Miwa T, Kawada N, Mori Y, Shibasaki Y, Tanaka Y, Fujiyama S, Koyama Y, Fujiyama A, Takahashi H & Iwasaka

T. (1999). Angiotensin II type 2 receptor overexpression activates the vascular kinin system and causes vasodilation. J Clin Invest 104, 925-935.

Vaniotis G, Glazkova I, Merlen C, Smith C, Villeneuve LR, Chatenet D, Therien M, Fournier A, Tadevosyan A, Trieu P, Nattel S, Hebert TE & Allen BG. (2013). Regulation of cardiac nitric oxide signalling by nuclear beta-adrenergic and endothelin receptors. J Mol Cell Cardiol 62, 58-68.

Wang SS & Augustine GJ. (1995). Confocal imaging and local photolysis of caged compounds: dual probes of synaptic function. Neuron 15, 755-760.

Yu H, Li J, Wu D, Qiu Z & Zhang Y. (2010). Chemistry and biological applications of photo-labile organic molecules. Chem Soc Rev 39, 464-473.

Zhang X, Wang G, Dupre DJ, Feng Y, Robitaille M, Lazartigues E, Feng YH, Hebert TE & Wu G. (2009). Rab1 GTPase and dimerization in the cell surface expression of angiotensin II type 2 receptor. J Pharmacol Exp Ther 330, 109-117.

Zimmerman B, Beautrait A, Aguila B, Charles R, Escher E, Claing A, Bouvier M & Laporte SA. (2012). Differential beta-arrestin-dependent conformational signaling and cellular responses revealed by angiotensin analogs. Sci Signal 5, ra33.

Figure Legends

Figure 1. Structures of the caged Ang-II analogues and competitive displacement of [^{125}I]Ang-II by caged Ang-II analogues. (A) Angiotensin-II (B) Ang-II-ODMNB (C) [Tyr(DMNB)^{4}]Ang-II (D) [Tyr(DMNB)^{4}]Ang-II-ODMNB. The position of the photo-sensitive 4,5-dimethoxy-2-nitrobenzyl moiety is indicated in brackets and was added either on the side chain of the tyrosine at position 4, the C-terminal carboxylic function of phenylalanine-8, or at both sites. Red and blue surfaces describe negative and positive electrostatic potentials (-3.5 kBT, +3.5 kBT), respectively. Three-dimensional structures were generated using the PyMol visualization software. The electrostatic potentials were calculated using the Adaptive Poisson-Boltzmann Solver with the PyMol tool. (E) and (F), Competitive displacement of [^{125}I]Ang-II by Ang-II or caged Ang-II analogues (n=6/condition) in HEK 293 cells transfected with AT1R or AT2R. Data are percentage of specific radioligand binding in absence of competitors. Non-specific binding was determined in presence of 1 µM Ang-II.

Figure 2. Concentration-dependent responses of rat thoracic aortic rings to various analogues without uncaging. Contraction-recordings were obtained with a curvilinear pen recorder for (A) Ang-II, (B) Ang-II-ODMNB (C) [Tyr(DMNB)^{4}]Ang-II, and (D) [Tyr(DMNB)^{4}]Ang-II-DMNB. (E) Immunoblotting for AT1R, AT2R and N-cadherin (positive control) in membranes isolated from rat thoracic aorta as well as HEK 293, HEK 293-AT1R and HEK 293-AT2R cells. (F) Overall results expressed as

percentage of contractile response induced by 40 mM KCl. Data are mean±SEM of at least 5 experiments/group performed on tissues isolated from separate animals for each experiment. Descending arrows on original recordings indicate baseline adjustment.

Figure 3. Photolysis kinetics of various analogues. Photolysis (100-W UV-lamp) of a 10-8 M solution of (A) [Tyr(DMNB)^4]Ang-II, (B) Ang-II-ODMNB and (C) [Tyr(DMNB)^4]Ang-II-ODMNB was performed in Krebs-Henseleit buffer and analyzed by mass spectrometry (n=3/group). (D) Caged peptide concentration over time following UV-irradiation. (E) Signal-intensity (Y-axis) versus wavelength (X-axis) and HPLC elution-time (Z-axis) at different times after photorelease of [Tyr(DMNB)^4]Ang-II as analyzed by analytical HPLC.

Figure 4. Contractile responses of rat thoracic aortic rings following photolysis of various analogues. Isometric aortic tension recording was obtained with a curvilinear pen recorder after 15-min incubation in the presence of caged analogues (10-8 M) followed by in situ photolysis with 30-W UV-lamp. (A) Control (B) [Tyr(DMNB)^4]Ang-II, (C) Ang-II-ODMNB and (D) [Tyr(DMNB)^4]Ang-II-DMNB. (E) Overall results as percentage of contractile response induced by 40 mM KCl. Data are mean±SEM (n=4 independent preparations from each of 4 animals/group).

Figure 5. AT1R-dependent ERK-phosphorylation following photolysis of [Tyr(DMNB)^4]Ang-II. Effects of (A) Ang-II, (B) [Tyr(DMNB)^4]Ang-II, (C) UV-irradiated [Tyr(DMNB)^4]Ang-II on serum starved HEK 293 cells transfected with AT1R. Phosphorylated ERK1/2 (p-ERK) and total ERK1/2 (ERK) immunoreactivity was determined on cell-lysates. (D) pERK immunoreactivity normalized to total ERK immunoreactivity (mean±SEM). (E) p-ERK and ERK immunoreactivity in AT1R transfected HEK 293 cells treated with vehicle, in the presence or absence of 10-nM Ang-II or [Tyr(DMNB)^4]Ang-II (cAng-II), or valsartan (Val; 1 μM, 30 min) with or without UV-irradiation (1 min). (F) Mean±SEM data corresponding to experiment in (E), N=3/concentration. **P<0.01, ***P<0.001, ns=non-significant.

Figure 6. AT2R-dependent cGMP production following photolysis of [Tyr(DMNB)^4]Ang-II. cGMP was measured in serum-starved HEK 293 cells transfected with AT2R following incubation with vehicle (control), Ang-II (10 nM) or [Tyr(DMNB)^4]Ang-II, 10 nM), in the presence of PD123319 (PD, 1 μM), L-NAME (1 mM), and UV-irradiation, as indicated. Data shown mean±SEM, n=3/condition, ***P<0.001, ##P<0.01 or ###P<0.001 vs. Ang II, §§§P<0.001 vs. [Tyr(DMNB)4]Ang-II, ns=non-significant.

Figure 7. Cellular uptake of fluorescein-[Ahx^0,Tyr(DMNB)^4]Ang-II. (A) Intracellular distribution of fluorescein-[Ahx^0]Ang-II, fluorescein-[Ahx^0,Tyr(DMNB)^4]Ang-II, fluorescein-[Ahx^0]PACAP(28-38) and fluorescein-[Ahx^0]TAT(48-60) upon confocal

microscopy in live non-permeabilized HEK 293 cells. Cell Mask and DRAQ5 were used to delineate the plasma membrane and nuclei, respectively. (B) Intracellular fluorescence intensity (mean±SEM, ***P<0.001). (C) Representative uptake efficiency of fluorescein-conjugated PACAP(28-38), TAT(48-60), Ang-II and [Tyr(DMNB)^4]Ang-II in HEK 293 cells upon flow cytometry; quantified (D) with fluorescence-activated cell sorting analysis software FlowJo (Mean±SEM, n=3/condition, *P<0.05, ***P<0.001).

Figure 8. Response of nucleoplasmic and cytosolic [Ca^{2+}] to photolysis of intracellular [Tyr(DMNB)^4]Ang-II. A) Nucleoplasmic and cytosolic [Ca^{2+}] recorded in canine cardiomyocytes before (t=10 s) and after (t=400 s) photolysis in cells loaded with vehicle (control), 20 nM [Tyr(DMNB)^4]Ang-II (cAng-II), 20 nM cAng-II + 1 μM valsartan, 20 nM cAng-II + 100 μM 2-APB, 1 μM valsartan alone or extracellularly administered 20 nM Ang-II with or without 1 μM Valsartan. Photolysis was induced by a pulse of UV-light (2-5 s, 70 μW) from a 405 nm/30 mW diode. (B) Nucleoplasmic (C) Cytosolic[Ca^{2+}] recorded in ventricular cardiomyocytes before and after photolysis in cells preincubated with [Tyr(DMNB)^4]Ang-II, vehicle (Ctl), valsartan, 2-APB along with non-photolysed [Tyr(DMNB)^4]Ang-II or vehicle. Dotted bracket: UV irradiation. DRAQ5 fluorescence was used to select the area corresponding to the nucleoplasm. Signals are presented as background-subtracted normalized fluorescence (%F/F0), where F is the fluorescence intensity and F0 is the resting fluorescence in the same cell prior to photolysis. (D) [Ca^{2+}] fluorescence in nucleus and cytosol normalized to

respective baseline (t=10 s) values. Nuclear changes are shown by dashed lines and cytosolic by solid lines. (E) For each condition (n=8-12 cells), mean nuclear Fluo-4 fluorescence at baseline (t=10 s; hatched bars) or after stimulation (t=400 s) was quantified. Data are mean±SEM, ***P<0.000, n.s.=nonsignificant.

Figure 9. Photolysis of intracellular [Tyr(DMNB)^4]Ang-II regulates gene-transcription. (A) 18S rRNA and (B) NF-κB mRNA quantified by qPCR. A stimulation-control (scr) condition was performed where cardiomyocytes were loaded with a slowly-photolysing Ang-II analogue, Ang-II-ODMNB. Myocytes were incubated with [Tyr(DMNB)^4]Ang-II or Ang-II-ODMNB (10 nM) for 30 min at room temperature. Following incubation, cells were washed, placed on ice, and exposed to a UV-lamp (30 W Pen-Ray lamp) for 1 min. In addition, cells were examined following treatment with buffer (Ctl) or extracellular Ang-II (Ang-II; 10 nM). Cells were then incubated at 37°C for 4 h prior to RNA extraction. Data are mean±SEM, *P<0.05, **P<0.01, ***P<0.0001.

Table 1. Physicochemical and binding properties of Ang-II and its photolabile analogues, as evaluated by competition binding assays using HEK 293-AT1 and HEK 293-AT2 transfected cells

Compound Name	[a]MS[calc] (g.mol^{-1})	[b]MS[found] (g.mol^{-1})	[c]Purity	Binding ^{125}I-Ang-II (HEK293-AT1R)			Binding ^{125}I-Ang-II (HEK293-AT2R)		
				IC_{50} (nM)	pIC_{50}	*n*	IC_{50} (nM)	pIC_{50}	*n*
Ang-II	**1046.18**	**1047.10**	**≥95%**	**3.2**	**8.58±0.10**	**8**	**32**	**7.65±0.18**	**6**
[Tyr(DMNB)^4]Ang-II	**1241.35**	**1241.52**	**≥95%**	**1110**	**6.01±0.11**	**6**	**1640**	**6.88±0.61**	**6**
Ang-II-ODMNB	**1241.35**	**1242.43**	**≥95%**	**915**	**6.13±0.27**	**6**	**470**	**6.45±0.28**	**5**
[Tyr(DMNB)^4]Ang-II-ODMNB	**1436.52**	**1437.52**	**≥95%**	**1140**	**6.31±0.27**	**6**	**1930**	**6.54±0.52**	**6**

[a]Theoretical monoisotopic molecular weight as calculated with ChemDraw Ultra 7.0.1. [b]M/z value assessed by MALDI-TOF-MS. [c]Percentage of purity determined by HPLC using the eluent system: A = H_2O containing 0.06% TFA and B = 40% CH_3CN in aqueous 0.06% TFA, with a gradient of 1% B/min and a flow rate of 1 ml/min on a Jupiter C_{18} column. Detection at 229 nm.

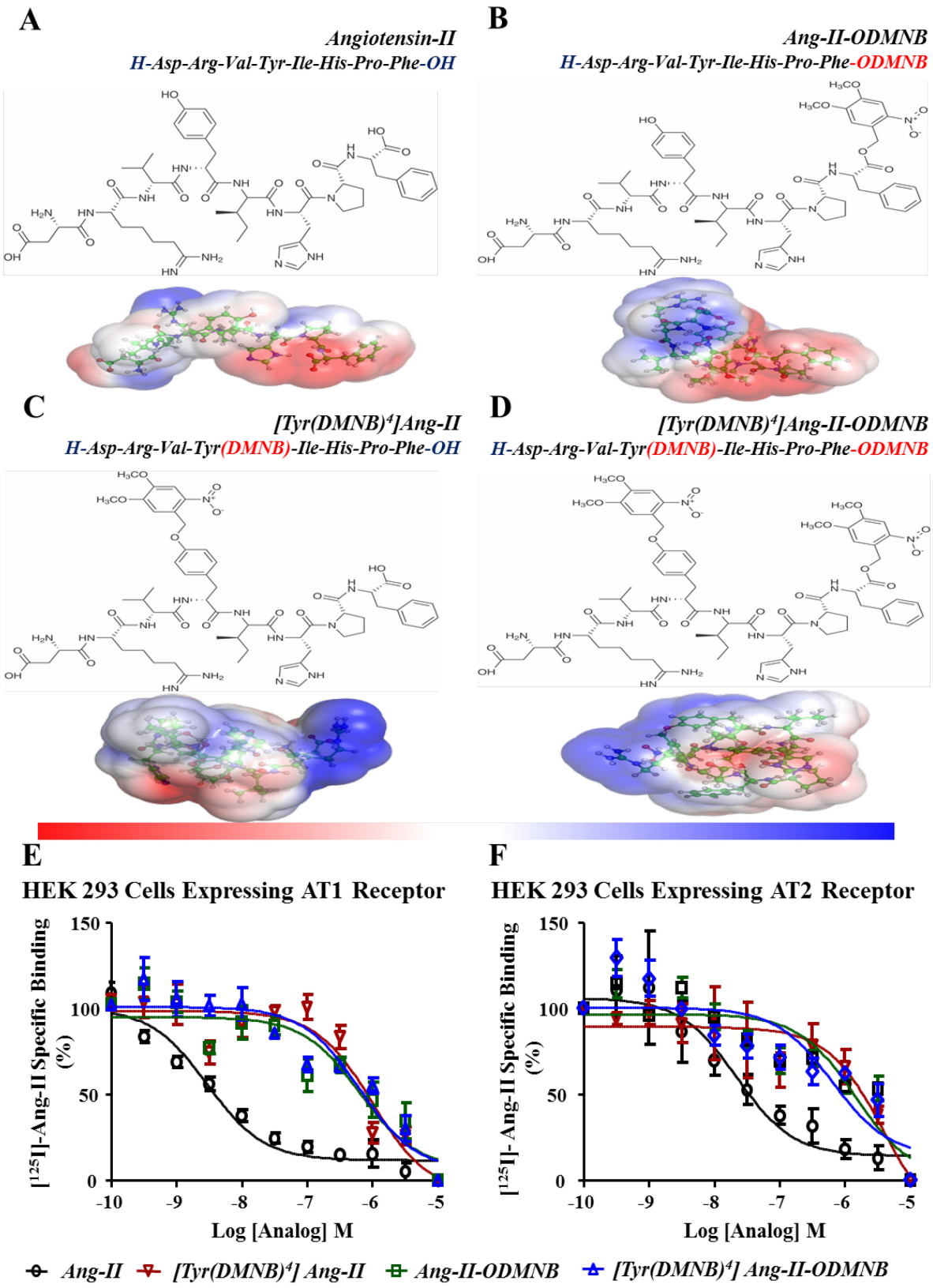
A
Angiotensin-II
H-Asp-Arg-Val-Tyr-Ile-His-Pro-Phe-OH
B
Ang-II-ODMNB
H-Asp-Arg-Val-Tyr-Ile-His-Pro-Phe-ODMNB
C
[Tyr(DMNB)4]Ang-II
H-Asp-Arg-Val-Tyr(DMNB)-Ile-His-Pro-Phe-OH
D
[Tyr(DMNB)4]Ang-II-ODMNB
H-Asp-Arg-Val-Tyr(DMNB)-Ile-His-Pro-Phe-ODMNB
E
HEK 293 Cells Expressing AT1 Receptor
[125I]-Ang-II Specific Binding (%)
Log [Analog] M
F
HEK 293 Cells Expressing AT2 Receptor
[125I]- Ang-II Specific Binding (%)
Log [Analog] M
Ang-II
[Tyr(DMNB)4] Ang-II
Ang-II-ODMNB
[Tyr(DMNB)4] Ang-II-ODMNB

Figure 1

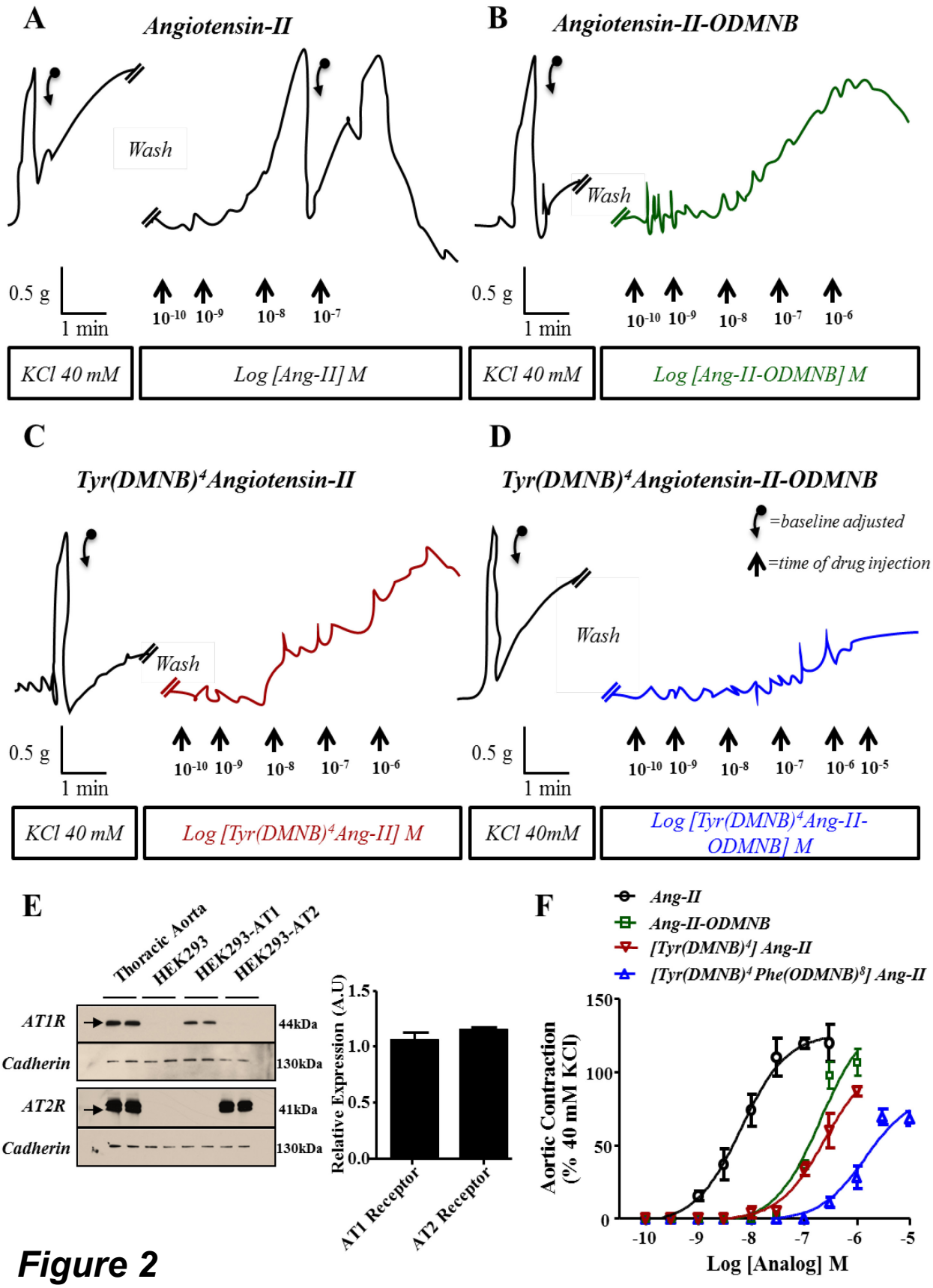
A
Angiotensin-II
Wash
0.5 g
1 min
10-10 10-9 10-8 10-7
KCl 40 mM
Log [Ang-II] M
B
Angiotensin-II-ODMNB
Wash
0.5 g
1 min
10-10 10-9 10-8 10-7 10-6
KCl 40 mM
Log [Ang-II-ODMNB] M
C
Tyr(DMNB)4Angiotensin-II
Wash
0.5 g
1 min
10-10 10-9 10-8 10-7 10-6
KCl 40 mM
Log [Tyr(DMNB)4Ang-II] M
D
Tyr(DMNB)4Angiotensin-II-ODMNB
=baseline adjusted
=time of drug injection
Wash
0.5 g
1 min
10-10 10-9 10-8 10-7 10-6 10-5
KCl 40mM
Log [Tyr(DMNB)4Ang-II-ODMNB] M
E
Thoracic Aorta
HEK293
HEK293-AT1
HEK293-AT2
AT1R
44kDa
Cadherin
130kDa
AT2R
41kDa
Cadherin
130kDa
Relative Expression (A.U)
1.5
1.0
0.5
0.0
AT1 Receptor
AT2 Receptor
F
Ang-II
Ang-II-ODMNB
[Tyr(DMNB)4] Ang-II
[Tyr(DMNB)4 Phe(ODMNB)8] Ang-II
Aortic Contraction (% 40 mM KCl)
150
100
50
0
-10 -9 -8 -7 -6 -5
Log [Analog] M

Figure 2

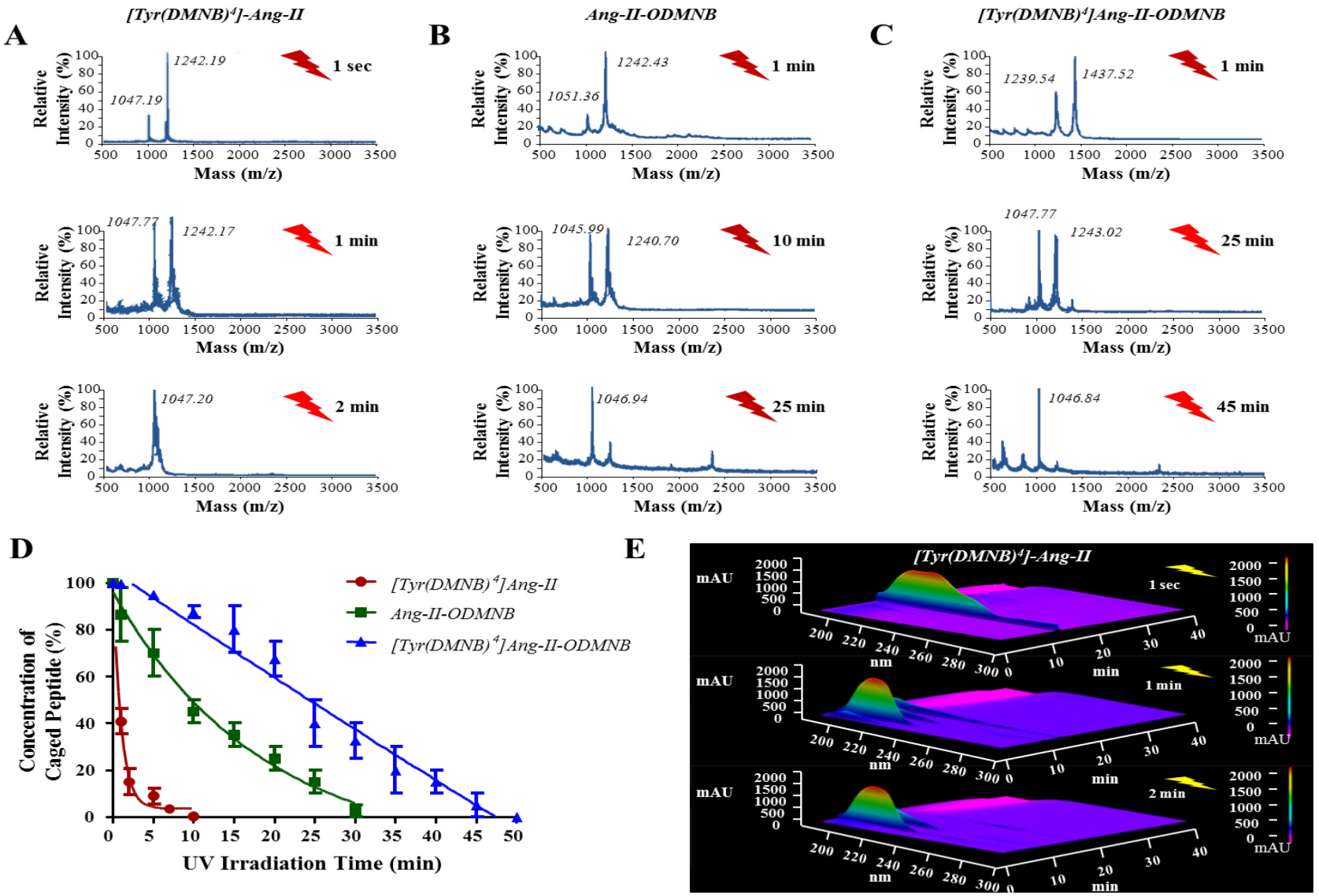
A
[Tyr(DMNB)4]-Ang-II
1242.19
1047.19
1 sec
1047.77
1242.17
1 min
1047.20
2 min
B
Ang-II-ODMNB
1242.43
1051.36
1 min
1045.99
1240.70
10 min
1046.94
25 min
C
[Tyr(DMNB)4]Ang-II-ODMNB
1239.54
1437.52
1 min
1047.77
1243.02
25 min
1046.84
45 min
Relative Intensity (%)
Mass (m/z)
D
Concentration of Caged Peptide (%)
UV Irradiation Time (min)
[Tyr(DMNB)4]Ang-II
Ang-II-ODMNB
[Tyr(DMNB)4]Ang-II-ODMNB
E
[Tyr(DMNB)4]-Ang-II
1 sec
1 min
2 min
mAU
nm
min

Figure 3

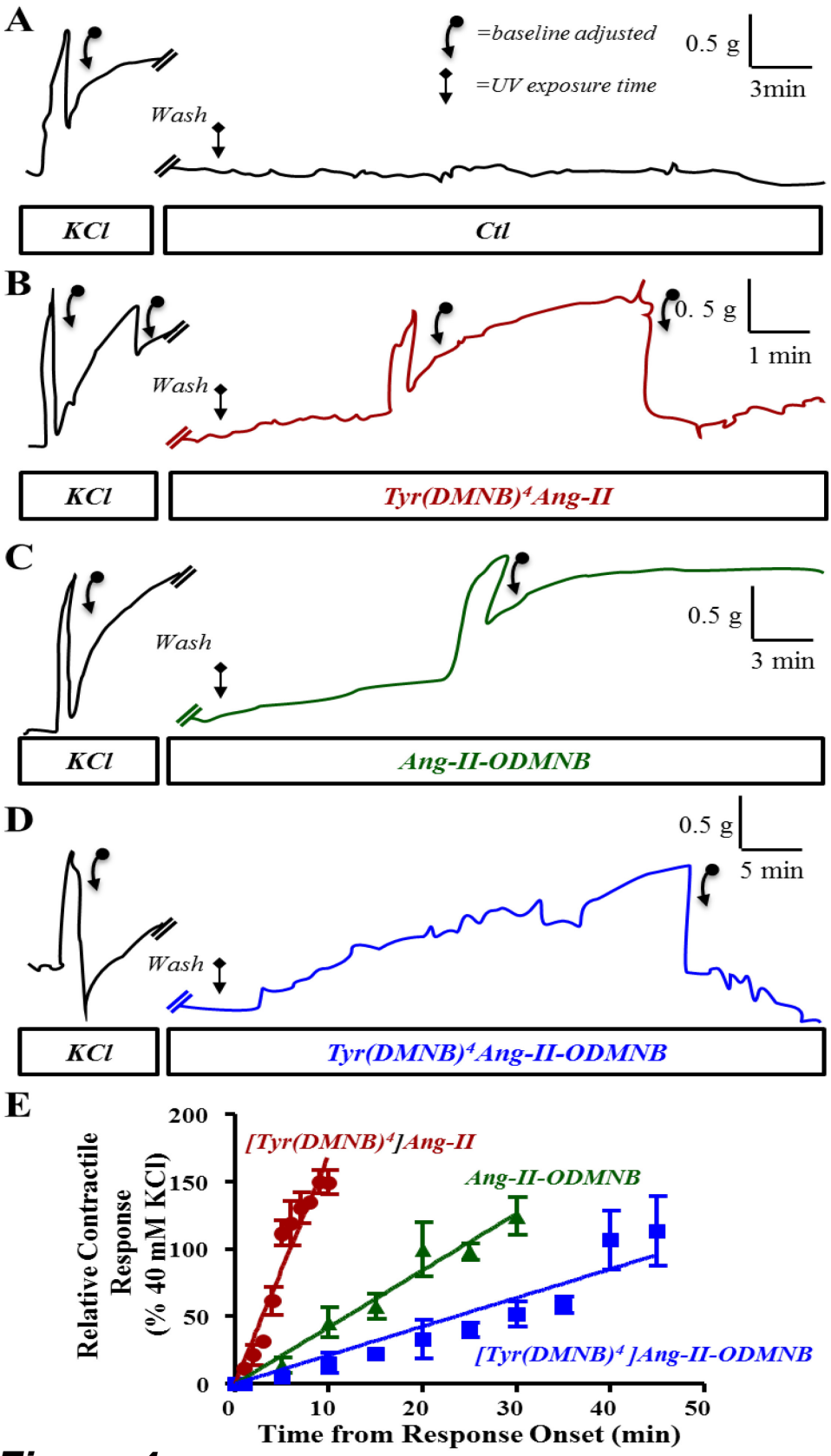
A
=baseline adjusted
=UV exposure time
0.5 g
3min
Wash
KCl
Ctl
B
0. 5 g
1 min
Wash
KCl
Tyr(DMNB)4Ang-II
C
0.5 g
3 min
Wash
KCl
Ang-II-ODMNB
D
0.5 g
5 min
Wash
KCl
Tyr(DMNB)4Ang-II-ODMNB
E
Relative Contractile Response (% 40 mM KCl)
200
150
100
50
0
[Tyr(DMNB)4]Ang-II
Ang-II-ODMNB
[Tyr(DMNB)4]Ang-II-ODMNB
0
10
20
30
40
50
Time from Response Onset (min)

Figure 4

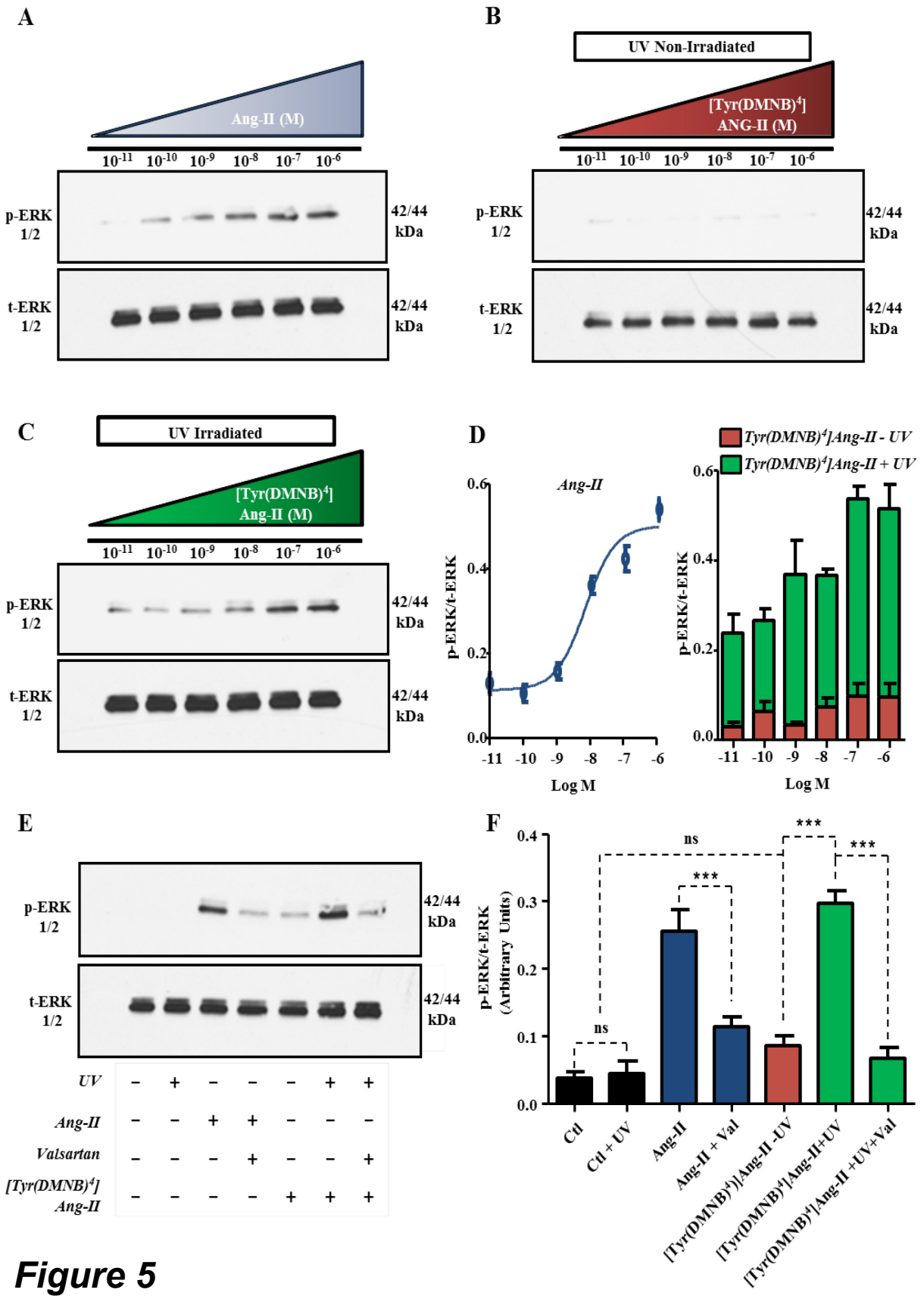
A
Ang-II (M)
10-11 10-10 10-9 10-8 10-7 10-6
p-ERK 1/2
t-ERK 1/2
42/44 kDa
B
UV Non-Irradiated
[Tyr(DMNB)4] ANG-II (M)
C
UV Irradiated
[Tyr(DMNB)4] Ang-II (M)
D
Ang-II
Tyr(DMNB)4]Ang-II - UV
Tyr(DMNB)4]Ang-II + UV
p-ERK/t-ERK
Log M
E
UV
Ang-II
Valsartan
[Tyr(DMNB)4] Ang-II
F
p-ERK/t-ERK (Arbitrary Units)
ns
***
Ctl
Ctl + UV
Ang-II
Ang-II + Val
[Tyr(DMNB)4]Ang-II -UV
[Tyr(DMNB)4]Ang-II+UV
[Tyr(DMNB)4]Ang-II +UV+Val

Figure 5

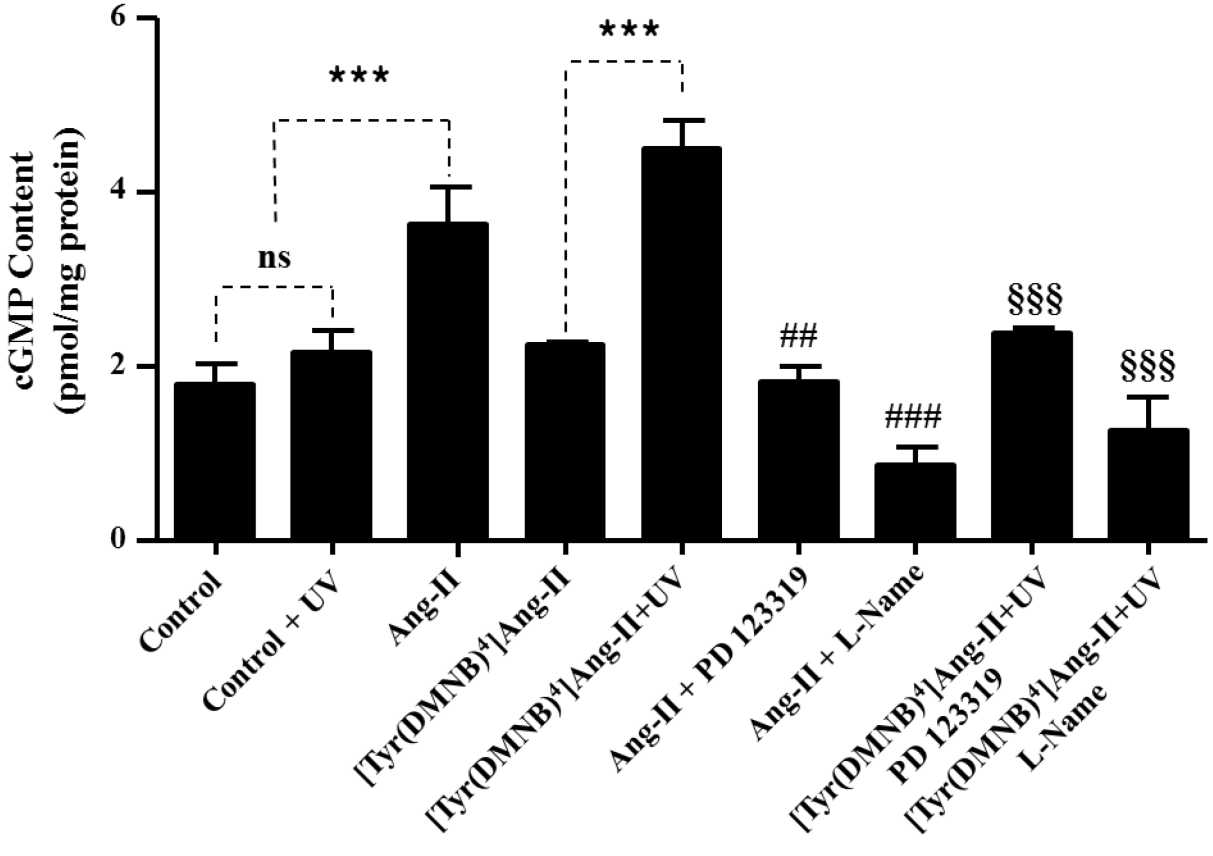
cGMP Content
(pmol/mg protein)
6
4
2
0
***
***
ns
##
###
§§§
§§§
Control
Control + UV
Ang-II
[Tyr(DMNB)4]Ang-II
[Tyr(DMNB)4]Ang-II+UV
Ang-II + PD 123319
Ang-II + L-Name
[Tyr(DMNB)4]Ang-II+UV
PD 123319
[Tyr(DMNB)4]Ang-II+UV
L-Name

Figure 6

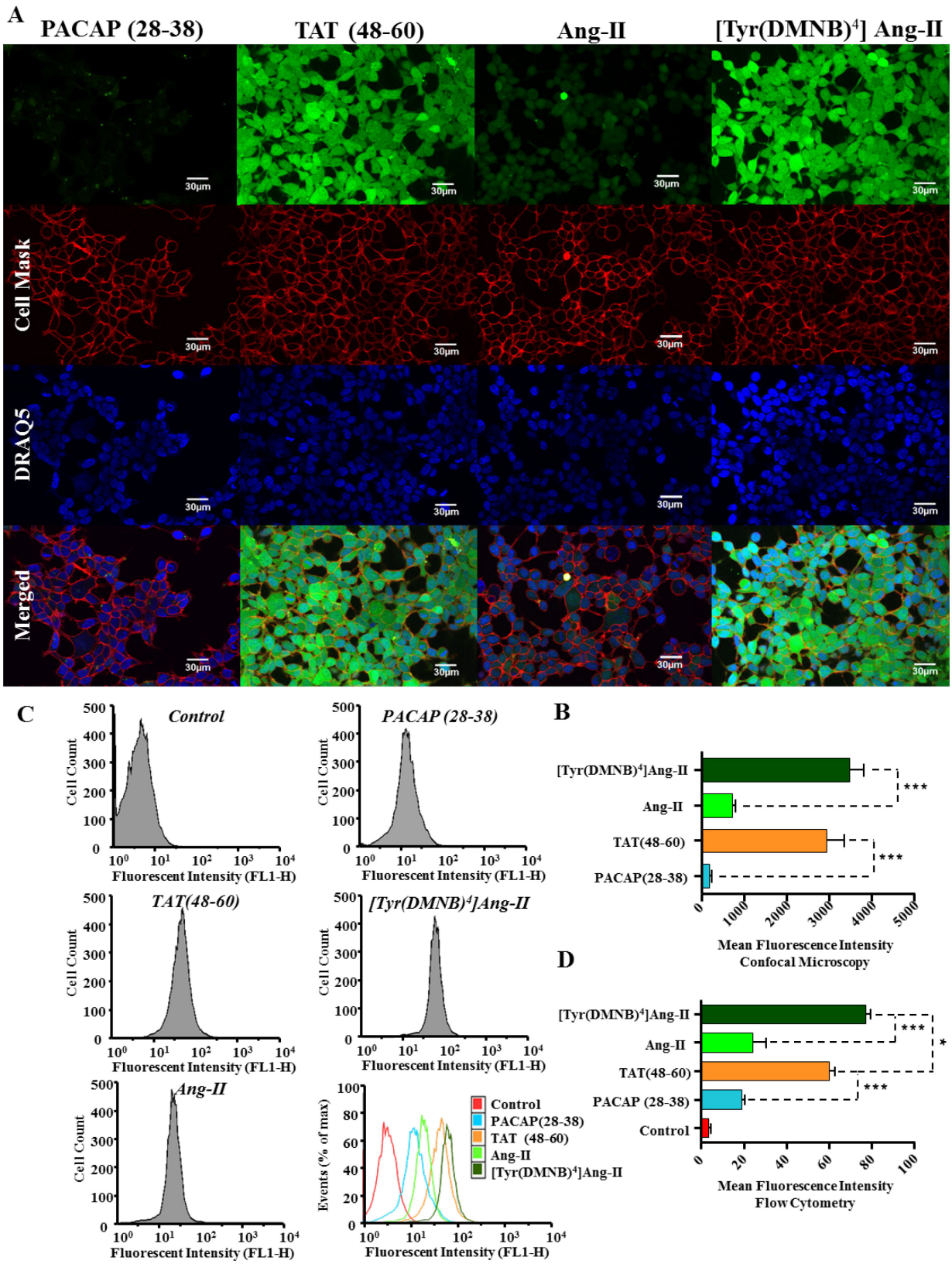
A
PACAP (28-38)
TAT (48-60)
Ang-II
[Tyr(DMNB)4] Ang-II
Cell Mask
DRAQ5
Merged
30µm
C
Control
PACAP (28-38)
TAT(48-60)
[Tyr(DMNB)4]Ang-II
Ang-II
Cell Count
Fluorescent Intensity (FL1-H)
Events (% of max)
Control
PACAP(28-38)
TAT (48-60)
Ang-II
[Tyr(DMNB)4]Ang-II
B
[Tyr(DMNB)4]Ang-II
Ang-II
TAT(48-60)
PACAP(28-38)
***
Mean Fluorescence Intensity
Confocal Microscopy
D
[Tyr(DMNB)4]Ang-II
Ang-II
TAT(48-60)
PACAP (28-38)
Control
***
*
Mean Fluorescence Intensity
Flow Cytometry

Figure 7

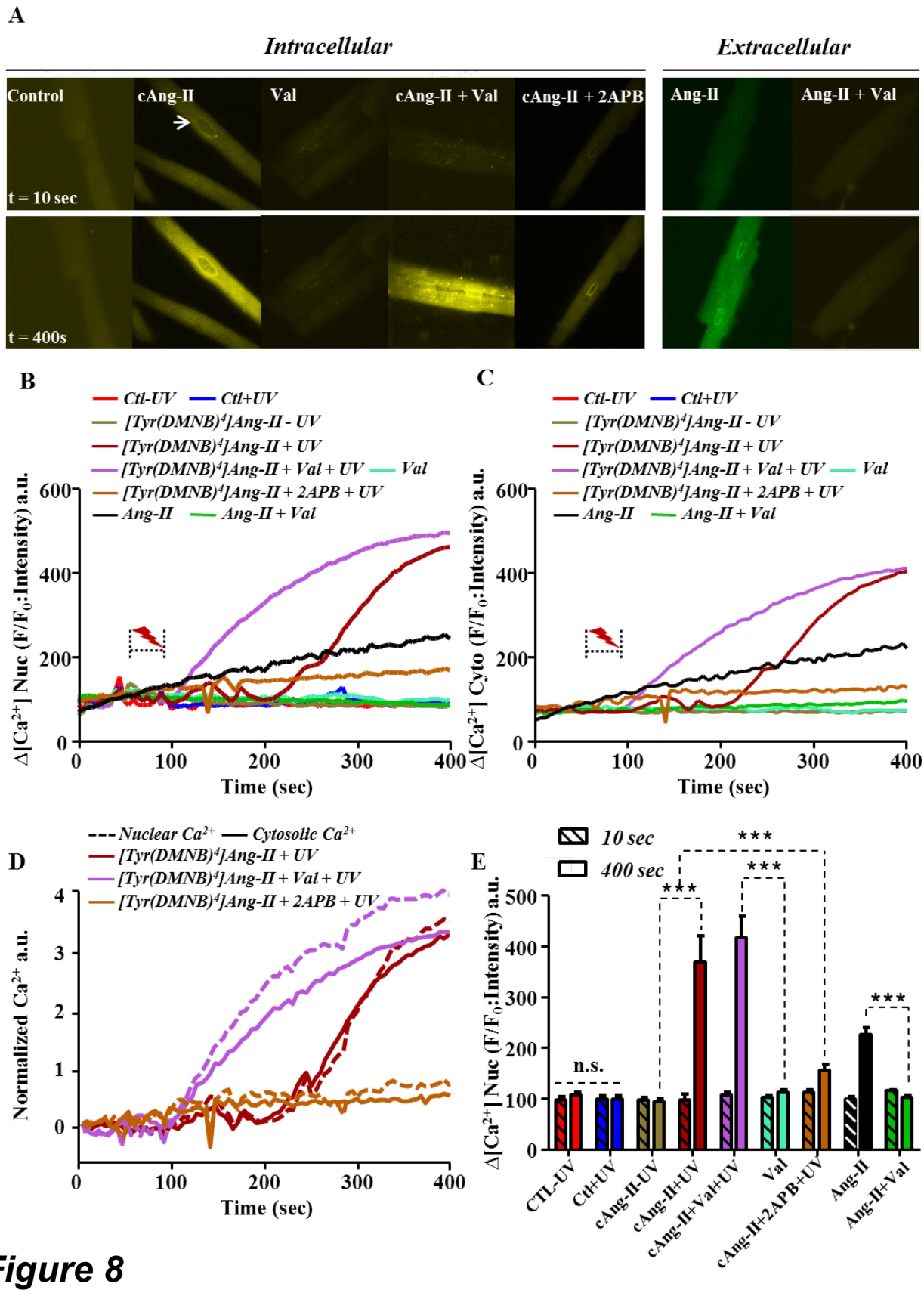
A
Intracellular
Extracellular
Control
cAng-II
Val
cAng-II + Val
cAng-II + 2APB
Ang-II
Ang-II + Val
t = 10 sec
t = 400s
B
C
Ctl-UV
Ctl+UV
[Tyr(DMNB)4]Ang-II - UV
[Tyr(DMNB)4]Ang-II + UV
[Tyr(DMNB)4]Ang-II + Val + UV
Val
[Tyr(DMNB)4]Ang-II + 2APB + UV
Ang-II
Ang-II + Val
Δ[Ca2+] Nuc (F/F0:Intensity) a.u.
Δ[Ca2+] Cyto (F/F0:Intensity) a.u.
Time (sec)
D
Nuclear Ca2+
Cytosolic Ca2+
[Tyr(DMNB)4]Ang-II + UV
[Tyr(DMNB)4]Ang-II + Val + UV
[Tyr(DMNB)4]Ang-II + 2APB + UV
Normalized Ca2+ a.u.
E
10 sec
400 sec
***
n.s.
CTL-UV
Ctl+UV
cAng-II-UV
cAng-II+UV
cAng-II+Val+UV
Val
cAng-II+2APB+UV
Ang-II
Ang-II+Val

Figure 8

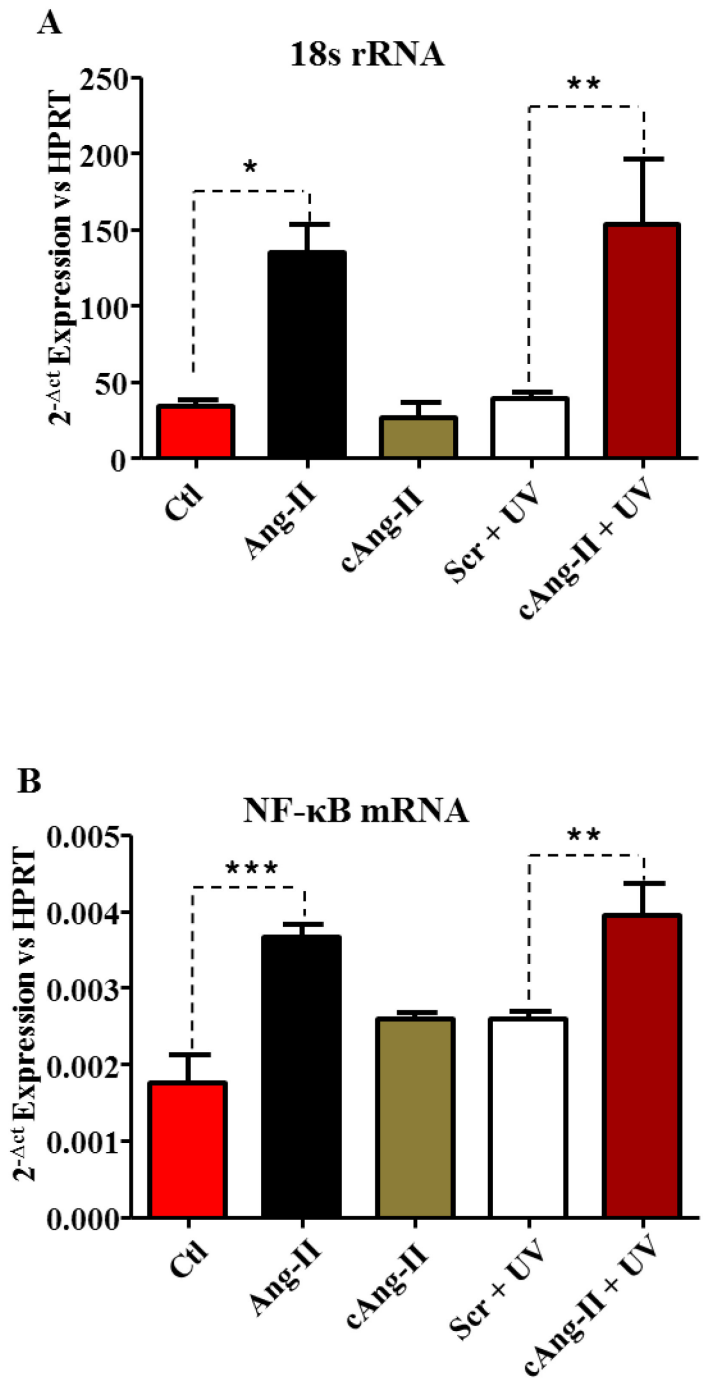
A
18s rRNA
2-Δct Expression vs HPRT
250
200
150
100
50
0
*
**
Ctl
Ang-II
cAng-II
Scr + UV
cAng-II + UV
B
NF-κB mRNA
2-Δct Expression vs HPRT
0.005
0.004
0.003
0.002
0.001
0.000
***
**
Ctl
Ang-II
cAng-II
Scr + UV
cAng-II + UV

Figure 9

CHAPTER 4 – Nuclear Compartmentalization of Angiotensin-II Receptor Signaling in Cardiac Fibroblasts Governs de Novo RNA Expression, Proliferation and Collagen Synthesis.

Linking Statement and Author Contribution

Cardiac fibroblasts make up the largest cell population of the heart in number, and are prominently affected by cardiac structural remodeling. Atrial fibroblasts, in contrast to ventricular fibroblasts, are more responsive to pro-fibrotic stimuli. Recent findings point to the synthesis and intracellular retention of Ang-II in fibroblasts. We hypothesized that intracellular Ang-II and associated nuclear AT1R and AT2R activation control the pattern of gene-expression in atrial fibroblasts via discrete signaling systems and thereby play a key role in the development of cardiac fibrosis

Tadevosyan A, Merlen C, Harada M, Qi XY, Villeneuve LR, Chatenet D, Fournier A, Allen BG, Nattel S. Nuclear Compartmentalization of Angiotensin-II Receptor Signaling in Cardiac Fibroblasts Governs de Novo RNA Expression, Proliferation and Collagen Synthesis. (Article in preparation)

A.T., B.G.A. and S.N. conceived the original research idea and experimental design. A.T. performed all of the experiments and generated Figures 1-8. A.T. also performed analysis and interpretation of data, and wrote the first draft of the manuscript. C.M., M.H. and Qi X.Y. assisted in cell isolation, purification of nuclei and transcription initiation assays. L.R.V. performed calcium imaging experiments. D.C, A.F, B.G.A. and S.N. supervised the project, provided intellectual input and edited the final manuscript.

Nuclear Compartmentalization of Angiotensin-II Receptor Signaling in Cardiac Fibroblasts Governs de Novo RNA Expression, Proliferation and Collagen Synthesis.

Artavazd Tadevosyan,[§] Clémence Merlen,[§] Masahide Harada,[*] Xiaoyan Qi,[§] David Chatenet,[#] Alain Fournier,[#] Bruce G Allen,[ϕ§†] Stanley Nattel[§†]

[§]Department of Medicine and Research Center; Montreal Heart Institute and Université de Montréal, Montreal, Quebec, Canada; [ϕ]Department of Biochemistry and Molecular Medicine; Université de Montréal, Montreal, Quebec, Canada; [#]Institut National de la Recherche Scientifique-Institut Armand Frappier, Laval, Québec, Canada *Department of Cardiology, Fujita Health University School of Medicine, Toyoake, Japan; [†]Department of Pharmacology and Therapeutics, McGill University, Montréal, QC, Canada

Running title: Intracrine Ang-II Signalling in Fibroblasts

Word count: 6843

Correspondence to: Stanley Nattel OR Bruce G. Allen, 5000 Bélanger St., Montréal, Québec, H1T 1C8, Canada. Tel.: (514)-376-3330; Fax: (514)-376-1355;

Abstract

Introduction: Cardiac fibroblasts are the most abundant cell type in the heart and govern cardiac structural remodeling. Recent findings indicate that the activation of the intracellular renin-angiotensin system (iRAS) in cardiomyocytes changes cell communication and alters cardiac excitability, but the functional importance of iRAS in cardiac fibroblasts is unknown.

Objective: To characterize intracellular Ang-II binding-sites and their functional role in atrial cardiac fibroblasts.

Methods and Results: Immunoblots of subcellular fractions obtained from isolated canine atrial fibroblast indicated the presence of nuclear AT1R and AT2R. AT1R was predominantly found on the inner nuclear membrane, whereas AT2R immunoreactivity localised to the inner nuclear membrane as well as the nucleoplasm. Ang-II-FITC binding assays and immunohistochemical analysis further confirmed the nuclear localization of AT1R and AT2R. AT1R mRNA and nuclear immunoreactivity- levels were significantly increased in atrial fibroblasts isolated from a canine heart failure (HF) model. In contrast, AT2R mRNA levels remained unchanged and nuclear AT2R was glycosylated. Nuclear expression of G proteins Gαq/11, Gαi/3, and Gβ was confirmed by immunoblotting and confocal microscopy. [α-^{32}P]UTP incorporation showed that nuclear AT1R and AT2R regulate de novo RNA synthesis via inositol trisphosphate receptor (IP3R)- and nitric-oxide (NO)-dependant pathways. In intact cultured fibroblasts, intracellular Ang-II release lead to IP3R-

dependant increases in nucleoplasmic Ca^{2+} concentration with IP3R3 being the predominant isoform detected. Intracellular Ang-II regulated fibroblast proliferation ([^{3}H]thymidine incorporation), collagen mRNA levels and collagen 1A1 secretion.

Conclusions: AT1R and AT2R are present on fibroblast nuclei. Nuclear AT1R are upregulated whereas AT2R are glycosylated in HF. Nuclear AT1R and AT2R, acting through NO and IP3R, regulate fibroblast transcription and intracellular Ang-II regulates fibroblast proliferation and ECM synthesis. Fibroblast nuclear AT1R/AT2R may play a key role in heart structural remodeling.

Keywords: Intracrine angiotensin system, nuclear receptors, cardiac fibroblasts, fibroblast regulation, remodeling

Introduction

Cardiac fibroblasts are the most predominant cell type of the myocardium and play a fundamental role in regulating the structural, mechanical and electrical properties of the heart [1, 2]. Fibroblast proliferation, which results in excessive extracellular matrix synthesis and cardiomyocyte uncoupling, leads to tissue fibrosis and myocardial remodeling. Many of the functional effects of cardiac fibroblasts are mediated by proinflammatory cytokines, vasoactive peptides and hormones [3].

The renin-angiotensin system (RAS) through primary reactive vasoconstrictor angiotensin-II (Ang-II) regulates fibroblast homeostasis [4]. Ang-II leads to progressive collagen production within the myocardium in a dose-dependent manner and has emerged as a key candidate promoting the development of myocardial fibrosis [5]. The classical RAS was considered for decades as a circulatory system in which the octapeptide Ang-II is delivered to target tissue or cells. Evidence is now available that independently of traditional RAS, cardiac cells can synthesize Ang-II intracellularly. Exposure of fibroblasts to isoproterenol or high glucose results in increased intracellular Ang-II levels [6]. Similarly, cardiomyocytes isolated from diabetic rats contains higher Ang-II concentrations compared to healthy animals [7]. Microinjection of Ang-II into cardiomyocytes changes physiological properties such as cell volume, cell communication and activation of ion channels [8].

In the present study we sought to assess in atrial fibroblasts the subcellular distribution of Ang-II type 1 (AT1R) and type 2 receptors (AT2R), to characterize the underlying subtype-specific signalling mechanisms and define potential functional

significance using a novel caged Ang-II analog, [Tyr(DMNB)^4]Ang-II [9]. We investigated atrial fibroblasts because of their important role in atrial fibrillation secondary to structural remodeling [2, 3]. A canine model of heart failure (HF) induced by ventricular tachypacing (VTP) was used to study the potential role of the iRAS in HF-related atrial arrhythmogenic remodeling as well as the effects of HF on Ang-II intracrine signalling [2, 3].

Materials and Methods

Heart Failure (HF) Animal Model

All animal protocols were approved by the institutional animal research ethics committee and were in accordance with the guidelines of the National Institutes of Health. Adult mongrel dogs were anesthetized with ketamine (5.0 mg/kg IV), diazepam (0.25 mg/kg IV) and halothane (1.5% PI). A unipolar pacing lead was inserted under fluoroscopy via the left internal jugular vein into the right ventricular apex and connected to an electronic pacemaker implanted in a subcutaneous pocket in the neck. After 24-hour post-operative recovery, the ventricular pacemaker was programmed to pace the ventricles at 240 bpm and an electrophysiological study was performed at the end of the VTP period.

Atrial Fibroblast Isolation

Adult mongrel dogs of either sex (20-30 kg) were anesthetized with morphine (2 mg/kg subcutaneous injection), α-chloralose (120 mg/kg intravenous), and heparin

(10,000 U). The heart was placed into 500 ml of ice-cold Tyrode solution (136 mM NaCl, 5.4 mM KCl, 1 mM $MgCl_2 \cdot 6H_2O$, 2 mM $CaCl_2$, 0.33 mM $NaH_2PO_4 \cdot H_2O$, 5 mM HEPES, 10 mM glucose, pH 7.4 at room temperature. Following cannulation of the left circumflex coronary artery and ligation of all leaks from arterial branches with silk to assure adequate perfusate pressure, the atria was perfused for 10 min with Ca^{2+} free Tyrode solution. The digestion of the atria was performed with constant recycling of collagenase solution containing 100 U/mL collagenase type II, 0.1 % bovine serum albumin (BSA) in Ca^{2+}-free Tyrode's solution. Digested tissue was sliced into small pieces and triturated with a transfer pipette to dissociate cell clumps in Dulbecco's modified eagle medium (DMEM). Debris was removed by filtration through a 500 µm nylon cell strainer and cells were centrifuged at 50 x g for 5 minutes, with slow deceleration, to pellet cardiomyocytes. The supernatant was centrifuged at 850 x g for 15 minutes to pellet cardiac fibroblasts. Cells were immediately frozen in liquid nitrogen (freshly isolated cells) or plated in T-75 culture flask and transferred to an incubator at 5% CO_2/95%-humidified air (37°C) in DMEM supplemented with 10% fetal bovine serum (FBS) and 2% penicillin/streptomycin. The medium was changed 2 hours after plating to remove dead and non-attached cells and every 24 hours thereafter

Cellular Fractionation and Western Blots

Cultured or freshly isolated cardiac fibroblasts were washed in ice-cold phosphate-buffered saline (PBS): 137 mM NaCl, 2.7 mM KCl, 4.2 mM $Na_2HPO_4 \cdot H_2O$, 1.8 mM KH_2PO_4, pH 7.4 at room temperature. Cells were then placed on an

orbital shaker for 20 min at 4°C and semi-permeabilized in a lysis buffer: 150 M NaCl, 0.2 mM EDTA, 20 mM Hepes-NaOH, 2 mM DTT, 2 mM $MgCl_2$, 40 µg/ml digitonin, supplemented with protease/phosphatase inhibitor cocktail just before use. The homogenate was then diluted with equal volume of lysis buffer without digitonin and transferred to a Dounce homogenizer. To further disrupt the cells and free the nuclei, 10 strokes with the tight pestle ('B') were performed. Freshly isolated nuclei are obtained after centrifugation at 850 x g for 15 min at 4°C in a swinging-bucket rotor (Sorvall 75-006-434 rotor). The supernatants are transferred to new tubes and further centrifuged at 80000 x g for 60 min 4°C (Beckman, TLA-100.3 rotor) to separate membrane and cytosolic fractions.

Membrane, cytosolic or nuclear cell extracts were diluted with Laemmli sample buffer and denatured by heating at 100°C for 5 min, and then protein was quantified by the Bradford assay. Fixed amounts of protein was separated by sodium dodecyl sulfate polyacrylamide gel electrophoresis (SDS-PAGE) (7.5-12%) and electrophoretically transferred to polyvinylidene difluoride (PVDF) membranes. Membranes were blocked for 1 hour at room temperature and probed with primary antibodies overnight at 4°C. After extensive washing, membranes were further incubated with the appropriate secondary antibody conjugated to horseradish peroxidase and immunoreactive bands were detected by enhanced chemiluminescence (ECL). After stripping in ReBlot-plus strong antibody solution, membranes were blocked and re-probed with additional primary and secondary antibodies.

To detect secreted collagen, 50 µl of culture media collected from constant quantities of cells was mixed with Laemmli sample buffer, heated, and separated on precast 7.5% SDS-PAGE gels. Following migration, proteins were transferred electrophoretically onto nitrocellulose membranes and blocked in 3% bovine serum albumin (BSA) in PBS on a rotator overnight at 4°C. Membranes were probed with the primary antibodies for 1 hour at room temperature, then washed and incubated with horseradish peroxidase-conjugated secondary antibodies for 1 hour at room temperature. Signals were detected with the ECL reagent and band intensities were quantified with Bio-Rad Quantity One software.

Nuclear Fractionation

Freshly isolated nuclei were suspended in 0.25 M sucrose, 50 mM Tris-HCl, 10 mM $MgCl_2$, 1 mM dithiothreitol. (pH 7.4) containing protease/phosphatase inhibitor cocktail and incubated for 30 min at 4 °C with 1% (w/v) sodium citrate. The nuclear suspension was centrifuged for 15 min at 500 x g and the supernatant, containing the outer nuclear membrane (ONM)-enriched fraction, was collected. The remaining pellet was re-suspended in 0.3 M sucrose, 50 mM Tris-HCl, 10 mM $MgCl_2$, 1 mM dithiothreitol. (pH 7.4). DNase (200 µg/ml) was added and samples were digested overnight at 4 °C on a rotating mixer. The homogenate was centrifuged for 2 h at 10 000 x g and the supernatant, containing the nucleoplasmic (NP) fraction, was collected. The pellet, containing the inner nuclear membrane (INM), was further purified using sucrose density (0.25 M/ 1.6 M / 2.4 M) gradients (20 min at 100000 x g).

RNA extraction and Quantitative Polymerase Chain Reaction (qPCR)

Total RNA was extracted using a kit from Macherey-Nagel, following the manufacturer's protocol. The concentration and purity of extracted RNA were assessed with a NanoDrop ND-1000 spectrophotometer. Single-stranded cDNA was synthesized from 1 µg of pure RNA with a High Capacity cDNA Reverse Transcription Kit. qPCR was performed with TaqMan probes and primers using a Stratagene Mx3000P system. Samples were assayed in duplicate and the results expressed relative to an internal housekeeping standard (HPRT).

[^{3}H]Thymidine Incorporation

Cultured atrial fibroblasts were plated in 24-well plates at 30,000 cells/well and serum-starved for 24 hours. Parallel series of cells were treated with various drugs and incubated for an additional 48 hours. DNA synthesis was assessed by adding 1 µCi/well of [^{3}H]thymidine 6 hours prior to the end of the treatment period. Cells were washed twice with ice-cold PBS, 5% trichloroacetic acid (TCA) was added, and then cells were kept for 1 hour at 4°C to precipitate DNA. The precipitate was then washed with ice-cold PBS, lysed with 0.5 M NaOH and resuspended in scintillation fluid. [^{3}H]Thymidine incorporation was determined using a beta-counter.

[α-^{32}P]UTP -Transcription Initiation Assay

Freshly isolated fibroblast nuclei were resuspended in 50 mM Tris, 0.15 M KCl, 1 mM $MnCl_2$, 6 mM $MgCl_2$, 1 mM ATP, 2 mM DTT, 1 U/µL RNAse inhibitor, pH 7.9 at room temperature, and incubated in the presence of agonist/antagonists and 10 µCi

[α-^{32}P]UTP (3,000 Ci/mmol) at 30°C for 30 min. Reactions were terminated by digestion with DNase and nuclei were lysed with 10 mM Tris–HCl 10 mM EDTA, 1% SDS, pH 8.0 at room temperature. Samples were then transferred onto Whatman GF/C glass microfiber-filter discs, washed twice with ice-cold 5% TCA containing 20 mM sodium pyrophosphate, and air-dried. Filters were then placed in vials containing scintillation fluid, and ^{32}P-incorporation was determined using a beta counter. The DNA content of each sample was determined spectrophotometrically using a NanoDrop ND-1000 spectrophotometer and [α-^{32}P]UTP incorporation was expressed as cpm/ng DNA.

Immunohistochemistry

Cardiac atrial fibroblasts plated in 18-mm coverslips were fixed for 20 min with 2% paraformaldehyde in PBS, pH 7.3, at room temperature, to preserve cell morphology. The cells were then incubated with the blocking/permeabilizing buffer (0.1% Triton X-100, 1% normal donkey serum (NDS), 1% BSA, pH 7.4) for 1 hour and then incubated overnight at 4°C with primary antibody diluted in 0.05% Triton X-100, 0.5% NDS, 0.5% BSA, pH 7.4. After three 5-min washes with PBS, cells were incubated at room temperature for 1 hour in a foil-covered plate with the appropriate Alexa-conjugated secondary antibodies diluted in 0.05% Triton X-100, 0.5% NDS, 0.5% BSA, pH 7.4. Cells were then carefully washed (3 x 5 min) with PBS, excess water was removed with a tissue and cells were placed onto a microscope slide containing a drop of 1,4-diazabicyclo[2.2.2]octane (DABCO) anti-quenching mounting medium (0.2% DABCO in glycerol) and the edges of the coverslip were sealed with

nail polish. Images were acquired with an Olympus FluoView FV1000 confocal laser-scanning microscope equipped with a 40X/1.3 oil immersion objective. For multichannel image acquisition, excitation and emission collection were carried out in a sequential mode for each channel. Acquisition parameters were tuned to optimize detection sensitivity and minimize photobleaching.

Fluorometric Nitric Oxide Assay

Isolated nuclei were preincubated with the fluorescent NO specific indicator 4,5-diaminofluorescein (DAF-2, 5 μg/ml) in a buffer containing 140 mM NaCl, 14 mM glucose, 4.7 mM KCl, 2.5 mM $CaCl_2$, 1.8 mM MgSO4, 1.8 mM KH_2PO_4, and 0.1 mM L-arginine (pH 7.4) for 30 min at 37°C. Nuclei were washed 3 times with HEPES buffer (20 mM HEPES, 115 mM NaCl, 5.4 mM KCl, 1.8 mM $CaCl_2$, 0.8 mM $MgCl_2$, 13.8 mM glucose, pH 7.4) to remove any unbound fluorescent dye and then incubated with various agonist/antagonists at 37°C. Samples were transferred to a 96-well microplate and the DAF-2 fluorescence was measured with a Biotek Synergy 2 microplate reader (excitation λ=488 nm, emission λ=510 nm)

[Tyr(DMNB)^4]Ang-II uncaging and intracellular Ca^{2+} measurement

To monitor changes in intracellular calcium concentration, freshly isolated cardiac fibroblasts cultured directly in FluoroDishes were loaded with 5 μM Fluo-4AM in DMEM in the presence or absence of [Tyr(DMNB)^4]Ang-II and placed into an incubator for 30 min at 37°C. Cells were washed three times with indicator-free medium and incubated for an additional 15 min to allow complete de-esterification of

AM-esters. DRAQ5, a membrane-permeable fluorescent dye with high affinity for double-stranded DNA, was used to stain the nucleus and to focus the UV-laser on a rectangular intracellular region overlapping the nucleus. Images were acquired using a Zeiss LSM 7 Duo microscope (combined LSM710 and Zeiss Live systems) with Zeiss Plan-Apochromat 63x/1.4 oil DIC objective lens equipped with a BC 405/561 dichroic mirror. Fluo-4AM was excited with an argon laser at 488 nm/100 mW diode (1-5% laser intensity) and fluorescence produced between 495 nm and 550 nm was measured. Cardiac fibroblasts were scanned in bi-directional mode at 30 fps, with pixel size set at 0.2 μm and the pinhole at 1.5 Airy units. After establishing a stable baseline, [Tyr(DMNB)^4]Ang-II was uncaged by a 70 μW pulse of UV-light using a 405-nm/30 mW diode. An X-Cite-optical power measurement system (XR2100) was used to monitor the optical power output at the stage level. Intracellular Ca^{2+} measurements were expressed as a percentage of fluorescence intensity relative to resting fluorescence prior to photolysis ($\Delta[Ca^{2+}]$ (F/F0;%)).

Statistical Analysis

Densitometric analyses were performed with Quantity One Bio-Rad software. Statistical analyses were performed with GraphPad Prism version 5.0 for Windows with one-way or two-way analysis of variance, as appropriate, with Bonferroni post hoc tests. All data are presented as mean±SEM. A two-tailed $P \leq 0.05$ was considered statistically significant.

Results

Endogenous Ang-II Receptors Localize to the Nucleus in Atrial Cardiac Fibroblasts

To assess the subcellular distribution of AT1R and AT2R in atrial cardiac fibroblasts, we isolated membrane, cytosolic and nuclear fractions. The fractionation was validated using organelle specific markers including pan-cadherin (membrane), HSP70 (cytosol) and lamin B (nuclei). Immunoblotting with subtype-specific antibodies revealed AT1R and AT2R immunoreactivity in all three fractions but band intensity was greatest in membrane and nuclear fractions (Figure 1A). To further examine the nuclear compartmentalization of AT1R and AT2R, we performed a nuclear subfractionation and isolated the ONM, INM and NP with minimal cross-contamination as defined by nesprin, emerin and HDAC2 immunoreactivity. AT1R immunoreactivity was detected more prominently on INM, whereas the AT2R immunoreactivity was observed in both INM and NP (Figure 1B). Ang-II binding was examined in intact nuclei using the fluorescently-labeled Ang-II analog (Ang-II-FITC) along with the DNA dye DRAQ5. Fluorescent labeling was detected at the nuclear envelope and to some extent in the nucleoplasm. Ang-II-FITC (100 nM) binding was displaced by both the AT1R selective antagonist, valsartan (1 μM) and the AT2R selective antagonist, PD 123,177 (1 μM). Pre-incubation with both valsartan and PD 123,177 completely inhibited Ang-II-FITC binding to isolated nuclei (Figure 1C-D). To further investigate the intracellular distribution of Ang-II receptors, permeabilized atrial fibroblasts cultured for three days were exposed to primary AT1R or AT2R

andtibodies and then incubated with secondary Alexa Fluor-conjugated fluorescent dyes. Immunofluorescence confocal microscopy was performed, with TOPRO-3 was used to delineate the nucleus and vimentin to show the intact fibroblast cytoskeleton (Figure 2A-B). These experiments revealed clear nuclear localisation for AT1R and AT2R.

Intracellular Ang-II Levels, Nuclear AT1R and Glycosylated Nuclear AT2R are Upregulated in HF

We studied changes in AT1R and AT2R mRNA expression as a function of VTP duration (control, 24 h and 2 week ventricular pacing). AT1R mRNA levels were significantly upregulated only after 2 weeks of VTP whereas AT2R mRNA levels remained unchanged (Figure 3A-B). Intracellular Ang-II concentrations, measured by competitive quantitative ELISA, were also upregulated at 2 week VTP (Ctl: 5.2±1.8 vs. CHF: 17.9±1.4 pmol/mg protein $P<0.01$) (Figure 3C). At the protein level, plasma-membrane AT1R immunoreactivity remained unchanged at 2-week VTP, whereas nuclear AT1R immunoreactivity was significantly increased (Figure 3D-E). Contrary to AT1R, AT2R immunoreactivity, both in membrane and nuclear fractions, were unaffected at 2-week VTP. However, we observed increased abundance of a higher molecular mass band of AT2R immunoreactivity in the nuclear fraction. To determine if the slower-migrating band corresponds to a glycosylated form of AT2R, we incubated the isolated membrane and nuclear fractions with peptide N-glycosidase F (PNGase F), which catalyzes the cleavage of N-linked oligosaccharides from N-linked glycoproteins [35]. PNGase F-digested samples showed a complete disappearance

of the higher mass AT2R band compared to non-treated groups (Figure 3F). The lower mass band that appeared in the treated group most likely represents the receptor in its totally deglycosylated form. These results suggest that at 2-week VTP the glycosylation status of nuclear AT2R has been altered whereas its abundance has not been changed

Nuclear AT1R and AT2R Regulate de Novo RNA Synthesis through NO and IP3R Signaling

To assess the potential functional role of nuclear AT1R and AT2R, we employed immunoblotting and immunofluorescence to localize downstream heterotrimeric G protein signaling partners (Figures 4A-B). Both Gαq/11 and Gαi/3 were present in the nuclear fraction and colocalized with TOPRO-3. Gαs was detected only in cytosolic fractions: no nuclear immunofluorescence was observed. Gβ immunoreactivity was also detected in nuclear fractions and immunofluorescence revealed intense staining of the nuclear membranes. Thus, Gα and Gβ subunits, known to mediate AT1R and AT2R signalling, are present on atrial cardiac fibroblast nuclear membranes.

To explore the functional consequences of nuclear AT1R and AT2R activation more directly, purified nuclei were incubated with [α-^{32}P]UTP to measure de novo RNA transcription in response to Ang-II. Ang-II produced a dose-dependent increase in de novo RNA transcription reaching statistical significance at 10 nM and plateaued at 100 nM (Figure 5A). Pretreated with 1 μM valsartan (AT1R-selective antagonist) or 1 μM PD 123,177 (AT2R-selective antagonist) prior to Ang-II (100 nM) exposure

significantly reduced [α-^{32}P]UTP incorporation (Ang-II: 420±41, Ang-II + valsartan: 111±14, Ang-II + PD 123,177: 220±1 cpm/ng DNA, N=4/group, P<0.001). RNA polymerase II is responsible for transcribing DNA to produce mRNA precursors and preincubating nuclei with an RNA polymerase II inhibitor, α-amanitin (5 μg/ml), prevented Ang-II from increasing transcription initiation (Figure 5B).

To determine the mechanisms whereby activating AT1R or AT2R lead to changes in gene expression, nuclei were preincubated with an nitric oxide (NO)-selective fluorescence dye 4,5-diaminofluorescein (DAF-2) and then exposed to Ang-II. Ang-II (100 nM) increased DAF-2 fluorescence and this increase was abolished by PD 123,177 (1 μM) but not by valsartan (1 μM), indicating that AT2R activate NO-synthase (NOS) in nuclear membranes whereas AT1R do not. Furthermore, the ANG II-induced production of NO was abolished when nuclei where pretreated with the NOS inhibitor L-NAME (1 mM) (Figure 5C). Immunoblotting subsequently revealed the presence of endothelial NOS (eNOS or NOS3) immunoreactivity in the nuclear fraction (Figure 5D).

We have previously demonstrated that cardiomyocyte nuclear AT1R are coupled to IP3R activation to increase nuclear Ca^{2+} concentration $[Ca^{2+}]_n$ that, in turn, plays a key role in regulating gene expression. To determine if this pathway also functions in fibroblast nuclei, we pretreated cardiac fibroblast nuclei with a specific AT1R agonist (L-162313, 1 μM) or AT2R agonist (CGP 42112A, 1 μM), in the presence or absence of the IP3R blocker 2-APB (100 μM) or L-NAME (1 mM), and assessed transcription initiation using [α–^{32}P]UTP incorporation. The results showed that the ability of AT1R to increase transcription initiation was reduced significantly by

2-APB and not L-NAME, whereas that of AT2R was reduced by L-NAME and not by 2-APB. These results indicate nuclear AT1R and AT2R regulate transcription via different signalling pathways (Figure 5E).

Intracellular Ang-II Mediates IP3R dependant Ca^{2+} Release

Here, we examined the ability of Ang-II to alter nuclear Ca^{2+} activity in intact atrial fibroblasts. A photolabile cell-permeable caged Ang-II (cAng-II) analog ([Tyr(DMNB)^4]Ang-II) was employed and changes in [Ca^{2+}] were determined using the cell-permeant fluorescent Ca^{2+} indicator, Fluo-4 AM. DRAQ5 fluorescence was used to localize nuclei. In contrast to control cells (Figure 6A), UV irradiation of cAng-II (100 nM) loaded fibroblasts generated a transient increase in nuclear Fluo4 fluorescence (white arrows indicate photobleached cells). Addition of valsartan (1 μM) in the extracellular medium failed to block the ability of cAng-II to increase $[Ca^{2+}]_n$ (Figures 6A-b), suggesting that the photolysed Ang-II is acting via intracellular receptors rather than being released into the media to act on nearby cells through autocrine or paracrine signaling. The addition of 2-APB (100 μM) significantly attenuated, but failed to totally block, the ability of photolyzed Ang-II to increase $[Ca^{2+}]_n$. Ang-II added directly to the extracellular media produced a rise in nuclear Ca^{2+} but with lower fluorescence intensity than observed upon intracellular photolysis of cAng-II (Figure 6A-C). Analysis of IP3R isoform expression by qPCR revealed that the IP3R3 isoform predominates over IP3R1 and IP3R2 (Figure 6D). Immunoblot analysis of IP3R isoforms in nuclear subfractions showed abundant IP3R3 in the INM and weaker

immunoreactivity in the ONM, with very weak signals for IP3R1 and IP3R2 (Figure 6D-E).

Intracellular Ang-II Regulates Fibroblast Proliferation

Here, we compared the growth stimulus-induced proliferative capacity of atrial fibroblasts originally plated at equal density. Stimulation of atrial fibroblast with Ang-II resulted in a significant increase in [^{3}H]thymidine incorporation compared to non-treated fibroblasts. Pretreatment with valsartan (AT1R blocker) and PD 123,177 (AT2R blocker) prior to the Ang-II treatment returned [^{3}H]thymidine incorporation to basal levels (Figure 7A). Fibroblasts loaded with cAng-II were UV-irradiated and [^{3}H]thymidine uptake was measured. Compared to basal UV-irradiated levels, [^{3}H]thymidine incorporation increased substantially (159.8±9.4 dpm in cAng-II vs 88.5±5.5 dpm in control). The ability of intracellular, photolyzed cAng-II to increase [^{3}H]thymidine incorporation was not prevented by extracellular AT1R and AT2R blockers (131±7.4 dpm). A caged, non-photolysable Ang-II analog was unable to increase [^{3}H]thymidine incorporation. The [^{3}H]thymidine incorporation in the UV-irradiated control group (no cAng-II loading) did not differ significantly from the non UV-irradiated control group (Figure 7B-C).

Intracellular Ang-II Regulates Collagen Expression

Finally, we evaluated the effect of Ang-II on collagen synthesis in atrial fibroblasts. Growth-arrested cultures were treated with extracellular Ang-II or loaded with cAng-II, alone or in combination with valsartan and PD123,177. Collagen 1A1,

1EX1 and 3A1 expression was determined at the mRNA level and secreted collagen 1 was measured by immunoblotting. Results are shown in Figure 8. When fibroblasts were treated with extracellular Ang-II, collagen 1EX1 and 3A1 mRNA levels were increased; collagen 1A1 secretion showed a small, but non-significant, increase. Photolysis of intracellular cAng-II resulting in a sustained increase in expression of all three collagen isoforms. This increase was not prevented by the addition of extracellular AT1R and AT2R blockers. Collagen-1 secretion showed changes similar to those in mRNA (Figure 8D,E).

Discussion

Main Findings and Significance

In the present study we have demonstrated: 1) the presence of nuclear AT1R and AT2R in atrial cardiac fibroblasts; 2) the upregulation of intracellular Ang-II, nuclear AT1R and alterations in the glycosylation of nuclear AT2R in HF; 3) the presence of nuclear heterotrimeric G protein subunits; 4) the involvement of NOS and IP3R in the activation of nuclear AT1R and AT2R to transcription; 5) intracellular Ang-II regulates nuclear Ca^{2+} homeostasis in intact atrial fibroblasts independent of plasma membrane AT1R; 6) the control of fibroblast proliferation and collagen-1 secretion by intracellular Ang-II. These findings suggest that intracellular Ang-II may participate in structural remodeling by controlling fibroblast function through activation of nuclear AT1R and AT2R.

Relation to Previous Studies of Nuclear Receptors

Cardiac fibroblasts play a key role in cardiac development, arrhythmogenesis and are fundamental in defining heart structure and function [10-12]. Although classical seven-transmembrane domain, G protein-coupled receptors (GPCRs) including angiotensin receptors (AT1R, AT2R) [13], endothelin receptors (ETA, ETB) [14], α-adrenergic receptors (α-1AR) [15], β-adrenergic receptors (β-1AR, β-3AR) [16] and urotensin receptors (U-II) [17] have increasingly been detected on cardiac nuclear membranes, almost nothing is known about their involvement in cardiac

fibroblasts. Most of the aforementioned studies were performed with cardiac myocytes or total cardiac nuclei preparations from dissected cardiac tissue, and hence could not define a role in fibroblasts. Both AT1R and AT2R were detected in adult human atrial fibroblasts [18, 19], dermal fibroblasts, synovial fibroblasts, lung fibroblasts [20], and AT1R are upregulated whereas AT2R remain unchanged in the left atrial tissue samples obtained from patients with atrial fibrillation [21]. Furthermore, earlier studies have identified putative nuclear localization signal (NLS) sequences in both AT1R and AT2R [22]. To our knowledge this is the first report to show the presence of subcellular Ang-II binding sites within isolated canine atrial fibroblasts and more precisely the presence of both AT1R and AT2R on the inner lipid bilayer of the nuclear envelope. Trafficking to the INM may occur following biosynthesis though a vesicle-mediated pathway, nuclear pore complex-dependent and -independent pathways and via diffusion-retention [23]. Furthermore, we have demonstrated and increase in nuclear AT1R immunoreactivity and altered glycosylation of nuclear AT2R in a model of HF. The upregulation of AT1R in earlier studies on chronic atrial fibrillation may reflect, at least in part, changes in AT1R at the nuclear level [21]. Our findings of altered AT2R post-translational modification in MI are consistent with previous reports in which 5 glycosylation sites in the extracellular N-terminal domain of AT2R were identified [24]. As the AT2R does not undergo internalization and trafficking, the glycosylated AT2R in the nucleus reflects the AT2R that was post-transnationally modified in the Golgi apparatus and trafficked to the nucleus [25].

Functional Role of Nuclear AT1R and AT2R

Heterotrimeric G proteins play a central role in GPCR-mediated signal transduction and serve as cellular switches to control at the molecular level the functional responses to GPCR activation [26]. In our study, Gαq/11, Gαi3, and Gβ were detected in the nuclear fraction whereas Gαs was only found in the cytoplasm. AT1R signalling is principally via Gαq11 and involves the production of inositol trisphosphate and mobilization of intracellular Ca^{2+}. In contrast, AT2R signal through Gαi3 to activate the cGMP/NO pathway [27, 28]. We have shown that, In nuclei isolated from cardiac atrial fibroblasts, AT2R is responsible for NO production as the AT1R selective antagonist, valsartan, had no effect on DAF-2 fluorescence, whereas the AT2R selective antagonist PD123,319 significantly reduced DAF-2 fluorescence to levels similar to those observed when nuclei were pretreated with NOS inhibitor, L-NAME. Consistent with previous findings in whole heart nuclei, eNOS immunoreactivity was detected in nuclei isolated from fibroblasts [29]. Furthermore, consistent with our previous studies on cardiomyocyte nuclei [13, 16, 30, 31], we observed a dose-dependent increase in de novo RNA synthesis in nuclei treated with Ang-II. We report that AT1R-mediated increase in transcriptional involves activation of IP3R whereas AT2R-mediated transcriptional involves NOS activation. IP3Rs are a family of Ca^{2+}-channels comprising three isoforms that differ in amino acid sequence and predominantly localize to the nuclear envelope. IP3R signalling requires the presence of phosphatidylinositol 4,5-bisphosphate, phosphatidylinositol kinases, phospholipase C and diacylglycerol kinases: all of these are present in the nuclear membrane [32]. Using a cell-permeable photoreleasable Ang-II analog in intact

fibroblasts, we demonstrated that intracellular Ang-II generates an IP3R-dependant increase in $[Ca^{2+}]_n$ that was not prevented by extracellular AT1R blockers

Role of Intracellular Ang-II in Fibroblast Proliferation and ECM Secretion

Fibroblasts respond to a wide range of neurohormonal stimuli with proliferation and increased production and secretion of components of the extracellular matrix, leading to pathological remodeling and altered cardiac function [1]. Ang-II-induced fibroblast proliferation is mediated through autocrine/paracrine factors [33]. Here, we report for the first time a novel regulatory aspect of fibroblast physiology: intracrine Ang-II-mediated proliferation and increased collagen synthesis and secretion. Extracellular Ang-II alone produced a significant increase in fibroblast number but not in collagen-1 synthesis and secretion, whereas intracellular photolysis of cAng-II significantly increased both fibroblast proliferation and collagen secretion. In intact fibroblasts, the effects of increased intracellular Ang-II were not prevented by the presence of valsartan and PD 123319 in the extracellular media, indicating the effects of intracellular Ang-II were not mediated by receptors at the cell surface.

Potential Limitations

Fibroblasts may be affected during enzymatic digestion of cardiac tissue and culture. Fibroblasts may lose their morphological and functional properties after 7 days of culture and may differentiate into myofibroblasts; therefore we used fibroblasts cultured for no more than 3-4 days in our experiments. Moreover, in vivo fibroblasts may be coupled to cardiomyocytes, hence our in vitro observations may

differ from those made using fibroblasts in the physiological in vivo milieu [2]. Mitochondrial Ang-II receptors have been recently described. In our cAng-II experiments in intact cells we cannot rule out the possibility of contributions from mitochondrial or other intracellular endomembrane ATRs [34].

Conclusions

The current study identifies novel participants in the profibrotic response by demonstrating the existence of nuclear AT1R and AT2R that are coupled to transcriptional responses through IP3R/NO pathways and regulate nuclear Ca2+ signaling and NO generation. Atrial fibroblast ATRs are altered in HF and cardiac fibroblasts exposed to intracellular Ang-II proliferate and secrete collagen-1. The identification and characterization of functional intracrine Ang-II signaling opens up new avenues of research involving the Ang-II system, with potential implications for the development of novel pharmacological interventions.

Acknowledgments: The authors thank Nathalie L'Heureux and Chantal St-Cyr for outstanding technical assistance and France Thériault for secretarial help with the manuscript.

Funding: This work was supported by the Canadian Institutes of Health Research and the Heart and Stroke Foundation of Canada. A.T. was supported by an FRQS-RSCV/HSFQ doctoral scholarship.

Disclosures: None.

References

[1] Souders CA, Bowers SL, Baudino TA. Cardiac fibroblast: the renaissance cell. Circulation research 2009;105:1164-76.

[2] Yue L, Xie J, Nattel S. Molecular determinants of cardiac fibroblast electrical function and therapeutic implications for atrial fibrillation. Cardiovascular research 2011;89:744-53.

[3] Burstein B, Nattel S. Atrial fibrosis: mechanisms and clinical relevance in atrial fibrillation. Journal of the American College of Cardiology 2008;51:802-9.

[4] Brilla CG. Renin-angiotensin-aldosterone system and myocardial fibrosis. Cardiovascular research 2000;47:1-3.

[5] Brilla CG, Zhou G, Matsubara L, Weber KT. Collagen metabolism in cultured adult rat cardiac fibroblasts: response to angiotensin II and aldosterone. Journal of molecular and cellular cardiology 1994;26:809-20.

[6] Singh VP, Baker KM, Kumar R. Activation of the intracellular renin-angiotensin system in cardiac fibroblasts by high glucose: role in extracellular matrix production. American journal of physiology Heart and circulatory physiology 2008;294:H1675-84.

[7] Singh VP, Le B, Khode R, Baker KM, Kumar R. Intracellular angiotensin II production in diabetic rats is correlated with cardiomyocyte apoptosis, oxidative stress, and cardiac fibrosis. Diabetes 2008;57:3297-306.

[8] De Mello WC. Beyond the circulating Renin-Angiotensin aldosterone system. Frontiers in endocrinology 2014;5:104.

[9] Tadevosyan A, Allen BG, Nattel S. Isolation and study of cardiac nuclei from canine myocardium and adult ventricular myocytes. Methods in molecular biology 2015;1234:69-80.

[10] Burstein B, Qi XY, Yeh YH, Calderone A, Nattel S. Atrial cardiomyocyte tachycardia alters cardiac fibroblast function: a novel consideration in atrial remodeling. Cardiovascular research 2007;76:442-52.

[11] Aguilar M, Qi XY, Huang H, Nattel S. Fibroblast electrical remodeling in heart failure and potential effects on atrial fibrillation. Biophysical journal 2014;107:2444-55.

[12] Qi XY, Huang H, Ordog B, Luo X, Naud P, Sun Y, et al. Fibroblast Inward-Rectifier Potassium Current Upregulation in Profibrillatory Atrial Remodeling. Circulation research 2015.

[13] Tadevosyan A, Maguy A, Villeneuve LR, Babin J, Bonnefoy A, Allen BG, et al. Nuclear-delimited angiotensin receptor-mediated signaling regulates cardiomyocyte gene expression. The Journal of biological chemistry 2010;285:22338-49.

[14] Boivin B, Chevalier D, Villeneuve LR, Rousseau E, Allen BG. Functional endothelin receptors are present on nuclei in cardiac ventricular myocytes. The Journal of biological chemistry 2003;278:29153-63.

[15] Wright CD, Chen Q, Baye NL, Huang Y, Healy CL, Kasinathan S, et al. Nuclear alpha1-adrenergic receptors signal activated ERK localization to caveolae in adult cardiac myocytes. Circulation research 2008;103:992-1000.

[16] Boivin B, Lavoie C, Vaniotis G, Baragli A, Villeneuve LR, Ethier N, et al. Functional beta-adrenergic receptor signalling on nuclear membranes in adult rat and mouse ventricular cardiomyocytes. Cardiovascular research 2006;71:69-78.

[17] Doan ND, Nguyen TT, Letourneau M, Turcotte K, Fournier A, Chatenet D. Biochemical and pharmacological characterization of nuclear urotensin-II binding sites in rat heart. British journal of pharmacology 2012;166:243-57.

[18] Brink M, Erne P, de Gasparo M, Rogg H, Schmid A, Stulz P, et al. Localization of the angiotensin II receptor subtypes in the human atrium. Journal of molecular and cellular cardiology 1996;28:1789-99.

[19] Tsutsumi Y, Matsubara H, Ohkubo N, Mori Y, Nozawa Y, Murasawa S, et al. Angiotensin II type 2 receptor is upregulated in human heart with interstitial fibrosis, and cardiac fibroblasts are the major cell type for its expression. Circulation research 1998;83:1035-46.

[20] Galindo M, Santiago B, Palao G, Gutierrez-Canas I, Ramirez JC, Pablos JL. Coexpression of AT1 and AT2 receptors by human fibroblasts is associated with resistance to angiotensin II. Peptides 2005;26:1647-53.

[21] Boldt A, Wetzel U, Weigl J, Garbade J, Lauschke J, Hindricks G, et al. Expression of angiotensin II receptors in human left and right atrial tissue in atrial fibrillation with and without underlying mitral valve disease. Journal of the American College of Cardiology 2003;42:1785-92.

[22] Lee DK, Lanca AJ, Cheng R, Nguyen T, Ji XD, Gobeil F, Jr., et al. Agonist-independent nuclear localization of the Apelin, angiotensin AT1, and bradykinin B2 receptors. The Journal of biological chemistry 2004;279:7901-8.

[23] Katta SS, Smoyer CJ, Jaspersen SL. Destination: inner nuclear membrane. Trends in cell biology 2014;24:221-9.

[24] Carey RM, Wang ZQ, Siragy HM. Role of the angiotensin type 2 receptor in the regulation of blood pressure and renal function. Hypertension 2000;35:155-63.

[25] Hunyady L, Bor M, Balla T, Catt KJ. Identification of a cytoplasmic Ser-Thr-Leu motif that determines agonist-induced internalization of the AT1 angiotensin receptor. The Journal of biological chemistry 1994;269:31378-82.

[26] Drake MT, Shenoy SK, Lefkowitz RJ. Trafficking of G protein-coupled receptors. Circulation research 2006;99:570-82.

[27] Li J, Zhao X, Li X, Lerea KM, Olson SC. Angiotensin II type 2 receptor-dependent increases in nitric oxide synthase expression in the pulmonary endothelium is mediated via a G alpha i3/Ras/Raf/MAPK pathway. American journal of physiology Cell physiology 2007;292:C2185-96.

[28] Hunyady L, Catt KJ. Pleiotropic AT1 receptor signaling pathways mediating physiological and pathogenic actions of angiotensin II. Molecular endocrinology 2006;20:953-70.

[29] Gwathmey TM, Shaltout HA, Pendergrass KD, Pirro NT, Figueroa JP, Rose JC, et al. Nuclear angiotensin II type 2 (AT2) receptors are functionally linked to nitric oxide production. American journal of physiology Renal physiology 2009;296:F1484-93.

[30] Vaniotis G, Gora S, Nantel A, Hebert TE, Allen BG. Examining the effects of nuclear GPCRs on gene expression using isolated nuclei. Methods in molecular biology 2015;1234:185-95.

[31] Vaniotis G, Del Duca D, Trieu P, Rohlicek CV, Hebert TE, Allen BG. Nuclear beta-adrenergic receptors modulate gene expression in adult rat heart. Cellular signalling 2011;23:89-98.

[32] Cardenas C, Liberona JL, Molgo J, Colasante C, Mignery GA, Jaimovich E. Nuclear inositol 1,4,5-trisphosphate receptors regulate local Ca2+ transients and modulate cAMP response element binding protein phosphorylation. Journal of cell science 2005;118:3131-40.

[33] Bouzegrhane F, Thibault G. Is angiotensin II a proliferative factor of cardiac fibroblasts? Cardiovascular research 2002;53:304-12.

[34] Abadir PM, Foster DB, Crow M, Cooke CA, Rucker JJ, Jain A, et al. Identification and characterization of a functional mitochondrial angiotensin system. Proceedings of the National Academy of Sciences of the United States of America 2011;108:14849-54.

[35] Norris GE, Stillman TJ, Anderson BF, Baker EN. The three-dimensional structure of PNGase F, a glycosylasparaginase from Flavobacterium meningosepticum. Structure 1994;2:1049-59.

Legends

Figure 1. Endogenous AT1R and AT2R localize to the nucleus in canine atrial fibroblasts. A, Cultured fibroblasts were fractionated by differential centrifugation and the purity of membrane, cytosolic and nuclear fractions (50 µg) were validated by immunoblotting with pan-cadherin, HSP70 and lamin B antibodies. The presence of AT1R and AT2R was determined by immunoblotting. B, Subfractionation of isolated fibroblast nuclei was performed to separate ONM, INM and NP. Nesprin, Emerin and HDAC2 served as markers of the ONM, INM/lamina and nucleoplasm, respectively. Immunoblotting detected AT1R and AT2R in nuclear subfractions. C, Isolated nuclei were plated on laminin-coated 18 mm coverslips and then incubated with 100 nM Ang-II-FITC at room temperature or preincubated with valsartan (1 µM) and/or PD123177 (1 µM) for 30 min prior to the addition of Ang-II-FITC. Nuclei were washed, stained with fluorescent DNA dye DRAQ5, and images acquired using an Olympus FluoView FV1000 confocal microscope. D, Quantification of Ang-II emitted fluorescence. Mean±SEM **P<0.01, ***P<0.001, N=5/condition.

Figure 2. AT1R and AT2R colocalize with TOPRO-3 nucleic acid stain in canine atrial fibroblasts. A, Permeabilized cultured atrial fibroblast were stained with AT1R conjugated with Alexa Fluor 488 (red), vimentin conjugated with Alexa Fluor 555 (green), and TOPRO-3 (blue). Merged images indicate the extent of colocalization. Bright field images confirm the purity of fibroblast isolation. B, Fibroblast were stained

for AT2R as above. Similar observations were obtained from five different canine atrial fibroblast preparations.

Figure 3. Ventricular tachypacing increases nuclear AT1R immunoreactivity and alters AT2R glycosylation in fibroblasts. A, Expression of AT1R in freshly isolated canine atrial fibroblast throughout the VTP time course (12 h, 24 h, 1 wk and 2 wk VTP). B, Expression of AT2R during the VTP-time course. C, Ang-II levels of control and 2 week VTP isolated fibroblasts. D, Immunoblotting for AT1R, AT2R, pan-cadherin and lamin-B in membrane and nuclear proteins from freshly-isolated CTL and 2 week VTP fibroblasts. E, Quantification (Mean±SEM) of AT1R and AT2R immunoreactivity in membrane and nuclear fractions normalized to, respectively, pan-cadherin and lamin-B. F, PNGase F treatment of nuclear AT2R. Nuclei were incubated with PNGase F at 37 °C for 7.5 hours followed by immunoblotting for AT2R. Glycosylation Ratio was calculated using non PNGase F treated samples by dividing the glycosylated band intensity over the nonglycosylated band. Mean±SEM *P<0.05, ***P<0.001 CTL vs. HF; N=4/group.

Figure 4. Presence of G protein subunits in fibroblast nuclei. A, Detection of Gαq/11, Gαi/3, Gαs, Gβ in membrane, cytosolic and nuclear subfractions by Western blot. B, Representative confocal images demonstrating the distribution of Gαq/11, Gαi/3, Gαs, and Gβ in atrial fibroblasts. Superimposed confocal image shows the colocalization of G proteins with TOPRO-3 nucleic acid dye. Similar observations were obtained from four different canine heart preparations.

Figure 5. Nuclear AT1R and AT2R regulate gene expression. A, Transcription initiation was measured as [α-^{32}P]UTP incorporation in isolated fibroblast nuclei treated with increasing concentrations of Ang-II. B, [α-^{32}P]UTP incorporation was measured in fibroblast nuclei treated with Ang-II (100 nM) alone, or pretreated with α-amanitin (5 μg/ml), Valsartan (1 μM) or PD123177 (1 μM) and then stimulated with Ang-II. C, NO production was determined as a measure of DAF-2 fluorescence in nuclei stimulated with Ang-II alone, or pretreated with Valsartan (1 μM), PD123177 (1 μM) or L-NAME (1 mM) and then stimulated with Ang-II. Data represent mean ± SEM of at least four separate experiments performed in triplicate and normalized to control. ***P<0.001 vs. control. D, Immunoblotting for eNOS in cytosolic and nuclear enriched fractions. E, [α-^{32}P]UTP incorporation measured in fibroblast nuclei treated with L-162313 (1 μM), CGP 42112A (1 μM) or in combination with either L-NAME (1 mM) or 2APB (100 μM). Mean±SEM *P<0.05, **P<0.01, ***P<0.001.

Figure 6. Photolysis of Intracellular cAng-II increases $[Ca^{2+}]_n$. A, Cultured atrial fibroblasts were plated on FluoroDishs and changes in nucleoplasmic $[Ca^{2+}]$ were recorded using fluorescent calcium dye Fluo4-AM. Cells were incubated with cAng-II (100 nM), cAng-II and Valsartan (1 μM), or cAng-II and 2-APB (100 μM). Where indicated Ang-II was added directly to the extracellular media. Images shown are before (T = 10 s) and after (T = 100 s) flash photolysis. White arrows indicate the cells selected for uncaging. B, Representative traces of nucleoplasmic $[Ca^{2+}]$ as measured above. C, Mean±SEM of fluorescence signals, presented as background-subtracted

normalized fluorescence (%F / F0), where F is the fluorescence intensity, and F0 is the resting fluorescence recorded in the same fibroblast under steady-state conditions prior to photolysis **P<0.01, ***P<0.001. D, Expression of IP3R1, IP3R2, IP3R3 as determined by qPCR. E, Immunoblotting for IP3R1, IP3R2, IP3R3 in nuclear subfractions.

Figure 7. Intracellular Ang-II regulates fibroblast proliferation. A, [^{3}H]thymidine incorporation in atrial fibroblasts treated with medium alone, Ang-II (100 nM), PD123177 (1 μM) and Valsartan (1 μM), or pretreated with PD123177 (1 μM) and Valsartan (1 μM) before Ang-II (100 nM) treatment. B, [^{3}H]thymidine incorporation in atrial fibroblasts treated with medium alone, cAng-II (100 nM), Scramble (Ang-II-ODMNB), PD123177 (1 μM) and Valsartan (1 μM), or treated with cAng-II before PD123177 (1 μM) and Valsartan (1 μM). C, Percent change of [^{3}H]thymidine uptake over applicable basal values. Mean±SEM *P<0.05, **P<0.01, ***P<0.001, N=4/group.

Figure 8. Intracellular Ang-II regulates collagen synthesis and secretion. Quantification of A, collagen 1A1 B, collagen 1EX1 and C, collagen 3A1 mRNA in cultured fibroblasts treated with control, Ang-II (100 nM), PD123177 (1 μM) and Valsartan (1 μM), pretreated with PD123177 (1 μM) and Valsartan (1 μM) before Ang-II (100 nM) or following photolysis of fibroblasts exposed to cAng-II (100 nM), PD123177 (1 μM) and Valsartan (1 μM), treated with cAng-II before PD123177 (1 μM) and Valsartan (1 μM). D, collagen 1 secretion expression was measured by immunoblot analysis of the cell culture media. E, Quantification of collagen 1

immunoblotting experiments. Band intensities were analyzed by densitometry. Mean±SEM *P<0.05, **P<0.01, ***P<0.001, N=4/group, N.S = non-significant from control.

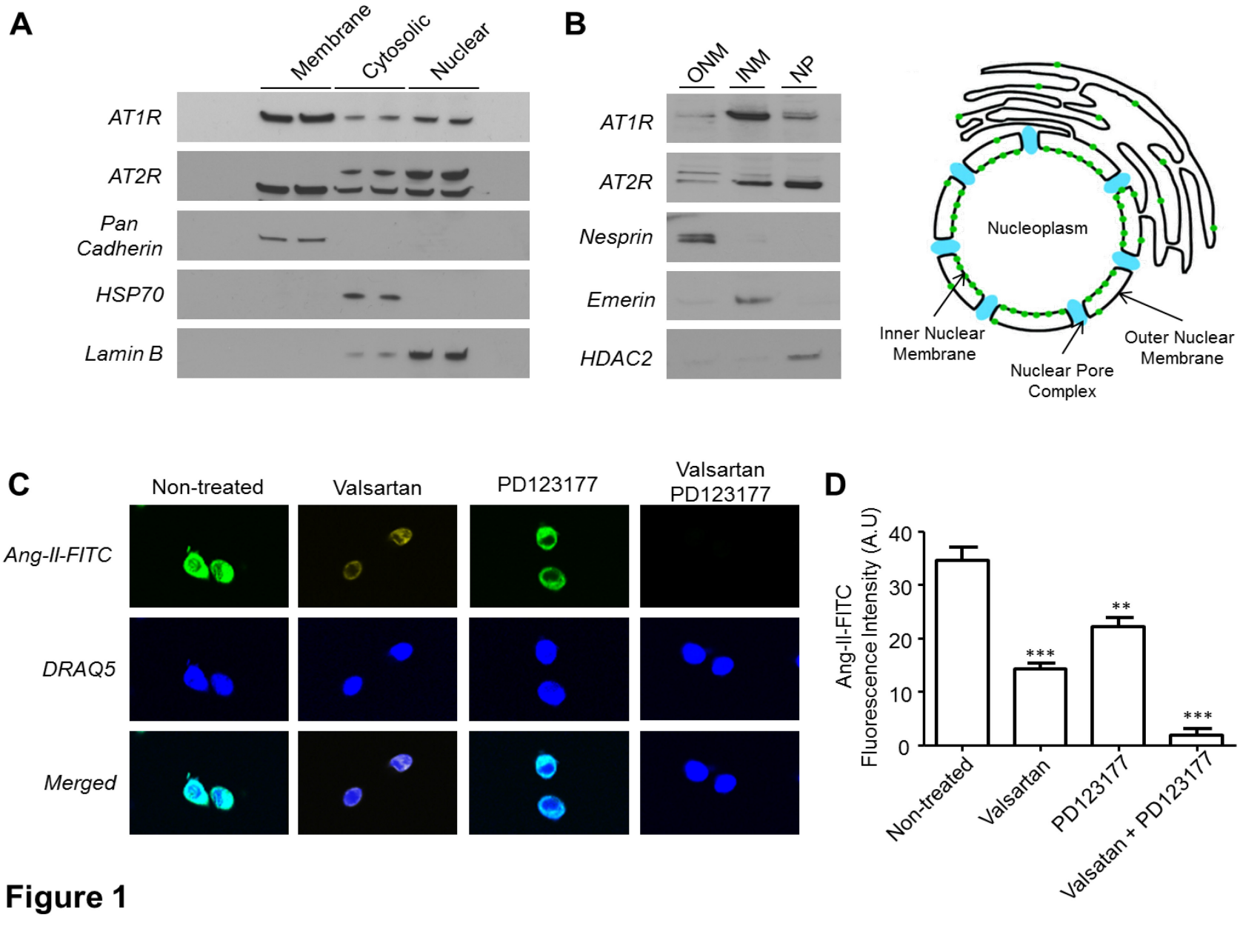
A
Membrane
Cytosolic
Nuclear
AT1R
AT2R
Pan Cadherin
HSP70
Lamin B
B
ONM
INM
NP
AT1R
AT2R
Nesprin
Emerin
HDAC2
Nucleoplasm
Inner Nuclear Membrane
Outer Nuclear Membrane
Nuclear Pore Complex
C
Non-treated
Valsartan
PD123177
Valsartan PD123177
Ang-II-FITC
DRAQ5
Merged
D
Ang-II-FITC Fluorescence Intensity (A.U)
40
30
20
10
0
***
**
***
Non-treated
Valsartan
PD123177
Valsatan + PD123177

Figure 1

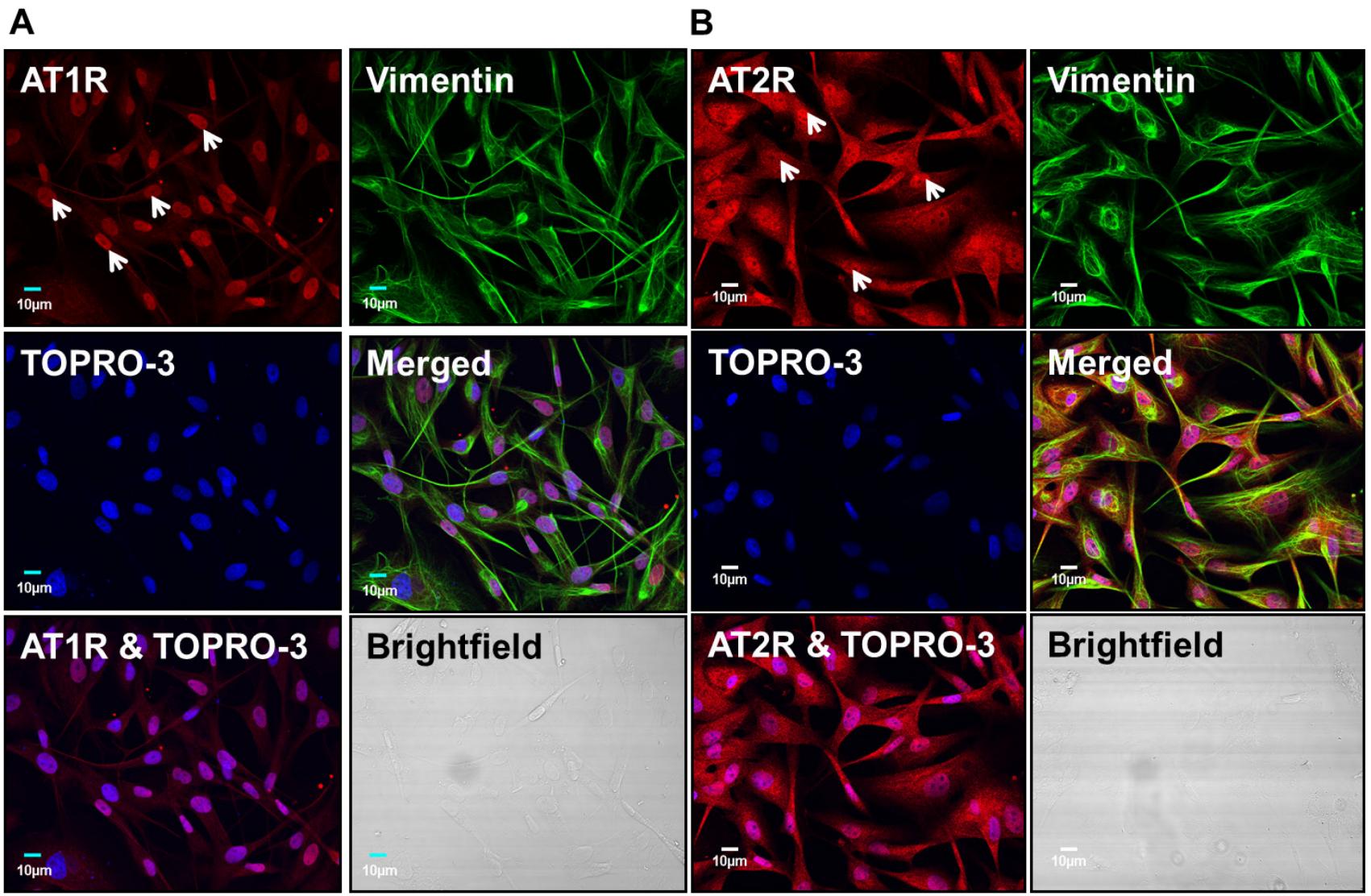
A
B
AT1R
Vimentin
AT2R
Vimentin
TOPRO-3
Merged
TOPRO-3
Merged
AT1R & TOPRO-3
Brightfield
AT2R & TOPRO-3
Brightfield
10µm

Figure 2

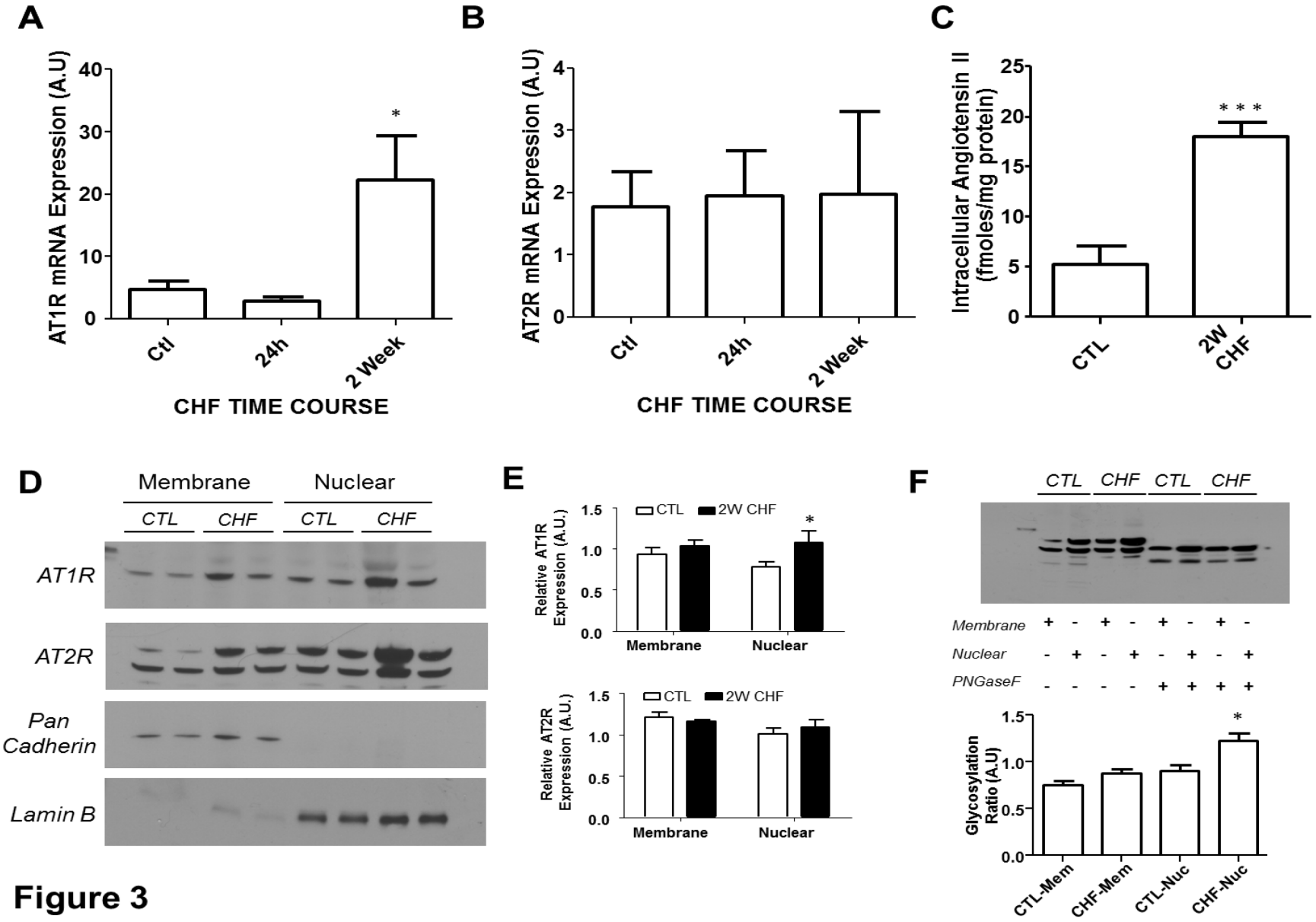
A
AT1R mRNA Expression (A.U)
40
30
20
10
0
*
Ctl
24h
2 Week
CHF TIME COURSE
B
AT2R mRNA Expression (A.U)
4
3
2
1
0
Ctl
24h
2 Week
CHF TIME COURSE
C
Intracellular Angiotensin II (fmoles/mg protein)
25
20
15
10
5
0
* * *
CTL
2W CHF
D
Membrane
Nuclear
CTL
CHF
CTL
CHF
AT1R
AT2R
Pan Cadherin
Lamin B
E
Relative AT1R Expression (A.U.)
1.5
1.0
0.5
0.0
CTL
2W CHF
*
Membrane
Nuclear
Relative AT2R Expression (A.U.)
1.5
1.0
0.5
0.0
CTL
2W CHF
Membrane
Nuclear
F
CTL
CHF
CTL
CHF
Membrane + - + - + - + -
Nuclear - + - + - + - +
PNGaseF - - - - + + + +
Glycosylation Ratio (A.U)
1.5
1.0
0.5
0.0
*
CTL-Mem
CHF-Mem
CTL-Nuc
CHF-Nuc

Figure 3

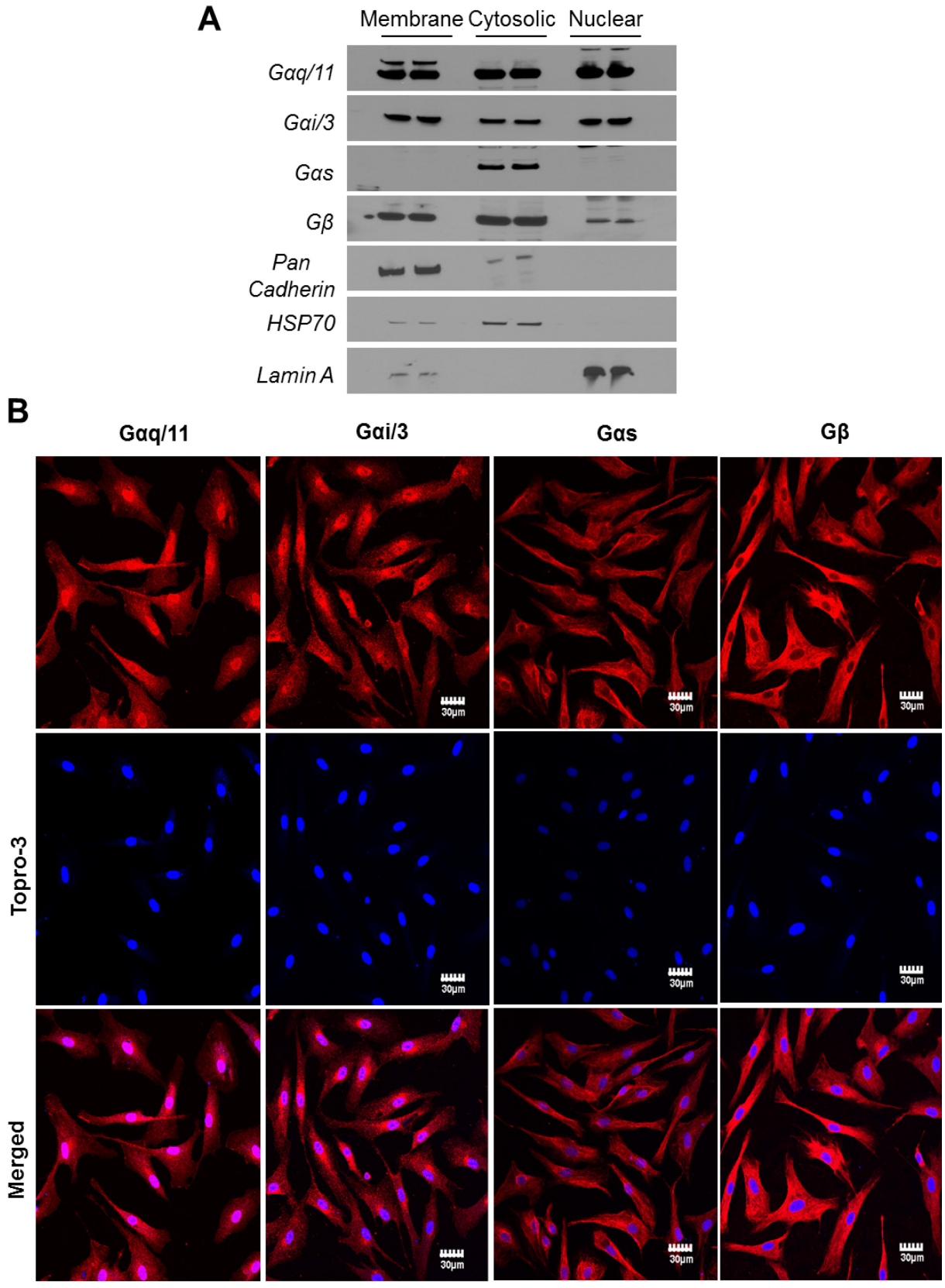
A
Membrane
Cytosolic
Nuclear
Gαq/11
Gαi/3
Gαs
Gβ
Pan Cadherin
HSP70
Lamin A
B
Gαq/11
Gαi/3
Gαs
Gβ
Topro-3
Merged
30μm

Figure 4

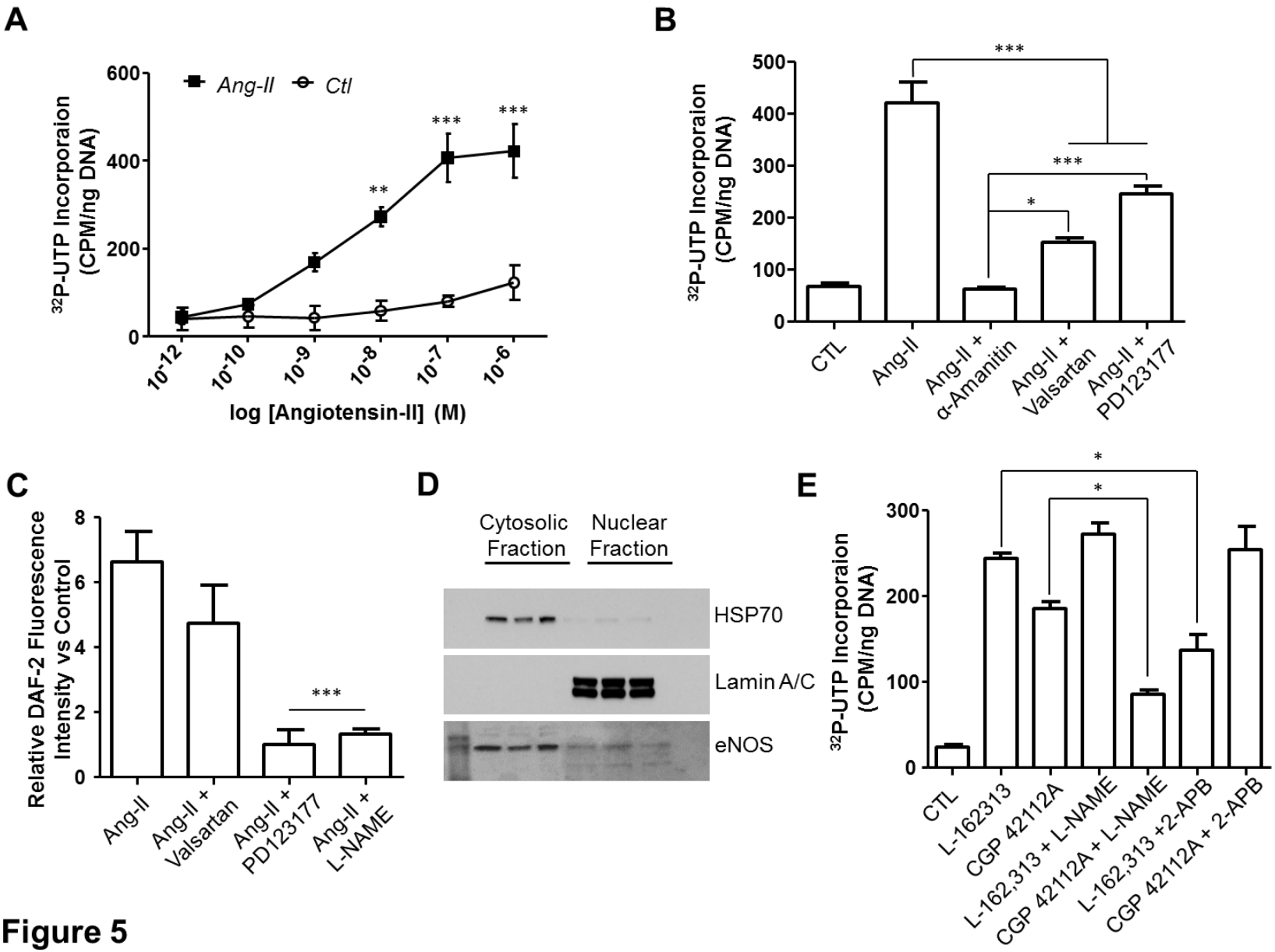
A
Ang-II
Ctl
32P-UTP Incorporaion (CPM/ng DNA)
log [Angiotensin-II] (M)
B
32P-UTP Incorporaion (CPM/ng DNA)
CTL
Ang-II
Ang-II + α-Amanitin
Ang-II + Valsartan
Ang-II + PD123177
C
Relative DAF-2 Fluorescence Intensity vs Control
Ang-II
Ang-II + Valsartan
Ang-II + PD123177
Ang-II + L-NAME
D
Cytosolic Fraction
Nuclear Fraction
HSP70
Lamin A/C
eNOS
E
32P-UTP Incorporaion (CPM/ng DNA)
CTL
L-162313
CGP 42112A
L-162,313 + L-NAME
CGP 42112A + L-NAME
L-162,313 +2-APB
CGP 42112A + 2-APB

Figure 5

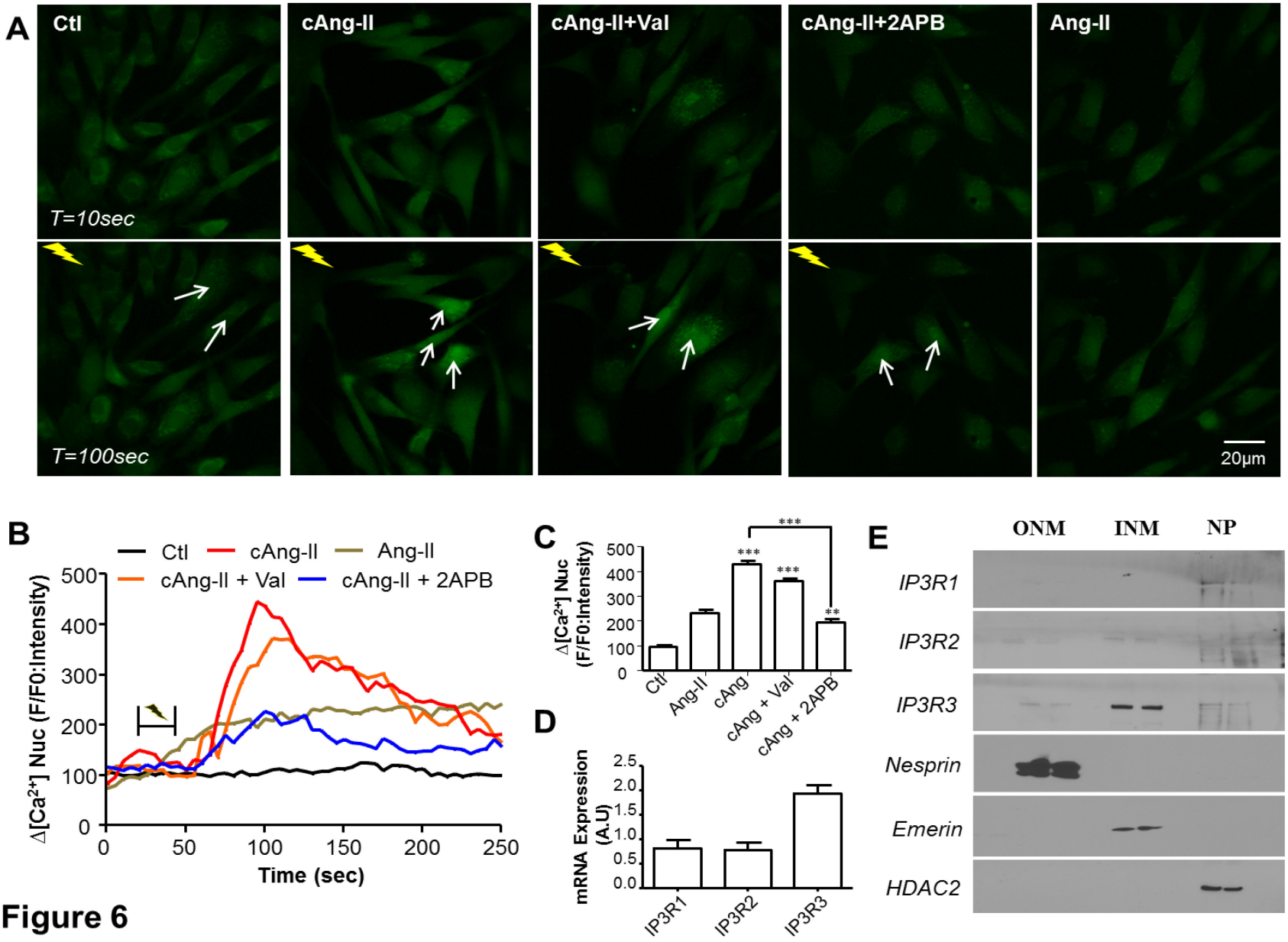
A
Ctl
cAng-II
cAng-II+Val
cAng-II+2APB
Ang-II
T=10sec
T=100sec
20μm
B
Ctl
cAng-II
Ang-II
cAng-II + Val
cAng-II + 2APB
Δ[Ca2+] Nuc (F/F0:Intensity)
Time (sec)
C
Δ[Ca2+] Nuc (F/F0:Intensity)
Ctl
Ang-II
cAng
cAng + Val
cAng + 2APB
D
mRNA Expression (A.U)
IP3R1
IP3R2
IP3R3
E
ONM
INM
NP
IP3R1
IP3R2
IP3R3
Nesprin
Emerin
HDAC2

Figure 6

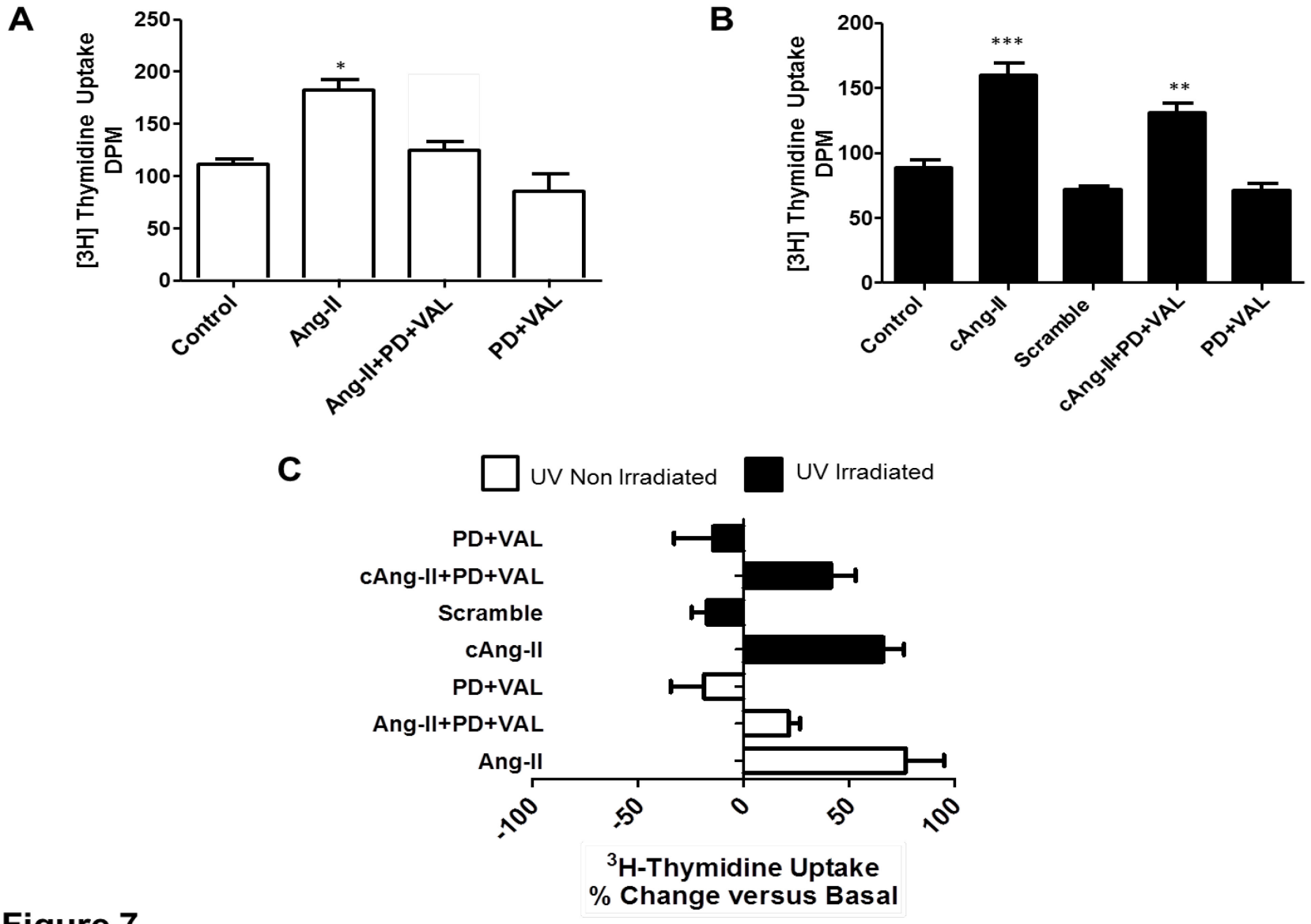
A
[3H] Thymidine Uptake DPM
250
200
150
100
50
0
*
Control
Ang-II
Ang-II+PD+VAL
PD+VAL
B
[3H] Thymidine Uptake DPM
200
150
100
50
0
***
**
Control
cAng-II
Scramble
cAng-II+PD+VAL
PD+VAL
C
UV Non Irradiated
UV Irradiated
PD+VAL
cAng-II+PD+VAL
Scramble
cAng-II
PD+VAL
Ang-II+PD+VAL
Ang-II
-100
-50
0
50
100
3H-Thymidine Uptake
% Change versus Basal

Figure 7

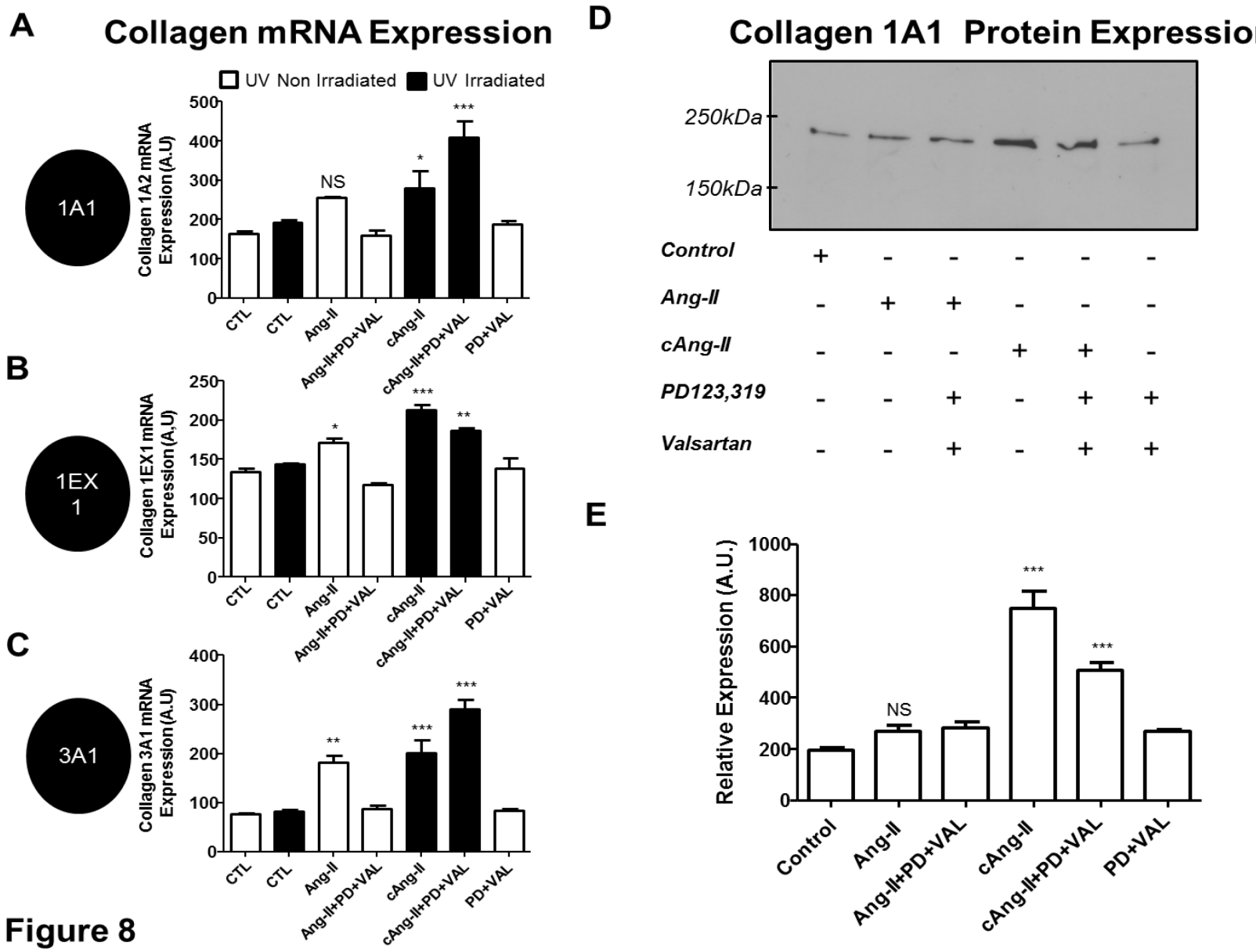
A
Collagen mRNA Expression
UV Non Irradiated
UV Irradiated
1A1
Collagen 1A2 mRNA Expression (A.U)
NS
*
***
B
1EX 1
Collagen 1EX1 mRNA Expression (A,U)
*
***
**
C
3A1
Collagen 3A1 mRNA Expression (A.U)
**
***
***
CTL
CTL
Ang-II
Ang-II+PD+VAL
cAng-II
cAng-II+PD+VAL
PD+VAL
D
Collagen 1A1 Protein Expression
250kDa
150kDa
Control + - - - - -
Ang-II - + + - - -
cAng-II - - - + + -
PD123,319 - - + - + +
Valsartan - - + - + +
E
Relative Expression (A.U.)
NS
***
***
Control
Ang-II
Ang-II+PD+VAL
cAng-II
cAng-II+PD+VAL
PD+VAL

Figure 8

CHAPTER 5 –General Discussion

5.1 Summary and Novel Contributions

Our understanding of the importance and role of the renin-angiotensin system has evolved enormously since the initial discovery of the rate-limiting enzyme, renin, by Tigerstedt and Bergman more than a century ago [213]. New frontiers are emerging, with the identification of novel components, subsystems, signalling transduction mechanisms and functional roles. Traditionally considered as a circulating endocrine system, recent experimental data provide evidence of a complete and functionally active RAS within cells, termed an 'intracrine' or intracellular system. Understanding the diversity of RAS signalling may lead to the development of novel pharmacological interventions for the prevention of cardiac disease and improved therapeutic outcomes.

In chapter 2, we advanced knowledge regarding intracrine RAS in cardiac cells in several ways. We identified, for the first time, the presence of nuclear AT1R and AT2R in ventricular cardiomyocytes. This nuclear localization of AT1R and AT2R was independent of G protein activation and therefore was not a result of clathrin-mediated internalization. Ang-II was detected in cardiomyocyte lysates and microinjected Ang-II localized primarily to the nuclear and perinuclear compartments. Transcriptomic analysis demonstrated that these intracellular receptors regulate de novo RNA synthesis through the activation of G proteins and affect the abundance of both ribosomal and messenger RNA. NF-κB mRNA is more abundant when isolated nuclei were exposed to Ang-II. Furthermore, nuclear AT1R but not AT2R is coupled to IP3R-dependent Ca^{2+} signalling and governs transcriptional regulation.

In chapter 3, we synthesized and pharmacologically characterized, novel cell-permeant photoreleasable Ang-II analogues to efficiently study for the first time intracrine RAS signalling directly in intact cells. In the Laboratory of Molecular and Pharmacological Studies on Peptides, we synthesized, using solid-phase peptide synthesis with Fmoc chemistry, caged Ang-II analogues by incorporating a photocleavable 4,5-dimethoxy-2-nitrobenzyl (DMNB) moiety onto the phenolic group of tyrosine-4 and/or the α-COOH of phenylalanine-8 of Ang-II. The incorporation of a DMNB residue on the active site of the Ang-II peptide prevents the recognition, binding, and subsequent activation of its target receptor (AT1R, AT2R). Our synthesized and highly purified Ang-II analogues ([Tyr(DMNB)^4]Ang-II, Ang-II-ODMNB and [Tyr(DMNB)^4]Ang-II-ODMNB) showed two to three orders of magnitude reduced binding affinity towards both AT1R and AT2R. Similarly, studies in rat thoracic aortic ring preparations revealed a similar rightward shift in the concentration-response curve for contraction. A study of the kinetics of photolysis for each of the three caged Ang-II analogues revealed that [Tyr(DMNB)^4]Ang-II exhibited the fastest rate of release of free Ang-II and therefore was the main focus of subsequent functional studies. Whereas [Tyr(DMNB)^4]Ang-II itself has no effect, Ang-II or photolyzed [Tyr(DMNB)^4]Ang-II increases dose dependently ERK phosphorylation in HEK 293 cells transfect with AT1R and activate NO/cGMP signalling in HEK 293 cells transfected with AT2R. In contrast to Ang-II, [Tyr(DMNB)^4]Ang-II is a potent cell penetrating peptide, showing similar characteristics to those of the HIV-1 derived TAT peptide (TAT48–60), which is regularly used for intracellular delivery of many therapeutically active and diagnostic agents. Photolysis of [Tyr(DMNB)^4]Ang-II inside

cardiomyocytes increases nuclear calcium through IP3R-mediated mechanisms which, in turn, regulates 18S rRNA and NF-*κ*B mRNA levels. These findings provide further pharmacological evidence in support of the functional intracrine RAS actions in cardiac cells. Hence, [Tyr(DMNB)^4]Ang-II is a novel pharmacological probe that could be used in medical research to investigate the role of intracrine RAS not only in cardiac cells, but in any cell type, to delineate specific roles of intracellular Ang-II.

In chapter 4, we presented the first study characterizing the functional role of intracrine RAS signalling in cardiac fibroblasts and investigated its potential involvement in HF. We present evidence that AT1R and AT2R are present on intracellular organelles and more specifically on the inner nuclear membrane. Furthermore, we demonstrate that intracellular Ang-II and nuclear AT1R are increased in HF, whereas the glycosylation of nuclear AT2R is altered. G protein subunits including Gαq/11, Gαi/3, and Gβ were detected in isolated nuclear fractions. Transcription initiation, analyzed by [α-^{32}P]UTP incorporation, showed that nuclear AT1R and AT2R regulate de novo RNA synthesis via IP3R and NO signal transduction pathways, respectively. Using Tyr(DMNB)^4]Ang-II, we demonstrated in intact cultured atrial fibroblasts that intracellular photorelease of Ang-II leads to increased $[Ca^{2+}]_n$, which is not prevented by extracellular AT1R blockers. The increase in $[Ca^{2+}]_n$ can be attenuated by an IP3R blocker and we showed for the first time that IP3R3 is the predominant IP3R isoform in atrial fibroblast nuclear membranes. Furthermore, increasing intracellular Ang-II results in fibroblast

proliferation, collagen synthesis and secretion independent of extracellular AT1R and AT2R.

5.2 Current Insights and Directions for Future Research

5.2.1 Concepts of Intracellular RAS

Major milestones in our understanding of RAS included the discovery of 1) Ang-II generating secretory proteins: renin and angiotensinogen, 2) membrane-anchored ACE with catalytic sites located on the extracellular domain, and 3) the fact that AT1R and AT2R belong to the GPCR superfamily. The accepted dogma has been that in GPCRs localize to the plasma membrane, become functional, and are activated in response to agonist binding. Hence, the concept of circulating and extracellular RAS dominated our thinking [214]. The intracellular synthesis and function of Ang-II was not explored in any detail until recently

To describe an intracrine RAS, defined by the existence of RAS components and the synthesis and actions of Ang-II within a cell, two potential models of the intracrine system were considered. First, intracellular RAS may act as a transient system where renin, angiotensinogen, and ACE are sorted in secretory vesicles, resulting in intravesicular Ang-II generation due to the close proximity of the substrates [215]. In support of the proposed model, renin and Ang-II immunoreactivity were observed within juxtaglomerular epitheloid granular cells [216]. Using

transmission electron microscopy Ang-II was colocalized by immunohistochemistry with renin and Ang-I in the cytoplasmic granules of the juxstaglomerular neonatal kidney cells, whereas angiotensinogen was localized throughout the cytosol [217]. By reverse haemolytic plaque assay it was revealed that kidney cortical cells retain approximately the number of Ang-I secreting cells as renin secreting cells and that the concentration of Ang-I and renin were upregulated when cells were treated with ACE [218]. Large amounts of Ang-II were reported in renin-containing storage granules and mechanistically Ang-II biosynthesis involved the action of resident renin on internalized, exogenous angiotensinogen [219]. Angiotensinogen, prorenin, and renin were also co-expressed in the same secretory granules of all glandular cell types isolated from rat anterior pituitary [220]. Stretch-induced Ang-II release from neonatal cardiomyocytes and low-passage cultures of cardiac microvascular endothelial cells further support the local biosynthesis, and subsequent storage and/or secretion theory [70,221].

The second model of the intracrine RAS involves non-secretory cellular compartments composed principally of the cytoplasm, mitochondria, and nucleus. The exact intracellular trafficking of RAS constituents under physiological and pathological conditions remains largely unknown; however, RAS components targeted to intracellular organelles may be generated as a result of alternative splicing, post-transcriptional processing of coding mRNA and/or post-translational modification. Human astrocytoma cell line, CCF-STTG1, and primary cultures of glial cells isolated from transgenic mice expressing human angiotensinogen expresses a

non-glycosylated form of angiotensinogen, which primarily localizes to the nucleus [222]. Alternatively-spliced renin transcripts generate a secretory renin or an alternative isoform lacking the pre-pro-fragment. In the adrenal gland, heart, and brain, the renin isoform lacking the pre-pro-fragment is retained intracellularly [223,224]. Furthermore, renin and ACE were localized within mitochondrial dense bodies of the rat adrenal cortex [225]. Overexpression of a non-secretory, intracellularly retained renin in transgenic rat hearts increases aldosterone production and in transgenic mice brains, increases arterial pressure and fluid consumption [226,227]. Cytoplasmic renin encoded by the alternatively-spliced renin transcript in H9c2 rat cardiomyoblasts promotes apoptotic cell death [228]. Endogenous ACE has been shown to be localized in the nucleus of mesangial, smooth muscle, and endothelial cells and administration of exogenous ACE correlates with activation of focal adhesion kinase, SRC homology 2 domain-containing protein-tyrosine phosphatase and modulation of platelet-derived growth factor receptor β signalling [229,230]. All of the above observations support the notion of subcellularly compartmentalized functional RAS.

5.2.2 Significance of the Cardiac Intracellular RAS

The rationale for examining the biological signal transduction mechanisms associated with intracrine RAS in the heart is related to accumulating clinical evidence suggesting that RAS blockade with either direct renin inhibitors, ACE inhibitors and/or AT1R blockers provides incomplete protection against cardiac

complications of a variety of remodeling-inducing conditions. A recent meta-analysis by The Blood Pressure Lowering Treatment Trialists' Collaborators combining 31 clinical trials with 190,606 participants showed no strong evidence between regimens to support recommendations for a particular blood pressure lowering drug class [231]. Furthermore, despite a strong biological rationale, in ONgoing Telmisartan Alone and in combination with Ramipril Global Endpoint Trial (ONTARGET), combination of ACE inhibitor, Ramipril, with AT1R blocker, Telmisartan, did not result in increased cardiovascular benefit but was associated with additional adverse events [232-234]. In Aliskiren Trial in Type 2 Diabetes Using Cardio-Renal Endpoints (ALTITUDE), combination of renin inhibitor (aliskeren) with either ACE inhibitor or AT1R blocker did not produce any beneficial outcome but rather, was associated with increased incidence of hypotension, hyperkalemia, renal complications, and nonfatal stroke [235,236]. Likewise in the The Aliskiren Trial on Acute Heart Failure Outcomes (ASTRONAUT) study, administration of alsikiren in addition to standard ACE inhibitor or AT1R blocker did not reduce cardiovascular death or heart failure rehospitalisation [237].

These results led to the following question: if AT1R blockers and ACE inhibitors have such well-documented benefits in preventing the cardiovascular consequences of heightened Ang-II activity, why are the benefits of dual RAS inhibition not superior to what can be obtained by other classes of antihypertensive drugs? We hypothesized that the discrepancy might be explained, at least in part, by the following possibilities: 1) Ang-II acts at intracellular locations where extracellular

ACE inhibitors or AT1R blockers might have limited access; 2) intracellular and tissue Ang-II biosynthesis may involve ACE independent enzymatic pathways, which in certain pathological conditions may become a dominant mechanism; 3) the clinical benefits of RAS inhibitors may be influenced by parallel mechanisms including the kallikrein–kinin system and/or peroxisome proliferator-activated receptor-gamma (PPARγ) activation. To specifically address the potential role of intracellular RAS, central to hypotheses 1) and 2) above, we performed the studies described in this thesis.

5.2.2.1 Intracellular ANG II Receptors and Actions

There is strong accumulating evidence that Ang-II, either produced within cellular compartments or incorporated through vesicular pathways from the extracellular biological environment, leads to hypertrophic, inflammatory, and fibrotic responses [238-240]. In Chapter 2, we demonstrated the presence of nuclear AT1R and AT2R in native cardiomyocytes and the functional role of nuclear AT1R and AT2R in the regulation of transcriptional and Ca^{2+}, thus providing a framework for the concept of intracrine RAS signalling. Other investigators have shown previously that intracellular Ang-II changes cellular electrophysiological properties including action potential duration, conduction velocity, and cardiac refractoriness, and can induce pathological events like early afterdepolarizations, [208,241]. Furthermore, microinjected Ang-II in vascular smooth muscle cells leads to a rapid increase in cytosolic and nuclear Ca^{2+} concentrations and the rise in intracellular Ca^{2+} is only

inhibited by intracellular, and not extracellular, administration of an AT1R blocker [242]. Cytosolic delivery of Ang-II using multilamellar liposomes, in de-endothelized aortic rings, resulted in a concentration-dependent contraction that was insensitive to extracellular administration of an AT1R blocker but pre-treatment with an intracellular AT1R blocker completely abolished the contractile response [243]. In chapter 3, we employed a novel photoreleasable [Tyr(DMNB)^4]Ang-II to demonstrate that intracellular Ang-II generated Ca^{2+} responses are not abolished by conventional extracellular AT1R blockers. Additionally, in chapter 4 we showed, in cultured cardiac fibroblasts, that intracellular Ang-II regulates proliferation plus the transcription and secretion of collagen, These effects are not prevented by the combination of PD123177 and valsartan in the extracellular medium. Thus, there is substantial evidence that intracellular Ang-II actions on intracellular AT1R and AT2R escapes inhibition from conventional pharmacological probes that act either in the extracellular compartment or the cell surface membrane. However, further studies are necessary to elucidate the mechanisms of intracrine RAS in pathological conditions, since sustained biological and pathological actions of RAS may represent a combination of both intracellular and extracellular Ang II-mediated pathways. A genetic model of mice lacking intracellular AT1 or AT2 receptor would provide solid insight on the role of intracrine Ang-II signalling in cardiac physiology. Nonetheless these in vivo models are, and will, remain a challenge as long as the mechanisms responsible for selective trafficking of ATRs to the cell surface and intracellular membranes are not understood. Moreover, the links between the development of HF and changes in nuclear AT1R/AT2R in whole heart preparations (physiologically close to an in vivo

condition), and complete transcriptome analysis need to be explored in future studies. GPCR regulators, including β-arrestin and GRK, were also found to be present in nuclei, but it's uncertain under which conditions the nuclear function of GPCR regulators are physiologically relevant. Thus more detailed studies will be required to clearly establish the role of GPCR regulators in mediating nuclear AT1R/AT2R signalling and allow the identification of novel biological functions [244,245].

5.2.2.2 Novel Routes for Intracellular Ang-II Biosynthesis

The concept of an ACE independent biosynthesis of Ang-II is gaining new momentum. Cardiac chymase-mediated Ang-II synthesis has emerged as an unconventional pathway in cardiac tissue and particularly under pathological conditions [246,247]. Chymase-generated Ang-II has been proposed to dominate over ACE in human heart and vasculature and to have a key role in cardiac remodeling, cardiomyopathies, heart failure and diabetes [76,247-249]. Electron microscopic immunocytochemistry showed that chymase, a chymotrypsin-like serine protease, is localized predominantly in cytosolic granules of mast cells, endothelial cells, and mesenchymal interstitial cells of the heart [250]. Paralleling these findings, studies identified in human atrial appendage tissue Ang-(1-12) as a non-renin dependent alternate precursor for the generation of cardiac Ang-II. In atrial cardiac cells Ang-(1-12) was primarily hydrolyzed by chymase whereas ACE contribution was almost undetectable [251-254]. Hearts perfused with Ang-(1-12) revealed a striking increase of Ang-II production that was not blocked by ACE inhibitors, whereas the

generation of Ang-II and consequent vasoconstriction and myocardial damage following ischemia were significantly attenuated by a chymase inhibitor (chymostatin) [255,256]. Hence, the primacy of chymase as a novel intracellular cardiac Ang-II producing enzyme should generate cautionary notes as to the direct applicability of animal models of cardiac ACE overexpression in addressing the role of cardiac RAS in human pathologies. In chapter 4, we observed that atrial fibroblasts isolated from HF animals contain significantly higher Ang-II levels as compared to control animals, which potently exerts trophic and profibrotic effects on the heart. It would be of great interest to investigate in further studies the role of chymase or ACE dependent hydrolytic activity in governing the biosynthesis of Ang-II in normal and pathological conditions.

5.2.2.3 Significance of Parallel Mechanisms

ACE inhibitors and AT1R blockers by acting at distinct points in the RAS may compensate to some extent and therefore reduce the influence of intracrine RAS signalling. In AT1R knockout mice, ACE inhibitors prevent cardiac fibrosis and improve myocardial function, suggesting that non-AT1R mediated mechanisms play a significant role in myocardial remodeling [257]. Several studies reported that kallikrein and bradykinin receptors are key determinants of the cardioprotective effect of ACE or AT1R blockade [258,259]. In tissue from kallikrein gene-deficient mice (TK –/–) subjected to 30 min of coronary artery occlusion followed by 3 h of reperfusion, administration of losartan prior to reperfusion did not reduce infarct size. Wild-type

mice pretreated with the bradykinin-2 receptor (B2R) antagonist icatibant reproduced the effect of TK deficiency [260]. AT1R-B2R heterodimerization was confirmed with BRET and FRET biophysical methods and in vitro / in vivo results established a role of the AT1R-B2R heterodimer in sensitizing AT1R-regulated vasoconstrictor activity [261]. Furthermore, AT1R blockers have been demonstrated to induce PPARγ activity [262]. PPARγ is a nuclear receptor that regulates the expression of genes by binding to peroxisome proliferator response elements. Telmisartan (AT1R blocker), acting through PPARγ, activates phosphoenolpyruvate carboxykinase-1 (PEPCK-C) and acetyl coenzyme A carboxylase 2 (ACC2) genes, markers of the differentiation of mouse embryonic fibroblasts into adipocytes [263]. Recently non-AT1R and non-AT2R binding sites with high affinity and specificity for Ang-II were described, however little is known about their functional significance [264]. Future research will need to focus on the role of non-classical RAS-mediated mechanisms, including investigating whether the AT1R and B2R heterodimerize at the nucleus and if they can be selectively targeted by biased ligands to deliver safer and more efficacious cardiac pharmacotherapy.

5.3 Conclusions

The concept of intracrine RAS signalling has evolved rapidly in the last decade. Once judged as an idiosyncratic phenomenon of unclear importance, intracrine RAS is now well characterized at the level of ligands (Ang-II), receptors (AT1R/AT2R), effectors, signalling mechanisms and actions, and increasingly, regarded as a viable cardiovascular drug target. This thesis has contributed to this field by providing novel tools with which to investigate the intracellular RAS and novel insights into its role and signalling mechanisms in cardiac cells. There remain many unanswered questions, before the translation of experimental research on intracrine RAS can head to the clinic, particularly those related to the origin of intracellular AT1R/AT2R, the precise site of intracellular Ang-II biosynthesis, and the exact in vivo role of intracrine RAS in pathological conditions.

References

1. Wong ND (2014) Epidemiological studies of CHD and the evolution of preventive cardiology. Nat Rev Cardiol 11: 276-289.
2. Tang CM, Insel PA (2004) GPCR expression in the heart; "new" receptors in myocytes and fibroblasts. Trends Cardiovasc Med 14: 94-99.
3. Hunt SA, Abraham WT, Chin MH, Feldman AM, Francis GS, et al. (2005) ACC/AHA 2005 Guideline Update for the Diagnosis and Management of Chronic Heart Failure in the Adult: a report of the American College of Cardiology/American Heart Association Task Force on Practice Guidelines (Writing Committee to Update the 2001 Guidelines for the Evaluation and Management of Heart Failure): developed in collaboration with the American College of Chest Physicians and the International Society for Heart and Lung Transplantation: endorsed by the Heart Rhythm Society. Circulation 112: e154-235.
4. Guyton AC (1981) The relationship of cardiac output and arterial pressure control. Circulation 64: 1079-1088.
5. Kang M, Chung KY, Walker JW (2007) G-protein coupled receptor signaling in myocardium: not for the faint of heart. Physiology (Bethesda) 22: 174-184.
6. Brette F, Orchard C (2003) T-tubule function in mammalian cardiac myocytes. Circ Res 92: 1182-1192.
7. Rivard K, Grandy SA, Douillette A, Paradis P, Nemer M, et al. (2011) Overexpression of type 1 angiotensin II receptors impairs excitation-

contraction coupling in the mouse heart. Am J Physiol Heart Circ Physiol 301: H2018-2027.

8. Hohendanner F, McCulloch AD, Blatter LA, Michailova AP (2014) Calcium and IP3 dynamics in cardiac myocytes: experimental and computational perspectives and approaches. Front Pharmacol 5: 35.

9. Sumandea MP, Steinberg SF (2011) Redox signaling and cardiac sarcomeres. J Biol Chem 286: 9921-9927.

10. Maeder MT, Kaye DM (2009) Heart failure with normal left ventricular ejection fraction. J Am Coll Cardiol 53: 905-918.

11. Oudot A, Vergely C, Ecarnot-Laubriet A, Rochette L (2003) Angiotensin II activates NADPH oxidase in isolated rat hearts subjected to ischaemia-reperfusion. Eur J Pharmacol 462: 145-154.

12. Donato AJ, Pierce GL, Lesniewski LA, Seals DR (2009) Role of NFkappaB in age-related vascular endothelial dysfunction in humans. Aging (Albany NY) 1: 678-680.

13. Johnson JL (2014) Emerging regulators of vascular smooth muscle cell function in the development and progression of atherosclerosis. Cardiovasc Res 103: 452-460.

14. Matsuzawa Y, Guddeti RR, Kwon TG, Lerman LO, Lerman A (2014) Treating Coronary Disease and the Impact of Endothelial Dysfunction. Prog Cardiovasc Dis.

15. Davignon J, Ganz P (2004) Role of endothelial dysfunction in atherosclerosis. Circulation 109: III27-32.

16. Stout KK, Verrier ED (2009) Acute valvular regurgitation. Circulation 119: 3232-3241.

17. Helske S, Lindstedt KA, Laine M, Mayranpaa M, Werkkala K, et al. (2004) Induction of local angiotensin II-producing systems in stenotic aortic valves. J Am Coll Cardiol 44: 1859-1866.

18. Bates ER (2011) Treatment options in severe aortic stenosis. Circulation 124: 355-359.

19. Nkomo VT, Gardin JM, Skelton TN, Gottdiener JS, Scott CG, et al. (2006) Burden of valvular heart diseases: a population-based study. Lancet 368: 1005-1011.

20. Neumar RW, Otto CW, Link MS, Kronick SL, Shuster M, et al. (2010) Part 8: adult advanced cardiovascular life support: 2010 American Heart Association Guidelines for Cardiopulmonary Resuscitation and Emergency Cardiovascular Care. Circulation 122: S729-767.

21. Kattwinkel J, Perlman JM, Aziz K, Colby C, Fairchild K, et al. (2010) Part 15: neonatal resuscitation: 2010 American Heart Association Guidelines for Cardiopulmonary Resuscitation and Emergency Cardiovascular Care. Circulation 122: S909-919.

22. Wakili R, Voigt N, Kaab S, Dobrev D, Nattel S (2011) Recent advances in the molecular pathophysiology of atrial fibrillation. J Clin Invest 121: 2955-2968.

23. Dobrev D, Nattel S (2010) New antiarrhythmic drugs for treatment of atrial fibrillation. Lancet 375: 1212-1223.

24. Tadros R, Ton AT, Fiset C, Nattel S (2014) Sex differences in cardiac electrophysiology and clinical arrhythmias: epidemiology, therapeutics, and mechanisms. Can J Cardiol 30: 783-792.

25. Nattel S, Maguy A, Le Bouter S, Yeh YH (2007) Arrhythmogenic ion-channel remodeling in the heart: heart failure, myocardial infarction, and atrial fibrillation. Physiol Rev 87: 425-456.

26. Doronin SV, Potapova IA, Lu Z, Cohen IS (2004) Angiotensin receptor type 1 forms a complex with the transient outward potassium channel Kv4.3 and regulates its gating properties and intracellular localization. J Biol Chem 279: 48231-48237.

27. Valderrabano M (2007) Influence of anisotropic conduction properties in the propagation of the cardiac action potential. Prog Biophys Mol Biol 94: 144-168.

28. Chen YJ, Chen YC, Tai CT, Yeh HI, Lin CI, et al. (2006) Angiotensin II and angiotensin II receptor blocker modulate the arrhythmogenic activity of pulmonary veins. Br J Pharmacol 147: 12-22.

29. Khandaker MH, Espinosa RE, Nishimura RA, Sinak LJ, Hayes SN, et al. (2010) Pericardial disease: diagnosis and management. Mayo Clin Proc 85: 572-593.

30. Little WC, Freeman GL (2006) Pericardial disease. Circulation 113: 1622-1632.

31. Miyazaki T, Pride HP, Zipes DP (1990) Prostaglandins in the pericardial fluid modulate neural regulation of cardiac electrophysiological properties. Circ Res 66: 163-175.

32. Rouleau JL (2011) New and emerging drugs and device therapies for chronic heart failure in patients with systolic ventricular dysfunction. Can J Cardiol 27: 296-301.

33. Cohn JN, Ferrari R, Sharpe N (2000) Cardiac remodeling--concepts and clinical implications: a consensus paper from an international forum on cardiac remodeling. Behalf of an International Forum on Cardiac Remodeling. J Am Coll Cardiol 35: 569-582.

34. Cohn JN (1995) Structural basis for heart failure. Ventricular remodeling and its pharmacological inhibition. Circulation 91: 2504-2507.

35. Mentz RJ, Kelly JP, von Lueder TG, Voors AA, Lam CS, et al. (2014) Noncardiac comorbidities in heart failure with reduced versus preserved ejection fraction. J Am Coll Cardiol 64: 2281-2293.

36. Bhuiyan T, Maurer MS (2011) Heart Failure with Preserved Ejection Fraction: Persistent Diagnosis, Therapeutic Enigma. Curr Cardiovasc Risk Rep 5: 440-449.

37. van Heerebeek L, Borbely A, Niessen HW, Bronzwaer JG, van der Velden J, et al. (2006) Myocardial structure and function differ in systolic and diastolic heart failure. Circulation 113: 1966-1973.

38. Kitzman DW, Little WC, Brubaker PH, Anderson RT, Hundley WG, et al. (2002) Pathophysiological characterization of isolated diastolic heart failure in comparison to systolic heart failure. JAMA 288: 2144-2150.

39. van Heerebeek L, Hamdani N, Handoko ML, Falcao-Pires I, Musters RJ, et al. (2008) Diastolic stiffness of the failing diabetic heart: importance of fibrosis,

advanced glycation end products, and myocyte resting tension. Circulation 117: 43-51.

40. Borbely A, van der Velden J, Papp Z, Bronzwaer JG, Edes I, et al. (2005) Cardiomyocyte stiffness in diastolic heart failure. Circulation 111: 774-781.

41. van Heerebeek L, Hamdani N, Falcao-Pires I, Leite-Moreira AF, Begieneman MP, et al. (2012) Low myocardial protein kinase G activity in heart failure with preserved ejection fraction. Circulation 126: 830-839.

42. Kehat I, Molkentin JD (2010) Molecular pathways underlying cardiac remodeling during pathophysiological stimulation. Circulation 122: 2727-2735.

43. Pfeffer MA, Braunwald E (1990) Ventricular remodeling after myocardial infarction. Experimental observations and clinical implications. Circulation 81: 1161-1172.

44. Sutton MG, Sharpe N (2000) Left ventricular remodeling after myocardial infarction: pathophysiology and therapy. Circulation 101: 2981-2988.

45. Rouleau JL, de Champlain J, Klein M, Bichet D, Moye L, et al. (1993) Activation of neurohumoral systems in postinfarction left ventricular dysfunction. J Am Coll Cardiol 22: 390-398.

46. Warren SE, Royal HD, Markis JE, Grossman W, McKay RG (1988) Time course of left ventricular dilation after myocardial infarction: influence of infarct-related artery and success of coronary thrombolysis. J Am Coll Cardiol 11: 12-19.

47. Ahuja P, Sdek P, MacLellan WR (2007) Cardiac myocyte cell cycle control in development, disease, and regeneration. Physiol Rev 87: 521-544.

48. Sadoshima J, Izumo S (1997) The cellular and molecular response of cardiac myocytes to mechanical stress. Annu Rev Physiol 59: 551-571.

49. Sadoshima J, Jahn L, Takahashi T, Kulik TJ, Izumo S (1992) Molecular characterization of the stretch-induced adaptation of cultured cardiac cells. An in vitro model of load-induced cardiac hypertrophy. J Biol Chem 267: 10551-10560.

50. Takemura G, Kanoh M, Minatoguchi S, Fujiwara H (2013) Cardiomyocyte apoptosis in the failing heart--a critical review from definition and classification of cell death. Int J Cardiol 167: 2373-2386.

51. Gonzalez A, Fortuno MA, Querejeta R, Ravassa S, Lopez B, et al. (2003) Cardiomyocyte apoptosis in hypertensive cardiomyopathy. Cardiovasc Res 59: 549-562.

52. Chiong M, Wang ZV, Pedrozo Z, Cao DJ, Troncoso R, et al. (2011) Cardiomyocyte death: mechanisms and translational implications. Cell Death Dis 2: e244.

53. Kung G, Konstantinidis K, Kitsis RN (2011) Programmed necrosis, not apoptosis, in the heart. Circ Res 108: 1017-1036.

54. Kalra D, Sivasubramanian N, Mann DL (2002) Angiotensin II induces tumor necrosis factor biosynthesis in the adult mammalian heart through a protein kinase C-dependent pathway. Circulation 105: 2198-2205.

55. Danial NN, Korsmeyer SJ (2004) Cell death: critical control points. Cell 116: 205-219.

56. Lipinski MM, Hoffman G, Ng A, Zhou W, Py BF, et al. (2010) A genome-wide siRNA screen reveals multiple mTORC1 independent signaling pathways regulating autophagy under normal nutritional conditions. Dev Cell 18: 1041-1052.

57. Levine B, Klionsky DJ (2004) Development by self-digestion: molecular mechanisms and biological functions of autophagy. Dev Cell 6: 463-477.

58. Gustafsson AB, Gottlieb RA (2009) Autophagy in ischemic heart disease. Circ Res 104: 150-158.

59. Souders CA, Bowers SL, Baudino TA (2009) Cardiac fibroblast: the renaissance cell. Circ Res 105: 1164-1176.

60. Camelliti P, Borg TK, Kohl P (2005) Structural and functional characterisation of cardiac fibroblasts. Cardiovasc Res 65: 40-51.

61. Manabe I, Shindo T, Nagai R (2002) Gene expression in fibroblasts and fibrosis: involvement in cardiac hypertrophy. Circ Res 91: 1103-1113.

62. Schuetze KB, McKinsey TA, Long CS (2014) Targeting cardiac fibroblasts to treat fibrosis of the heart: focus on HDACs. J Mol Cell Cardiol 70: 100-107.

63. Gan Q, Yoshida T, Li J, Owens GK (2007) Smooth muscle cells and myofibroblasts use distinct transcriptional mechanisms for smooth muscle alpha-actin expression. Circ Res 101: 883-892.

64. Bai J, Zhang N, Hua Y, Wang B, Ling L, et al. (2013) Metformin inhibits angiotensin II-induced differentiation of cardiac fibroblasts into myofibroblasts. PLoS One 8: e72120.

65. Olson ER, Naugle JE, Zhang X, Bomser JA, Meszaros JG (2005) Inhibition of cardiac fibroblast proliferation and myofibroblast differentiation by resveratrol. Am J Physiol Heart Circ Physiol 288: H1131-1138.

66. Louault C, Benamer N, Faivre JF, Potreau D, Bescond J (2008) Implication of connexins 40 and 43 in functional coupling between mouse cardiac fibroblasts in primary culture. Biochim Biophys Acta 1778: 2097-2104.

67. Krenning G, Zeisberg EM, Kalluri R (2010) The origin of fibroblasts and mechanism of cardiac fibrosis. J Cell Physiol 225: 631-637.

68. Burchfield JS, Xie M, Hill JA (2013) Pathological ventricular remodeling: mechanisms: part 1 of 2. Circulation 128: 388-400.

69. Grossman W, Jones D, McLaurin LP (1975) Wall stress and patterns of hypertrophy in the human left ventricle. J Clin Invest 56: 56-64.

70. Sadoshima J, Xu Y, Slayter HS, Izumo S (1993) Autocrine release of angiotensin II mediates stretch-induced hypertrophy of cardiac myocytes in vitro. Cell 75: 977-984.

71. Francis GS (2011) Neurohormonal control of heart failure. Cleve Clin J Med 78 Suppl 1: S75-79.

72. Parsons KK, Coffman TM (2007) The renin-angiotensin system: it's all in your head. J Clin Invest 117: 873-876.

73. Witherow FN, Helmy A, Webb DJ, Fox KA, Newby DE (2001) Bradykinin contributes to the vasodilator effects of chronic angiotensin-converting enzyme inhibition in patients with heart failure. Circulation 104: 2177-2181.

74. Kramkowski K, Mogielnicki A, Buczko W (2006) The physiological significance of the alternative pathways of angiotensin II production. J Physiol Pharmacol 57: 529-539.

75. Rykl J, Thiemann J, Kurzawski S, Pohl T, Gobom J, et al. (2006) Renal cathepsin G and angiotensin II generation. J Hypertens 24: 1797-1807.

76. Li M, Liu K, Michalicek J, Angus JA, Hunt JE, et al. (2004) Involvement of chymase-mediated angiotensin II generation in blood pressure regulation. J Clin Invest 114: 112-120.

77. Leung PS (2007) The physiology of a local renin-angiotensin system in the pancreas. J Physiol 580: 31-37.

78. Zisman LS, Meixell GE, Bristow MR, Canver CC (2003) Angiotensin-(1-7) formation in the intact human heart: in vivo dependence on angiotensin II as substrate. Circulation 108: 1679-1681.

79. Vickers C, Hales P, Kaushik V, Dick L, Gavin J, et al. (2002) Hydrolysis of biological peptides by human angiotensin-converting enzyme-related carboxypeptidase. J Biol Chem 277: 14838-14843.

80. Dias-Peixoto MF, Santos RA, Gomes ER, Alves MN, Almeida PW, et al. (2008) Molecular mechanisms involved in the angiotensin-(1-7)/Mas signaling pathway in cardiomyocytes. Hypertension 52: 542-548.

81. Gomes ER, Lara AA, Almeida PW, Guimaraes D, Resende RR, et al. (2010) Angiotensin-(1-7) prevents cardiomyocyte pathological remodeling through a nitric oxide/guanosine 3',5'-cyclic monophosphate-dependent pathway. Hypertension 55: 153-160.

82. Regitz-Zagrosek V, Fielitz J, Fleck E (1998) Myocardial angiotensin receptors in human hearts. Basic Res Cardiol 93 Suppl 2: 37-42.

83. Booz GW, Baker KM (1996) Role of type 1 and type 2 angiotensin receptors in angiotensin II-induced cardiomyocyte hypertrophy. Hypertension 28: 635-640.

84. Hou M, Pantev E, Moller S, Erlinge D, Edvinsson L (2000) Angiotensin II type 1 receptors stimulate protein synthesis in human cardiac fibroblasts via a Ca2+-sensitive PKC-dependent tyrosine kinase pathway. Acta Physiol Scand 168: 301-309.

85. de Gasparo M, Catt KJ, Inagami T, Wright JW, Unger T (2000) International union of pharmacology. XXIII. The angiotensin II receptors. Pharmacol Rev 52: 415-472.

86. Sadoshima J, Izumo S (1996) The heterotrimeric G q protein-coupled angiotensin II receptor activates p21 ras via the tyrosine kinase-Shc-Grb2-Sos pathway in cardiac myocytes. EMBO J 15: 775-787.

87. Eguchi S, Iwasaki H, Inagami T, Numaguchi K, Yamakawa T, et al. (1999) Involvement of PYK2 in angiotensin II signaling of vascular smooth muscle cells. Hypertension 33: 201-206.

88. Murasawa S, Mori Y, Nozawa Y, Gotoh N, Shibuya M, et al. (1998) Angiotensin II type 1 receptor-induced extracellular signal-regulated protein kinase activation is mediated by Ca2+/calmodulin-dependent transactivation of epidermal growth factor receptor. Circ Res 82: 1338-1348.

89. Higuchi S, Ohtsu H, Suzuki H, Shirai H, Frank GD, et al. (2007) Angiotensin II signal transduction through the AT1 receptor: novel insights into mechanisms and pathophysiology. Clin Sci (Lond) 112: 417-428.

90. Ohtsu H, Suzuki H, Nakashima H, Dhobale S, Frank GD, et al. (2006) Angiotensin II signal transduction through small GTP-binding proteins: mechanism and significance in vascular smooth muscle cells. Hypertension 48: 534-540.

91. Fujii T, Onohara N, Maruyama Y, Tanabe S, Kobayashi H, et al. (2005) Galpha12/13-mediated production of reactive oxygen species is critical for angiotensin receptor-induced NFAT activation in cardiac fibroblasts. J Biol Chem 280: 23041-23047.

92. Pracyk JB, Tanaka K, Hegland DD, Kim KS, Sethi R, et al. (1998) A requirement for the rac1 GTPase in the signal transduction pathway leading to cardiac myocyte hypertrophy. J Clin Invest 102: 929-937.

93. Tilley DG (2011) G protein-dependent and G protein-independent signaling pathways and their impact on cardiac function. Circ Res 109: 217-230.

94. Gaborik Z, Szaszak M, Szidonya L, Balla B, Paku S, et al. (2001) Beta-arrestin- and dynamin-dependent endocytosis of the AT1 angiotensin receptor. Mol Pharmacol 59: 239-247.

95. Violin JD, Lefkowitz RJ (2007) Beta-arrestin-biased ligands at seven-transmembrane receptors. Trends Pharmacol Sci 28: 416-422.

96. Boerrigter G, Lark MW, Whalen EJ, Soergel DG, Violin JD, et al. (2011) Cardiorenal actions of TRV120027, a novel ss-arrestin-biased ligand at the

angiotensin II type I receptor, in healthy and heart failure canines: a novel therapeutic strategy for acute heart failure. Circ Heart Fail 4: 770-778.

97. Kim KS, Abraham D, Williams B, Violin JD, Mao L, et al. (2012) beta-Arrestin-biased AT1R stimulation promotes cell survival during acute cardiac injury. Am J Physiol Heart Circ Physiol 303: H1001-1010.

98. Anderson KM, Murahashi T, Dostal DE, Peach MJ (1993) Morphological and biochemical analysis of angiotensin II internalization in cultured rat aortic smooth muscle cells. Am J Physiol 264: C179-188.

99. Kule CE, Karoor V, Day JN, Thomas WG, Baker KM, et al. (2004) Agonist-dependent internalization of the angiotensin II type one receptor (AT1): role of C-terminus phosphorylation in recruitment of beta-arrestins. Regul Pept 120: 141-148.

100. Wyse BD, Prior IA, Qian H, Morrow IC, Nixon S, et al. (2003) Caveolin interacts with the angiotensin II type 1 receptor during exocytic transport but not at the plasma membrane. J Biol Chem 278: 23738-23746.

101. Carey RM, Wang ZQ, Siragy HM (2000) Role of the angiotensin type 2 receptor in the regulation of blood pressure and renal function. Hypertension 35: 155-163.

102. Bedecs K, Elbaz N, Sutren M, Masson M, Susini C, et al. (1997) Angiotensin II type 2 receptors mediate inhibition of mitogen-activated protein kinase cascade and functional activation of SHP-1 tyrosine phosphatase. Biochem J 325 (Pt 2): 449-454.

103. Horiuchi M, Akishita M, Dzau VJ (1999) Recent progress in angiotensin II type 2 receptor research in the cardiovascular system. Hypertension 33: 613-621.

104. van Kesteren CA, van Heugten HA, Lamers JM, Saxena PR, Schalekamp MA, et al. (1997) Angiotensin II-mediated growth and antigrowth effects in cultured neonatal rat cardiac myocytes and fibroblasts. J Mol Cell Cardiol 29: 2147-2157.

105. Yamada T, Horiuchi M, Dzau VJ (1996) Angiotensin II type 2 receptor mediates programmed cell death. Proc Natl Acad Sci U S A 93: 156-160.

106. Tanaka M, Ohnishi J, Ozawa Y, Sugimoto M, Usuki S, et al. (1995) Characterization of angiotensin II receptor type 2 during differentiation and apoptosis of rat ovarian cultured granulosa cells. Biochem Biophys Res Commun 207: 593-598.

107. Dimmeler S, Rippmann V, Weiland U, Haendeler J, Zeiher AM (1997) Angiotensin II induces apoptosis of human endothelial cells. Protective effect of nitric oxide. Circ Res 81: 970-976.

108. Yamada T, Akishita M, Pollman MJ, Gibbons GH, Dzau VJ, et al. (1998) Angiotensin II type 2 receptor mediates vascular smooth muscle cell apoptosis and antagonizes angiotensin II type 1 receptor action: an in vitro gene transfer study. Life Sci 63: PL289-295.

109. Turu G, Szidonya L, Gaborik Z, Buday L, Spat A, et al. (2006) Differential beta-arrestin binding of AT1 and AT2 angiotensin receptors. FEBS Lett 580: 41-45.

110. Ruilope LM, Schmieder RE (2008) Left ventricular hypertrophy and clinical outcomes in hypertensive patients. Am J Hypertens 21: 500-508.

111. Drazner MH (2011) The progression of hypertensive heart disease. Circulation 123: 327-334.

112. Schillaci G, Verdecchia P, Porcellati C, Cuccurullo O, Cosco C, et al. (2000) Continuous relation between left ventricular mass and cardiovascular risk in essential hypertension. Hypertension 35: 580-586.

113. Cuspidi C, Sala C, Muiesan ML, De Luca N, Schillaci G, et al. (2013) Right ventricular hypertrophy in systemic hypertension: an updated review of clinical studies. J Hypertens 31: 858-865.

114. Sadoshima J, Izumo S (1993) Molecular characterization of angiotensin II--induced hypertrophy of cardiac myocytes and hyperplasia of cardiac fibroblasts. Critical role of the AT1 receptor subtype. Circ Res 73: 413-423.

115. Schunkert H, Dzau VJ, Tang SS, Hirsch AT, Apstein CS, et al. (1990) Increased rat cardiac angiotensin converting enzyme activity and mRNA expression in pressure overload left ventricular hypertrophy. Effects on coronary resistance, contractility, and relaxation. J Clin Invest 86: 1913-1920.

116. Suzuki J, Matsubara H, Urakami M, Inada M (1993) Rat angiotensin II (type 1A) receptor mRNA regulation and subtype expression in myocardial growth and hypertrophy. Circ Res 73: 439-447.

117. Sadoshima J, Izumo S (1993) Signal transduction pathways of angiotensin II--induced c-fos gene expression in cardiac myocytes in vitro. Roles of phospholipid-derived second messengers. Circ Res 73: 424-438.

118. Sadoshima J, Izumo S (1995) Rapamycin selectively inhibits angiotensin II-induced increase in protein synthesis in cardiac myocytes in vitro. Potential

role of 70-kD S6 kinase in angiotensin II-induced cardiac hypertrophy. Circ Res 77: 1040-1052.

119. Aoki H, Izumo S, Sadoshima J (1998) Angiotensin II activates RhoA in cardiac myocytes: a critical role of RhoA in angiotensin II-induced premyofibril formation. Circ Res 82: 666-676.

120. Milavetz JJ, Raya TE, Johnson CS, Morkin E, Goldman S (1996) Survival after myocardial infarction in rats: captopril versus losartan. J Am Coll Cardiol 27: 714-719.

121. Liu YH, Yang XP, Sharov VG, Nass O, Sabbah HN, et al. (1997) Effects of angiotensin-converting enzyme inhibitors and angiotensin II type 1 receptor antagonists in rats with heart failure. Role of kinins and angiotensin II type 2 receptors. J Clin Invest 99: 1926-1935.

122. Kjeldsen SE, Dahlof B, Devereux RB, Julius S, Aurup P, et al. (2002) Effects of losartan on cardiovascular morbidity and mortality in patients with isolated systolic hypertension and left ventricular hypertrophy: a Losartan Intervention for Endpoint Reduction (LIFE) substudy. JAMA 288: 1491-1498.

123. Mathew J, Sleight P, Lonn E, Johnstone D, Pogue J, et al. (2001) Reduction of cardiovascular risk by regression of electrocardiographic markers of left ventricular hypertrophy by the angiotensin-converting enzyme inhibitor ramipril. Circulation 104: 1615-1621.

124. Yang LY, Ge X, Wang YL, Ma KL, Liu H, et al. (2013) Angiotensin receptor blockers reduce left ventricular hypertrophy in dialysis patients: a meta-analysis. Am J Med Sci 345: 1-9.

125. Verdecchia P, Sleight P, Mancia G, Fagard R, Trimarco B, et al. (2009) Effects of telmisartan, ramipril, and their combination on left ventricular hypertrophy in individuals at high vascular risk in the Ongoing Telmisartan Alone and in Combination With Ramipril Global End Point Trial and the Telmisartan Randomized Assessment Study in ACE Intolerant Subjects With Cardiovascular Disease. Circulation 120: 1380-1389.

126. Nishida K, Datino T, Macle L, Nattel S (2014) Atrial fibrillation ablation: translating basic mechanistic insights to the patient. J Am Coll Cardiol 64: 823-831.

127. Benjamin EJ, Levy D, Vaziri SM, D'Agostino RB, Belanger AJ, et al. (1994) Independent risk factors for atrial fibrillation in a population-based cohort. The Framingham Heart Study. JAMA 271: 840-844.

128. Wolf PA, Abbott RD, Kannel WB (1991) Atrial fibrillation as an independent risk factor for stroke: the Framingham Study. Stroke 22: 983-988.

129. Fuster V, Ryden LE, Cannom DS, Crijns HJ, Curtis AB, et al. (2006) ACC/AHA/ESC 2006 guidelines for the management of patients with atrial fibrillation-executive summary: a report of the American College of Cardiology/American Heart Association Task Force on Practice Guidelines and the European Society of Cardiology Committee for Practice Guidelines (Writing Committee to Revise the 2001 Guidelines for the Management of Patients with Atrial Fibrillation). Eur Heart J 27: 1979-2030.

130. Allessie M, Ausma J, Schotten U (2002) Electrical, contractile and structural remodeling during atrial fibrillation. Cardiovasc Res 54: 230-246.

131. Nattel S, Burstein B, Dobrev D (2008) Atrial remodeling and atrial fibrillation: mechanisms and implications. Circ Arrhythm Electrophysiol 1: 62-73.

132. Xiao HD, Fuchs S, Campbell DJ, Lewis W, Dudley SC, Jr., et al. (2004) Mice with cardiac-restricted angiotensin-converting enzyme (ACE) have atrial enlargement, cardiac arrhythmia, and sudden death. Am J Pathol 165: 1019-1032.

133. Li D, Shinagawa K, Pang L, Leung TK, Cardin S, et al. (2001) Effects of angiotensin-converting enzyme inhibition on the development of the atrial fibrillation substrate in dogs with ventricular tachypacing-induced congestive heart failure. Circulation 104: 2608-2614.

134. Goette A, Staack T, Rocken C, Arndt M, Geller JC, et al. (2000) Increased expression of extracellular signal-regulated kinase and angiotensin-converting enzyme in human atria during atrial fibrillation. J Am Coll Cardiol 35: 1669-1677.

135. Pellman J, Lyon RC, Sheikh F (2010) Extracellular matrix remodeling in atrial fibrosis: mechanisms and implications in atrial fibrillation. J Mol Cell Cardiol 48: 461-467.

136. Xu J, Cui G, Esmailian F, Plunkett M, Marelli D, et al. (2004) Atrial extracellular matrix remodeling and the maintenance of atrial fibrillation. Circulation 109: 363-368.

137. Lin CS, Pan CH (2008) Regulatory mechanisms of atrial fibrotic remodeling in atrial fibrillation. Cell Mol Life Sci 65: 1489-1508.

138. Casaclang-Verzosa G, Gersh BJ, Tsang TS (2008) Structural and functional remodeling of the left atrium: clinical and therapeutic implications for atrial fibrillation. J Am Coll Cardiol 51: 1-11.

139. Investigators G-A, Disertori M, Latini R, Barlera S, Franzosi MG, et al. (2009) Valsartan for prevention of recurrent atrial fibrillation. N Engl J Med 360: 1606-1617.

140. Investigators AI, Yusuf S, Healey JS, Pogue J, Chrolavicius S, et al. (2011) Irbesartan in patients with atrial fibrillation. N Engl J Med 364: 928-938.

141. Goette A, Schon N, Kirchhof P, Breithardt G, Fetsch T, et al. (2012) Angiotensin II-antagonist in paroxysmal atrial fibrillation (ANTIPAF) trial. Circ Arrhythm Electrophysiol 5: 43-51.

142. Tardif JC TM (2007) Perindopril and prevention of atrial fibrillation. European Heart Journal 9: E25-E29.

143. Go AS, Mozaffarian D, Roger VL, Benjamin EJ, Berry JD, et al. (2014) Heart disease and stroke statistics--2014 update: a report from the American Heart Association. Circulation 129: e28-e292.

144. Chatterjee K (2005) Neurohormonal activation in congestive heart failure and the role of vasopressin. Am J Cardiol 95: 8B-13B.

145. Writing Committee M, Yancy CW, Jessup M, Bozkurt B, Butler J, et al. (2013) 2013 ACCF/AHA guideline for the management of heart failure: a report of the American College of Cardiology Foundation/American Heart Association Task Force on practice guidelines. Circulation 128: e240-327.

146. Granger CB, McMurray JJ, Yusuf S, Held P, Michelson EL, et al. (2003) Effects of candesartan in patients with chronic heart failure and reduced left-ventricular systolic function intolerant to angiotensin-converting-enzyme inhibitors: the CHARM-Alternative trial. Lancet 362: 772-776.

147. Pfeffer MA, McMurray JJ, Velazquez EJ, Rouleau JL, Kober L, et al. (2003) Valsartan, captopril, or both in myocardial infarction complicated by heart failure, left ventricular dysfunction, or both. N Engl J Med 349: 1893-1906.

148. Leask A, Abraham DJ (2004) TGF-beta signaling and the fibrotic response. FASEB J 18: 816-827.

149. Dobaczewski M, Chen W, Frangogiannis NG (2011) Transforming growth factor (TGF)-beta signaling in cardiac remodeling. J Mol Cell Cardiol 51: 600-606.

150. Munger JS, Huang X, Kawakatsu H, Griffiths MJ, Dalton SL, et al. (1999) The integrin alpha v beta 6 binds and activates latent TGF beta 1: a mechanism for regulating pulmonary inflammation and fibrosis. Cell 96: 319-328.

151. Hyytiainen M, Penttinen C, Keski-Oja J (2004) Latent TGF-beta binding proteins: extracellular matrix association and roles in TGF-beta activation. Crit Rev Clin Lab Sci 41: 233-264.

152. Shi Y, Massague J (2003) Mechanisms of TGF-beta signaling from cell membrane to the nucleus. Cell 113: 685-700.

153. Lo RS, Massague J (1999) Ubiquitin-dependent degradation of TGF-beta-activated smad2. Nat Cell Biol 1: 472-478.

154. Almendral JL, Shick V, Rosendorff C, Atlas SA (2010) Association between transforming growth factor-beta(1) and left ventricular mass and diameter in hypertensive patients. J Am Soc Hypertens 4: 135-141.

155. Villar AV, Cobo M, Llano M, Montalvo C, Gonzalez-Vilchez F, et al. (2009) Plasma levels of transforming growth factor-beta1 reflect left ventricular remodeling in aortic stenosis. PLoS One 4: e8476.

156. Gramley F, Lorenzen J, Koellensperger E, Kettering K, Weiss C, et al. (2010) Atrial fibrosis and atrial fibrillation: the role of the TGF-beta1 signaling pathway. Int J Cardiol 143: 405-413.

157. Rosenkranz S, Flesch M, Amann K, Haeuseler C, Kilter H, et al. (2002) Alterations of beta-adrenergic signaling and cardiac hypertrophy in transgenic mice overexpressing TGF-beta(1). Am J Physiol Heart Circ Physiol 283: H1253-1262.

158. Kuwahara F, Kai H, Tokuda K, Kai M, Takeshita A, et al. (2002) Transforming growth factor-beta function blocking prevents myocardial fibrosis and diastolic dysfunction in pressure-overloaded rats. Circulation 106: 130-135.

159. Koyanagi M, Egashira K, Kubo-Inoue M, Usui M, Kitamoto S, et al. (2000) Role of transforming growth factor-beta1 in cardiovascular inflammatory changes induced by chronic inhibition of nitric oxide synthesis. Hypertension 35: 86-90.

160. Moussad EE, Brigstock DR (2000) Connective tissue growth factor: what's in a name? Mol Genet Metab 71: 276-292.

161. Abreu JG, Ketpura NI, Reversade B, De Robertis EM (2002) Connective-tissue growth factor (CTGF) modulates cell signalling by BMP and TGF-beta. Nat Cell Biol 4: 599-604.

162. Koitabashi N, Arai M, Niwano K, Watanabe A, Endoh M, et al. (2008) Plasma connective tissue growth factor is a novel potential biomarker of cardiac dysfunction in patients with chronic heart failure. Eur J Heart Fail 10: 373-379.

163. Ohnishi H, Oka T, Kusachi S, Nakanishi T, Takeda K, et al. (1998) Increased expression of connective tissue growth factor in the infarct zone of experimentally induced myocardial infarction in rats. J Mol Cell Cardiol 30: 2411-2422.

164. Finckenberg P, Inkinen K, Ahonen J, Merasto S, Louhelainen M, et al. (2003) Angiotensin II induces connective tissue growth factor gene expression via calcineurin-dependent pathways. Am J Pathol 163: 355-366.

165. Koitabashi N, Arai M, Kogure S, Niwano K, Watanabe A, et al. (2007) Increased connective tissue growth factor relative to brain natriuretic peptide as a determinant of myocardial fibrosis. Hypertension 49: 1120-1127.

166. Hishikawa K, Oemar BS, Nakaki T (2001) Static pressure regulates connective tissue growth factor expression in human mesangial cells. J Biol Chem 276: 16797-16803.

167. Ahmed MS, Oie E, Vinge LE, Yndestad A, Oystein Andersen G, et al. (2004) Connective tissue growth factor--a novel mediator of angiotensin II-stimulated cardiac fibroblast activation in heart failure in rats. J Mol Cell Cardiol 36: 393-404.

168. Recchia AG, Filice E, Pellegrino D, Dobrina A, Cerra MC, et al. (2009) Endothelin-1 induces connective tissue growth factor expression in cardiomyocytes. J Mol Cell Cardiol 46: 352-359.

169. Lipson KE, Wong C, Teng Y, Spong S (2012) CTGF is a central mediator of tissue remodeling and fibrosis and its inhibition can reverse the process of fibrosis. Fibrogenesis Tissue Repair 5: S24.

170. Blom IE, Goldschmeding R, Leask A (2002) Gene regulation of connective tissue growth factor: new targets for antifibrotic therapy? Matrix Biol 21: 473-482.

171. Chen MM, Lam A, Abraham JA, Schreiner GF, Joly AH (2000) CTGF expression is induced by TGF- beta in cardiac fibroblasts and cardiac myocytes: a potential role in heart fibrosis. J Mol Cell Cardiol 32: 1805-1819.

172. Duncan MR, Frazier KS, Abramson S, Williams S, Klapper H, et al. (1999) Connective tissue growth factor mediates transforming growth factor beta-induced collagen synthesis: down-regulation by cAMP. FASEB J 13: 1774-1786.

173. Booth AJ, Csencsits-Smith K, Wood SC, Lu G, Lipson KE, et al. (2010) Connective tissue growth factor promotes fibrosis downstream of TGFbeta and IL-6 in chronic cardiac allograft rejection. Am J Transplant 10: 220-230.

174. Liu C, Zhao W, Meng W, Zhao T, Chen Y, et al. (2014) Platelet-derived growth factor blockade on cardiac remodeling following infarction. Mol Cell Biochem 397: 295-304.

175. Shim AH, Liu H, Focia PJ, Chen X, Lin PC, et al. (2010) Structures of a platelet-derived growth factor/propeptide complex and a platelet-derived growth factor/receptor complex. Proc Natl Acad Sci U S A 107: 11307-11312.

176. Heldin CH, Eriksson U, Ostman A (2002) New members of the platelet-derived growth factor family of mitogens. Arch Biochem Biophys 398: 284-290.

177. Simon AR, Rai U, Fanburg BL, Cochran BH (1998) Activation of the JAK-STAT pathway by reactive oxygen species. Am J Physiol 275: C1640-1652.

178. Reif S, Lang A, Lindquist JN, Yata Y, Gabele E, et al. (2003) The role of focal adhesion kinase-phosphatidylinositol 3-kinase-akt signaling in hepatic stellate cell proliferation and type I collagen expression. J Biol Chem 278: 8083-8090.

179. Fan B, Ma L, Li Q, Wang L, Zhou J, et al. (2014) Role of PDGFs/PDGFRs signaling pathway in myocardial fibrosis of DOCA/salt hypertensive rats. Int J Clin Exp Pathol 7: 16-27.

180. Zhao W, Zhao T, Huang V, Chen Y, Ahokas RA, et al. (2011) Platelet-derived growth factor involvement in myocardial remodeling following infarction. J Mol Cell Cardiol 51: 830-838.

181. Liao CH, Akazawa H, Tamagawa M, Ito K, Yasuda N, et al. (2010) Cardiac mast cells cause atrial fibrillation through PDGF-A-mediated fibrosis in pressure-overloaded mouse hearts. J Clin Invest 120: 242-253.

182. Shindo T, Manabe I, Fukushima Y, Tobe K, Aizawa K, et al. (2002) Kruppel-like zinc-finger transcription factor KLF5/BTEB2 is a target for angiotensin II signaling and an essential regulator of cardiovascular remodeling. Nat Med 8: 856-863.

183. Burstein B, Libby E, Calderone A, Nattel S (2008) Differential behaviors of atrial versus ventricular fibroblasts: a potential role for platelet-derived growth factor in atrial-ventricular remodeling differences. Circulation 117: 1630-1641.

184. Ponten A, Li X, Thoren P, Aase K, Sjoblom T, et al. (2003) Transgenic overexpression of platelet-derived growth factor-C in the mouse heart induces cardiac fibrosis, hypertrophy, and dilated cardiomyopathy. Am J Pathol 163: 673-682.

185. Tuuminen R, Nykanen A, Keranen MA, Krebs R, Alitalo K, et al. (2006) The effect of platelet-derived growth factor ligands in rat cardiac allograft vasculopathy and fibrosis. Transplant Proc 38: 3271-3273.

186. Zhao T, Zhao W, Chen Y, Li VS, Meng W, et al. (2013) Platelet-derived growth factor-D promotes fibrogenesis of cardiac fibroblasts. Am J Physiol Heart Circ Physiol 304: H1719-1726.

187. Liao S, Bodmer J, Pietras D, Azhar M, Doetschman T, et al. (2009) Biological functions of the low and high molecular weight protein isoforms of fibroblast growth factor-2 in cardiovascular development and disease. Dev Dyn 238: 249-264.

188. Kaye D, Pimental D, Prasad S, Maki T, Berger HJ, et al. (1996) Role of transiently altered sarcolemmal membrane permeability and basic fibroblast growth factor release in the hypertrophic response of adult rat ventricular myocytes to increased mechanical activity in vitro. J Clin Invest 97: 281-291.

189. Florkiewicz RZ, Anchin J, Baird A (1998) The inhibition of fibroblast growth factor-2 export by cardenolides implies a novel function for the catalytic subunit of Na+,K+-ATPase. J Biol Chem 273: 544-551.

190. Clarke MS, Caldwell RW, Chiao H, Miyake K, McNeil PL (1995) Contraction-induced cell wounding and release of fibroblast growth factor in heart. Circ Res 76: 927-934.

191. Mignatti P, Morimoto T, Rifkin DB (1991) Basic fibroblast growth factor released by single, isolated cells stimulates their migration in an autocrine manner. Proc Natl Acad Sci U S A 88: 11007-11011.

192. Detillieux KA, Sheikh F, Kardami E, Cattini PA (2003) Biological activities of fibroblast growth factor-2 in the adult myocardium. Cardiovasc Res 57: 8-19.

193. Bogoyevitch MA, Glennon PE, Andersson MB, Clerk A, Lazou A, et al. (1994) Endothelin-1 and fibroblast growth factors stimulate the mitogen-activated protein kinase signaling cascade in cardiac myocytes. The potential role of the cascade in the integration of two signaling pathways leading to myocyte hypertrophy. J Biol Chem 269: 1110-1119.

194. Mima T, Ueno H, Fischman DA, Williams LT, Mikawa T (1995) Fibroblast growth factor receptor is required for in vivo cardiac myocyte proliferation at early embryonic stages of heart development. Proc Natl Acad Sci U S A 92: 467-471.

195. Jiang ZS, Padua RR, Ju H, Doble BW, Jin Y, et al. (2002) Acute protection of ischemic heart by FGF-2: involvement of FGF-2 receptors and protein kinase C. Am J Physiol Heart Circ Physiol 282: H1071-1080.

196. Sheikh F, Sontag DP, Fandrich RR, Kardami E, Cattini PA (2001) Overexpression of FGF-2 increases cardiac myocyte viability after injury in isolated mouse hearts. Am J Physiol Heart Circ Physiol 280: H1039-1050.

197. Hellman U, Hellstrom M, Morner S, Engstrom-Laurent A, Aberg AM, et al. (2008) Parallel up-regulation of FGF-2 and hyaluronan during development of cardiac hypertrophy in rat. Cell Tissue Res 332: 49-56.

198. Schultz JE, Witt SA, Nieman ML, Reiser PJ, Engle SJ, et al. (1999) Fibroblast growth factor-2 mediates pressure-induced hypertrophic response. J Clin Invest 104: 709-719.

199. Tang W, Wei Y, Le K, Li Z, Bao Y, et al. (2011) Mitogen-activated protein kinases ERK 1/2- and p38-GATA4 pathways mediate the Ang II-induced activation of FGF2 gene in neonatal rat cardiomyocytes. Biochem Pharmacol 81: 518-525.

200. Pellieux C, Foletti A, Peduto G, Aubert JF, Nussberger J, et al. (2001) Dilated cardiomyopathy and impaired cardiac hypertrophic response to angiotensin II in mice lacking FGF-2. J Clin Invest 108: 1843-1851.

201. Peters J, Farrenkopf R, Clausmeyer S, Zimmer J, Kantachuvesiri S, et al. (2002) Functional significance of prorenin internalization in the rat heart. Circ Res 90: 1135-1141.

202. Baker KM, Chernin MI, Schreiber T, Sanghi S, Haiderzaidi S, et al. (2004) Evidence of a novel intracrine mechanism in angiotensin II-induced cardiac hypertrophy. Regul Pept 120: 5-13.

203. Frustaci A, Kajstura J, Chimenti C, Jakoniuk I, Leri A, et al. (2000) Myocardial cell death in human diabetes. Circ Res 87: 1123-1132.

204. Singh VP, Baker KM, Kumar R (2008) Activation of the intracellular renin-angiotensin system in cardiac fibroblasts by high glucose: role in extracellular matrix production. Am J Physiol Heart Circ Physiol 294: H1675-1684.

205. Singh VP, Le B, Bhat VB, Baker KM, Kumar R (2007) High-glucose-induced regulation of intracellular ANG II synthesis and nuclear redistribution in cardiac myocytes. Am J Physiol Heart Circ Physiol 293: H939-948.

206. Singh VP, Le B, Khode R, Baker KM, Kumar R (2008) Intracellular angiotensin II production in diabetic rats is correlated with cardiomyocyte apoptosis, oxidative stress, and cardiac fibrosis. Diabetes 57: 3297-3306.

207. De Mello WC (1998) Intracellular angiotensin II regulates the inward calcium current in cardiac myocytes. Hypertension 32: 976-982.

208. De Mello WC (2011) Intracrine action of angiotensin II in the intact ventricle of the failing heart: angiotensin II changes cardiac excitability from within. Mol Cell Biochem 358: 309-315.

209. De Mello WC (1996) Renin-angiotensin system and cell communication in the failing heart. Hypertension 27: 1267-1272.

210. Filipeanu CM, Brailoiu E, Kok JW, Henning RH, De Zeeuw D, et al. (2001) Intracellular angiotensin II elicits Ca2+ increases in A7r5 vascular smooth muscle cells. Eur J Pharmacol 420: 9-18.

211. Filipeanu CM, Henning RH, de Zeeuw D, Nelemans A (2001) Intracellular Angiotensin II and cell growth of vascular smooth muscle cells. Br J Pharmacol 132: 1590-1596.

212. Weber MA, Giles TD (2006) Inhibiting the renin-angiotensin system to prevent cardiovascular diseases: do we need a more comprehensive strategy? Rev Cardiovasc Med 7: 45-54.

213. Tigerstedt RB, PG. (1898) Niere und Kreislauf. Scand Arch Physiol 8: 221-271.

214. Basso N, Terragno NA (2001) History about the discovery of the renin-angiotensin system. Hypertension 38: 1246-1249.

215. Kumar R, Thomas CM, Yong QC, Chen W, Baker KM (2012) The intracrine renin-angiotensin system. Clin Sci (Lond) 123: 273-284.

216. Celio MR, Inagami T (1981) Angiotensin II immunoreactivity coexists with renin in the juxtaglomerular granular cells of the kidney. Proc Natl Acad Sci U S A 78: 3897-3900.

217. Hunt MK, Ramos SP, Geary KM, Norling LL, Peach MJ, et al. (1992) Colocalization and release of angiotensin and renin in renal cortical cells. Am J Physiol 263: F363-373.

218. Carey RM, Geary KM, Hunt MK, Ramos SP, Forbes MS, et al. (1990) Identification of individual renocortical cells that secrete renin. Am J Physiol 258: F649-659.

219. Mercure C, Ramla D, Garcia R, Thibault G, Deschepper CF, et al. (1998) Evidence for intracellular generation of angiotensin II in rat juxtaglomerular cells. FEBS Lett 422: 395-399.

220. Vila-Porcile E, Corvol P (1998) Angiotensinogen, prorenin, and renin are Co-localized in the secretory granules of all glandular cells of the rat anterior pituitary: an immunoultrastructural study. J Histochem Cytochem 46: 301-311.

221. Fischer TA, Ungureanu-Longrois D, Singh K, de Zengotita J, DeUgarte D, et al. (1997) Regulation of bFGF expression and ANG II secretion in cardiac myocytes and microvascular endothelial cells. Am J Physiol 272: H958-968.

222. Sherrod M, Liu X, Zhang X, Sigmund CD (2005) Nuclear localization of angiotensinogen in astrocytes. Am J Physiol Regul Integr Comp Physiol 288: R539-546.

223. Lee-Kirsch MA, Gaudet F, Cardoso MC, Lindpaintner K (1999) Distinct renin isoforms generated by tissue-specific transcription initiation and alternative splicing. Circ Res 84: 240-246.

224. Clausmeyer S, Reinecke A, Farrenkopf R, Unger T, Peters J (2000) Tissue-specific expression of a rat renin transcript lacking the coding sequence for the prefragment and its stimulation by myocardial infarction. Endocrinology 141: 2963-2970.

225. Peters J, Kranzlin B, Schaeffer S, Zimmer J, Resch S, et al. (1996) Presence of renin within intramitochondrial dense bodies of the rat adrenal cortex. Am J Physiol 271: E439-450.

226. Lavoie JL, Liu X, Bianco RA, Beltz TG, Johnson AK, et al. (2006) Evidence supporting a functional role for intracellular renin in the brain. Hypertension 47: 461-466.

227. Peters J, Wanka H, Peters B, Hoffmann S (2008) A renin transcript lacking exon 1 encodes for a non-secretory intracellular renin that increases aldosterone production in transgenic rats. J Cell Mol Med 12: 1229-1237.

228. Wanka H, Kessler N, Ellmer J, Endlich N, Peters BS, et al. (2009) Cytosolic renin is targeted to mitochondria and induces apoptosis in H9c2 rat cardiomyoblasts. J Cell Mol Med 13: 2926-2937.

229. Camargo de Andrade MC, Di Marco GS, de Paulo Castro Teixeira V, Mortara RA, Sabatini RA, et al. (2006) Expression and localization of N-domain ANG I-converting enzymes in mesangial cells in culture from spontaneously hypertensive rats. Am J Physiol Renal Physiol 290: F364-375.

230. Lucero HA, Kintsurashvili E, Marketou ME, Gavras H (2010) Cell signaling, internalization, and nuclear localization of the angiotensin converting enzyme in smooth muscle and endothelial cells. J Biol Chem 285: 5555-5568.

231. Blood Pressure Lowering Treatment Trialists C, Turnbull F, Neal B, Ninomiya T, Algert C, et al. (2008) Effects of different regimens to lower blood pressure on major cardiovascular events in older and younger adults: meta-analysis of randomised trials. BMJ 336: 1121-1123.

232. Scheen AJ, Krzesinski JM (2008) [ONTARGET: similar protection of telmisartan and ramipril and lack of benefit of combined therapy in patients at high risk for vascular events]. Rev Med Liege 63: 213-219.

233. Mann JF, Schmieder RE, McQueen M, Dyal L, Schumacher H, et al. (2008) Renal outcomes with telmisartan, ramipril, or both, in people at high vascular

risk (the ONTARGET study): a multicentre, randomised, double-blind, controlled trial. Lancet 372: 547-553.

234. Investigators O, Yusuf S, Teo KK, Pogue J, Dyal L, et al. (2008) Telmisartan, ramipril, or both in patients at high risk for vascular events. N Engl J Med 358: 1547-1559.

235. Messerli FH, Bangalore S (2013) ALTITUDE trial and dual RAS blockade: the alluring but soft science of the surrogate end point. Am J Med 126: e1-3.

236. Mallat SG (2013) Dual renin-angiotensin system inhibition for prevention of renal and cardiovascular events: do the latest trials challenge existing evidence? Cardiovasc Diabetol 12: 108.

237. Gheorghiade M, Bohm M, Greene SJ, Fonarow GC, Lewis EF, et al. (2013) Effect of aliskiren on postdischarge mortality and heart failure readmissions among patients hospitalized for heart failure: the ASTRONAUT randomized trial. JAMA 309: 1125-1135.

238. Danser AH (2010) Cardiac angiotensin II: does it have a function? Am J Physiol Heart Circ Physiol 299: H1304-1306.

239. Baker KM, Kumar R (2006) Intracellular angiotensin II induces cell proliferation independent of AT1 receptor. Am J Physiol Cell Physiol 291: C995-1001.

240. Kumar R, Singh VP, Baker KM (2008) The intracellular renin-angiotensin system: implications in cardiovascular remodeling. Curr Opin Nephrol Hypertens 17: 168-173.

241. De Mello WC (2009) Cell swelling, impulse conduction, and cardiac arrhythmias in the failing heart. Opposite effects of angiotensin II and angiotensin (1-7) on cell volume regulation. Mol Cell Biochem 330: 211-217.

242. Haller H, Lindschau C, Erdmann B, Quass P, Luft FC (1996) Effects of intracellular angiotensin II in vascular smooth muscle cells. Circ Res 79: 765-772.

243. Brailoiu E, Filipeanu CM, Tica A, Toma CP, de Zeeuw D, et al. (1999) Contractile effects by intracellular angiotensin II via receptors with a distinct pharmacological profile in rat aorta. Br J Pharmacol 126: 1133-1138.

244. Beaulieu JM, Caron MG (2005) Beta-arrestin goes nuclear. Cell 123: 755-757.

245. Martini JS, Raake P, Vinge LE, DeGeorge BR, Jr., Chuprun JK, et al. (2008) Uncovering G protein-coupled receptor kinase-5 as a histone deacetylase kinase in the nucleus of cardiomyocytes. Proc Natl Acad Sci U S A 105: 12457-12462.

246. Miyazaki M, Takai S (2006) Tissue angiotensin II generating system by angiotensin-converting enzyme and chymase. J Pharmacol Sci 100: 391-397.

247. Bacani C, Frishman WH (2006) Chymase: a new pharmacologic target in cardiovascular disease. Cardiol Rev 14: 187-193.

248. Koka V, Wang W, Huang XR, Kim-Mitsuyama S, Truong LD, et al. (2006) Advanced glycation end products activate a chymase-dependent angiotensin II-generating pathway in diabetic complications. Circulation 113: 1353-1360.

249. Dell'Italia LJ, Husain A (2002) Dissecting the role of chymase in angiotensin II formation and heart and blood vessel diseases. Curr Opin Cardiol 17: 374-379.

250. Urata H, Boehm KD, Philip A, Kinoshita A, Gabrovsek J, et al. (1993) Cellular localization and regional distribution of an angiotensin II-forming chymase in the heart. J Clin Invest 91: 1269-1281.

251. Ahmad S, Simmons T, Varagic J, Moniwa N, Chappell MC, et al. (2011) Chymase-dependent generation of angiotensin II from angiotensin-(1-12) in human atrial tissue. PLoS One 6: e28501.

252. Carey RM (2013) Newly discovered components and actions of the renin-angiotensin system. Hypertension 62: 818-822.

253. Ahmad S, Wei CC, Tallaj J, Dell'Italia LJ, Moniwa N, et al. (2013) Chymase mediates angiotensin-(1-12) metabolism in normal human hearts. J Am Soc Hypertens 7: 128-136.

254. Ahmad S, Varagic J, Groban L, Dell'Italia LJ, Nagata S, et al. (2014) Angiotensin-(1-12): a chymase-mediated cellular angiotensin II substrate. Curr Hypertens Rep 16: 429.

255. Prosser HC, Forster ME, Richards AM, Pemberton CJ (2009) Cardiac chymase converts rat proAngiotensin-12 (PA12) to angiotensin II: effects of PA12 upon cardiac haemodynamics. Cardiovasc Res 82: 40-50.

256. Zheng J, Wei CC, Hase N, Shi K, Killingsworth CR, et al. (2014) Chymase mediates injury and mitochondrial damage in cardiomyocytes during acute ischemia/reperfusion in the dog. PLoS One 9: e94732.

257. Yoshiyama M, Nakamura Y, Omura T, Izumi Y, Matsumoto R, et al. (2005) Angiotensin converting enzyme inhibitor prevents left ventricular remodelling

after myocardial infarction in angiotensin II type 1 receptor knockout mice. Heart 91: 1080-1085.

258. Liu YH, Yang XP, Mehta D, Bulagannawar M, Scicli GM, et al. (2000) Role of kinins in chronic heart failure and in the therapeutic effect of ACE inhibitors in kininogen-deficient rats. Am J Physiol Heart Circ Physiol 278: H507-514.

259. Yang XP, Liu YH, Mehta D, Cavasin MA, Shesely E, et al. (2001) Diminished cardioprotective response to inhibition of angiotensin-converting enzyme and angiotensin II type 1 receptor in B(2) kinin receptor gene knockout mice. Circ Res 88: 1072-1079.

260. Messadi-Laribi E, Griol-Charhbili V, Pizard A, Vincent MP, Heudes D, et al. (2007) Tissue kallikrein is involved in the cardioprotective effect of AT1-receptor blockade in acute myocardial ischemia. J Pharmacol Exp Ther 323: 210-216.

261. Quitterer U, AbdAlla S (2014) Vasopressor meets vasodepressor: The AT1-B2 receptor heterodimer. Biochem Pharmacol 88: 284-290.

262. Schupp M, Janke J, Clasen R, Unger T, Kintscher U (2004) Angiotensin type 1 receptor blockers induce peroxisome proliferator-activated receptor-gamma activity. Circulation 109: 2054-2057.

263. Benson SC, Pershadsingh HA, Ho CI, Chittiboyina A, Desai P, et al. (2004) Identification of telmisartan as a unique angiotensin II receptor antagonist with selective PPARgamma-modulating activity. Hypertension 43: 993-1002.

264. Wangler NJ, Santos KL, Schadock I, Hagen FK, Escher E, et al. (2012) Identification of membrane-bound variant of metalloendopeptidase neurolysin

(EC 3.4.24.16) as the non-angiotensin type 1 (non-AT1), non-AT2 angiotensin binding site. J Biol Chem 287: 114-122.